REAL-TIME METABOLIC FLUX IN CHRONIC LYMPHOCYTIC LEUKAEMIA CELLS ADAPTING TO THE HYPOXIC NICHE

by

KATARZYNA MAŁGORZATA KOCZUŁA

A thesis submitted to the University of Birmingham for the degree of

DOCTOR OF PHILOSOPHY

School of Cancer Sciences

College of Medical and Dental Sciences

University of Birmingham

February 2015

ABSTRACT

Although knowledge of metabolic adaptations in cancer has increased dramatically, little is known about the spontaneous adoptive adaptations of cancer cells to changing conditions in the body. This is particularly important for chronic lymphocytic leukaemia (CLL) cells which continually circulate between different microenvironments in the blood, bone marrow and lymph nodes.

To study such metabolic adaptations, a nuclear magnetic resonance (NMR) based approach; capable of monitoring real-time metabolism in primary CLL cells was developed. Using this setup, this thesis demonstrates fast, reversible metabolic plasticity in CLL cells during transition from normoxic to hypoxic conditions, associated with elevated HIF-1α dependent glycolysis. This work also demonstrates differential utilisation of pyruvate in oxygenated and hypoxic conditions where in the latter, pyruvate was actively transported into CLL cells to protect against oxidative stress. Moreover, real-time NMR experiments provided initial evidence that CLL metabolism in hypoxia correlates with stage of disease, adding significant relevance of our method for patient stratification. Additionally, to further investigate alterations between normoxic and hypoxic metabolism, Metabolic Flux Analysis (MFA) was carried out using primary CLL cell extracts, revealing modifications in pyruvate carboxylase (PC) activity and the pentose phosphate pathway (PPP).

Despite the recent advent of promising new agents, CLL currently remains incurable and new therapeutic approaches are required. Understanding CLL cell adaptation to changing oxygen availability will permit the development of therapies that interfere with disease aetiology. This study makes several significant contributions towards this goal. Moreover, the findings may be relevant to all migratory cancer cells, and may have importance for the development of strategies to prevent cancer metastasis.

Moim Rodzicom i Dziadkom,

Za ich miłość oraz niekończące się wsparcie

To my Parents and Grandparents,

For their love and endless support

ACKNOWLEDGEMENTS

I would like to say thank you to my supervisors Professor Ulrich Günther, Professor Christopher Bunce and Doctor Farhat Khanim for giving me the opportunity to undertake this PhD project in their groups. Thank you for encouraging my research and for allowing me to grow as a research scientist. Thank you for your ideas, for new and interesting experiments and for the critical opinion you gave about my work. Being a part of the Marie Curie project METAFLUX was a great privilege and I would like to say thank you to everyone who contributed to creating this exceptional network.

My work would not be possible without the help of very skilled and helpful academic staff from both the School of Biosciences and HWB-NMR Facility. I would like to express my special appreciation to Scientific Officer Christian Ludwig, who with enormous patience, taught me the basics of NMR theory as well as the practice. Chris, it was always a great pleasure to work with you and your charisma and sense of humour makes the most boring peak picking or shimming, a very nice and pleasant experience. I am so grateful for all the extra time you spent helping with the project, for all the urgent help during the work with the spectrometer and the data analysis. Thank you for listening to our needs and constantly updating our software, making our work more efficient.

I would also like to say a big thank you to Rachel, Andy, Nikos and Laura who were always very understanding, warm and caring; always ready to help in the laboratory and discuss all the PhD problems. I was very lucky to have you around.

I would like to warmly thank all my NMR colleagues: Karen, Sue and Sarah – three super women of the NMR facility, who ensured that our facility was running smoothly and who were always ready to solve urgent problems. It was a pleasure to work with you. I also want to say thank you for your support and well done to Mei, Tatiana and Sotiris, with whom we shared the ups and downs of the METAFLUX adventure. I would also like to acknowledge all of my great colleagues from the 4th and 3rd floors in Biosciences for creating a friendly atmosphere to work in, with a special thank you to Kay and Dorthe for their support in the most difficult moments.

More people without whom my work could not be conducted are Guy Pratt and Helene Parry, thanks to whom every week I could work on fresh primary CLL cells. Thank you for being very reliable and working hard to provide samples and clinical data. I am also grateful to Dr Daniel Tennant for very many fruitful scientific discussions.

Now I would also like to a say big thank you to my amazing friend and flatmate Iza, for her everyday support and encouragement, cooking and baking together and sharing all of the good and bad moments of PhD life.

Now it is time for Massive and Biggest thanks to Chib for being with me through the major part of my PhD, and being the best award compensating all the struggles I faced through the PhD time. Thank you for your support, patience and understanding and for always being able to make me laugh, when I would least expect it.

At the end I would like to say thank you to my Family; my Parents, Grandparents and my Sister Ania for supporting me, making me feel their presence and believing in me, even from far away.

TABLE OF CONTENTS

ABSTRACT II

ACKNOWLEDGEMENTS V

TABLE OF CONTENTS VI

LIST OF FIGURES XI

LIST OF TABLES XV

ABBREVIATIONS XVI

CHAPTER I - INTRODUCTION

1.1 HALLMARKS OF CANCER 2

1.2 UNDERSTANDING CANCER METABOLISM 4

1.2.1 Metabolism pervades every aspect of biology 4
1.2.2 Lessons from Warburg 6
1.2.3 The advantage of altered cancer metabolism 7
1.2.4 Role of ROS in cancer cells 9
1.2.5 Glutamine metabolism 11

1.3 THE HYPOXIC TUMOUR ENVIRONMENT 15

1.3.1 HIF-1α 16

1.4. HAEMATOLOGICAL CANCERS 19

1.4.1 Inhibitors of glycolysis in leukaemic cells 20
1.4.2 IDH1/2 mutations 24
1.4.3 Mitochondrial uncoupling 25

1.5. CHRONIC LYMPHOCYTIC LEUKAEMIA (CLL) 27

1.5.1 CLL microenvironment 31
1.5.2 Current CLL therapies 33
1.5.3 CLL cell metabolism 37
1.5.4 Metabolism of quiescent cells 38

1.6 TOOLS USED FOR INVESTIGATING CANCER METABOLISM 40

1.6.1 Spectroscopic methods used in metabolic analysis 40
1.6.2 Metabolic Flux analysis 43
1.6.3 NMR as a tool for metabolomics studies 45
1.6.3.1 Metabolic profiles of cancer cells 47
1.6.4 Leading NMR techniques for cancer metabolomics 48
1.6.4.1 Magic Angle Spinning (MAS) 48
1.6.4.2 NMR measurements of cell extracts 49

1.6.4.3 Dynamic Nuclear Polarization (DNP) 49
1.6.4.4 Measurement of living cells in NMR 50
1.6.4.4.1 ^{31}P NMR as an indicator of pH in samples 51
1.6.4.4.2 Challenges of recording real-time metabolic changes 52
1.6.4.4.3 Flow systems 54

1.7. FUTURE PROSPECTS **55**

1.8. AIM OF THIS THESIS **56**

CHAPTER II - MATERIALS AND METHODS

2.1 CELLS FROM PATIENTS **59**
2.1.1 Purification of primary CLL cells 59
2.1.2 Isolation of CD^{19+ve} cells 60

2.2 ANALYSIS OF CELL PHENOTYPE USING FLOW CYTOMETRY **60**

2.3 ASSESSMENT OF CELL VIABILITY AND PROLIFERATION **62**
2.3.1 AV/PI staining 62
2.3.2 Cell cycle analysis. 62

2.4 CELL MORPHOLOGY: JENNER-GIEMSA STAINING **63**

2.5 REAL TIME NMR EXPERIMENTS WITH LIVING CELLS **63**
2.5.1 Sample preparation 63
2.5.2 Set up of the NMR experiment 64
2.5.3 Real time NMR measurement 1D ^{1}H NOESY 67
2.5.4 Proton-Carbon 1D spectra 67
2.5.5 NMR time course data processing 71
2.5.6 NMR time course data analysis 72
2.5.7 Determination of the intracellular pH inside the NMR tube 74

2.6 CLL CELL EXTRACTION **76**
2.6.1 Incubation with the ^{13}C labelled precursor 76
2.6.2 Quenching 76
2.6.3 Extraction 77

2.7 NMR METABOLIC FLUX EXPERIMENTS USING CELL EXTRACTS **78**
2.7.1 Sample preparation 78
2.7.2 HSQC acquisition 78
2.7.3 HSQC data processing 79
2.7.4 HSQC data analysis 79

2.8 QUANTITATIVE REAL-TIME POLYMERASE CHAIN REACTION (QRT-PCR) ... **80**
2.8.1 RNA extraction 80

2.8.2 RNA quantification 81
2.8.3 Reverse transcription 81
2.8.4 β-actin PCR 82
2.8.5 Agarose gel electrophoresis 83
2.8.6 Real-time PCR 83
2.8.6.1 Measurement of gene expression. 83
2.8.6.2 Q-PCR data analysis. 84
2.9 PROTEIN ANALYSIS: WESTERN BLOTTING **85**
2.9.1 Protein extraction and quantification. 85
2.9.2 Sample preparation and protein separation by sodium dodecyl sulphate – polyacrylamide gel electrophoresis (SDS PAGE) 85
2.9.3 Protein transfer 86
2.9.4 Immunodetection of proteins 86
2.10 INVESTIGATION OF OXIDATIVE STRESS **88**
2.10.1 Assessment of accumulation of Reactive Oxygen Species (ROS) 88
2.10.2 Assessment of accumulation of Mitochondrial Superoxide 88
2.11 TREATMENTS OF CLL CELLS WITH INHIBITORS **89**
2.11.1 HIF-1α inhibition with Chetomin 89
2.11.2 Alanine aminotransferase inhibition with cycloserine and β-chloro-l-alanine. 89
2.11.3 Pyruvate cellular transporter (MCT1) inhibition with CHC 89
2.12 HRP CHROMOGENIC STAINING OF CYTOSPINS **90**
2.12.1 Staining 90
2.12.2 Counterstain 91
2.12.3 Dehydration and Mounting 91
2.13 FLUORESCENT STAINING OF CYTOSPINS **91**
2.14 STATISTICAL ANALYSIS OF EXPERIMENTS **93**
2.15 METABOLAB ROUTINES USED FOR DATA ANALYSIS **93**
2.15.1 MATLAB scripts 93
2.15.1.1 Scale TMSP 93
2.15.1.2 Peaking shifting peaks 94
2.15.1.3 Fit pH curve 95
2.15.1.4 Calculate pH 96
2.15.1.5 Calculate percentage of Keto and Enol form of pyruvate 96

CHAPTER III - ESTABLISHING NMR METHOD TO MEASURE METABOLIC CHANGES IN LIVING CLL CELLS

3.1 INTRODUCTION **99**
3.2 RESULTS **102**

3.2.1 1D ^{1}H NMR spectrum of living CLL cells 102
3.2.2 Viability of CLL cells was not affected by the NMR experiment 106
3.2.3 Changes can be seen in the intensity of metabolites 107
3.2.4 Changes of intensities of metabolite signals 111
3.2.5 Apparently quiescent CLL cells show high metabolic activity 111
3.2.6 Metabolic changes were not affected by the stabilisation of extracellular pH . 115
3.2.7 Primary CLL cells survive extreme hypoxia 118
3.2.8 Kinetics of the metabolic changes 119

3.3 DISCUSSION **125**

CHAPTER IV - METABOLIC PLASTICITY OF CLL CELLS

4.1. INTRODUCTION **137**

4.2 RESULTS **141**
4.2.1 Primary CLL cells adapt their metabolism to hypoxic conditions 141
4.2.2 HIF-1α shows hypoxia-inducible nuclear import 145
4.2.3 Primary CLL cells exhibit reversible metabolic plasticity during the transition between different oxygen environments 149
4.2.4 HIF-1α inhibition reverses changes in metabolism associated with hypoxia. . 153
4.2.5 HIF-1α inhibition by chetomin is toxic to CLL cells regardless of the oxygen level 155
4.2.6 Alanine aminotransferase is not involved in the mechanism of hypoxic adaptation. 157

4.3 DISCUSSION **162**

CHAPTER V - INVESTIGATING THE ROLE OF PYRUVATE IN ADAPTING TO HYPOXIA

5.1 INTRODUCTION **170**

5.2 RESULTS **173**
5.2.1 Analysis of pyruvate changes during the NMR time course. 173
5.2.2. CLL cells export pyruvate in normoxia and take it up again in hypoxia. 175
5.2.3 Pyruvate dynamics were not HIF-1α dependent. 178
5.2.4 Inhibition by MCT1 prevents pyruvate re-uptake and causes apoptosis of CLL cells. 180
5.2.5 Methyl pyruvate does not rescue CLL cells from CHC. 183
5.2.6 Exogenous pyruvate reduces mitosox and ROS levels in CLL cells. 186
5.2.7 Keto-enol tautomerism of pyruvate 189

5.3 DISCUSSION **193**

CHAPTER VI - METABOLIC FLUX ANALYSIS OF CLL CELLS IN DIFFERENT OXYGEN ENVIRONMENTS

6.1. INTRODUCTION **200**

6.2 RESULTS **206**

6.2.1 [1,2-^{13}C]glucose flux through Glycolysis and Pentose Phosphate Pathway 206
6.2.2 Pyruvate carboxylase is active only in hypoxic conditions 213
6.2.3 Glucose flux into the TCA cycle via PDH/PC 219
6.2.4 ^{13}C-3-Glutamine flux 221

6.3 DISCUSSION **228**

CHAPTER VII - GENERAL DISCUSSION

7.1 GENERAL DISCUSSION **237**

7.2 FUTURE WORK **242**

7.3 THE FUTURE OF NMR METABOLOMICS FOR BEATING CANCER **244**

7.4 CONCLUDING REMARKS **247**

REFERENCES **249**

APPENDICES **267**

APPENDIX A1: Buffers and Recipes 268
APPENDIX A2: Purity of CLL preparations 270
APPENDIX A3: Chetomin killing curves 271

LIST OF FIGURES

Chapter 1

Figure 1.1. Hallmark of cancer cells 3

Figure 1.2. HIF-1α regulation by proline hydroxylation 18

Figure 1.3. The role of mTOR activation in supporting cancer cell survival 23

Figure 1.4. Model of the lifecycle of a CLL B cell 30

Figure 1.5. New therapeutic agents and their targets in a chronic lymphocytic leukaemia cell 36

Chapter 2

Figure 2.1. Example of flow cytometry analysis, assessment of CLL preparations purity.....61

Figure 2.2. Scheme of NMR time course experiment 66

Figure 2.3. The pulse sequence for a set of two 1D-$^{1}H^{13}C$ decoupled NMR spectra 69

Figure 2.4. The principle of obtaining ^{13}C% incorporation data from the 1D ^{1}H spectra 70

Figure 2.5. Colour time gradient of the 1D ^{1}H noesy spectra 73

Figure 2.6. Changes of pH in the NMR tube 75

Chapter 3

Figure 3.1. 1D ^{1}H NMR spectrum of CLL cells 103

Figure 3.2. J-res and HSQC spectra of the used medium 105

Figure 3.3. CLL cells can tolerate NMR analyses 106

Figure 3.4. Changes in the NMR spectrum are the result of metabolic activity of CLL cells 108

Figure 3.5. Spectrum of CLL cells in medium with agarose overlaid with spectrum of medium alone 110

Figure 3.6. Representative peaks for chosen metabolites, changes over time 113

Figure 3.7. Cell cycle analysis of CLL cells. CLL cells remain in G_0/G_1 phases of cell cycle in both normoxia and hypoxia 114

Figure 3.8. Metabolic changes of CLL cells were not dependent of the extracellular pH changes 116
Figure 3.9. Spectrum of RPMI with HEPES vs spectrum of standard RPMI 117
Figure 3.10. Change of oxygen concentration over the time course experiment 119
Figure 3.11.A Real-time changes in metabolite peaks intensities during the NMR time course 121
Figure 3.11.B Real-time changes in metabolite peaks intensities during the NMR time course 122
Figure 3.12. Kinetics of different peaks corresponding to the same metabolite were similar 124
Figure 3.13. Metabolic map presenting all of the metabolites assigned in the ^{1}H NOESY spectra recorded on samples with primary CLL cells 131

Chapter 4

Figure 4.1. HIF-1α level increases immediately after CLL cells reach hypoxia 142
Figure 4.2. Level of HIF-1α increases in hypoxia together with the expression of its target genes, which can be blocked by chetomin 144
Figure 4.3. HIF-1α shows hypoxia-inducible nuclear import 146
Figure 4.4. HIF-1α is present at a low level in the cytoplasm of normoxic CLL cells 147
Figure 4.5. HIF-1α is present in the nuclei of hypoxic CLL cells 148
Figure 4.6. Viability of CLL cells is not affected by extreme changes in oxygen levels 150
Figure 4.7. CLL cells are metabolically robust and plastic 151
Figure 4.8. Metabolic adaptation of CLL cells to hypoxia involves HIF-1α 154
Figure 4.9. HIF-1α inhibition by chetomin is toxic to CLL cells in both normoxia and hypoxia 156
Figure 4.10. Alanine aminotransferase (ALAT) inhibition in CLL cells 159
Figure 4.11. Alanine aminotransferase (ALAT) inhibition did not affect the viability of CLL cells 160
Figure 4.12. Membrane permeable αKG did not affect ALAT inhibition 161

Chapter 5

Figure 5.1. Analysis of the pyruvate concentration during the time course with CLL cells .174
Figure 5.2. Flux of pyruvate 177
Figure 5.3. The transition in pyruvate dynamics was independent of HIF-1α activation 179
Figure 5.4. Inhibition of pyruvate transporter with CHC 181
Figure 5.5. Metabolic changes during CHC treatment 182
Figure 5.6. Methyl pyruvate does not rescue cells from CHC induced apoptosis 185
Figure 5.7. Exogenous pyruvate reduces mitosox and ROS level in CLL cells 187
Figure 5.8. Exogenous pyruvate reduces mitosox and ROS level in CLL cells 188
Figure 5.9. Keto-enol pyruvate tautomerism 191
Figure 5.10. Keto-enol pyruvate tautomerism in the NMR spectrum 192

Chapter 6

Figure 6.1. ^{13}C labelled glucose flux to lactate through glycolysis and PPP 202
Figure 6.2. ^{13}C labelling patterns and corresponding multiplet structures 204
Figure 6.3. ^{13}C NMR multiplet structures in metabolites with label incorporation in various adjacent atoms, with different coupling constants 205
Figure 6.4. Simplified presentation of ^{13}C labelling patterns of metabolites after incubating cells with [1,2-^{13}C]glucose 207
Figure 6.5. The theoretical label distribution in the glutamate molecule coming from the [1,2-^{13}C]glucose after multiple TCA rounds 208
Figure 6.6. Glucose flux in CLL cells in normoxia 210
Figure 6.7. Glucose flux in CLL cells in hypoxia 211
Figure 6.8. Pentose Phosphate Pathway is more active in normoxia 212
Figure 6.9. Aspartate HSQC signals prove the presence of pyruvate carboxylase activity in CLL cells incubated for 24 h in hypoxia 215
Figure 6.10. The glutamate HSQC signal proves pyruvate carboxylase activity in CLL cells is higher in hypoxia than in normoxia 217
Figure 6.11. A 1D ^{13}C column from the HSQC experimental data proves pyruvate carboxylase activity in CLL cells is higher in hypoxia than in normoxia 218

Figure 6.12. Glutamine flux in CLL cells in normoxia 222
Figure 6.13. Glutamine flux in CLL cells in hypoxia 223
Figure 6.14. In normoxia lactate can be labelled from glucose but not from glutamine in CLL cells 225
Figure 6.15. In hypoxia lactate can be labelled from glucose but not from glutamine in CLL cells 226
Figure 6.16. In CLL cells lactate can be labelled from glucose in normoxia and hypoxia in the similar percentage 227
Figure 6.17. Metabolic shift of CLL cells entering hypoxia 230
Figure 6.18. Glycolysis is interconnected with PPP in CLL cells 231

LIST OF TABLES

Chapter 1

Table 1.1. Binet and Rai staging systems for classification of CLL 28

Table 1.2. Comparison of analytical methods used for metabolomics 42

Chapter 2

Table 2.1. Media with the ^{13}C labelled precursors 76

Table 2.2. Antibodies used for the western blot analysis 87

Table 2.3. Antibodies used for cytospin staining 92

Chapter 3

Table 3.1. Clinical characteristics of CLL patients 123

Chapter 4

Table 4.1. Kinetics of metabolic changes in CLL cells measured by the NMR during two normoxia-hypoxia cycles 152

ABBREVIATIONS

2DG	2-Deoxyglucose
2HG	2-Hydroxyglutarate
3BrPa	3-Bromopyruvate
3HB	3-Hydroxybutyrate
Acetyl-CoA	Acetyl coenzyme A
ADCC	Antibody-dependent cell-mediated cytotoxicity
ADP	Adenosine diphosphate
ALAT	Alanine aminotransferase
ALL	Acute lymphoid leukaemia
AML	Acute myeloid leukaemia
Ang-1	Angiopoietin 1
APRIL	Proliferation-inducing ligand
aq	Acquisition time
Asp	Aspartate
AST	Aspartate aminotransferase
ATP	Adenosine triphosphate
AV	Annexin V
BaP	The redeployed drug combination of bezafibrate and medroxyprogesterone acetate
BAFF	B-cell-activating factor of the tumour necrosis factor (TNF) family
BCL2	B-cell lymphoma 2
BCR	B-cell Receptor
BF	Back-flux
bFGF	Basic fibroblast growth factor
BPTES	Bis-2-(5-phenylacetamido-1,2,4-thiadiazoyl-2-yl)ethyl sulfide
BR	Bendamustine
BSA	Bovine serum albumin
BTK	Bruton's tyrosine kinase
CAIX	Carbonic anhydrase 9
CBP	CREB-binding protein
CD19+	Positive for CD19
CD5	Cluster of differentiation 5
cDNA	Complementary DNA
CHC	α-cyano-4-hydroxycinnamate
CLL	Chronic Lymphocytic Leukaemia

CML	Chronic myeloid leukaemia
coA	Coenzyme A
CTM	Chetomin
CXCL12	C-X-C motif chemokine 12
CXCR4	Chemokine (C-X-C motif) receptor type 4
d1	Interscan relaxation delay
DCA	Dichloroacetate
DMSO	Dimethyl sulfoxide
DNA	Deoxyribonucleic acid
DNP	Dynamic Nuclear Polarization
dNTPs	Deoxynucleotide triphosphates
EM	Exponential multiplication
ERK	Extracellular signal-regulated kinase
FACS	Fluorescence-activated cell sorting
FBA	Flux Balance Analysis
FC	Flow Cytometry
FCR	Fludarabine and cyclophosphamide
FDG-PET	Fluorodeoxyglucose positron emission tomography
FIMA	Field Independent Metabolic Analysis
GAAC	General amino acid control
GAPDH	Glyceraldehyde 3-phosphate dehydrogenase
GC–MS	Gas chromatography– mass spectrometry
GLUT1	Glucose transporter 1
GS	Glutamine synthetase
GSH	Glutathione
H2DCFDA	5-(and-6)-carboxy-2′,7′ dichlorodihydrofluorescein diacetate
HIF-1α	Hypoxia-inducible factor 1-alpha
HMBD	Human Metabolite Database
HPLC	High-performance liquid chromatography
HREs	Hypoxia-response elements
HRMAS	High-Resolution Magic Angle Spinning
HRP	Horseradish peroxidase
HSCs	Haematopoietic stem cells
HSQC	Heteronuclear single quantum coherence spectroscopy
Hx-PRTase	Hypoxanthineguanine phosphoribosyl transferase
Hz	Hertz
IDH1	Isocitrate dehydrogenase 1
IgVH	Immunoglobulin variable region heavy chain
IMP	Inosine 5′-monophosphate

ITS+	Culture supplement containing insulin, human transferrin and selenous acid
JNK	JUN N-terminal kinase
J-RES	J-resolved
Lat1	Large neutral amino acid transporter
LDHA	Lactate dehydrogenase A
MAPK	Mitogen-activated protein kinase
MAS	Magic Angle Spinning
Mcl-1	Myeloid cell leukaemia 1
MCT1	Monocarboxylate Transporter 1
MFA	Metabolic Flux Analysis
Mitosox	Mitochondrial superoxide
MNCs	Mononuclear cells
MRI	Magnetic Resonance Imaging
mRNA	Messenger RNA
MRS	Magnetic resonance spectroscopy
mTOR1	Mammalian target of rapamycin complex 1
NADH	Nicotinamide adenine dinucleotide reduced
NADPH	Nicotinamide adenine dinucleotide phosphate
NFkB	Nuclear factor-kappa-B
NLCs	Nurse-like cells
NMR	Nuclear Magnetic Resonance
NOESY	Nuclear Overhauser effect spectroscopy
NS	Number of scans
OAA	Oxaloacetate
p21	Cyclin-dependent kinase inhibitor 1
PAG	Phosphate activated glutaminase
PBS	Phosphate buffered saline
PC	Pyruvate Carboksylase
PDGF	Platelet-derived growth factor
PDH	Pyruvate Dehydrogenase
PDK1	Pyruvate Dehydrogenase Kinase 1
PI	Propidium Iodide
PI3K	Phosphoinositide 3-kinase
PKC	Protein kinase C
PKM2	Pyruvate kinase M2
PLC	Phospholipase C.
ppm	Parts per million
PPP	Pentose Phosphate Pathway
PTEN	Phosphatase and tensin homolog

PTPs	Protein tyrosine phosphatases
pVHL	The product of the von Hippel–Lindau tumour suppressor gene
QRT-PCR	Quantitative real-time polymerase chain reaction
RNA	Ribonucleic acid
ROS	Reactive Oxygen Species
RPMI	Roswell Park Memorial Institute medium
RT	Room temperature
RT-PCR	Reverse Transcription PCR
SDF-1	Stromal cell-derived factor 1
SEM	Standard error of the mean
Syk	Spleen tyrosine kinase
TCA	Tricarboxylic Acid Cycle
TD	Data points
TLC	Thin-Layer Chromatography
TLR	Toll-like receptor
TMSP	Sodium 3-(trimethylsilyl) propionate-2,2,3,3-d4
TNFα	Tumour necrosis factor alpha
TRX	Thioredoxin
Ub	Ubiquitin
UPLC	Ultra performance liquid chromatography
UV	Ultraviolet
VEGF	Vascular endothelial growth factor
WT	Wild-Type
α-KG	α-ketoglutarate

Chapter I

Introduction

1.1 HALLMARKS OF CANCER

Cancer is a disease involving dynamic changes in the genome. The foundation of cancer research was set by the discovery of the mutations leading to the production of oncogenes, as well as tumour suppressor genes specific for different types of cancer. However studies carried out within the last two decades have shown that the features that regulate the transformation of normal human cells into malignant cancers are shared amongst cancers. Tumourigenesis is a multistep process and these steps reflect genetic alterations that drive the progressive transformation of normal human cells into highly malignant derivatives (Hanahan and Weinberg 2000). Ten essential alterations in cell physiology that collectively dictate malignant growth of the cell have been proposed (Figure 1.1). The main hallmarks shared between the majority of cancer types include: genome instability and mutations, self-sufficiency in growth signals, insensitivity to antigrowth signals, tumour promoting inflammation, resistance to programmed cell death (apoptosis), sustained angiogenesis, tissue invasion and metastasis, avoidance of immune destruction, limitless replicative potential and deregulated cellular energetics. The work presented in this thesis will focus on the final hallmark listed, the ability to modify, or reprogram cellular metabolism in order to meet the bioenergetic and biosynthetic demands of increased cell proliferation, and to survive environmental fluctuations in external nutrient and oxygen availability.

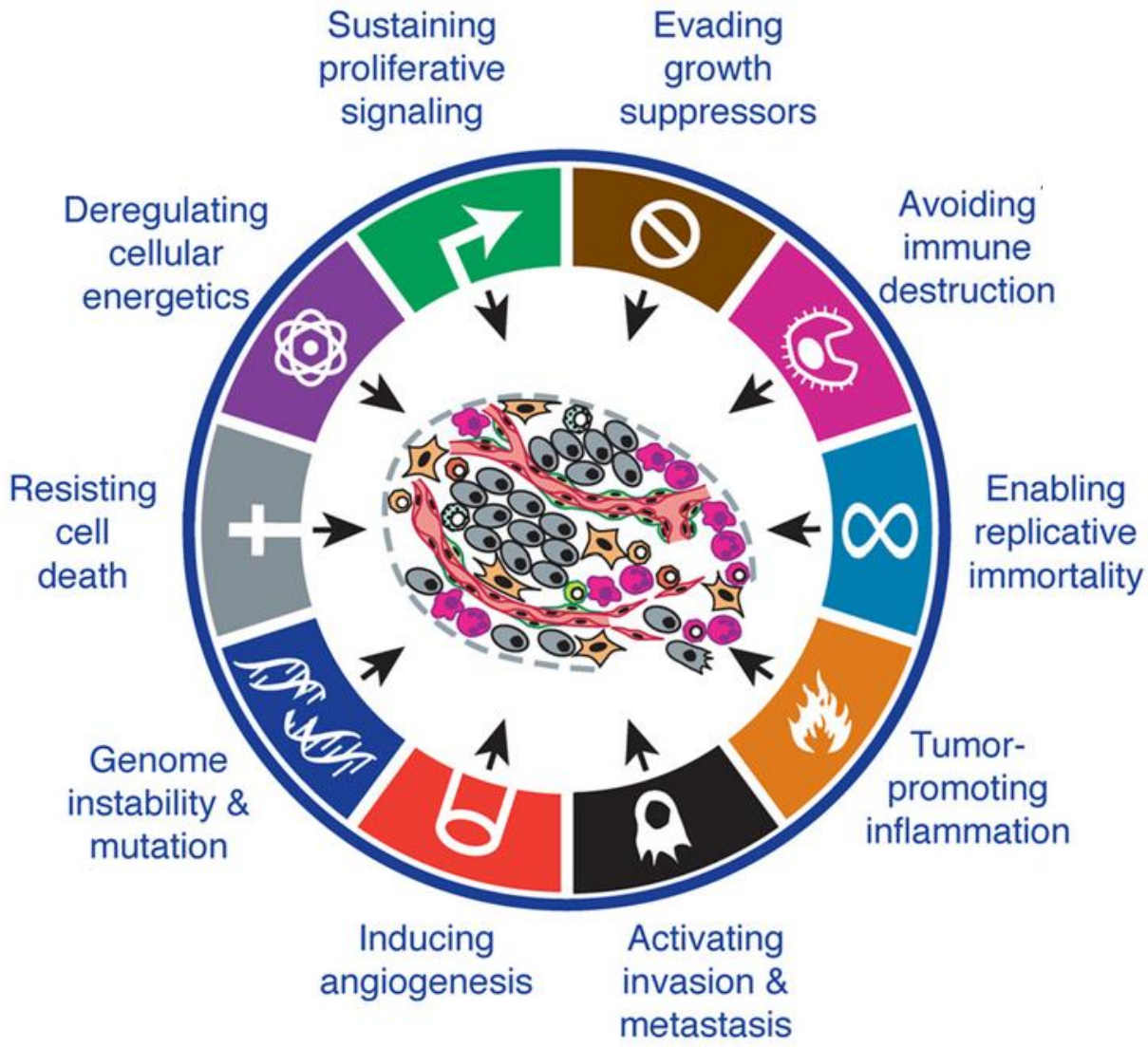

Figure 1. 1. Hallmarks of cancer cells.

The main hallmarks shared between the majority of cancer types (Adapted from Hanahan and Weinberg 2011).

1.2 UNDERSTANDING CANCER METABOLISM

The metabolism of cancer cells differs from healthy cells and various types of cancer are characterised by specific metabolic alterations. Despite many recent studies, our understanding of cancer metabolism remains enigmatic. It is crucial to improve our understanding of metabolic deregulations in cancer since they have also been shown to be linked to drug resistance in cancer therapy (Zhou, Zhao et al. 2010; Zhao, Liu et al. 2011). A better understanding of the reprogrammed cellular pathways in cancer is expected to lead to the identification of new therapeutic targets (Hamanaka and Chandel 2012).

1.2.1 Metabolism pervades every aspect of biology

Metabolism is defined as the sum of biochemical processes in living organisms that either consume or produce energy (DeBerardinis and Thompson 2012). At present, there are over 16,000 metabolites and 8,700 reactions annotated in the Kyoto Encyclopedia of Genes and Genomes (http://www.genome.jp /kegg/pathway.html). Core metabolism can be simplified to the pathways involving carbohydrates, fatty acids and amino acids essential to homeostasis and macromolecule synthesis. These pathways can be separated into three classes: anabolic pathways – energy requiring pathways that construct molecules from smaller units; catabolic pathways – which degrade molecules to release energy; and waste disposal pathways – which eliminate toxic by-products.

Most of these metabolic networks were defined during the "golden age of biochemistry" (1920s - 1960s). They include core pathways like glycolysis (Embden, Meyerhof, and Parnas), respiration (Warburg), the tricarboxylic acid (TCA) and urea cycles, glycogen catabolism (Cori and Cori), oxidative phosphorylation (Mitchell), and the importance of ATP in energy transfer reactions (Lipmann). In the latter half of the 20th century, interest in metabolism gradually disappeared as new areas of biology, such as genetics, became more popular (DeBerardinis and Thompson 2012). However, recent investigations of cell biology and disease have renewed interest in metabolism (Recent reviews: (McKnight 2010; Benjamin, Cravatt et al. 2012; Cantor and Sabatini 2012; Ward and Thompson 2012). Recent years have revealed new metabolites and connections between their pathways which could not have been predicted from the conventional understanding of biochemistry (Gross, Cairns et al. 2010). This has resulted in our current awareness of the relevance of metabolism to all other cellular processes.

Interest in the altered metabolism exhibited by cancer cells has grown with the discovery of oncogenic mutations in metabolic enzymes and has been aroused by the development of tools that monitor metabolism in living cells. Abnormal metabolism has now become the key target for anti-cancer therapies.

1.2.2 Lessons from Warburg

Altered cancer metabolism contributes to its malignant transformation, as well as to the initiation, growth and maintenance of tumours (Chen, Hewel et al. 2007; Hanahan and Weinberg 2011). Common hallmarks for many cancer types are, energy production based on aerobic glycolysis, increased fatty acid synthesis and increased glutamine metabolism (Zhao, Butler et al. 2013). The principle of abnormal metabolism in cancer is long-standing, dating back to the early 1920s when Otto Warburg initiated investigations into cancer metabolism, studying the behaviour of tissue slices *ex vivo*. He observed that cancer cells tended to convert glucose to lactate, using anaerobic pathways (which are less efficient in ATP production), despite the presence of oxygen. This was interpreted as a fundamental change in the way glucose metabolism is regulated in cancer cells (Warburg, Wind et al. 1927; Warburg 1956). Amongst Warburg's many other seminal contributions to biochemistry (including work on respiration for which he received the Nobel Prize in 1931) he is best remembered and most frequently cited for this observation, now called the Warburg effect. Warburg suggested that the reason for these metabolic alterations may be a consequence of mitochondrial defects that inhibited the ability of cancer cells to effectively oxidize glucose carbon to CO_2 (Koppenol, Bounds et al. 2011). A later extension to this hypothesis, that dysfunctional mitochondria caused cancer was also proposed (Koppenol, Bounds et al. 2011). Warburg's seminal finding was

supported by many studies performed on various cancer types. Later, other hypotheses appeared claiming that mitochondria are functional in most tumour cells and able to carry out oxidative phosphorylation and produce the majority of ATP for cancer cells (Weinhouse 1976). Nowadays, Warburg's observation of increased glucose fermentation by cancer cells is successfully exploited in clinics for diagnostic purposes, to detect tumours in the body. Using 2-18F-fluoro-2-deoxy-D-glucose (FDG), a radiolabelled glucose analogue, positron emission tomography identifies malignant tissues which consume much more glucose than healthy tissues (Gambhir 2002).

1.2.3 The advantage of altered cancer metabolism

The current challenge is to understand why cancer cells utilise a less efficient metabolic pathway, despite their need to intensively grow and divide. In order to determine the reason for increased aerobic glycolysis, it is important to realise the purpose of cell metabolism in general and what the specific requirements of a cancer cell may be. All cells take up nutrients from their environment and incorporate them into pathways in order to sustain homeostasis. Cells need to carry out many reactions that are energetically unfavourable, such us maintaining ion gradients across membranes, actively transporting molecules through the membranes and synthesising proteins. The coupling of these reactions with ATP hydrolysis, providing free energy, enables them to proceed.

Cancer cells need efficient ways to produce ATP, but they must also adapt to their specific environment. As a consequence of irregular vascularization, the tumour microenvironment is often lacking nutrients (Hirayama, Kami et al. 2009; Ackerman and Simon 2014). Therefore, cancer cells are forced to shift their metabolism to anabolic reactions. It has been proposed that in order to produce all of the necessary metabolites, cells attempt to save glucose for the synthesis of those that can solely be produced from glucose – such as ribose for nucleotides. Other metabolites such as lipids, are produced from alternative sources e.g. glutamine (Anastasiou and Cantley 2012).

In general, cancer cells benefit from their abnormal metabolism in several ways. Firstly, their metabolism ensures that they have a ready supply of the building blocks required for the synthesis of NADPH, acetyl-CoA, ATP and other macromolecules. Secondly, by claiming more nutrients than healthy cells, tumour cells contribute to the starvation of neighbouring cells, gaining more space for expansion and growth (Kaelin and Thompson 2010). Thirdly, an excessive uptake of nutrients may lead to the increased generation of reactive oxygen species (ROS), if reactions in the TCA occur at a rate exceeding the capacity of electron capture within the electron transport chain (Wellen and Thompson 2010). High ROS levels may promote cancer-cell proliferation by inactivating growth-inhibiting phosphatase

enzymes. Enhanced ROS may also lead to an enhanced mutation rate by inducing DNA damage (Kaelin and Thompson 2010).

1.2.4 Role of ROS in cancer cells

Reactive oxygen species are a diverse class of radical species which retain a more reactive state than molecular oxygen and are produced in all cells as a normal metabolic by-product. ROS are heterogeneous in their properties and cause various effects, depending on their levels. At low concentrations, ROS contribute to cell proliferation and survival through the post-translational modification of phosphatases and kinases (Lee, Yang et al. 2002; Giannoni, Buricchi et al. 2005). The production of low ROS levels is also required for homeostatic signalling events, cell differentiation and cell mediated immunity. Moderate levels of ROS induce the expression of stress-responsive genes such as HIF-1α, triggering the expression of pro-survival proteins (Gao, Zhang et al. 2007). On the other hand, high levels of ROS may lead to damage to cellular macromolecules including lipids, proteins, mitochondrial and nuclear DNA and cause the induction of senescence (Takahashi, Ohtani et al. 2006). The permeabilisation of mitochondria, resulting in the release of cytochrome c and apoptosis can also be caused by ROS (Garrido, Galluzzi et al. 2006). In order to neutralise the destructive effect of ROS, cells produce antioxidant molecules, such as reduced glutathione (GSH) and thioredoxin (TRX) as well as a range of antioxidant enzymes (Nathan and Ding 2010). These molecules reduce

excessive levels of ROS, preventing irreversible cellular damage and restoring redox homeostasis.

The first time a link between ROS and cellular transformation was identified was in 1981, when it was shown that insulin elevated intracellular H_2O_2 levels and increased the proliferation of tumour cells (Oberley 1988). Cancer cells have a high demand for ATP due to their increased proliferation rate. However, the consequence of this uncontrolled energy production is the accumulation of ROS. In order to ensure their survival, transformed cells protect themselves by up-regulating antioxidant systems, creating a paradox of high ROS production in the presence of high antioxidant levels (Schafer, Grassian et al. 2009). Many studies have evaluated ROS levels and production under various circumstances, with the goal of characterising the stages at which ROS are oncogenic or tumour suppressive (Trachootham, Alexandre et al. 2009).

At low to moderate levels, ROS have been shown to contribute to tumour formation either by acting as signalling molecules or, by promoting DNA mutations. For example, ROS can stimulate the phosphorylation of mitogen-activated protein kinase (MAPK) and extracellular signal-regulated kinase (ERK), cyclin D1 expression and JUN N-terminal kinase (JNK) activation, which promotes growth and survival of cancer cells (Martindale and Holbrook 2002; Ranjan, Anathy et al. 2006). ROS have also been shown to reversibly inactivate tumour suppressors such as phosphatase

and tensin homolog (PTEN) and protein tyrosine phosphatases (PTPs) because of the presence of the redox-sensitive cysteine residues in their catalytic centre (Leslie, Bennett et al. 2003).

At high levels, ROS promote severe cellular damage and cell death. Cancer cells need to fight high levels of ROS, especially at early stages of tumour development. It has been shown that conditions inducing oxidative stress also increase the selective pressure on pre-neoplastic cells to develop potent antioxidant mechanisms. High ROS levels are also induced by detachment from the cell matrix. This aspect represents a challenge for metastatic cancer cells that need to survive during migration to distant organs (Schafer, Grassian et al. 2009; Gorrini, Harris et al. 2013). Therefore, cancer cells have a high antioxidant capacity that regulates ROS to levels that are compatible with their cellular functions but still higher than in healthy cells. Targeting these enhanced antioxidant defence mechanisms may represent a strategy that can specifically kill cancer cells, including tumour-initiating cells, while leaving healthy cells intact.

1.2.5 Glutamine metabolism

Although mitochondrial dysfunction was considered a feature of cancer cells that contributes to the Warburg effect, more recently it has been shown that the mitochondria of cancer cells are fully functional and required for cancer cell metabolism (Wallace 2012). However since glucose is mainly used in aerobic

glycolysis, glutamine becomes the major substrate required for the TCA cycle and production of NADPH and fatty acids. In fact some cancer cell lines display 'addiction' to glutamine (Yuneva, Zamboni et al. 2007; Wise, DeBerardinis et al. 2008). This is particularly interesting due to the fact that glutamine is a nonessential amino acid that can be synthesised from glucose. It has been observed that as an artefact of *in vitro* culture, glutamine is switched from a nonessential to an essential amino acid (Eagle 1955). These are aspects that may explain why some cancers seem not to be able to survive in the absence of exogenous glutamine.

The role of glutamine in cell growth and signalling pathways has been widely explored in recent years (DeBerardinis, Mancuso et al. 2007; Wise and Thompson 2010). The most obvious role for glutamine is in providing nitrogen for protein and nucleotide synthesis. The growing cancer must synthesise nitrogenous compounds in the form of nucleotides and non-essential amino acids. When glutamine donates its amide group it is converted to glutamate. Glutamic acid is the primary nitrogen donor for the synthesis of alanine, serine, aspartate and ornithine, as well as contributing its carbon and nitrogen to proline synthesis. Serine is a precursor for glycine and cysteine biosynthesis, ornithine is a precursor of arginine, and aspartate is a precursor for asparagine biosynthesis (Newsholme, Procopio et al. 2003).

The contribution of glutamine in amino acid biosynthesis explains its key role in the protein translation needs of cancer cells. Moreover, glutamine also plays an

important regulatory role in protein translation (Hurtaud, Gelly et al. 2007). It has been shown that glutamine starvation activates the general amino acid control (GAAC) pathway, which results in the up-regulation of amino acid transporters, leading to increased amino acid uptake. This elevates the intracellular amino acid level, which results in an elevation of the mammalian target of rapamycin complex 1 (mTOR1) (Chen, Zou et al. 2014). This complex is an evolutionarily conserved master regulator of cell growth that activates protein translation and inhibits the macroautophagy pathway which is a vacuolar degradation process (Wullschleger, Loewith et al. 2006). The essential glutamine requirements of proliferating cells were described for the first time by Harry Eagle in 1955, when it was observed that cells could not proliferate in the absence of glutamine and that many of them did not maintain their viability (Eagle 1955). Later it was observed that carbons from glutamine can be incorporated into carbon dioxide that is released by cells and that the consumption of glutamine in certain cancer cells is substantially higher than any other amino acid (Kovacevic 1971). Using NMR analysis with labelled glutamine, it was shown that in a glioblastoma cell line, a significant fraction of carbon from glutamine is converted into lactic acid (DeBerardinis, Mancuso et al. 2007). Anaplerotic pathways (those that replenish TCA cycle intermediates) are dominant in most cancer cells (DeBerardinis and Cheng 2010; Wise and Thompson 2010) and they are often a consequence of pyruvate kinase M2 (PKM2) activity (Mazurek, Boschek et al. 2005), resulting in a decoupling of glycolysis and the TCA cycle. It can

also be caused by the deactivation of pyruvate dehydrogenase (PDH) by pyruvate dehydrogenase kinases (PDK), thus preventing it from catalysing the acetylation of coenzyme A (coA) and therefore blocking this entry point into the TCA cycle.

In cancer cells, glutamine catabolism is also regulated by multiple oncogenic signals, including those transmitted by the Rho family of GTPases and by c-Myc. Activation of c-Myc, makes cells glutamine-dependent for survival (Yuneva, Zamboni et al. 2007). Myc induces glutaminase which transforms glutamine into glutamate and also inhibits the expression of microRNA miR-23a and miR-23b which are translational inhibitors of glutaminase. It has been shown that glutamate can be converted to α-ketoglutarate which fuels the TCA cycle in order to produce oxaloacetate (OAA), showing that glutamine is the major anaplerotic substrate for proliferating glioblastoma cells (DeBerardinis, Mancuso et al. 2007; Wise, DeBerardinis et al. 2008; Wise and Thompson 2010). This anaplerotic activity is required to maintain the TCA cycle when rapidly proliferating cells are using citrate as a precursor for lipid biosynthesis. Another product of glutaminolysis, ammonia, has been shown to promote basal autophagy, limit proliferation under physiological stress and prevent cells from TNFα- induced apoptosis (Sakiyama, Musch et al. 2009).

Intriguing recent research suggests that under hypoxic conditions, the Krebs cycle may proceed in the reverse direction (Metallo, Gameiro et al. 2012). Glutamine

derived α-KG produces citrate through reductive carboxylation to support *de novo* synthesis of fatty acids. This phenomenon was shown in some cancer cell lines (such as renal cell carcinoma (Mullen, Wheaton et al. 2012) or melanoma (Filipp, Scott et al. 2012)) but has not been reported for other cancers (including leukaemia) so far. Flexibility of metabolism to use either of the anaplerotic pathways, as well as possible altered pathways in various cancer cells must be taken into consideration when thinking about therapies targeting metabolism of specific cancer types.

Distinct inhibitors of glutaminase have been identified, these are glutamine mimetics such as 6-diazo-5-oxo-l-norleucine (Ahluwalia, Grem et al. 1990; Griffiths, Keast et al. 1993) or selective inhibitors such as 968 and BPTES [bis-2-(5-phenylacetamido-1,2,4-thiadiazoyl-2-yl)ethyl sulfide] (Robinson, McBryant et al. 2007; Wang, Erickson et al. 2010). The potential to selectively block cellular transformation, may contribute to successfully targeting glutamine metabolism in cancer therapy (Lukey, Wilson et al. 2013).

1.3 THE HYPOXIC TUMOUR ENVIRONMENT

A fundamental problem for solid tumours is that they consume all their oxygen supplies from blood and so must survive in hypoxia – usually defined as the condition when the level of $O_2 < 1\%$ (compared to 2 to 9% O_2 in the adjacent tissue) (Favaro, Lord et al. 2011). Existence of tumour hypoxia has been validated using biochemical markers of hypoxia, such as EF5 and pimonidazole, or endogenous

molecular markers, such as hypoxia inducible factor (HIF) and carbonic anhydrase 9 (CAIX). As shown in a series of studies, hypoxia induces a wide range of biological changes, such as decreased cell proliferation (Evans, Hahn et al. 2001), increased expression of genes responsible for drug-resistance (Wartenberg, Ling et al. 2003), selection of clones resistant to apoptosis (Graeber, Osmanian et al. 1996), enhanced tumour invasion and metastasis (Subarsky and Hill 2003) and elevated mutagenesis (Subarsky and Hill 2003). These mechanisms undoubtedly contribute to the evolution of malignant tumour cells. However, it remains to be fully understood why hypoxic tumour cells tend to be more aggressive in nature and more resistant to treatment than non-hypoxic tumour cells within the same tumour, despite their similar genetic background (Kim, Lin et al. 2009).

1.3.1 HIF-1α

Hypoxia-induced signalling is primarily mediated by HIF, which accumulates and promotes the transcription of over 200 genes. Many of these genes support cell survival, promote glycolysis and supress oxidative phosphorylation. HIFs are transcription factor complexes comprised of an α and β subunit and they function as an integral part of the hypoxia response, allowing cell survival during periods of low oxygen supply. Although HIF plays an important protective role during development and oxygen stress, it has been shown to enhance tumourigenesis and promote the development of a more malignant phenotype. HIF activity is high in

most, if not all tumours, either owing to hypoxia or conditions leading to HIF stabilization under normoxia (pseudohypoxia) (Gottlieb and Tomlinson 2005).

Accumulation of HIF is supressed by oxygen-dependent prolyl hydroxylase domain (PHD) enzymes. On the other hand, changes in the levels of reactive oxygen species or TCA cycle metabolites such as fumarate and succinate may promote HIF accumulation (Kaelin and Thompson 2010). HIF-1α regulation is presented in Figure 1.2. Understanding of the role of HIF in hypoxic metabolism could lead to the development of chemotherapies that specifically target the hypoxic regions of tumours.

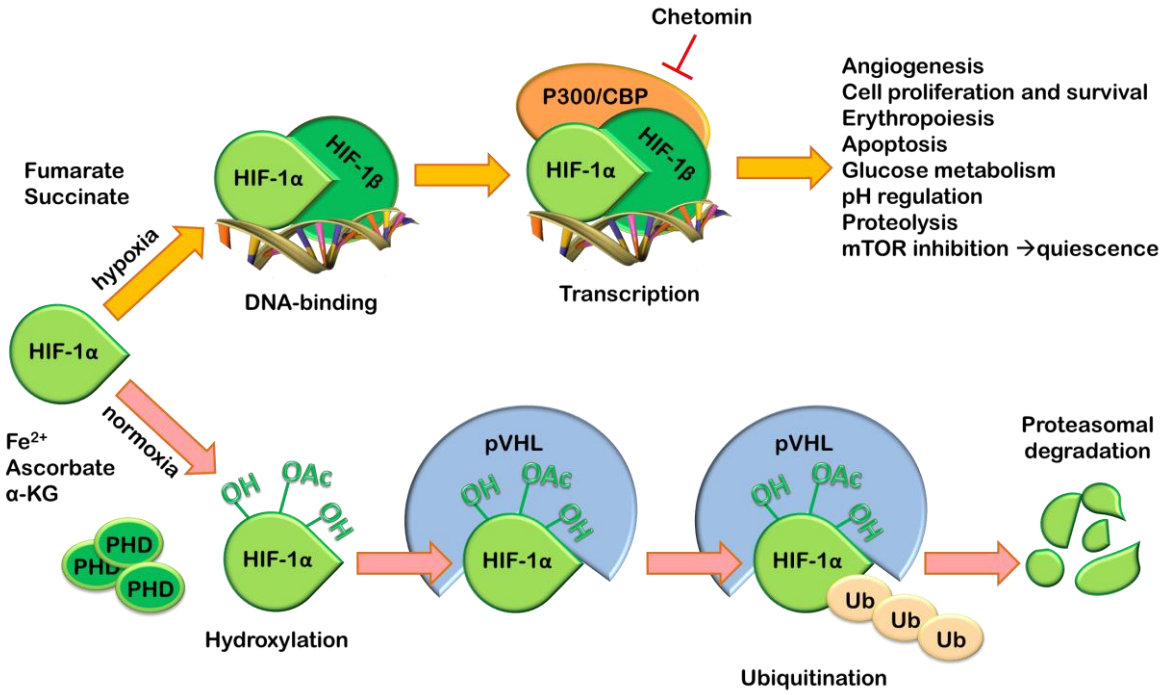

Figure 1. 2. HIF-1α regulation by proline hydroxylation.

In response to hypoxia, HIF-1α accumulates and translocates to the nucleus. There, HIF-1α dimerises with HIF-1β, binds to hypoxia-response elements (HREs) within the promoters of target genes and recruits transcriptional co-activators such as p300/CBP for transcriptional activity. A range of cell functions are regulated by the target genes, as indicated. Chetomin, a commonly used inhibitor of HIF-1α transcriptional activity, binds to p300, disrupting its interaction with HIF-1α and attenuating hypoxia-inducible transcription. In response to normoxia, HIF-1α is hydroxylated by proline hydroxylases (PHD). Hydroxylated HIF-1α (OH) is recognised by pVHL (the product of the von Hippel–Lindau tumour suppressor gene), which, together with a multisubunit ubiquitin ligase complex, tags HIF-1α with polyubiquitin; this allows recognition by the proteasome and subsequent degradation. Acetylation of HIF-1α (OAc) also promotes pVHL binding. *Abbreviations: CBP, CREB-binding protein; Ub, ubiquitin; α-KG, α-ketoglutarate.

1.4. HAEMATOLOGICAL CANCERS

It is likely that haematological malignant transformation begins in the bone marrow, where blood cells are produced, leading to their uncontrolled growth and abnormal functions. Tumour cells interfering with normal haematopoiesis disrupt blood functions such as protection from infection or prevention of bleeding. There are three main types of blood cancer: lymphoma, myeloma and leukaemia.

The lymphomas are a complex group of tumours of lymphocytes and present predominantly at localised sites in lymphoid tissues such as lymph nodes and spleen. Myeloma is a cancer of plasma cells (antibody producing lymphocytes). Myeloma invariably arises within the bone marrow. The leukaemias are a complex group of cancers but are united by the presence of significant circulating leucocytes in the blood. The term leukaemia is derived from the Greek for 'white blood'. Leukaemia can be of myeloid or lymphoid origin and either acute or chronic; giving rise to the categories: acute myeloid (AML), acute lymphoid (ALL), chronic myeloid (CML) and chronic lymphocytic (CLL). Some of the metabolic aspects are common for all types of leukaemia, while others are entirely unique to a particular leukaemia type (Jitschin, Hofmann et al. 2014; Wang, Israelsen et al. 2014). Moreover, metabolic pathways may differ between cells of the same origin and are dependent on their microenvironment (Bailey, Wojtkowiak et al. 2012).

1.4.1 Inhibitors of glycolysis in leukaemic cells

During the last decade, there has been a strong focus on neoplastic related metabolism in cancer research. Many solid tumours are known for their altered, highly glycolytic metabolism described as the Warburg effect but the occurrence of this phenomenon in blood cancers has only recently been reported. There is significant evidence that targeting glycolytic pathways in leukaemic cells may re-program cells and inhibit cancer proliferation. Compounds such as 3-bromopyruvate (3BrPa), are known inhibitors of glycolytic pathway, however, are required in high concentrations due to low solubility and biodistribution. Such concentrations often result in toxicity (Ko, Smith et al. 2004; Xu, Pelicano et al. 2005). New inhibitors used in combination with or without standard chemotherapy, may present a new therapeutic strategy (Leni, Parakkal et al. 2013). In this respect, it is important to identify the enzymes and metabolic processes that are crucial for haematological cancer cell proliferation and survival.

So far, studies focused on AML and ALL have shown that they are dependent on glycolysis in aerobic conditions (Boag, Beesley et al. 2006). Levels of HIF-1α and the HIF-1α dependent proteins; GLUT1, GLUT3, CA9 and GAPDH, were significantly higher in the blood of AML and ALL patients compared to cells derived from the blood of healthy donors. Moreover, leukaemias with higher glycolytic rates showed stronger resistance to chemotherapy. For example, it has been shown that

inhibition of glycolysis using 2DG (2-deoxyglucose) rendered otherwise resistant leukaemia cells, susceptible to glucocorticoid treatment (Hulleman, Kazemier et al. 2009). 2DG was also shown to affect the pentose phosphate pathway and alter protein glycosylation. However decreased viability of cells also observed in normoxia, may indicate that 2DG toxicity in aerobic conditions results from the inhibition of glycosylation, rather than glycolysis (Kurtoglu, Maher et al. 2007). Combinations of the glycolytic pathway inhibitor, 3BrPa, with antimycin A – an inhibitor of electron transport in the mitochondrial complex III - showed a dramatic decrease of ATP in cancer cells followed by increased cell death (Ko, Smith et al. 2004). This data shows that acute leukaemia depends on glycolysis but also that oxidative respiration is important for survival. It is however still unclear how this inhibitor combination affects healthy cells.

In order to potentiate the effects of inhibition of glycolysis, mTOR inhibitors could be used as additional therapeutics. mTOR plays multiple roles in supporting cancer cell survival directly, by affecting cell cycle regulators and indirectly, by sustaining nutrient supply. mTOR is also responsible for the regulation of energy metabolism and cellular survival of cancer cells (see Figure 1.3). Therefore, combined inhibition of glycolysis and mTOR would induce severe metabolic deregulation and cell death. It has been shown that in leukaemia and lymphoma cells, a combination of 3BrPa with rapamycin effectively depleted ATP, limited the nutrient uptake, cell

proliferation and cell survival. Importantly, this combination has been shown to have low toxicity to healthy cells (Xu, Pelicano et al. 2005).

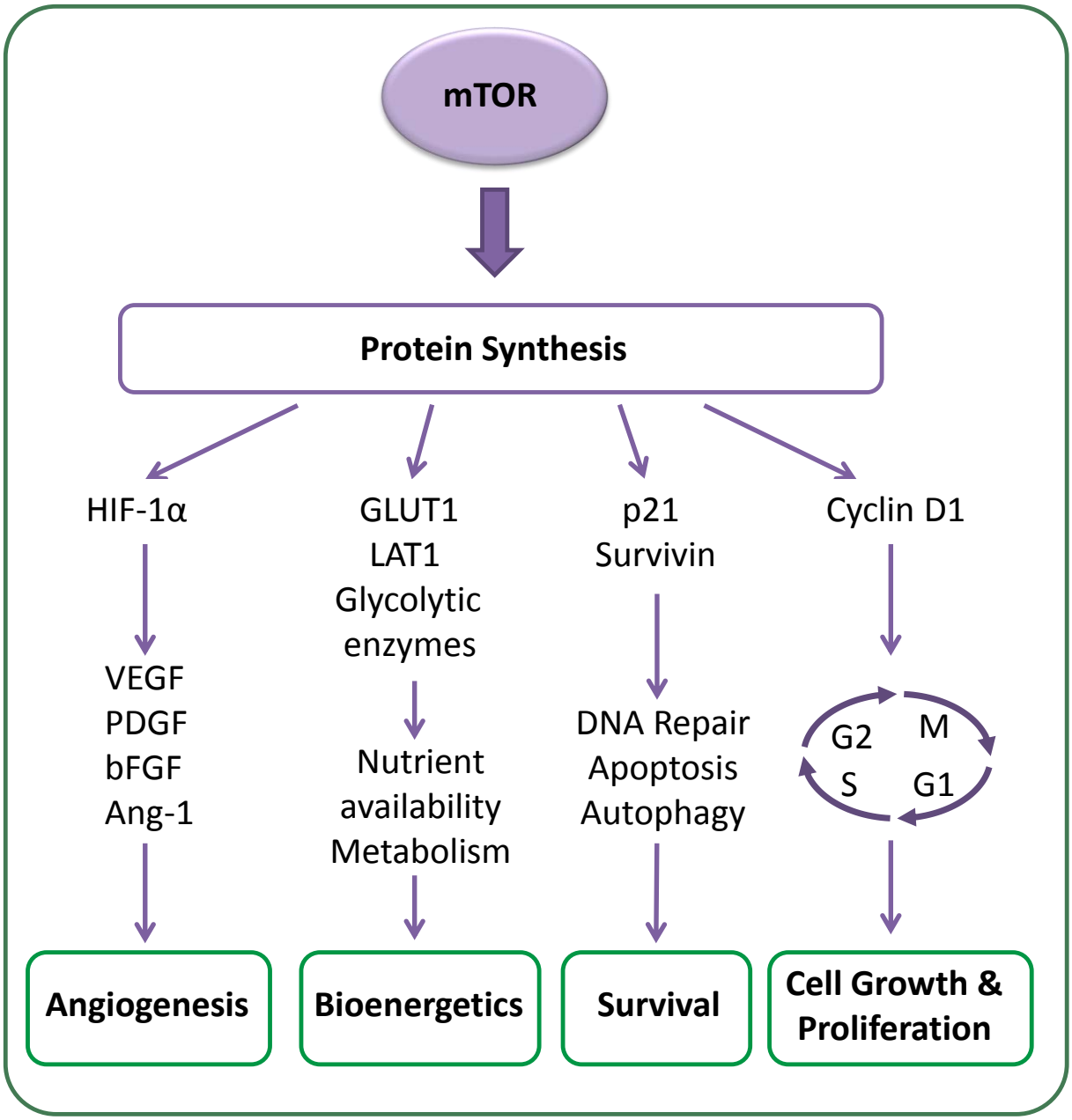

Figure 1. 3. The role of mTOR activation in supporting cancer cell survival.

Overactivation of mTOR due to dysregulation of upstream pathways, leading to abnormal activities in cell angiogenesis, cell metabolism, apoptosis and proliferation, has been implicated in various cancer types (based on (Advani 2010)).

Studies with metabolic inhibitors have also shown promising results in the *in vivo* model of multiple myeloma. Dichloroacetate (DCA) inhibits pyruvate dehydrogenase kinase which limits Acetyl-coA production from pyruvate. As a result more Acetyl-CoA is produced and more NADH electrons may be donated to the electron transport chain. This may lead to increased ROS production, contributing to the loss in generation of membrane potential and ultimately the suppression of cell proliferation (Fujiwara, Kawano et al. 2013).

Targeting glycolysis in haematological malignancies has emerged as a promising approach. However more studies are needed to investigate molecular mechanisms and potential chemoresistance.

1.4.2 IDH1/2 mutations

Gene sequencing studies identified somatic mutations in isocitrate dehydrogenase 1 (IDH1) in AML and glioma patients but not in those suffering from other human malignances (Dang, White et al. 2009; Mardis, Ding et al. 2009; Zhao, Lin et al. 2009). Mutated IDH1 transforms α-ketoglutarate to the oncometabolite 2-hydroxyglutarate (2-HG). The ability of 2-HG to alter the epigenetic landscape (through the inhibition of a family of αKG-dependent Jumonji-C domain histone demethylases) has contributed to changing the way we think about metabolism and its effects on other cellular processes. When the wild-type IDH1/2 converts isocitrate to α-KG, NADPH is produced; this contributes significantly to the synthesis of

glutathione, protecting cells from ROS. In IDH1 mutants however, during the reaction in which 2-HG is produced, NADPH is consumed. Moreover, the level of α-KG also decreases. α-KG is known to activate proline hydroxylases that inactivate HIF-1α as a result of IDH (Xu, Yang et al. 2011). Therefore the overall effects are increased levels of ROS and HIF-1α.

Inhibitors of IDH tested in different types of leukaemias were found to reduce the amount of 2-HG and inhibit the growth of cancer cells (Popovici-Muller, Saunders et al. 2012). IDH inhibition led to histone demethylation and to the induction of haemopoietic/neural differentiation, suggesting that these agents might induce differentiation in IDH-mutant cells through alterations in the epigenetic state (Rohle, Popovici-Muller et al. 2013; Wang, Travins et al. 2013). Extensive *in vivo* studies in IDH-mutant models are still being reported and the role of IDH in malignant cells after oncogenic transformation requires additional, extensive investigation.

1.4.3 Mitochondrial uncoupling

Leukaemia cells, like most cancers, are 'addicted' to glucose in the generation of energy, but recent research shows that they also have the ability to reduce molecular oxygen, utilising electrons from carbon sources other than pyruvate to grow and evade cell death (Samudio, Fiegl et al. 2008; Samudio, Fiegl et al. 2009). Recent evidence suggests that fatty acid derived acetyl-CoA can fuel Krebs cycle

activity and the molecular reduction of oxygen (Samudio, Harmancey et al. 2010). In leukaemia cells mitochondrial uncoupling – the continuing reduction of oxygen without the synthesis of ATP – can mimic the Warburg effect in the absence of permanent alterations to the oxidative capacity of cells. However, the benefits of this metabolic shift to cells are not fully understood.

The model proposed by Velez (Velez, Hail et al. 2013) presents reprogrammed pathways of intermediary metabolism in leukaemic cells. In this model, pyruvate is converted to lactate in order to regenerate NAD^+. This results in the absence of OAA production from pyruvate. In this situation, the only source of α-KG that can supply the TCA cycle is glutamine, however OAA may also be produced through aspartate anaplerosis. Regeneration of the citrate pool, on the other hand, would rely on acetyl-CoA derived from fatty acids.

It has been shown that in several human solid tumours, DCA shifts pyruvate metabolism from glycolysis and lactate production to glucose oxidation in the mitochondria, which results in high ROS production, leading to cell death (Bonnet, Archer et al. 2007). This shows that using an alternative source of carbon to pyruvate for oxygen reduction may protect against cell death. Despite not yet being shown in leukaemia cells, this possibility should be considered.

1.5. CHRONIC LYMPHOCYTIC LEUKAEMIA (CLL)

Chronic lymphocytic leukaemia (CLL) is the most common form of leukaemia in Western countries (D'Arena, Di Renzo et al. 2003; Chiorazzi, Rai et al. 2005). Although there have been recent improvements in prolonging survival with combination chemoimmunotherapy regimens, the disease remains incurable using current therapies. Patients suffering from CLL present highly variable clinical courses. Some patients die within two years of initial diagnosis, while others may lead an almost normal life without the need for treatment (Chiorazzi, Rai et al. 2005). There are two widely accepted staging methods of CLL: the Binet and the modified Rai systems (presented in Table 1.1.). These staging systems are simple and inexpensive, based only on standard laboratory tests and physical examination. Staging is useful to predict prognosis and also to stratify patients to achieve comparisons for interpreting specific treatment results.

Table 1.1. Binet and Rai staging systems for classification of CLL.

System	Stage	Description	Median survival (years)
Binet system*			
	A	Haemoglobin ≥ 10 g/dL and platelets ≥ 100,000/mm^3 and < 3 involved nodal areas	11.5
	B	Haemoglobin ≥ 10 g/dL and platelets ≥ 100,000/mm^3 and ≥ 3 involved nodal areas	8.6
	C	Haemoglobin < 10 g/dL and/or platelets < 100,000/mm^3 and any number of involved nodal areas	7.0
Rai system			
	0 (low risk)	Lymphocytosis, lymphocytes in blood > 15,000 / mcL and > 40% lymphocytes in the bone marrow	11.5
	I (intermediate risk)	Stage 0 with enlarged node(s)	11.0
	II (intermediate risk)	Stage 0-I with splenomegaly, hepatomegaly, or both	7.8
	III (high risk)	Stage 0-II with haemoglobin < 11.0 g/dL or haematocrit <33%	5.3
	IV (high risk)	Stage 0-III with platelets < 100,000 /mcL	7.0

The International Workshop on CLL has recommended integrating the Rai and Binet systems as follows: A0, AI, AII, BI, BII and CIII, CIV (1989). Adapted from the 2008 NCI guidelines (Hallek, Cheson et al. 2008), *Areas of involvement considered for staging are as follows: head and neck, axillae, groins, palpable spleen, palpable liver.

CLL is characterised by both circulating peripheral disease, as well as accumulation of proliferating monoclonal B-lymphocytes in bone marrow and lymphoid organs (Caligaris-Cappio 2000). Clinical data show that, although therapies are often effective at killing CLL cells in the peripheral blood, residual disease remains in the bone marrow and lymph nodes (Davids and Burger 2012). It is likely that these malignant cells sequestered in the tissue, receive protection from a wide variety of treatments through pro-survival signals and inhibition of apoptosis, fostered by the stromal microenvironment (Ramsay and Rodriguez-Justo 2013). The complex biology underlying how these CLL cells are recruited, maintained, and released from the stroma is an area of active investigation (see Figure 1.4).

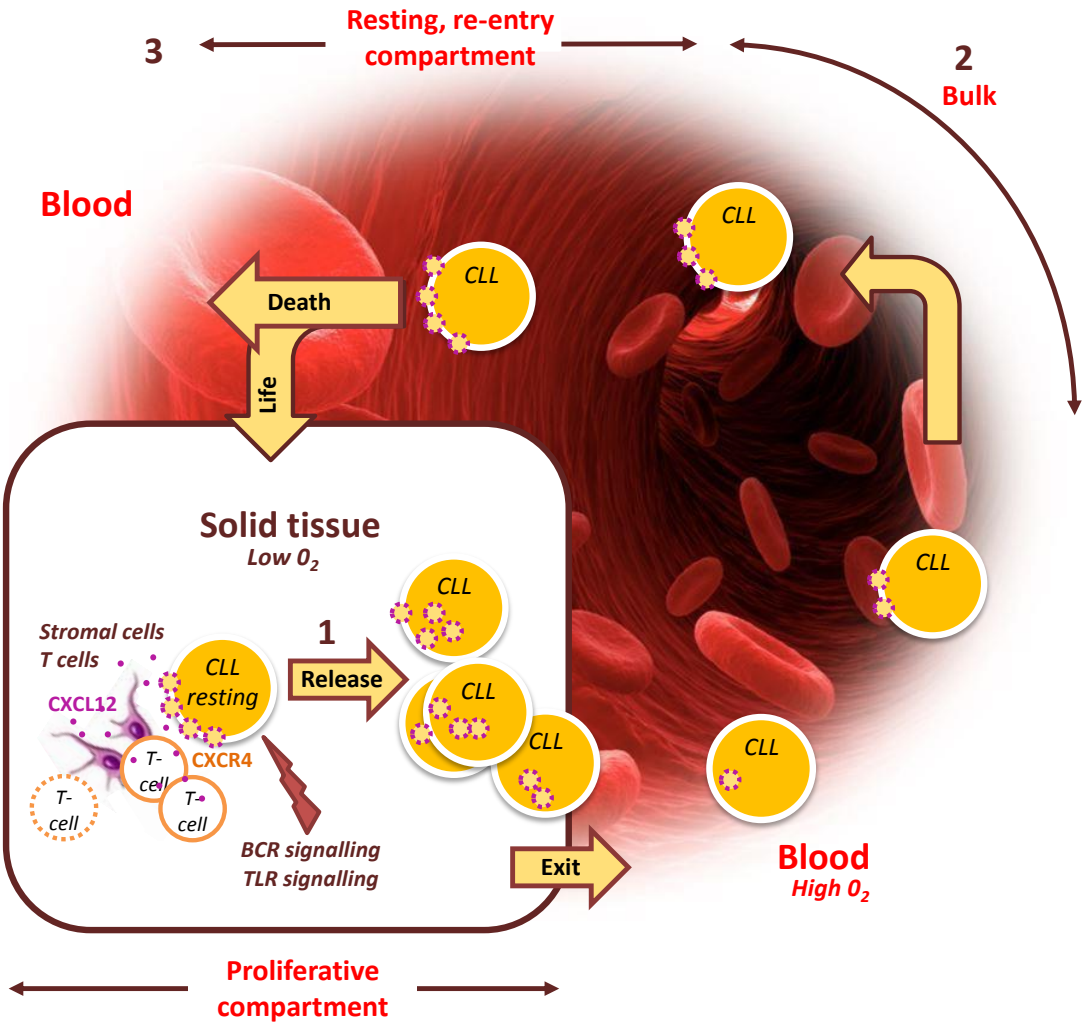

Figure 1.4. Model of the lifecycle of a CLL B cell.

1) CLL cells rest on the stromal cells due to CXCR4-CXCL12 (SDF-1) interactions. Additionally, activated T cells in the presence of CXCL12 enhance the activation and proliferation of the leukemic clone. When stimulated, CLL cells are activated and divide, regulating CD5, internalising CXCR4 and detaching from stroma. The process could be ligand-induced (for example, BCR or toll-like (TLR) or other pathways) or spontaneous. Recently divided (low CXCRX4) CLL cells are more likely to exit solid tissue and reach peripheral blood. 2) Recently born/divided CLL cells reach peripheral blood. Over time, possibly because of a lack of trophic input from the solid tissue microenvironment, cells begin to re-express CXCR4 to return to nutrient-rich niches. 3) CXCR4 bright CLL cells have the greatest chance of re-entering lymphoid solid tissue and receiving pro-survival stimuli. Those that do not re-enter, die by exhaustion. (Based on (Calissano, Damle et al. 2011) and (Borge, Nannini et al. 2013), background picture adapted from http://dxline.info/).

In order to allow transit between different environments, the metabolism of CLL cells must be able to quickly adapt to new conditions. Levels of oxygen and pH differ between peripheral blood and between centres of proliferation in lymph nodes and bone marrow, thus influencing metabolism (Star-Lack, Adalsteinsson et al. 2000; Sison and Brown 2011). Understanding the changes in metabolism of CLL cells linked to the transition between oxygen states, may lead to the development of new therapeutic targets.

1.5.1 CLL microenvironment

Recent reports have emphasised the importance of the microenvironment in the development and pathophysiology of malignancies. Although most of these reports investigated interactions between stromal and neoplastic cells, hypoxia has emerged as another component of the microenvironment. Although hypoxia in solid tumours is well studied, it is unclear what role, if any, it has in the physiology of haematological neoplasias. Lymphomas in this context may resemble solid tumours, but the hypoxic sanctuary for leukaemias is thought to be bone marrow. There is an additional interest in comparisons of the role of hypoxia within the bone marrow of healthy individuals and cancer patients, as it may affect haematopoietic progenitors and their differentiation as well as bone metastases (Fiegl, Samudio et al. 2010).

The cellular microenvironment of CLL cells in the bone marrow and secondary lymphatic tissues, consists of stromal cells and matrix (Burger, Ghia et al.

2009). Interactions of CLL cells with their cellular environment affect the survival of CLL cells and proliferation and provide drug resistance that may be responsible for residual disease after conventional therapy. Key cellular players were shown to be mesenchymal stromal cells, monocyte-derived nurse-like cells (NLCs), and T cells (Panayiotidis, Jones et al. 1996; Burger, Tsukada et al. 2000; Bagnara, Kaufman et al. 2011). The B-cell Receptor (BCR) expressed on CLL cells is responsible for the maintenance and expansion of the CLL clone, through its downstream kinases such as the spleen tyrosine kinase (Syk), Bruton's tyrosine kinase (BTK), and phosphatidylinositide 3-kinase (PI3K). Chemokine receptors such as CXCR4 and CXCR5, together with adhesion molecules, regulate CLL cell trafficking and tissue homing (Burger, Burger et al. 1999). Members of tumour necrosis factor (TNF) family such as the CD40 ligand, B cell-activating factor of the tumour necrosis factor family (BAFF), and a proliferation-inducing ligand (APRIL) activate CLL cells, and promote immune recognition and survival which leads to the expansion of malignant cells (Nishio, Endo et al. 2005). Moreover, as a consequence of BCR activation, CLL cells secrete cytokines (such as CCL3), which influence the microenvironment by attracting accessory cells such as monocytes and T cells (Burger, Quiroga et al. 2009).

1.5.2 Current CLL therapies

At present, CLL remains incurable without allogeneic stem cell transplantation, although treatment outcomes have improved considerably in the last decade through the use of novel therapeutic agents, as well as risk stratification (Bottcher, Ritgen et al. 2012).

The standard first-line treatment of fit CLL patients is the combination of the monoclonal antibody rituximab, with the cytostatic drugs fludarabine and cyclophosphamide (FCR) or with bendamustine (BR) (Keating, O'Brien et al. 2005; Eichhorst, Busch et al. 2006). Rituximab is an antibody against the B-cell antigen CD20, expressed on the CLL cell surface and has been shown to activate complement-dependent cytotoxicity, opsonisation to macrophages causing antibody-dependent cell-mediated cytotoxicity (ADCC) and apoptosis (Maloney, Smith et al. 2002). Another CD20 antibody, oftatumimab which targets a different epitope of CD20, was shown to be efficient both in combination with chemotherapeutics, and as a single agent; unlike rituximab which has limited efficacy as a monotherapy (Wierda, Kipps et al. 2010). Obinutuzumab (GA101) is another antibody targeting CD20 characterised by increased antibody-dependent cellular cytotoxicity and inducing a direct, non-apoptotic lysosome mediated cell death (Alduaij, Ivanov et al. 2011). In cases of fludarabine-refractory CLL, alemtuzumab - the CD52 antibody - has been confirmed to be effective (Faderl, Thomas et al. 2003). However,

alemtuzumab was withdrawn from the market in Europe and the US for treatment of CLL and is available only through named patient programmes (Tausch, Mertens et al. 2014).

Another class of CLL treatments are immune modulatory drugs such as Lenalidomide. This compound acts by inhibiting cytokines such as TNF-α, interleukin-7, and VEGF and stimulating T and natural killer cells. In addition, it resolves immunosuppressive mechanisms against healthy T cells induced by lymphoma cells. Lenalidomide is a replacement of thalidomide with fewer side effects and improved potency (Sharma, Steward et al. 2006).

The B-cell receptor signalling pathway has been shown to be essential for CLL cell survival (Wiestner 2013) and inhibition of this pathway became a new therapeutic target. The small-molecule ibrutinib is one of the new drugs in clinical development that is effective in CLL through inhibition of this pathway. Ibrutinib binds to the cysteine 481 of the Bruton's tyrosine kinase and interrupts activation of the BCR pathway, resulting in reduced migration and proliferation of the malignant cells and induced apoptosis. Importantly, ibrutinib is a very well tolerated drug, with few side effects (Byrd, Furman et al. 2013). Another agent targeting the BCR pathway is the (PI3K) inhibitor, idelalisib. Activated PI3K is linked to the nuclear factor-kappa-B (NFkB) activation and expression of B-cell lymphoma (BCL)-XL and Mcl-1, mediating inhibition of pro-survival pathways (Longo, Laurenti et al. 2008).

Moreover, PI3K inhibition has been shown to decrease chemotaxis of CLL cells into protective tissue microenvironments, resulting in higher susceptibility to chemotherapy (Hoellenriegel, Meadows et al. 2011).

Another promising drug, ABT-199 is an orally bioavailable antagonist of the anti-apoptotic protein BCL-2. It induces apoptosis by mimicking the BH3 domain. ABT-199 has been shown to dramatically reduce the number of CLL cells within 12 hours after administration. Currently ABT-199 is in clinical development as a monotherapy as well as in combination with antibodies and chemotherapy (Souers, Leverson et al. 2013).

As presented above, a broad range of novel agents with different mechanisms of action have entered clinical trials in the last decade (See Figure 1.5). They have already proven their efficacy as well as improved safety profile compared to chemotherapy, showing a potential to change the treatment paradigm of CLL.

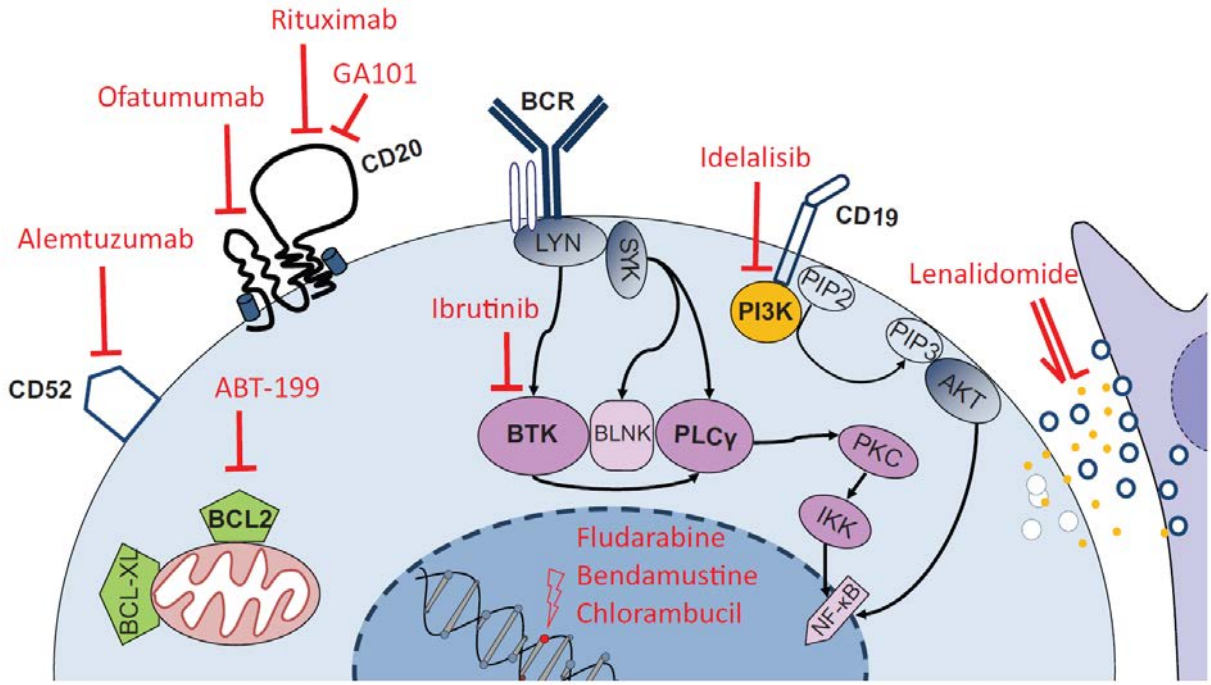

Figure 1.5. New therapeutic agents and their targets in a chronic lymphocytic leukaemia cell.

BCL2, B-cell lymphoma 2; BCR, B-cell receptor; BTK, Bruton's tyrosine kinase; NFkB, nuclear factor kappa B; PI3K, phophoinositide 3-kinase; PKC, protein kinase C; PLC, phospholipase C. (Adapted from (Tausch, Mertens et al. 2014)).

1.5.3 CLL cell metabolism

Recent technological developments have allowed global analyses of biochemical alterations in cancer and enabled the discovery of potential molecules involved in cancer cell survival and drug resistance. It was found that GSH is particularly important for CLL cells, owing to the unique biological properties of this leukaemia. CLL cells intrinsically have higher levels of reactive oxygen species (ROS) when compared with normal lymphocytes, and are highly sensitive to agents that induce further oxidative stress (Zhang, Trachootham et al. 2012). The elevated ROS level renders CLL cells more dependent on cellular antioxidants such as GSH to maintain the redox balance. However, CLL cells are unable to maintain GSH once they are isolated from patients and cultured *in vitro*, exhibiting a high level of spontaneous apoptosis (Collins, Verschuer et al. 1989; Silber, Farber et al. 1992). Recently, it was shown that the bone marrow stromal cells promote GSH metabolism in CLL cells and enhance leukaemia cell survival and drug resistance (Zhang, Trachootham et al. 2012). This finding could lead to a novel therapeutic strategy. Alongside this, the adaptations of CLL cells to ROS by up-regulating the stress-responsive heme-oxygenase-1 (HO-1), may be a feasible metabolic alteration to target therapeutically. However, due to the limited knowledge in the area of CLL cell metabolism, further exploration is required (Jitschin, Hofmann et al. 2014).

1.5.4 Metabolism of quiescent cells

Unlike CLL cells present in proliferation centres, CLL cells circulating in the peripheral blood are in the reversible, cell-cycle arrest state, called quiescence. The transition between proliferation and quiescence has been shown to be associated with changes in gene expression, histone modification and the extension of chromatin compaction; although it remains unclear if chromatin state changes are responsible for cell cycle exit, initiating quiescence (Evertts, Manning et al. 2013). Entry into the quiescent state is often correlated with dramatic changes in metabolism, as the requirements of proliferating and quiescent cells are different. Many, but not all quiescent cells down-regulate their protein synthesis. In some cases, cellular quiescence is associated with lower metabolic activity, characterised by low glucose consumption and glycolysis, decreased translation rates and activation of autophagy in order to provide nutrients for survival (Valcourt, Lemons et al. 2012).

In different quiescence models including mammalian lymphocytes, haematopoietic stem cells and *Saccharomyces cerevisiae*, the PI3Kinase/TOR signalling pathway is involved in growth control. Quiescent fibroblasts are an example of cells that exhibit metabolism where glucose uptake and flux are not reduced. They maintain comparable metabolic rates to proliferating fibroblasts, however the mechanism through which metabolites enter the TCA cycle is different. In quiescent

fibroblasts, pyruvate is transformed into oxaloacetate by pyruvate carboxylase, while in dividing fibroblasts, metabolic intermediates enter the TCA cycle from pyruvate via transfer of the acetyl group of acetyl-CoA to oxaloacetate. A possible explanation for the maintenance of high metabolic rates during quiescence of fibroblasts is that in this state, they have an important biosynthetic function, the secretion of extracellular matrix proteins (Lemons, Feng et al. 2010).

Different metabolic adaptations to quiescence are shown by adult haematopoietic stem cells (HSCs). They maintain a quiescent state in order to avoid cellular damage from ROS and to ensure life-long tissue renewal capacity (Jang and Sharkis 2007). Slow cycling cells are more resistant to cytotoxic agents such as UV, ionising radiation and chemicals affecting cells that are in the S or M phase of the cell cycle. Quiescent HSCs depend more on glycolysis than on oxidative phosphorylation for ATP production, although it is not clear if this metabolic program is intrinsically required for stem cell self-renewal, or if it is an adaptive response to the hypoxic environment (Shyh-Chang, Daley et al. 2013). This phenotype has been shown to be programmed by the HSC transcription factor MEIS1, via its target HIF-1α which up-regulates many glycolytic enzymes. Therefore HIF-1α plays an essential role in the maintenance of HSC quiescence and stress resistance (Takubo, Goda et al. 2010; Shyh-Chang, Daley et al. 2013).

1.6 TOOLS USED FOR INVESTIGATING CANCER METABOLISM

Recently, there has been increasing interest in investigating metabolic flux in cells. Technological advances in instrumentation have allowed for the quantification and analysis of dynamic changes in metabolites under either biological or certain culture conditions, or in response to treatment. This approach is described by the term metabolic flux analysis (MFA), often using an experimental approach based on isotopically labelled tracers. This is distinctly different from 'metabolomics' which describes the analysis of complete sets of metabolites, simply based on profiles arising from metabolite concentrations (Griffin and Shockcor 2004). MFA is a more powerful tool for the study of metabolism as the distribution of isotopically labelled metabolic precursors allows for the monitoring of metabolic fluxes and mapping of metabolic pathways. By using different tracer molecules, MFA can detect fluxes even for steady-state concentrations. This chapter will focus on the capabilities and recent achievements in the field of nuclear magnetic resonance (NMR) spectroscopy for investigating metabolic flux in cancer cells.

1.6.1 Spectroscopic methods used in metabolic analysis

Understanding the aetiology and progression of disease through metabolic profiling is not a new concept — ^{31}P, ^{1}H and ^{13}C NMR spectroscopy, along with gas chromatography– mass spectrometry (GC–MS) and liquid chromatography – mass spectrometry (LC-MS) are tools that have been widely used for metabolic analysis

since the early 1970s (Hoult, Busby et al. 1974; Gates and Sweeley 1978). NMR spectroscopy has also been used to differentiate between different cancer cell lines (Florian, Preece et al. 1995; Florian, Preece et al. 1995; Lodi, Tiziani et al. 2013) and to monitor metabolic processes that occur in cancer cells during events such as apoptosis (Hakumaki, Poptani et al. 1998; Williams, Anthony et al. 1998). However, due to technical challenges, current methods still face many limitations which prevent them from reaching this ideal. Using NMR-based approaches, 20–40 metabolites can typically be detected in tissue extracts while 100–200 can be detected in urine samples. Using the more sensitive approach of LC–MS, around 1,000 metabolites can be detected in these sample types. Various other analytical tools can also be used for metabolomics, provided that the data sets are rich in molecular information. Fourier-transform infrared (FT-IR) spectrometry, metabolite arrays (Bochner, Gadzinski et al. 2001), Raman spectroscopy (Hanlon, Manoharan et al. 2000) and Thin-Layer Chromatography (TLC) (Tweeddale, Notley-McRobb et al. 1998) have been used in metabolomics analysis. However, these techniques do not allow for the distinguishing of metabolites within the same class of compounds. As a result, they may only be useful for initial screening. The advantages and disadvantages of the most commonly used techniques are compared in Table 1.2.

Table 1.2. Comparison of analytical methods used for metabolomics. Adapted from (Vernocchi, Vannini et al. 2012).

Analytical method	Advantages	Disadvantages	Comments
NMR	• Rapid analysis • High resolution • No derivatisation • Non-destructive • Easy sample preparation • Fully quantitative • Highly reproducible • Non-selective (detects all metabolites simultaneously)	• Low sensitivity • Convoluted spectra • More than one peak per component • Slow	• **Chemical consideration:** gives detailed structural information for individual metabolites, particularly using 2D NMR • **Chemical bias:** NMR has no chemical bias and can be used directly on the sample • **Speed:** few minutes to hours, depends on the concentration of samples and on the NMR instrument (strength of the magnet, type of probes)
GC-MS	• Sensitive • Robust • Large linear range • Large commercial and public libraries	• Slow • Often requires derivatisation • Many analytes thermally- unstable or too large for analysis	• **Chemical consideration:** on its own will not generally lead to metabolite identification. However coupled with MS is very powerful for analyte identification • **Chemical bias:** solvent extraction bias: non-polar vs. polar analytes. Need for chemical derivatisation • **Speed:** very useful separation, typically takes 10-30 min
LC-MS	• No derivatisation required • Many models of separation available • Large sample capacity • High sensitivity, can identify ~2000 compounds	• Slow • Limited commercial libraries • Quantification requires isotope labelled libraries	• **Chemical consideration:** on its own will not lead to metabolite identification. However coupled with MS is very powerful for analyte identification • **Chemical bias:** solvent bias means it is usually more applicable to polar compounds; lipid analysis requires a second sample • **Speed:** typically takes 10-30 min
FT-IR	• Rapid analysis • Complete fingerprint of sample chemical composition • No derivatisation needed	• Extremely convoluted spectra • Many peaks per component • Difficult identification of metabolites in mixtures • Requires samples drying	• **Chemical consideration:** provides limited structural information, but useful for identification of functional groups • **Chemical bias:** these methods have little chemical bias and can be used directly on the sample • **Speed:** 10-60 sec

Among all of these techniques, the most powerful and commonly used are NMR spectroscopy and Mass Spectrometry. They both provide structural and quantitative information on multiple classes of compounds in a single analytical run. ^{1}H-NMR is a universal detector that will give a spectrum for all homogeneous samples, if the molecule containing protons (^{1}H) is present above the detection limit. NMR spectroscopy permits analysis of all metabolites present in a biofluid at the same time, while MS usually requires samples to be fractioned prior to analysis. Therefore, MS is coupled to a chromatography technique such as HPLC or UPLC. Both techniques provide information on a wide range of metabolites, without the need for selection of a particular analyte to focus on (Lindon, Holmes et al. 2006). The remainder of this chapter presents NMR spectroscopy as a leading tool for metabolic studies.

1.6.2 Metabolic Flux analysis

Isotope tracer-based metabolic flux analysis has developed over the past two decades as the primary approach to quantifying the rates of turnover of metabolites through metabolic pathways; that is, metabolic fluxes. MFA utilises isotopically labelled metabolic precursors such as glucose and glutamine as tracers and observes the flux of individual-labelled atoms across metabolic networks. This allows for the monitoring of metabolic fluxes and the mapping of metabolic pathways and it is

especially important for detecting the fate of metabolites which are part of many different pathways.

Tracing metabolic profiles has the potential to reveal crucial enzymatic steps that could be targeted in the drug discovery process. It is well known that tumours are associated with substantial rewiring of metabolic networks. Many recent studies show approaches for the analysis of metabolism that make it possible to simultaneously assess metabolite concentrations and pathway fluxes for a large number of the key components involved in the central metabolism of human cells. Labelled cell extracts can be analysed by mass spectrometry or by NMR. There are several reports where one-dimensional ^{13}C-NMR spectra have been used, although two-dimensional NMR analysis using HSQC spectra has been shown to have great advantages (Szyperski 1995). Comprehensive isotopomer models, predicting the tracer label distribution facilitate the quantitative analysis of fluxes through key central metabolic pathways including glycolysis, pentose phosphate pathway, tricarboxylic acid cycle, anaplerotic reactions, and biosynthetic pathways of fatty acids and amino acids (Günther et al., 2014). The validity and strength of this approach is illustrated by its application in a number of perturbations to cancer cells, including exposure to hypoxia, drug treatment and tumour progression.

The term "Metabolic Flux Analysis" is also used in the context of computational biology, using flux balance analysis (FBA) where metabolic pathways

are modelled across a network of biochemical reactions on a genome scale (Wiechert 2001).

1.6.3 NMR as a tool for metabolomics studies

Spin ½ isotopes behave like small magnets when placed in a magnetic field. The spins align with or against the magnetic field. Because of the energy difference between parallel and anti-parallel aligned spins, the parallel state is populated more than the anti-parallel state, causing magnetisation of the entire sample. By applying a radiofrequency to the nuclei, one can cause the nuclei to switch to the opposing magnetic state and this transfer is associated with the generation of transverse magnetisation. When there is transverse magnetisation, the magnetisation starts to precess around the axes of the external magnetic field, which can be detected as a radio frequency. Nuclei in different molecules as well as in different chemical environments exhibit distinct resonance frequencies resulting in a unique pattern of chemical shifts visible in the NMR spectrum. This property makes NMR a useful tool for chemical analysis as structure elucidation is possible based on these frequency differences.

NMR analysis for metabolomics has centred on ^{1}H and ^{13}C NMR spectroscopy, although ^{31}P NMR spectroscopy has been used to measure high-energy phosphate metabolites (such as ATP) and phosphorylated lipid intermediates. Other nuclei such as ^{2}H and ^{19}F have also been used, the latter is found in a range of neuroleptic drugs,

and has been introduced as a tracer for drug discovery approaches (Dalvit and Vulpetti 2011).

NMR is a relatively insensitive technique but has the strong advantage that it can be used in a non-invasive manner, allowing metabolic profiling of intact tissue. This has formed the basis for MRI, the most common application of NMR. The non-invasiveness of NMR has been exploited in this thesis where intact human cells were studied. Various approaches have been used to study intact tissue by NMR, starting from measuring structural and functional properties of proteins in whole cells (in-cell NMR) (Selenko and Wagner 2007; Borcherds, Theillet et al. 2014), through to small pieces of intact tissue measured by high-resolution magic angle spinning (MAS) ^{1}H NMR spectroscopy (Cheng, Lean et al. 1996; Griffin, Sang et al. 2002), or *in vivo* spectroscopy of whole organs (Pfeuffer, Tkac et al. 1999). Alternatively, tissue extracts can be used for the analysis of hydrophilic metabolites (Beckonert, Keun et al. 2007).

The detection limit for ^{1}H-NMR spectroscopy is typically in the order of 10 μM in a tissue extract or biofluid, although lower concentrations can be measured using excessively long acquisition times. Typical acquisition times for one-dimensional ^{1}H-NMR spectra are about 10 minutes. NMR-spectroscopy analysis of biofluids has been shown to be highly reproducible, as samples analysed by this method have produced

similar results to those measured on other types of spectrometers (Lindon, Nicholson et al. 2003; Dona, Jimenez et al. 2014).

1.6.3.1 Metabolic profiles of cancer cells

Metabolomics in cancer has developed almost in parallel with a new era of research in cancer metabolism. Although these two fields are closely related, they represent the expertise of two different scientific communities: cancer biologists and analytical chemists. Over the last decade, collaborations of scientists from these fields have resulted in significant advancements in our knowledge.

NMR spectroscopy, including *in vivo* magnetic resonance spectroscopy (MRS) and high-resolution solution-state analysis of tissue extracts, has been widely used for several years. Although NMR spectroscopy detects only a relatively small number of metabolites, it can be used to monitor the activity of many cellular processes. As many metabolic pathways are connected, changes detected in the metabolome can be used to follow seemingly unrelated pathways. Despite limitations in sensitivity and the ability to measure a broad range of metabolites, MRS has been used to analyse tumour types in humans and in animal models of cancer (Tate, Crabb et al. 1996; Tate, Griffiths et al. 1998). *In vitro* NMR metabolomics studies have also demonstrated differences between tumour types, in terms of various biochemical pathways (Florian, Preece et al. 1995).

1.6.4 Leading NMR techniques for cancer metabolomics

1.6.4.1 Magic Angle Spinning (MAS)

As mentioned previously, high-resolution magic angle spinning (HRMAS) ^{1}H-NMR spectroscopy, can produce high-resolution spectra from small pieces of intact tissue (Denkert, Bucher et al. 2012). A biopsy or post-mortem sample of tissue is spun at an angle of ca. 54.74° (the so-called magic angle) to the applied magnetic field. The spinning results in a significant improvement in the resolution of the spectrum obtained by eliminating dipolar interactions and magnetic susceptibility effects which cause wide lines (Renault, Shintu et al. 2013). This approach has several advantages over NMR spectroscopy of tissue extracts. Both aqueous and lipid-soluble metabolites can be observed simultaneously *in situ*, whereas solution-state NMR would require separate extraction procedures. One of the first applications of this technique was to distinguish between healthy and malignant lymph nodes (Cheng, Lean et al. 1996). Information about the metabolic environment of the tumour can also be obtained using HRMAS ^{1}H-NMR spectroscopy, which can be used to identify metabolites with a range of physical properties. These approaches have also been used to follow the effects of therapeutics on tumour cells *in vitro* and *in vivo* (Griffin and Shockcor 2004).

1.6.4.2 NMR measurements of cell extracts

Obtaining cell extracts requires concentrated samples in order to obtain a sufficiently good signal-to-noise ration in NMR spectra. If the signal overlap is not significant, parameters such as chemical shift and spin multiplicity can be obtained using simple one-dimensional spectra (usually one-dimensional nuclear Overhauser effect spectroscopy (NOESY) with solvent presaturation). When the spectral overlap becomes too extensive, two dimensional NMR experiments can be used to overcome this problem by significantly increasing the resolution and dispersing the peaks into two-dimensions. 2D ^{1}H-^{1}H TOCSY (TOtal Correlation SpectroscopY), 2D ^{1}H-^{13}C HSQC (Heteronuclear Single-Quantum Correlation) and 2D ^{1}H-^{1}H JRES (J-resolved spectroscopy) are the three most commonly used 2D NMR methods in metabolomics (Gebregiworgis and Powers 2012). These methods not only improve the resolution, but also allow various spin correlations to be observed and recorded using the natural abundance of isotopes, and may be sufficient to identify and quantify metabolites to answer important questions about cell metabolism, tumour progression and efficiency of treatment.

1.6.4.3 Dynamic Nuclear Polarization (DNP)

It has recently been shown that NMR of hyperpolarised precursors has the potential to become a suitable modality for monitoring metabolism and for measuring changes in metabolic fluxes (Golman, in 't Zandt et al. 2006; Schroeder,

Atherton et al. 2009). In these studies, ^{13}C-labeled metabolites are hyperpolarised using stable radicals. ^{13}C chemical shifts can be exploited to distinguish between the original molecules and their metabolic products and gradient-based imaging techniques can localise the spatial source of these spectral signatures.

To obtain a thorough understanding of the cellular processes, it was important to develop *in vitro* cell systems in which conditions could be carefully controlled and manipulated. So far, a number of studies have monitored the metabolism of hyperpolarised molecules in concentrated cell suspensions (Chen, Albers et al. 2007; Day, Kettunen et al. 2007). This method has also been used to measure breast cancer cells cultivated on beads and maintained by continuous perfusion under physiological conditions. This enabled a reliable characterisation of the kinetics and mechanism of hyperpolarised pyruvate-to-lactate conversions in T47D cell line (Harris, Eliyahu et al. 2009). DNP based approaches are however limited to the short time frames in the order of the longitudinal relaxation time of the metabolites that were polarised.

1.6.4.4 Measurement of living cells in NMR

NMR spectroscopy was developed in the 1960s, and by the early 1970s it had already been used for *in vivo* measurements using intact red blood cell suspensions, although in non-viable conditions (Morris 1988). Since then, multiple applications in fields such as medicine, toxicology and environmental sciences have been reported

and its usage continues to increase (Cohen, Motiei et al. 2004; Palomino-Schatzlein, Escrig et al. 2011). The popularity of NMR arises from its non-invasive and non-destructive nature, as well as its capacity to measure metabolite levels in complex mixtures without the need for separation.

1.6.4.4.1 ^{31}P NMR as an indicator of pH in samples

Tumour pH has long been of interest because it can alter the therapeutic efficiency of chemotherapeutic agents, radiation or hyperthermia. Tumour thermal sensitivity depends primarily on intracellular pH (pH_{in}) and its lowering has been proposed as a target for tumour specific therapies. Therefore, particular methods are required to accurately measure pH_{in} in tumours. NMR spectroscopy provides a non-invasive technique for measuring the pH_{in} of tumour cells *in situ* by the observation of the ^{31}P signal from ionisable intracellular phosphates. Since the ^{31}P chemical shift of readily observable inorganic phosphate (Pi) is sensitive to pH changes in the physiological range (i.e. pKa= 6.6), it has been used routinely in a wide range of tissues as the NMR indicator of pH_{in} measurements performed *in vivo* (Soto, Zhu et al. 1996). This is also feasible *in vivo* in particular in MRS applications. With new technology it is also possible to use dual receiver probes that allow recording spectra of the same sample simultaneously, for example ^{1}H and ^{31}P. This may enable monitoring changes in metabolic flux together with pH changes.

1.6.4.4.2 Challenges of recording real-time metabolic changes

The development of effective therapies against malignant diseases and monitoring their effect in a non-invasive manner is one of the most important challenges for biomedical research in the area of personalised medicine. NMR is a very useful experimental approach in this context as it enables continuous monitoring of biochemical processes. The approach of measuring living, patient derived cells and their metabolic changes in real-time is new and therefore challenging. Firstly, to record real-time metabolic fluxes in cells, the problem of cellular sedimentation needs to be solved, in order to obtain a homogenous sample in the NMR tube. To avoid the disruption of metabolic process to be measured, cells need to be kept in conditions mimicking their natural environment. Constant perfusion can potentially be applied to keep cells in suspension during NMR experiments and various flow-systems have been reported (Keshari, Kurhanewicz et al. 2010; Khajeh, Bernstein et al. 2010).

Secondly, in order to record spectra within a short time period, proton spectra need to be used as ^{1}H is the most sensitive NMR nucleus. ^{1}H-NMR is intrinsically 14 times more sensitive than ^{31}P, thus allowing shorter acquisition times to be used. Moreover, proton NMR offers the advantage that numerous natural biological compounds, as well as drugs and their metabolites, can be detected. However, the presence of signals originating from extracellular compounds and the immense water

signal, as well as many overlapping proton signals, have limited the application of proton NMR in studies of biological samples. Some proton NMR studies have been reported *in vivo* (Garcia-Segura, Sanchez-Chapado et al. 1999); however, these have not yet attained translation to routine clinical application. It was also shown that Diffusion Weighted Proton Magnetic Resonance Spectroscopy can be used to selectively observe only the intracellular metabolites of several cell lines *in vitro* (Mardor, Kaplan et al. 2000). This method is based on differences in motional properties of cellular components, as larger molecules (such as proteins) exhibit slower rotational tumbling. Interaction with small molecules may also affect their motional properties within cells. Owing to such interactions, intracellular components have a lower apparent diffusion constant (ADC) than extracellular components and free water. Diffusion Weighted Proton Magnetic Resonance Spectroscopy can select small molecules that maintain fast rotational diffusion, however this requires large concentrations of intracellular metabolites.

There has been progress in measuring living cells using NMR in recent years and techniques are still being improved to obtain the full picture of cellular metabolites which could be detected within short time frames. This will eventually create the possibility of monitoring real-time metabolic fluxes in living cells, in different conditions and responding to various treatments.

1.6.4.4.3 Flow systems

In order to obtain accurate quantitative metabolic data, studies should be performed on intact living cells - *ex vivo* or *in vitro* as opposed to metabolite extraction from cells, which often exhibits low reproducibility. For measurements to be conducted on living cells, combinations of small-scale bioreactors with NMR spectrometers have been designed to reduce cellular sedimentation and to allow for the acquisition of metabolic data, in a defined and controlled environment. However, the high cell density required in the NMR tube causes many constraints, especially for primary human cells where limited numbers are available.

For any bioreactor, the maintenance of oxygen levels is important. Low solubility of oxygen in media entails that gas diffusion alone will not adequately provide for the metabolic needs of cells. Furthermore, mammalian cells respond to high oxygen concentrations by changes in their metabolism and it is generally recommended that pO_2 is maintained between 25 and 50%. Increasing perfusion rates would be the simplest solution to ensure that the oxygen consumption rate of cells can be satisfied. However, increasing flow rates to suitable levels will most definitely cause cell wash-out from the bioreactor, due to the low cell density. In this sense, the major challenge is to construct the appropriate configuration that will allow for high flow rates, while maintaining freely suspended cells in the NMR reading zone.

As a part of the presented thesis, a novel approach for measuring the metabolism of living primary human cells has been developed. The use of low percentage agarose containing embedded suspension cells is an alternative method providing both the homogeneity of the NMR sample as well as prevention of cellular sedimentation.

1.7. FUTURE PROSPECTS

Most of today's anti-cancer drugs are far from specific in attacking tumours. Rather, they represent poisons that tend to kill cancer cells more than normal cells. As a consequence of this incomplete specificity, they can cause severe side effects. Fortunately, cancer researchers are rapidly progressing to more targeted treatments, and pioneering new approaches to diagnose and classify cancers more effectively. The necessity for tests that can predict or at least monitor the response of an individual patient to specific treatment is still increasing.

Metabolomics can be used in this context in several ways. The most important approach is to detect changes on a metabolite level that can be used as a fundamental component for new targeted therapeutic strategies. This is particularly promising in the context of cancer as the disease involves significant metabolic reprogramming.

Metabolism is involved directly or indirectly in all functional activities of cells. There is mounting evidence for cross-talk between signalling pathways and

metabolic control in every multicellular organism studied (Vander Heiden, Cantley et al. 2009). However, there is still much to learn about how proliferating cell metabolism is regulated. Despite a long and rich history of research, the complex connection between metabolism and proliferation is an increasingly exciting area of investigation and it is possible that additional pathways have yet to be described. Understanding this important aspect of biology is likely to have a major impact on our understanding of cell proliferation control and cancer. Based on the findings presented above, we can say that the developed metabolomics approach constitutes a promising analytical tool for revealing specific metabolic phenotypes in a variety of cell types and pathological conditions.

1.8. AIM OF THIS THESIS

The overall objective of this thesis was to demonstrate a method of monitoring metabolism in living cells using NMR and to follow the kinetic changes of metabolites, without disturbing cells.

The use of cell lines in metabolomics studies has significant limitations for studying metabolic adaptations or changes in the rates of cell growth and proliferation, as cell lines never represent the phenotype of an individual patient's cancer cells. Therefore, it is important to test patient derived primary cancer cells. The choice of CLL cells arises from the realisation that these cells can be grown in solution and they can be maintained alive for extended periods of time.

Specifically, using primary CLL cells the aims of the study presented were:

- To develop a method for measuring the metabolism of living CLL cells in real time.
- To compare the metabolism of CLL cells as they transit and cycle from oxygenated to hypoxic environments and are subject to pH changes.
- To investigate factors responsible for the metabolic plasticity of CLL cells.
- To analyse metabolic mechanisms using metabolic flux analysis on CLL cell extracts.

Chapter II

Materials and Methods

All chemicals were purchased from Sigma-Aldrich (Poole, U.K.), unless stated otherwise and all FC analyses were conducted using a FACSCalibur and Cell QuestPro software (BD, Oxford, U.K.).

2.1 Cells from patients

Unselected patients with B-cell CLL attending the outpatient clinic at Birmingham Heartlands Hospital and Queen Elizabeth Hospital were recruited for this study. The patients had been diagnosed according to standard morphologic, immunophenotypic and clinical criteria (Oscier, Dearden et al. 2012) and had provided informed written consent for the study which had received local ethical approval.

2.1.1 Purification of primary CLL cells

The mononuclear cells (MNCs) were isolated from blood using Leucosep tubes (Greiner Bio-one, Gloucester) loaded with 15 ml Ficoll-Paque plus (G.E Healthcare, Amersham). MNCs were cultured in RPMI 1640 (Invitrogen Gibco, Paisley) with 1% ITS^+ (culture supplement containing insulin, human transferrin and selenous acid) (BD Biosciences), 100 U/ml penicillin and 100 μg/ml streptomycin (Invitrogen Gibco). Cells were seeded at the concentration $5x10^6$ cells/ml and incubated in a humidified chamber at 37°C and with 5% CO_2. When cultured in these conditions, CLL cells stay quiescent in the G_0/G_1 phase of the cell cycle.

2.1.2 Isolation of CD^{19+ve} cells

For experiments using $CD19^{+ve}$ cells isolated from the blood of healthy donors, MNCs were isolated as above (section 2.1.1). In cases where the purity was < 70%, negative selection was performed using the Dynabeads® Untouched™ human B Cells kit (Invitrogen) to purify $CD19^{+ve}$ cells without affecting their metabolism.

2.2 Analysis of cell phenotype using flow cytometry

Following positive selection of CD19 cells, a cell purity check was carried out, using CD19 marker. Staining was carried out on $3x10^5$ cells made up to a final volume of 200 µl in phosphate buffered saline (PBS) (Invitrogen Gibco) and incubated with 2 µl of the appropriate antibodies at room temperature (RT) in the dark. Cells were subsequently washed in 2 ml PBS by centrifugation at 1500 rpm for 5 minutes, suspended in 300 µl of PBS and analysed. Data were analysed using BD FACSCalibur™, and 10,000 events were collected after manually performed compensation, using single colour controls. Flow cytometry analysis representative for CLL preparation are shown in Figure 2.1 and purity of all CLL preparations is demonstrated in Appendix A2.

2.3 Assessment of cell viability and proliferation

2.3.1 AV/PI staining

Single Annexin V (AV) and co-Annexin V/Propidium Iodide (PI) positivity was assessed by flow cytometry (FC) following staining using an AV FITC kit (BD), according to the manufacturer's instructions. Briefly, 100 µl of cell suspension ($5x10^6$ cells/ml) was transferred to a FACS tube and 1 ml of cold PBS was added. Cells were centrifuged for 5 minutes at 1500 rpm. The supernatant was removed and cells were resuspended in 100 µl of 1xAV binding buffer. Subsequently 5 µl of AV FITC antibody and 5 µl of PI stain was added and mixed. Samples were incubated at RT in the dark for 15 minutes. Staining was analysed using the flow cytometer within one hour.

2.3.2 Cell cycle analysis.

An aliquot of $3x10^5$ cells was removed from the cell culture and filled with PBS to obtain a final volume of 1 ml. Following the 5 minute centrifugation at 1500 rpm, the supernatant was removed and 500 µl of cell cycle buffer (see buffers and recipes in Appendix) was added. Cell suspension was vortexed and stored in the dark at 4°C for 24 hours before the analysis.

2.4 Cell morphology: Jenner-Giemsa staining

Aliquots of 100 µl cell suspension was loaded onto slides and spun down at 500 rpm for 3 minutes using a Cytospin 3 Centrifuge. Slides were air-dried and fixed with ethanol for 5 minutes. Using a Coplin jar, slides were immersed in Jenner staining solution (diluted 1 in 3 in 1 mM sodium phosphate buffer, pH 5.6) and left for 5 minutes, after which they were washed with distilled water. Slides were then placed in Giemsa Staining solution (diluted 1 in 20 in 1 mM sodium phosphate buffer pH 5.6) and left for 10 minutes, after which they were washed with distilled water again. Slides were left to dry followed by mounting onto coverslips using DePex (VWR, UK). Cytospins were observed at 40x magnification.

2.5 Real time NMR experiments with living cells

2.5.1 Sample preparation

Cell populations characterised as healthy (> 80% Annexin V negative) were selected for NMR experiments. Two concentrations of cells were used: $5x10^7$ cells/ml or $1x10^7$ cells/ml. Directly before the start of each experiment, cells were washed twice with warm RPMI medium and gently suspended in pre-warmed (37°C) 0.1% low melting agarose (Sigma) in RPMI (supplemented with 100 U/ml penicillin, 100 µg/ml streptomycin (Invitrogen Gibco) and 1% ITS^+ (BD Biosciences)) and 1 mM sodium 3-(trimethylsilyl) propionate-2,2,3,3-d4 (TMSP, Cambridge Isotope

Laboratories) in D_2O (GOSS Scientific Instruments Ltd.). After suspending cells in the agarose matrix, 550 µl of cell suspension was loaded into 5 mm NMR tubes using long, glass NMR pipettes. The Oxygen Sensor connected to a Fiber Optic Oxygen Meter (World Precision Instruments) was inserted into the NMR tube and sealed together with Parafilm M®. The NMR tube with the immersed oxygen sensor was transferred into the 500 MHz NMR magnet after pre-warming to 310 K. Measurements were started within 15 minutes of sample injection into the magnet.

2.5.2 Set up of the NMR experiment

After injecting the sample into the magnet, the probe was tuned, the spectrometer was locked for field frequency stabilisation (H_2O + D_2O), and finally the sample was shimmed using automated shimming. This was facilitated by shimming a 0.1% agarose in RPMI sample before the cell sample was prepared. A series of automated 3D shims was performed until no changes were seen, followed by a series of 1D shims and an adjustment of the Z-shim to compensate for temperature gradients across the sample. This adjustment was previously optimised to minimise the TMSP line width. When the cell sample was in the magnet, the series of 1D shims was usually sufficient to obtain a good line width of TMSP (< 2 Hz). On occasions when the line width was higher than 2.5 Hz, additional manual shimming was performed. Following this, the pulse calibration was applied and the receiver gain determined followed by the acquisition of series of 1D ^1H NOESY spectra over 24

hours. The oxygen measurement was started together with the acquisition. After the measurement, cells can be recovered for further analysis. A scheme of the NMR time course is presented in Figure 2.2.

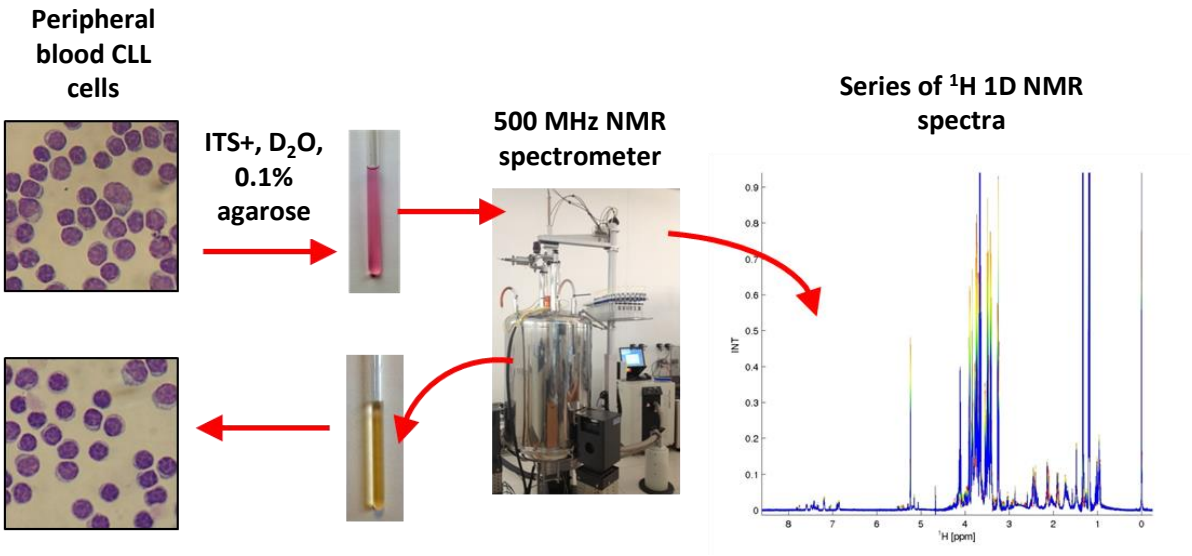

Figure 2. 2. Scheme of NMR time course experiment.

Peripheral blood CLL cells were suspended in RPMI 1640 medium with 1% ITS+, TMSP, D_2O and 0.1% agarose and transferred to the NMR tube. Spectra are acquired over 24 hours using a 500 MHz NMR spectrometer with the temperature set to 37°C.

2.5.3 Real time NMR measurement 1D ^{1}H NOESY

1D ^{1}H NOESY spectra were acquired at 37°C, using a 500 MHz Bruker spectrometer equipped with a cryogenically cooled probe. The spectral width of the acquired spectra was 12 ppm, with 16384 acquired complex data points. The transmitter frequency offset was set to 4.696 ppm to suppress the water signal by presaturation. For apodisation an exponential multiplication (EM) window function with a line broadening of 0.3 Hz was used and the NMR data was zero filled to 32768 points. Measurements were carried out with deuterium frequency locking after shimming. For time course experiments, a series of 144 1D spectra were acquired over 24 hours. Each spectrum was acquired over 10 minutes (which included the time of shimming between each sample), acquiring 64 transients and a recycle delay of 4 s.

2.5.4 Proton-Carbon 1D spectra

In order to investigate carbon flux in real time, a set of two 1D-^{1}H^{13}C decoupled NMR spectra were acquired. One spectrum contained NMR signals originating from all protons in the sample, while the second acquired spectrum contained only signals originating from protons bound to ^{13}C (the pulse sequences are presented in Figure 2.3). Quantitation of this spectral approach was ascertained by scaling the first spectrum down to 1% and then comparing the signal intensity of the TMSP signal in both spectra. Due to the 1% natural abundance of ^{13}C, both signals

had to have the same intensity after scaling down the first spectrum. Then by comparing relative signal intensities in both spectra, the percentage of incorporation of the ^{13}C label could be determined from a single sample in real time (see Figure 2.4). The time resolution achieved was 5 minutes per spectrum or 10 minutes per data point.

As an alternative, in principle the first increment of an HSQC spectrum could also be used, but due to non-adiabatic 90° pulses, magnetisation is not quantitatively recovered at chemical shifts far away from the carrier frequencies. The sequence presented here does not edit through ^{13}C, but rather filters out ^{12}C bound ^{1}H signals and only uses adiabatic 180° pulses on the carbon channel and therefore omits these artefacts.

2.5.5 NMR time course data processing

The NMR data was processed using the MATLAB based NMRLab/MetaboLab software (Gunther, Ludwig et al. 2000; Ludwig and Gunther 2011). A script for automated data processing of all the spectra was created using the ScriptBuilder module of MetaboLab. To further suppress the residual solvent resonance, a convolution filter using a gauss function was applied. Zero filling was set to 131072 data points and phase correction was performed using the automatic phase correction of MetaboLab. Exponential like broadening of 0.3 Hz was applied prior to Fourier transformation of the data. Subsequently a spline based baseline correction (Gunther, Ludwig et al. 2000) was applied simultaneously to all acquired spectra. The chemical shift of TMSP changes with pH, but in order to compare the linewidths and ensure that they did not change throughout the timecourse, all spectra were aligned to the TMSP signal which was set to 0 ppm. As the change in chemical shift for TMSP was very small from spectrum to spectrum, the automatic peak picking algorithm for shifting peaks for other metabolites was able to cope with automatically determining the correct signal and therefore did not compromise any results. Also, pH measurement (described in chapter 5.2.7) which only depends on the difference between the two shifts of histidine, was not affected by the TMSP alignment to 0 ppm.

2.5.6 NMR time course data analysis

NMR resonances of metabolites were assigned using the Chenomx software and HMBD (Human Metabolite Database). In cases of uncertain peaks, samples were spiked with the known metabolite at the concentration similar to that predicted from the obtained NMR spectrum. In order to distinguish peaks which changed their intensity or chemical shift during the time course, spectra were coloured using a rainbow gradient starting from red for the first spectrum, going through yellow and green and finishing with blue for the final spectrum (see Figure 2.5).

For peaks exhibiting intensity changes over time, kinetic modelling was performed using the time series analysis tool (TSATool) from the Metabolab software. Peaks of interest were selected from the first or last spectrum, depending on whether the associated metabolite concentration increased or decreased over time. Selected peaks were then propagated automatically to the rest of the spectra in the time course. For the analysis, the time axis was obtained automatically from the Bruker acquisition data files. First order mono or bi-exponential kinetics were assumed to compare metabolic turnover between cells from different patients or from different treatments.

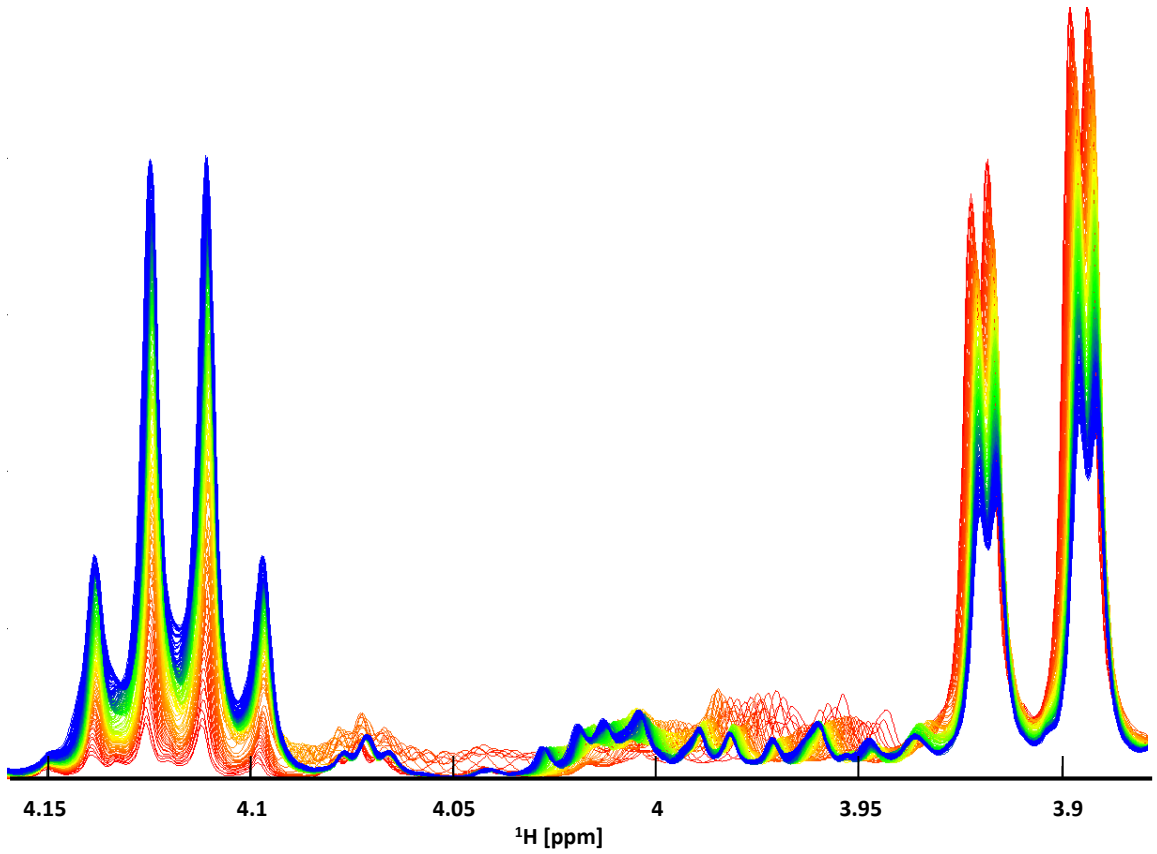

Figure 2. 5. Colour time gradient of the 1D ^{1}H noesy spectra.

Spectra were recorded every 10 minutes over the course of 24 hours. Then data was processed in NMRLab, spectra were superimposed and coloured. The first spectrum is coloured red, with the colour scheme proceeding through yellow and green to blue for the final spectra of the series. This fragment of spectra shows peaks of lactate increasing (quartet at 4.125; 4.111; 4.098; 4.084 ppm) and peaks of glucose decreasing (doublets at 3.877; 3.881; 3.897; 3.901 ppm*). Glucose peaks are shifting to the right as the pH becomes more acidic.

* Peaks were assigned using the HMDB database (The Human Metabolome Database), due to the different temperature and pH, the actual chemical shift values may differ.

2.5.7 Determination of the intracellular pH inside the NMR tube

The extracellular pH inside the NMR tube was determined using the pH sensitivity of the chemical shift of the 2 side chain resonances from histidine (see figure 2.6). In order to obtain the pH curve, 23 media samples with increasing pH were measured (ranging from pH=3 to pH=8.5) in triplicate. Using the chemical shift difference Δδ between the peaks corresponding to imidazole ring protons H2 and H5, attached to C2 and C5 and C5-H peaks (Kintner, Anderson et al. 2000; Cohen, Motiei et al. 2004), we were able to measure the pH of the NMR sample at each particular time point. A calibration curve for the H2 and H5 histidine protons was determined in a solution of RPMI medium adjusted to pH 3-8.5. Curve fitting was carried out in MATLAB using a custom made script with the equation (Schechter, Sachs et al. 1972):

$$pH = pKa + log10\frac{\Delta\delta - \delta BH}{\delta B - \Delta\delta}$$

where pKa is the acid dissociation constant reflecting the inflection point of the titration curve, Δδ represents the difference between the chemical shift of the histidine protons in solution, δBH is the limiting chemical shift value at acid pH and δB is the limiting chemical shift value at basic pH.

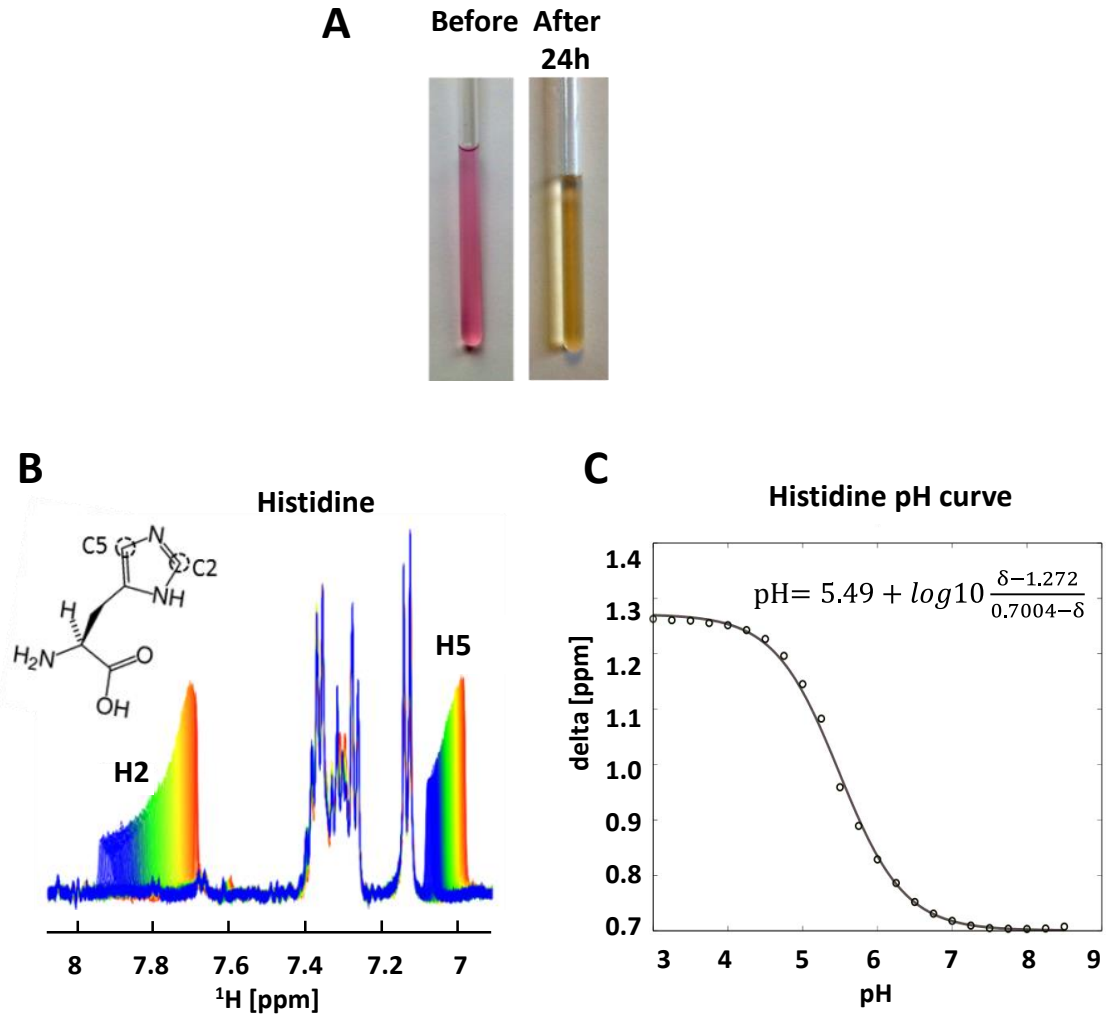

Figure 2. 6. Changes of pH in the NMR tube.

A) Picture of the NMR tube with CLL cells suspended in 0.1% agarose RPMI at $5x10^7$ cells/ml before and after the 24 h time course experiment. B) Chemical structure of histidine with C2 and C5 marked and histidine region of 144 overlaid 24 h time course ^1H spectra (sample contained $5x10^7$/ml CLL cells in 0.1% agarose RPMI with 1% ITS$^+$). Spectra are coloured starting from the first data point in red, and the last data point in blue. Peaks of protons connected to C2 (H2) and connected to C5 (H5) of histidine are shifting to the left. C) Histidine pH curve with the equation of fitted line. Samples of RPMI medium with different pH (x axes) were measured and the difference in chemical shift between frequency [ppm] of two histidine peaks was calculated (y axes). The pH value was calculated using the equation: pH= 5,49 + log10 ((δ−1,272)/(0.7004−δ)).

2.6 CLL cell extraction

2.6.1 Incubation with the ^{13}C labelled precursor

For the extracts analysis ≥180x10^6 cells were required per sample. Media for particular samples were prepared according to Table 2.1. Cells were washed once with the appropriate medium, seeded at 5x10^6/ml and incubated for 24 hours in an incubator under normoxic (22% O_2) or hypoxic (1% O_2) conditions before quenching.

Table 2. 1. Media with the ^{13}C labelled precursors

Sample	RPMI 1640 medium (Invitrogen, catalogue number)	Added precursors
Control	No glutamine (31870-082)	300 mg/l, 2 mM Glutamine (Sigma)
^{13}C-1,2-Glucose	No glucose (11879-020)	2000 mg/l, 11.11 mM of ^{13}C-1,2-Glucose (Sigma Isotopes)
^{13}C-3-Glutamine	No glutamine (31870-082)	300 mg/L, 2 mM ^{13}C-3-Glutamine (Sigma Isotopes)

2.6.2 Quenching

The centrifuge was pre-chilled to -9°C and the fixed angle centrifuge rotor was pre-chilled in the -20°C freezer for 1 hour. The 2 ml Eppendorf tubes were labelled and weighed (for the estimation of the cell pellet biomass). HPLC grade methanol (1.6 ml, 60%, prepared using HPLC grade water) was added to each Eppendorf and

put on dry ice for a minimum of 15 minutes to cool the quenching solution to -40°C. The cell suspension from the sample to be quenched was poured into a 50 ml Falcon tube and centrifuged at room temp (1500 rpm, 5 min). Supernatant (1 ml) was transferred into an Eppendorf and snap frozen in liquid nitrogen. The remainder of the supernatant was discarded. The cell pellet was resuspended in the residual media in the Falcon tube and 200 µl of this suspension was ejected directly into the 2 ml Eppendorf containing quenching solution, mixed and returned to dry ice. Next, all samples were placed in the pre-chilled rotor and centrifuged at -9°C, 2500 *g* for 5 min. The quenching solution was removed with a glass Pasteur pipette. Tubes with pellet were weighed to estimate the pellet mass. Pellets were frozen in -80°C until extraction.

2.6.3 Extraction

Quenched cell pellets were kept on dry ice. Pre-chilled HPLC grade methanol was added to each pellet 8 µl/mg (of pellet) and vortexed for 30 seconds. Then pre-chilled HPLC grade chloroform was added (8 µl/mg) to each Eppendorf and pulse vortexed. Following this, 7.2 µl/mg of HPLC grade water was added and samples were vortexed for 30 seconds and left on ice for 10 min. Next, samples were centrifuged at 1500 *g* (4000 rpm) for 10 min at 4°C. Subsequently, samples were left on the bench for 5 min. After the centrifugation samples were bi-phasic: the upper layer contained polar metabolites and the lower layer contained lipids. The same

volume from the upper layer was transferred to the new Eppendorf vials and aliquots were dried in the vacuum concentrator (SpeedVac) for 3-6 hours. Dry pellets were stored at -80°C until required. The non-polar fraction was also collected (in glass vials) and stored in -80°C for potential future lipid analysis.

2.7 NMR Metabolic Flux experiments using cell extracts

2.7.1 Sample preparation

The dried polar extracts were dissolved in 90% H_2O/10% D_2O (GOSS Scientific Instruments Ltd, Essex UK) prepared as 100 mM phosphate buffer (pH 7.0), containing 0.5 mM sodium 3-(trimethylsilyl)propionate-2,2,3,3-d4 (TMSP, Cambridge Isotope Laboratories) as an internal reference.

2.7.2 HSQC acquisition

The 2D ^{1}H ^{13}C- HSQC spectra were acquired on a 600 MHz UltraShield plus Bruker magnet with a 4-channel Bruker Avance III console using a low volume 1.7 mm CryoProbe™ with a 35 µl sample volume. This spectrometer was also equipped with a SampleJet automated sample changer with sample cooling at 6°C. After the sample was inserted into the magnet, it was temperature equilibrated for 30 s at 300 K (27°C). The probe was then automatically tuned and matched for each sample, followed by sample locking to the D_2O resonance, automatic shimming (shimming is

a procedure which makes the magnetic field as homogenous as possible across the sample) and automated pulse calibration (Wu and Otting 2005) which included: spectral widths (13 ppm & 160 ppm), number of acquired data points (TD), interscan relaxation delay (d1), acquisition time (aq), number of scans (NS) and quadrature detection (Echo/Antiecho).

2.7.3 HSQC data processing

All data processing and analysis was performed using the MATLAB based NMRLab/MetaboLab software package (Gunther, Ludwig et al. 2000; Ludwig and Gunther 2011). Prior to Fourier transformation, the NMR data was apodized using a 90° phase shifted quadratic sine function, then zero filled to 1024 and 4096 data points for ^{1}H and ^{13}C dimension respectively. The NMR spectra were manually phase corrected to obtain pure absorption line shapes and referenced to the methyl signal of alanine using the HMDB based library shifts of the MetaboLab software. To further suppress the residual solvent resonance, a convolution filter using a gauss function was applied to the fids in the ^{1}H dimension (Marion, Ikura et al. 1989).

2.7.4 HSQC data analysis

Assignment and analysis were all carried out in MetaboLab using the HMDB based chemical shift library. A combination of various analyses were used, including an approach using an unlabelled reference sample, multiplet analysis (quantum

mechanical reconstruction of the NMR spectrum using pygamma (Smith, Levante et al. 1994)), as well as the absolute label incorporation into C3 of lactate via 1D spectra.

2.8 Quantitative real-time polymerase chain reaction (QRT-PCR)

2.8.1 RNA extraction

RNA was extracted from a pellet of $1x10^6$ cells using a Qiagen RNeasy mini kit (Qiagen, Crawley, U.K.) according to the manufacturer's instructions. Briefly, cells were resuspended in 350 μl buffer RLT (plus β-mercaptoethanol; Sigma). The sample was then homogenised using a QIAshredder spin column. One volume of 70% ethanol (Fischer Loughborough, U.K.) was added to the homogenised sample and 700 μl of this mixture added to an RNeasy mini column. The column was centrifuged for 15 seconds at 14000 rpm in a microfuge. Further DNA removal was carried out using the RNase-free DNase set. 350 μl buffer RW1 was added to the column and the column centrifuged for 15 seconds at 14000 rpm in a microfuge. The DNase I stock solution was added to buffer RDD according to manufacturer's instructions and 80 μl of this mix was added to the column and incubated for 15 minutes at room temperature. Buffer RW1 (350 μl) was added to the column and the column was centrifuged for 15 seconds at 14000 rpm in a microfuge. Buffer RPE (500 μl) was added to the column and centrifuged for 15 seconds at 14000 rpm in a microfuge.

Another 500 µl RPE was applied to the column prior to centrifugation for 2 minutes at 14000 rpm in a microfuge. The RNeasy column was transferred to a 1.5 ml collection tube, RNA was eluted with the addition of 30 µl RNase-free water and was isolated by centrifugation for 1 minute at 14000 rpm in a microfuge, and stored at –20°C.

2.8.2 RNA quantification

RNA samples were diluted 1 in 50 with RNase-free water (Invitrogen Gibco) in a total volume of 100 µl. The absorbance at 260 nm was measured at OD 260 and the RNA concentration was calculated using the following equation:

RNA concentration (µg/µl) = (OD260 x 40 x dilution factor)/1000.

2.8.3 Reverse transcription

cDNA was produced from 100 ng RNA using reverse transcription. Unless stated otherwise, all constituents were obtained from Invitrogen (Paisley, U.K.) and the procedure carried out as follows: 1 µl of both random primers (Promega) and deoxynucleotide triphosphates (dNTPs) (Bioline, London, U.K.) were added to 100 ng RNA, the volume made up to 12 µl with DNase RNase-free water (Invitrogen Gibco), and the mix heated to 65°C for 5 minutes, transferred to ice and centrifuged for 15 seconds at 14000 rpm in a microfuge. A solution comprising the following components was prepared: 1x buffer, 0.1 M DTT, RNase Out (Promega) and

Superscript. After centrifugation, 8 μl of this solution was added to the RNA, primer and dNTPs. The mix was incubated at 25°C for 10 minutes, 42°C for 90 minutes and 70°C for 15 minutes in a thermocycler.

2.8.4 β-actin PCR

To confirm that the reverse transcriptase reaction had worked, PCR reactions for β-actin were performed. The sequences of these primers were as follows:

Forward 5′ GTCACCAACTGGGACGACA 3'

Reverse 5′ TGGCCATCTCTTGCTCGAA 3'

The 1x reaction mix was prepared as follows: Taq buffer, primers (33 μM), dNTP's (10 mM), $MgCl_2$ (50 mM), Taq polymerase, cDNA and DNase RNase-free water to 50 μl. The PCR cycle included an initial denaturation step (95°C for 2 minutes), followed by 38 cycles of 94°C for 20 seconds, 55°C for 30 seconds and 72°C for 60 seconds and a final incubation at 72°C for 5 minutes. Subsequently, 6 μl of a product was mixed with 2 μl 10x DNA gel loading buffer (Bioline), loaded onto a 1% agarose gel and electrophoresed in 1x Tris-borate-EDTA buffer (TBE) (see Appendix) at 60 V, for 45 minutes.

2.8.5 Agarose gel electrophoresis

Gel electrophoresis was used to analyse β-actin products. Powdered agarose (Bioline, London, UK) was dissolved by heating in 50 ml 1x TBE buffer supplemented with a fluorescent dye used for staining nucleic acids - ethidium bromide (0.5 μg/ml). The gel was set in the tank at RT and submerged in 1x TBE buffer containing ethidium bromide (0.5 μg/ml). Nucleic acid samples were combined with 1 μl of 6x gel loading dye (New England Biolabs, UK) and loaded into sample wells alongside the DNA molecular weight ladder (New England Biolabs, UK). Samples were subjected to electrophoresis at 80 V for 40 minutes and the gel visualised by UV illumination using bio imaging unit (Geneflow, UK).

2.8.6 Real-time PCR

2.8.6.1 Measurement of gene expression.

Reactions were performed using an ABI Prism 7700 sequence detector (Applied Biosystems) using the SensiFast SYBR Hi-Rox kit (Bioline, UK). Thermocycler conditions were 50°C for 2 minutes, 95°C for 10 minutes, followed by 44 cycles of 95°C for 15 seconds and 60°C for 1 minute. Each PCR reaction contained 900 nM gene specific 5′ and 3′ primers: VEGF (Hs_VEGFA_1_SG), GLUT1 (Hs_SLC2A1_1_SG), LDHA (Hs_LDHA_1_SG) (all from Qiagen), 1x SensiMix™ SYBR Low-ROX MasterMix (Bioline) (containing pre-optimized dNTPs, $MgCl_2$, molecular probe and ROX dye), and cDNA (1 μl) in a total volume of 20 μl with

dH_2O. Three biological replicates were used for each of the target genes, with each individual assessed in triplicate. Results were normalised to the internal reference gene 18S rRNA. Control 18S reactions contained 50 nM 18S 5′ and 3′ primers (Sigma), SensiMix™ (Biolone) and cDNA in a total volume of 20 μl.

2.8.6.2 Q-PCR data analysis.

Q-PCR data was first analysed using ABI Prism 7000 software (Applied Biosystems) according to manufacturer's guidelines. Briefly, cycle threshold (CT) values were determined for both 18S internal control and genes of interest in each sample by placing a threshold line over the exponential phase of the PCR cycle profiles. The average CT values were calculated from the duplicates. The 18S internal control value was then subtracted from the value for the gene of interest to give ΔCT values. This value was converted to fold change in gene expression relative to control using the equation:

$$\text{Fold change} = 2^{-\Delta\Delta CT}$$

and fold change was converted to percentage expression relative to control via multiplication by 100. The average and standard error of the mean of samples were calculated.

2.9 Protein analysis: western blotting

2.9.1 Protein extraction and quantification.

For protein extraction, $2.5x10^7$ cells were resuspended in 150 μl RIPA buffer (see Appendix), supplemented with 1x protease inhibitor (Sigma), and incubated for 30 minutes on ice prior to centrifugation at 14000 rpm at 4°C for 10 minutes in a microfuge. The supernatant was transferred to a 1.5 ml centrifuge tube and frozen at -20°C.

For protein quantification, the Dc protein assay protocol (Bio-Rad, Hemel Hempstead, U.K.) was followed according to manufacturer's instructions. Briefly, 5 μl BSA standards (0, 0.625, 1.25, 2.5, 5 and 10 mg/ml) were added to duplicate wells of a 96 well plate and 2 μl of each protein sample were added to 3 μl distilled water in replicate wells. 20 μl reagent S was added to each ml of reagent A required to make solution 'A', and 25 μl A' added to each well. Reagent B (200 μl) was then added to each well, wells were mixed and the reaction allowed to develop for 15 minutes before the optical density was measured at 645 nm, using a plate reader.

2.9.2 Sample preparation and protein separation by sodium dodecyl sulphate – polyacrylamide gel electrophoresis (SDS PAGE).

Protein samples (20-40 μg) were mixed in a 3:1 ratio with 4x SDS gel loading buffer (see buffer and recipes in Appendix), heated to 100°C for 10 minutes in boiling

water. A 10% resolving gel mix was prepared (see Appendix) and allowed to fully polymerise at RT for 40 minutes prior to the addition of the stacking gel; prepared as described in Appendix. Protein samples, and 5 µl pre-stained precision dual stained markers (Bio-Rad) were loaded onto the gel and electrophoresed at 150 V with 1x SDS gel running buffer for 90-100 minutes.

2.9.3 Protein transfer

The polyvinylidene difluoride (PVDF) membrane (Millipore, Watford, U.K.) was soaked in methanol (Fischer) for 2 seconds, dH_2O for 2 minutes and equilibrated in transfer buffer (see Appendix) for 10 minutes. Semi-dry transfer was carried out using four layers of pre-transfer buffer-soaked 3 mm paper (Fischer) on the cathode and anode and the transfer was carried out using a Mini-Protean transfer tank (Bio-Rad) at 25 V for 1 hour.

2.9.4 Immunodetection of proteins

The membrane was rinsed in TBS-T (see buffer and recipes in Appendix) and then blocked for 45 minutes in 5% blocking solution (see Appendix). Primary antibody was diluted (according to table 2.2) in 5% blocking solution and the membrane was incubated overnight at 4°C with rocking. On the following day, the membrane was washed three times for 5 minutes in TBS-T and incubated for 45 minutes at RT, with rocking in the 5% blocking solution with the secondary antibody

(horseradish peroxidase (HRP)) diluted according to Table 2.2. Then the membrane was washed as above and signal developed using Supersignal West Pico Chemiluminescent substrate (Pierce, Northumberland, U.K.) and signal detected by exposure to Xomat scientific imaging film (Kodak, Sigma) for 5 minutes. Films were developed using an AGFA CURIX 60 (Agfa, Mortsel, Belgium). Equal loading was checked using mouse anti-human β-actin antibody (Sigma) and secondary rabbit anti-mouse following the same protocol (dilutions 1 in 10000 for each).

Table 2. 2. Antibodies used for the western blot analysis

Antibody	Source	Company	Cat no.	Dilution
Anti-HIF-1α	mouse	BD Biosciences	610959	1:500
Anti-VEGF	rabbit	Abcam	ab46154	1:1000
Anti-GLUT1 (H-43)	rabbit	SantaCruz Biotechnology	sc-7903	1:1000
Anti-β-actin	mouse	Sigma	A2228-100UL	1:10000
Anti-rabbit	goat	Sigma	A6154-1ML	1:1000
Anti-mouse	goat	Sigma	A2554-1ML	1:1000

2.10 Investigation of oxidative stress

2.10.1 Assessment of accumulation of Reactive Oxygen Species (ROS)

Carboxy-H2DCFDA (H2DCFDA) (Invitrogen Molecular Probes, Paisley, U.K) binds to all ROS and was dissolved in dimethyl sulfoxide (DMSO) to yield a 2000x stock, of 10 μM. This was aliquoted into 10 μl volumes and was stored at -20°C. Immediately prior to use, a 1 μM working dilution was made in warm RPMI medium. 500 μl of cell suspension was placed in the FACS tube and 5 μl of medium with H2DCFDA was added, mixed and incubated at 37°C, for 40 minutes. Immediately after the incubation, FACS tubes were analysed.

2.10.2 Assessment of accumulation of Mitochondrial Superoxide

MitoSOX Red (Invitrogen Molecular Probes, Paisley, U.K) was used to assess the presence of mitochondrial superoxide (mitosox) in cells, according to the manufacturer's instructions. Briefly, 1 ml of warm PBS was added to 200 μl of cell suspension and centrifuged at 1500 rpm for 5 minutes. The supernatant was removed and a vial of MitoSOX Red was diluted in 13 μl of DMSO to yield a 10 mM stock. A working stock of 10 μl MitoSOX Red was prepared in warm PBS (Invitrogen Gibco) and this was added to the cells, prior to incubation at 37°C for 10 minutes.

2.11 Treatments of CLL cells with inhibitors

Stock solutions of inhibitors in DMSO were aliquoted and stored at −80°C prior to use. For cell treatment, these stock solutions were diluted 1:1000 in medium to a final DMSO concentration of 0.1%.

2.11.1 HIF-1α inhibition with Chetomin

Cells were pre-treated for 3 hours with 0.1 μM, 1 μM and 5 μM chetomin (CTM) dissolved in DMSO. In order to obtain hypoxic conditions, cells were incubated in the hypoxic incubator (Mini Galaxy A, O_2 control) with 1% O_2 and 5% CO_2 at 37°C for 24 hours.

2.11.2 Alanine aminotransferase inhibition with cycloserine and β-chloro-l-alanine.

Cells were treated with two concentrations of cycloserine and β-chloro-l-alanine: 10 μM and 250 μM for 24 hours in normoxia and hypoxia.

2.11.3 Pyruvate cellular transporter (MCT1) inhibition with CHC

Alpha-cyano-4-hydroxycinnamate (CHC) (Sigma) was dissolved in DMSO and used at 2 mM and 5 mM concentrations. Cells were pre-treated for 3 hours before transfefrring into hypoxic conditions.

2.12 HRP chromogenic staining of cytospins

2.12.1 Staining

After spinning and drying, of the cytospins, they were fixed for 10 minutes in cold acetone and air dried. Then the spot of cells was circled with a hydrophobic pen to create a barrier and 80 µl of peroxidase block was added and incubated at RT protected from light for 10 minutes. Following this, the cytospins were rinsed twice in fresh wash buffer for 3 minutes each time followed by incubation with 80 µl of FcR block at RT protected from light for 10 minutes. Next, cytospins were rinsed twice in fresh wash buffer for 3 minutes each time.

Primary HIF-1α antibody (Sigma) was diluted 1:100 in Dako Antibody Diluent, applied on the slides and incubated for 30 minutes at RT, protected from light. Then cytospins were rinsed as previously. Secondary Antibody – Anti rabbit/mouse HRP Dako premade solution, was applied on the slides, incubated for 30 minutes at RT protected from light and rinsed as previously. Chromogenic developer was then prepared using 20 µl of stock added to 1 ml of diluent and added to each slide separately and incubated at RT for up to 10 minutes while monitoring under a microscope. Once clear staining was seen or high background developed, the solution was rinsed off by dropping slides into fresh buffer.

2.12.2 Counterstain

Slides were immersed in haematoxylin for 15 seconds, then rinsed in Scotts water, freshened and rinsed again. Subsequently, slides were dipped in acid alcohol wash for less than 5 seconds and rinsed well in Scotts water, then rinsed with running tap water for 30 seconds-1 min.

2.12.3 Dehydration and Mounting

Cytospins were immersed twice in 50% ethanol, twice in 70% ethanol, once in 96% ethanol for 3 minutes, once in 96% ethanol for 2 minutes, twice in 98% ethanol for 2 minutes each and once in 100% ethanol for 2 minutes. Then cytospins were air dried and mounted with the coverslip using mounting medium (Dako).

2.13 Fluorescent staining of cytospins

After spinning and drying, the cytospins were fixed for 10 minutes in cold acetone and air dried. Then the cells spot was circled with a hydrophobic pen to create a barrier and 80 μl of donkey serum (Jackson ImmunoResearch) was added and incubated at RT protected from light for 10 minutes. Then the cytospins were rinsed twice in fresh wash buffer for 3 minutes each time followed by 30 minute incubation at RT protected from light with first primary antibodies: rabbit anti HIF-1α (Sigma) diluted 1:100 (see table 2.3). Next, cytospins were rinsed twice in fresh wash buffer for 3 minutes each time. Secondary antibody – donkey anti rabbit

(Jackson ImmunoResearch) was applied on the slides, incubated for 30 minutes at RT protected from light and rinsed as previously. Cytospins were then stained with PAX-5 which is a B cell marker. The procedure was the same as previously, IgG control was stained with anti-goat antibody. All the antibody dilutions are presented in table 2.3. After the last wash, cytospins were mounted to the coverslips using the ProLong® Gold anti fade reagent with DAPI dye, staining the nuclei of cells (Life Technologies).

Table 2. 3. Antibodies used for cytospin staining

Antibody	Source	Company	Cat no.	Dilution
Anti-HIF-1α	rabbit	Sigma	HPA001275	1:100
Human Pax5/BSAP	goat	R&D systems	AF3487	1:10
Normal rabbit IgG	rabbit	R&D systems	AB-105-C	1:100
Normal Goat IgG	goat	R&D systems	AB-108-C	1:10
Anti-Rabbit HRP	goat	Dako	P 0448	premade solution
Anti-Rabbit	donkey	Jackson ImmunoResearch	711-001-003-JIR	1:100
Alexa Fluor® 568 Donkey Anti-Goat	donkey	Life Technologies	P36930	1:100

2.14 Statistical analysis of experiments

Normal distribution and homogeneity of variance of all data sets was assessed by Shapiro-Wilk and Levene's tests respectively using SPSS version 16 software. All the data were normally distributed and displayed homogeneity of variance. Statistical significance was assessed using the student's t-test for paired data, calculated using the statistics package within Microsoft Excel™. p values below 0.05 are indicated by * as described in the legends of figures.

2.15 MetaboLab routines used for data analysis

Together with the progress of the project, development of MetaboLab was carried out. The HSQC library of chosen metabolites was built, based on the HMDB data.

2.15.1 MATLAB scripts

In order to perform the analysis of the time course NMR spectra, specific MATLAB scripts were created.

2.15.1.1 Scale TMSP

Scale TMSP height script has been used to scale all of the TMSP signal heights from the time course experiment to 1. This enabled us to compare peak heights in the different experiments as well as overcome the line width instability between spectra of the same time course. TMSP is the reference point for 0 ppm.

```
function scale_tmsp_height(stepsize)

if(nargin<1)
    stepsize = 1;
end

global NMRDAT
global NMRPAR

s = NMRPAR.CURSET(1);
e = NMRPAR.CURSET(2);

ref  = NMRDAT(s,1).PROC(1).REF;
nexp = NMRDAT(s,1).ACQUS(1).NE;

for k = 1:nexp
    NMRDAT(1,k).MAT       = NMRDAT(1,k).MAT/NMRDAT(1,k).MAT(ref(2));
    NMRDAT(1,k).DISP.PLOT = 0;
end

for k=1:stepsize:nexp
    NMRDAT(1,k).DISP.PLOT=1;
end
```

2.15.1.2 Peaking shifting peaks

This script was built in order to pick all of the peaks from the time course dataset, including shifting peaks (like histidine), crossing through other peaks.

```
% pick the first spectrum and transfer, then


nspc = 147;

pp = {};

for k = 1:147
    pp{k} = NMRDAT(1,k).MANINT;
end

% then pick last spectrum and transfer, then
% determine until which spectrum it's fine (83)


for k = 1:100
    NMRDAT(1,k).MANINT = pp{k};
end
```

2.15.1.3 Fit pH curve

The "fit pH curve" script was built in order to create pH curves from the differences of the chemical shifts of histidine peaks from 21 spectra, acquired on the medium samples with differing pH (3.5-8.5).

```
nPeaks = 2;
nSpc   = 21;
pH     = [8.5, 8.25, 8, 7.75, 7.5, 7.25, 7, 6.75, 6.5, 6.25, 6,
5.75, 5.5, 5.25, 5, 4.75, 4.5, 4.25, 4, 3.75, 3.5];
fitfun = '(10.^(t-pk)*DB+DA))./(1+10.^(t-pk))';



%-------------------------------------------

ppm    = zeros(nSpc,nPeaks);
for k = 1:nSpc
    ppm(k,:) = NMRDAT(1,k).MANINT.peakMaxPPM;
end

diffData = abs(diff(ppm')');
pars     = parse_command_string(fitfun,1);

fitpars = zeros(1,length(pars));
for k = 1:length(pars)
    fitpars(k) = pars(k).value;
end

opts                    = optimset();
opts.MaxFunEvals         = 1e7;
opts.MaxIter             = 1e7;
opts.TolFun              = 1e-7;
opts.TolX                = 1e-7;


[par_eval, fval, status] =
fminsearch(@gen_fit,fitpars,opts,pH,diffData,fitfun,pars);
[chi2,simFct]            = gen_fit(par_eval,t,data,fitfun,pars);


figure
```

2.15.1.4 Calculate pH

In order to get the value of the chemical shift differences (Δδ) between two histidine peaks for each spectrum automatically, the following script was used.

```
nspc = 144
;


shifts = zeros(nspc,2);
for k = 1:nspc
    shifts(k,:) = NMRDAT(1,k).MANINT.peakMaxPPM;
end
difference = diff(shifts')';
```

Subsequently the series of Δδ was inserted in the pH curve equation to obtain the pH value for each NMR spectrum.

2.15.1.5 Calculate percentage of keto and enol form of pyruvate

In order to calculate percentage of keto and enol form of pyruvate at any particular time point of the time course, the following script was used. This script combines the information about the pyruvate tautomers together with the pH values.

```
% Pick 4 peaks (Keto/Enol-Pyruvate and the 2 Histidine signals)

global NMRPAR
global NMRDAT
global extractPeaks


s = NMRPAR.CURSET(1);
e = NMRPAR.CURSET(2);

nspc = NMRDAT(s,1).ACQUS(1).NE;
t    = extractPeaks(1).t;
t    = t(:);


shifts = zeros(nspc,4);
```

```
for k = 1:nspc
    shifts(k,:) = NMRDAT(s,k).MANINT.peakMaxPPM;
end


pHshifts = shifts(:,3:4);
deltaCS  = diff(pHshifts')';


ph = 5.49 + log10((deltaCS - 1.272)./(0.7004-deltaCS));

pyr1 = extractPeaks(2).peak(1).expInt;
pyr2 = extractPeaks(2).peak(2).expInt;

enolPyruvate = 100*pyr2./(pyr1+pyr2);
enolPyruvate = enolPyruvate(:);
ketoPyruvate = 100*pyr1./(pyr1+pyr2);
ketoPyruvate = ketoPyruvate(:);


%figure; plot(ph,enolPyruvate);
%title('pH vs enol %')
%print -dpdf pyruvate_ph_vs_enol.pdf
%plot(t,ph);
%title('pH over time')
%print -dpdf pyruvate_ph_over_time.pdf
plot(t,enolPyruvate,'b-',t,ketoPyruvate,'r-');
title('Keto-r-/Enol-b- % over time')
%print -dpdf pyruvate_enol_over_time.pdf

data = [t'; ph'; enolPyruvate'; ketoPyruvate'];

csvwrite('pyruvate_ph_data.csv',data);
```

Chapter III

Establishing NMR method to measure metabolic changes in living CLL cells

3.1 INTRODUCTION

Metabolomics has been widely used to examine the metabolic phenotype of cells, usually exploiting either hydrophilic or lipophilic extracts (Gromova and Roby 2010; Fernando, Bhopale et al. 2011). Performing time course analyses in this way requires large amounts of biological material, which is a limiting factor for studies using primary human cells. However, NMR represents a non-invasive analytical method that is, in principle, able to analyse the metabolism of living cells, and monitor its dynamics over extended periods of time in a single batch of cells.

NMR is a powerful tool that can be used to monitor labelling patterns in key metabolic intermediates, which can be used to calculate fluxes in mammalian tissues (Griffin and Corcoran 2005). While metabolomics measures static metabolite concentrations, metabolic flux analysis observes the flux of individual atoms across metabolic networks employing isotopically labelled metabolic precursors such as glucose and glutamine as tracers. However, because of the limited sensitivity of ^{13}C NMR, it has not been widely applied to the study of isolated cells in culture. Such studies require a very large number of cells to fill the sample volume of an NMR tube. A number of different methods have been used to immobilise dense cultures of cells inside an NMR tube. A key parameter that must be considered with any cell immobilisation technique is the transport of metabolites and nutrients. Oxygen can be particularly problematic, because it is poorly soluble in aqueous media. In dense

masses of cells, metabolic rates are often limited by the rate of oxygen diffusion. Such limitations can hinder the determination of the true intrinsic metabolic characteristics of a population of cells. To avoid such limitations either the diffusion distance in the cell mass must be short, or the density of the cell mass must be relatively low. It has previously been shown that the metabolism of human cancer cells can be monitored using NMR perfusion systems with various adherent cell lines grown on microcarrier beads. Methods involving microcarriers can be used with cell lines, where the amount of biological material can easily be multiplied. In published experiments, 3-8x10^8 cells grown on beads were used, filling a 20 mm NMR tube (Pianet, Canioni et al. 1992). Similar methods have been used for the metabolic flux analyses in glioma cells after enriching the metabolic substrates with ^{13}C labels. Microbeads were mixed with SF188 cells at a ratio of 10^7 cells per gram (DeBerardinis, Mancuso et al. 2007). As the cells usually need to grow in the microcarriers for 8-9 days, this method can be effectively used solely with cells that proliferate and adhere to microbeads (Mancuso, Beardsley et al. 2004; Mancuso, Zhu et al. 2005).

As a result of the non-invasiveness of NMR, in-cell NMR is widely used for protein investigation. This method allows for the determination of the conformation and functional properties of proteins inside living cells (for example *Xenopus laevis* oocytes) (Selenko and Wagner 2007).

Despite well-developed systems for measuring metabolites using proliferating, adherent cells, little has been reported on NMR metabolomics using quiescent, suspension cells. A "continuous cell cultivator" providing convective oxygen and nutrient transport was constructed for ^{31}P NMR experiments using *Saccharomyces cerevisiae* where large amounts of cells can easily be grown (Meehan, Eskey et al. 1992). More recently, a perfusion small-scale bioreactor for on-line monitoring of the cell energetic state was developed for free-suspension mammalian cells (Chinese hamster ovary cell line) (Ben-Tchavtchavadze, Chen et al. 2010), however, no metabolomics work on human suspension cells has been published to date.

In order to investigate the metabolism of primary CLL cells which are non-dividing, an NMR system for cells in suspension that does not require microcarriers, perfusion systems or large amounts of cells, was developed. In order to suspend cells evenly in the NMR tube and for the duration of the experiment, cells were embedded in a medium-agarose matrix. To monitor the oxygen concentration in the tube, an oxygen sensor was used and the pH was calculated using the histidine resonances (as described in materials and methods).

3.2 RESULTS

3.2.1 1D ^{1}H NMR spectrum of living CLL cells

A typical 1D ^{1}H-NMR spectrum obtained from $5x10^{7}$ CLL cells is shown in Figure 3.1. NMR spectra were obtained with a time resolution of 7-10 minutes over 24 hours permitting a well-resolved time course of metabolic activity. The spectrum contains signals of > 30 metabolites, of which alanine, glutamate, formate, hypoxanthine, uridine, pyroglutamate, phosphocholine, pyruvate, succinate, lactate and 3-hydroxybutyrate (3-HB) arise from the cells. Some peaks such as hypoxanthine or 3-HB were visible only after a few hours of running the experiment. The rest of the assigned peaks were the ingredients of the RPMI medium or their derivatives. Around 10 resonances were not assigned owing to the lack of corresponding signal assignments in existing metabolomics spectral libraries. Signals which were difficult to distinguish due to signal overlap were not assigned (with the exception of pyruvate). Some metabolites were pH sensitive (such as histidine), resulting in changing chemical shifts during the time course, as the extracellular pH was changing, which made them difficult to categorise. One of the unassigned peaks placed at 5.06 ppm was increasing over time in all the samples.

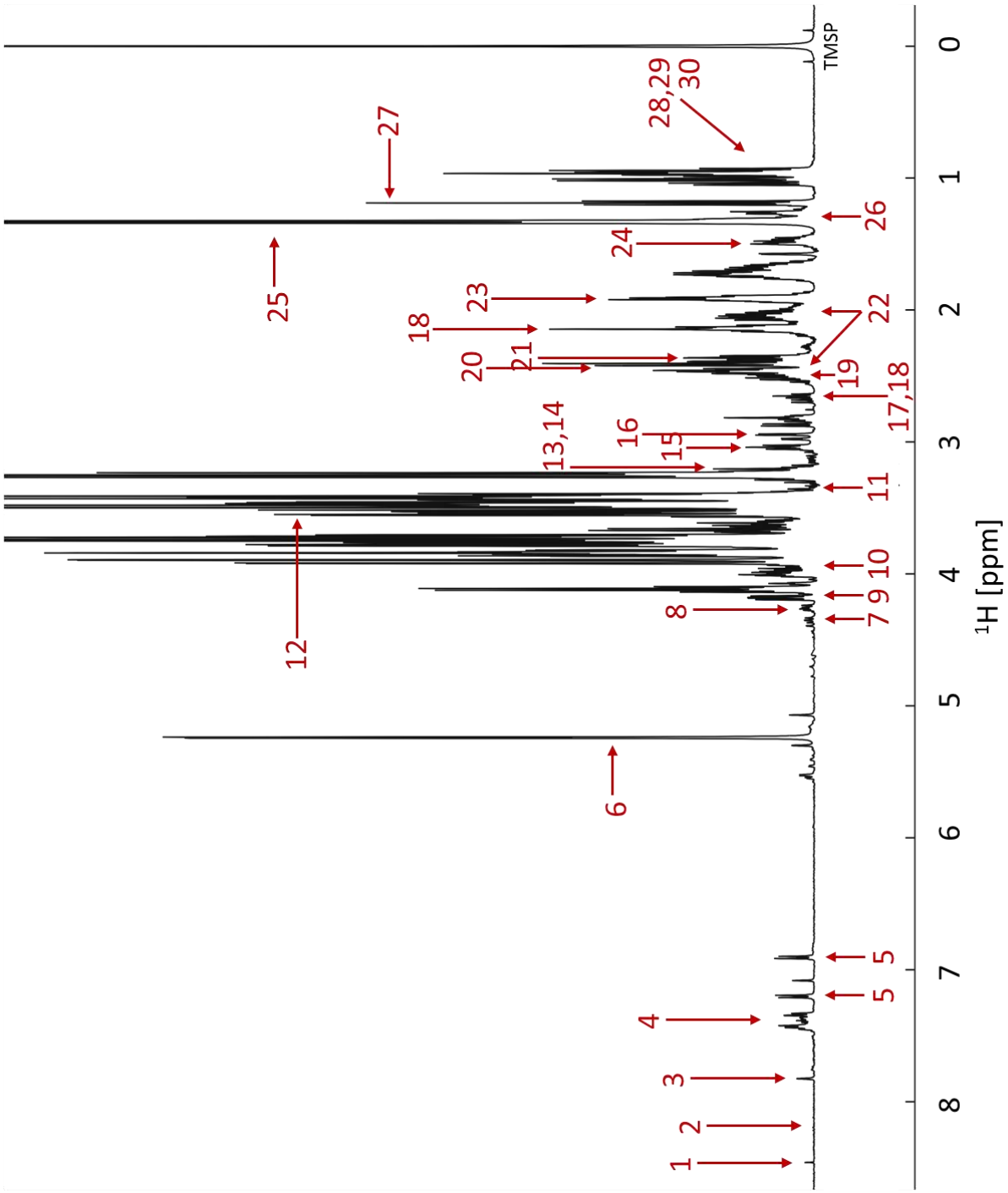

Figure 3. 1. 1D ^{1}H NMR spectrum of CLL cells.

Metabolites assigned: 1-formate, 2-hypoxanthine*, 3-histidine, 4-phenylalanine, 5-tyrosine, 6-glucose, 7-trans-4-hydroxyl-L-proline, 8-uridine, 9-pyroglutamate, 10-serine, 11-myo-inositol, 12-glycine, 13-phosphocholine, 14-choline, 15-lysine, 16-asparagine, 17-aspartate, 18-methionine, 19-glutamine, 20-succinate, 21-pyruvate, 22-glutamate, 23-arginine, 24-alanine, 25-lactate, 26-3-hydroxybutyrate, 27-ethanol, 28-valine, 29-isoleucine and 30-leucine.

* hypoxanthine was detectable after a few hours of the time course.

In order to confirm the assignment of the most abundant peaks, the agarose matrix and cells were removed by centrifugation, the pH of the medium was re-adjusted to 7.0 and placed back in the NMR tube to acquire another 1D NOESY, 2D $^{1}H^{1}H$ J-resolved (J-res) and 2D $^{1}H^{13}C$ HSQC spectrum (Figure 3.2). J-res spectra were analysed using automatic metabolic quantification – FIMA (Field Independent Metabolic Analysis) through the online service at http://www.bml-nmr.org/. The major advantage of using two-dimensional NMR spectra is the reduction of signals overlap due to the introduction of a second independent chemical shift axis. In J-res spectra reduction of overlap is achieved by the ability to create a proton decoupled 1D spectrum, which has less overlap compared to a normal 1D proton spectrum.

3.2.2 Viability of CLL cells was not affected by the NMR experiment

High cell viability was maintained during NMR measurements, as proven by flow cytometric Annexin V / Propidium Iodide analyses of cell death and apoptosis, and confirmed by cell morphology (Figure 3.3). The ability to recover viable cells after the time course experiment allowed cells to be used for parallel analyses such as Western Blotting and PCR.

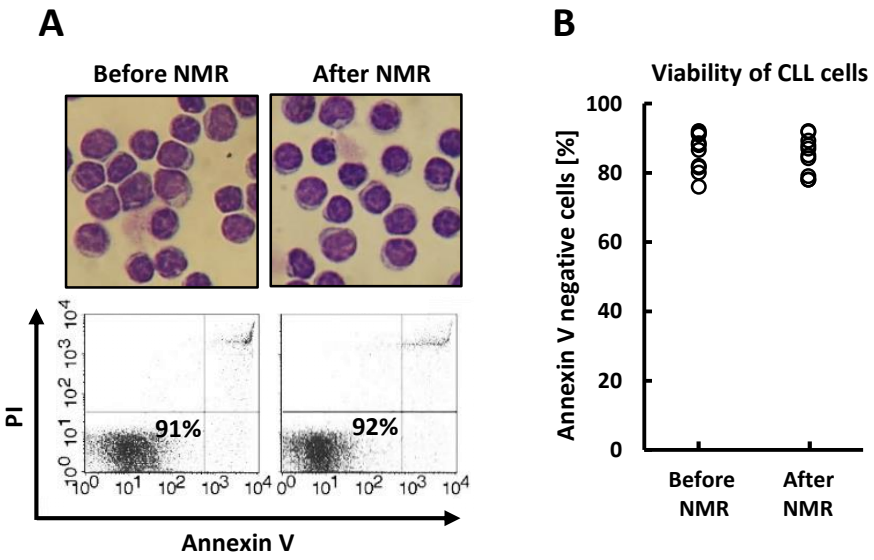

Figure 3. 3. CLL cells can tolerate NMR analyses.

A) Representative image of CLL cells before and after the NMR experiment, stained using Jenner-Giemsa stain and representative scatter plot for Annexin V/PI staining of CLL cells before and after NMR measurement. Lower left corner: healthy cells which are both propidium iodide and annexin V negative. B) Viability data for 10 primary CLL samples.

3.2.3 Changes can be seen in the intensity of metabolites

NMR time course analyses showed changes of the intensity of some metabolites. The most profound increase was exhibited by lactate peaks (δ: 1.31; 1.324 ppm) visible as an orange peak on the Figure 3.4 A. The most visible decrease of intensity was observed by the signals of glucose (the majority of peaks between 3.2-4 ppm) clearly visible in the 2D spectrum in Figure 3.4 A. In order to investigate whether the changes seen were the result of the metabolism of CLL cells, a control time course was recorded on the sample containing RPMI medium and agarose only (Figure 3.4 B). Looking at both, the 3D projection and the overlaid first (red) and last (blue) spectra, it appeared that there were no changes in metabolite concentrations and the signals were stable over the 24 hours. Moreover, the lactate peak was not detected in the control sample. Results from control spectra recorded without cells confirmed that the observed changes in intensities arose from the metabolic activity of the CLL cells.

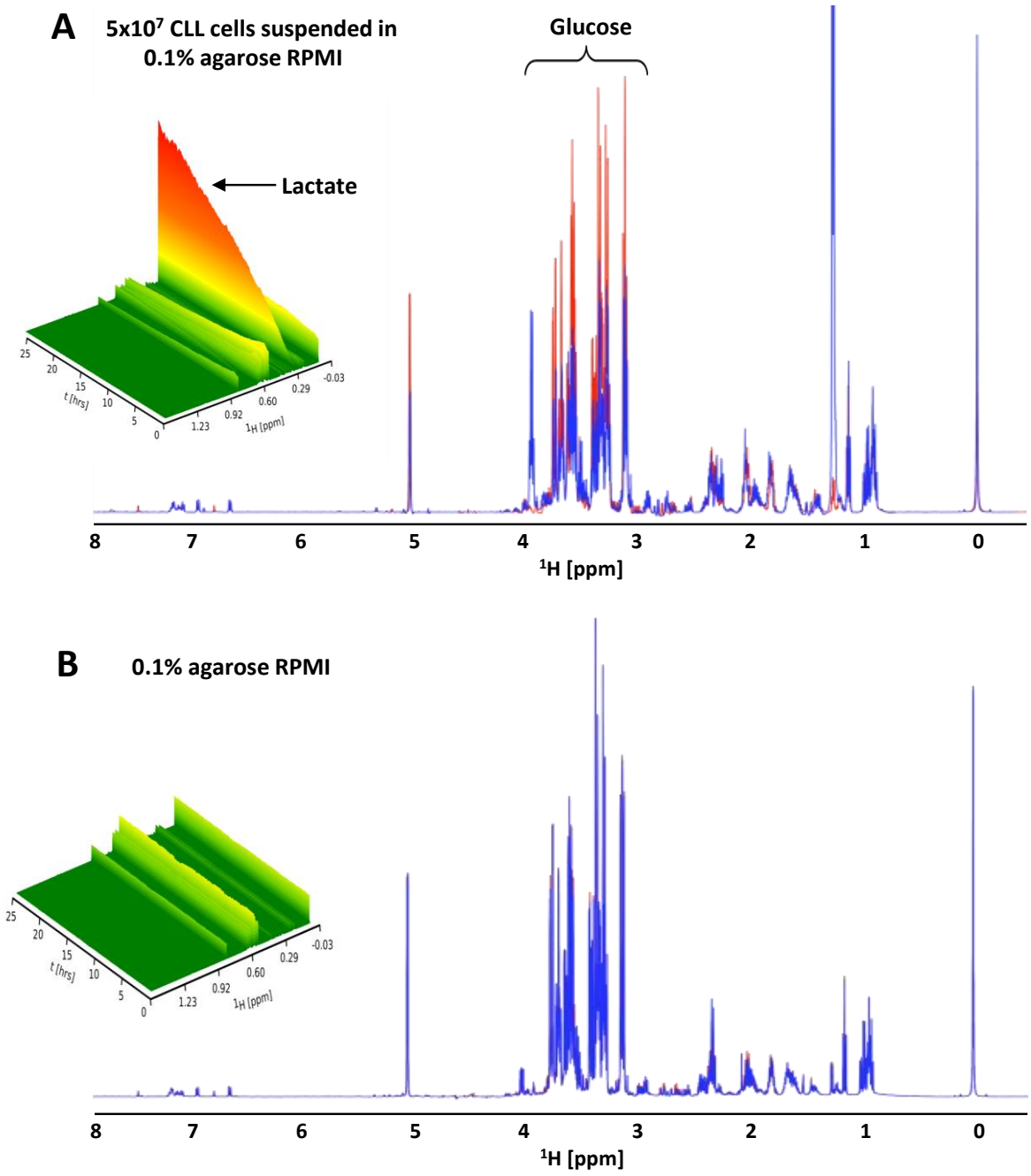

Figure 3. 4. Changes in the NMR spectrum are the result of metabolic activity of CLL cells.

3D view of the NMR time course experiment. The sample contains A) $5x10^7$ CLL cells/ml suspended in RPMI medium with ITS^+ and 0.1% low melting agarose; B) control sample without CLL cells. The largest signal coloured orange corresponds to lactate which is increasing over time. Superimposed first (red) and last (blue) ^1H spectra of the 24 hour time course show the most profound decrease for glucose in the CLL sample.

In order to find out if any of the metabolites observed arose from the intracellular environment the spectrum of medium with CLL cells in agarose was compared with spectrum of medium alone retrieved from the supernatant after spinning down the agarose and cells. Figure 3.5 shows that the superimposed spectra are overlapping, suggesting that all the metabolites seen in the sample with cells are largely extracellular. Slight differences between some peaks are the consequence of pH dependent shift. The fact that we were not able to see signals of metabolites inside cells may be due to the small volume of cells (3-5 μl) compared to the total sample volume (550 μl). Because the biomass is so small, we also do not see lipids which would not be secreted from cells in large amounts.

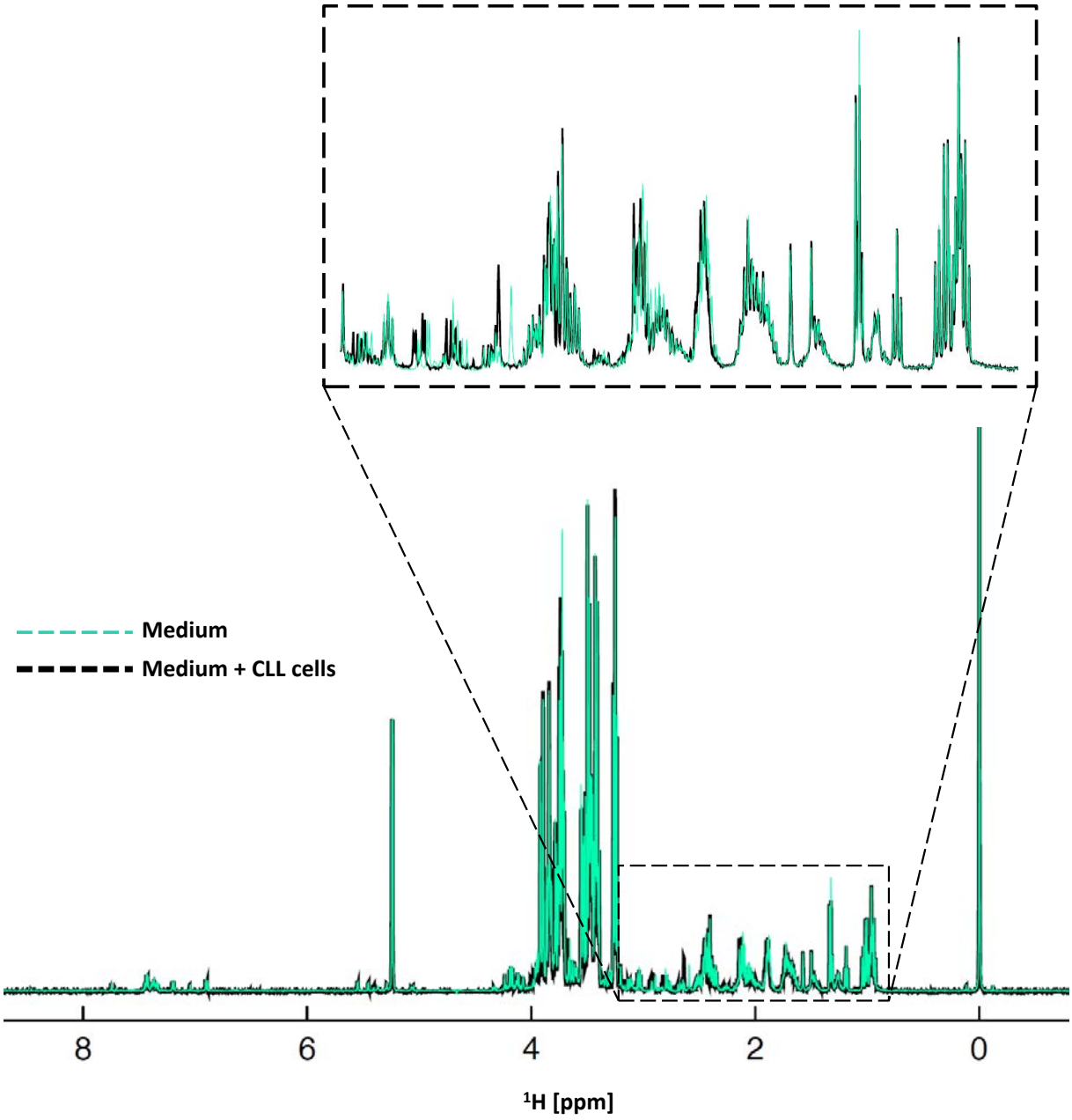

Figure 3. 5. Spectrum of CLL cells in medium with agarose overlaid with spectrum of medium alone.

The black spectrum is the last spectrum of $1x10^7$ CLL cells embedded in RPMI medium supplemented with 1% ITS$^+$ and 0.1% low melting agarose. After acquiring the spectrum, sample was spun down so that pellet contained agarose and cells. Medium supernatant was transferred back to the NMR tube and spectrum (shown in teal colour) was obtained. The line width of the black spectrum was broadened for the better visibility. Fragment from 0.5- 3.5 ppm was enlarged and presented in the top rectangle.

3.2.4 Changes of intensities of metabolite signals

In order to distinguish between signals which changes intensity and those that are stable over time course of 24 hours, sections from spectra representing several metabolites were compared (Figure 3.6). Colours move from red to blue over the time course. Signals of metabolites that were consumed by cells (such as glucose or glutamine) decreased over time, while those of metabolites secreted by cells (such as lactate, alanine, glutamate, hypoxanthine and 3-hydroxybutyrate) increased. Some metabolites showed up or downfield changes in their chemical shift caused by pH changes (such as histidine, glutamine and arginine). To allow for scaling of the spectrum to its frequency as well as to its intensity, for the comparison of different samples, it was crucial that the internal reference compound - TMSP, stayed stable throughout time course experiments. The stability of TMSP peak was achieved by shimming between the acquisition of subsequent spectra of the time course.

3.2.5 Apparently quiescent CLL cells show high metabolic activity

Peripheral blood CLL cells are out of cell cycle (Messmer, Messmer et al. 2005), have relatively scant cytoplasms (see Fig 3.3.A), and are generally considered to be quiescent (Calissano, Damle et al. 2011). Cell cycle analysis confirmed that all CLL cells were in the G_0 phase (Figure 3.7). Despite this, marked metabolic activity in these cells was observed, notably evidenced by increases in signals for lactate,

glutamate, alanine, 3-hydroxybutyrate and histidine (Figure 3.6) as well as consumption of glucose and glutamine.

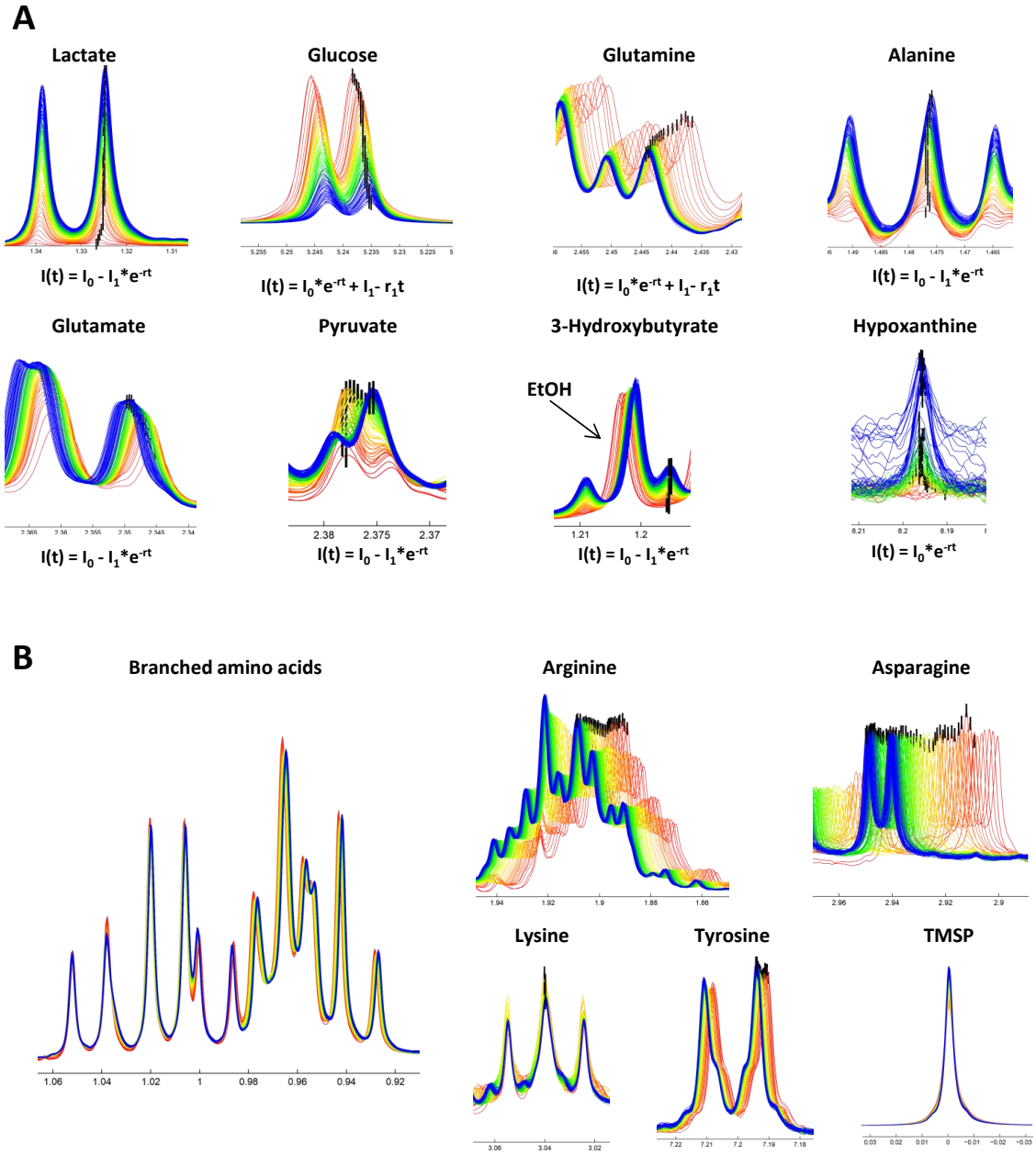

Figure 3. 6. Representative peaks for chosen metabolites, changes over time.

144 superimposed ^{1}H spectra recorded over 24 hours. Spectra are colour coded for the time course: the first spectrum is red, and the last one is blue. The equation under each spectral section indicates which formula was used for fitting kinetics for experimental data points. The equation below the pyruvate could only be used for the first phase where the signal grows. A) Metabolites the intensity of which changed over time; B) Metabolites the intensity of which reminded stable during 24 hour experiment. Some of the signals which are pH sensitive are shifting to the left or right. TMSP - internal standard.

3.2.6 Metabolic changes were not affected by the stabilisation of extracellular pH

As it would be expected, lactate production was associated with a progressive acidification of the medium. We used the chemical shift of histidine signals (Cohen, Motiei et al. 2004), which is a component of RPMI medium, to determine the *in situ* changes in pH during each acquisition. As shown in Figure 3.8, pH changed from ~7.8 to 6.5 over a 24 h time course and displayed a pattern which correlated with the accumulation of lactate (Figure 3.8 B). In order to stabilise the pH, medium with additional HEPES buffer was used. Experiments performed using RPMI medium with 25 mM HEPES demonstrated that lactate production was unaffected by the stabilisation of the extracellular pH (Figure 3.8). RPMI medium with HEPES buffer was not used routinely as HEPES signals obscured a large part of the spectrum (Figure 3.9).

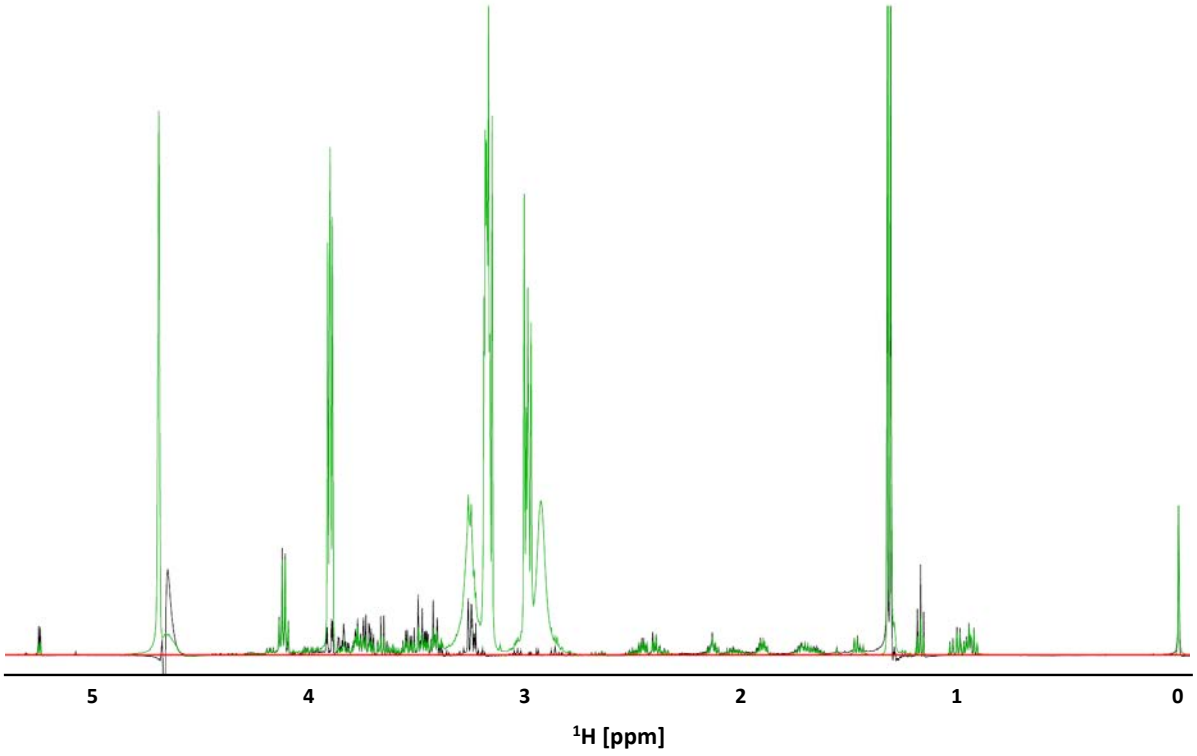

Figure 3. 9. Spectrum of RPMI with HEPES vs spectrum of standard RPMI.

The green spectrum was recorded using $1x10^7$ CLL cells in RPMI medium with 25 mM HEPES and the black one using $1x10^7$ CLL cells in the standard RPMI medium. The intense multiple peaks around 2.9, 3.2 and 3.75 ppm correspond to protons of HEPES.

3.2.7 Primary CLL cells survive extreme hypoxia

The external diameter of the glass tubes used for NMR analyses was 5 mm, with an inner diameter of approximately 4.2 mm, whereas the volume of the semi-solid culture was 550 μl. This large ratio of volume to surface area, in combination with the previously unrecognised high metabolic activity of CLL cells, suggested that oxygen within the cultures would be rapidly depleted. In order to investigate changes of oxygen levels over time a fibre optic oxygen sensor was placed in the agarose matrix during the spectra acquisition (see Figure 3.10 A). Oxygen measurements were recorded every 10 minutes parallel to each 1D NMR spectrum. These measurements indeed confirmed that oxygen was progressively and rapidly depleted and that CLL cells experienced profound hypoxia for the majority of each 24 hour exposure. The level of oxygen stabilised after reaching a value between 0.1-0.8%. The rate of oxygen consumption was cell number dependent, indicating that it was driven by cellular consumption (Figure 3.10 B). In experiments using $5x10^7$ cells/ml, oxygen was consumed within ≈70 minutes (Figure 3.10 B).

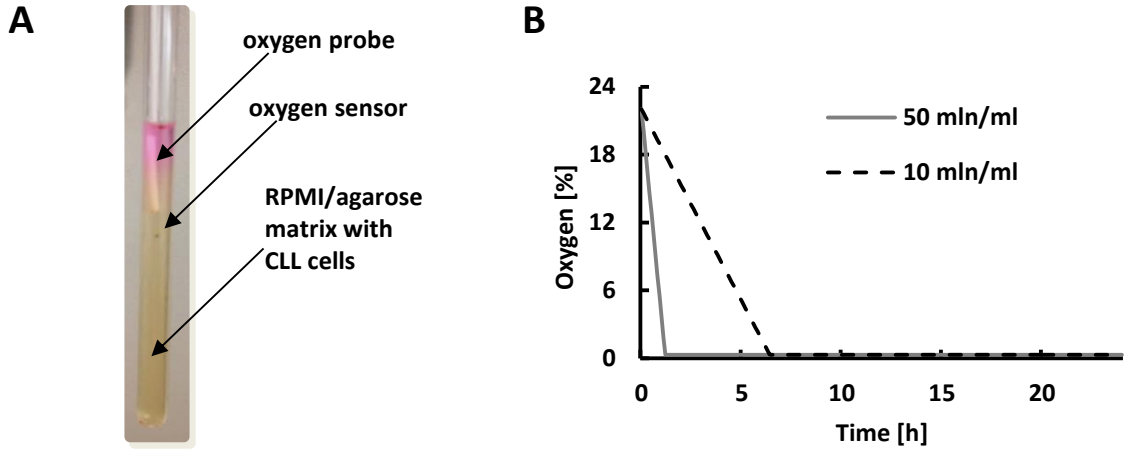

Figure 3. 10. Change of oxygen concentration over the time course experiment.

A) Fibre optic oxygen probe immersed in the NMR tube with CLL cells. B) Oxygen consumption for the samples containing $10x10^6$ cells/ml and $50x10^6$ cells/ml.

3.2.8 Kinetics of the metabolic changes

Real-time measurements of metabolites over 24 hours showed that production of lactate was associated with glucose consumption, as expected (Figure 3.11). Some CLL samples consumed glucose more rapidly than others. Concordantly, the production of lactate showed the greatest correlation with those samples that consumed the most glucose. The production of alanine also mirrored the extent of glucose consumption and lactate production. Similarly, the consumption of glutamine reflected glucose consumption and lactate production. Overall these observations appear to indicate that CLL may be divided into tumours with higher and lower metabolic states (Figure 3.11.A). Interestingly all the CLL samples

exhibiting lower metabolic activity came from patients diagnosed with the A0 stage of the disease whereas the rest of the patients were at more advanced stage at the time of sampling (See Table 3.1). However, there were too few patients to draw any statistically relevant conclusion about correlations between CLL cellular behaviour and clinical or prognostic markers.

Glutamate variably accumulated across all the samples with one sample displaying particularly marked accumulation. 3-Hydroxybutarate peaks were very close to the ethanol peaks (see Figure 3.6). In order to obtain the intensity values corresponding to 3-hydroxybutyrate only, the ethanol peak intensity values were subtracted from the overlapping peaks. Hypoxanthine, another increasing metabolite, was observed to be secreted only after a few hours of hypoxic conditions. Although the peak intensity was not very high, the increase was consistent for all the samples containing $5x10^7$ cells/ml and for some samples containing $1x10^7$ cells/ml. Other metabolites including lysine, arginine and valine were remarkably stable during the acquisition of spectra (Figure 3.11.B). Table 3.1 shows the patient characteristics for all of the primary CLL cell donors, compared in Figure 3.11.

As some metabolites are represented by multiple peaks seen in different parts of spectrum, it was crucial to show that individual peaks of the same metabolite exhibit identical kinetics. Figure 3.12 presents an example of lactate and glucose representative peaks, together with fitted kinetics.

Table 3. 1. Clinical characteristics of CLL patients.

CLL samples used to obtain data presented in Figure 3.11. Patients were attending the outpatient clinic at Birmingham Heartlands Hospital or Queen Elizabeth Hospital in Birmingham, UK.

Patient	Sex	Age (Y)	Stage	Additional clinical features	Leukocyte count	CD19+ at the time of sampling [%]	Length of time with disease	Treatment when sampled	Previous treatment
1	M	85	C	CD38 neg, Zap70 pos, Normal cytogenetics.	150	91	14y 3m	Observation	First treated with chlorambucil in 1998 then in 2012.
2	M	71	A0	CD38 neg	150	90	2y 11m	Observation	none
3	M	58	A0	CD38 neg	58	74	1y 9m	Observation	None
4	F	92	C	ATM, p53 WT. CD38 unknown	191	88	18y 2m	Chlorambucil	24/9/02 then 04/07/08 and 2012
5	F	76	B	ATM and p53 WT -	170	85	6y 1m	Observation	None. Progressive on that date though with sweats, LN and high WCC. No cytopenia
6	M	58	A	CD38 neg	58	80	1y 9m	Observation	None
7	F	77	A	nil	76	89	8y 9m	Observation	None. Had eyelid swelling but RT given locally after this date.
8	M	82	A0	nil	132	75	7y 9m	Observation	none
9	M	65	A	CD38 neg	147	59	2y 3m	Observation	none
10	F	92	A0	CD38 neg	60	76	18y 2m	Chlorambucil	none
11	M	83	A0	Additional 1q on karyotype. ATM, p53 WT	177	92.5	6y 11m	Observation	Previous FC in 2009 x 2 courses, BaP started week after this sample

LN; lymph node, RT; Rituximab, FC; Fludarabine and Cyclophosphamide, WCC; white cell count, BaP; The redeployed drug combination of bezafibrate and medroxyprogesterone acetate (Murray, Khanim et al. 2010)

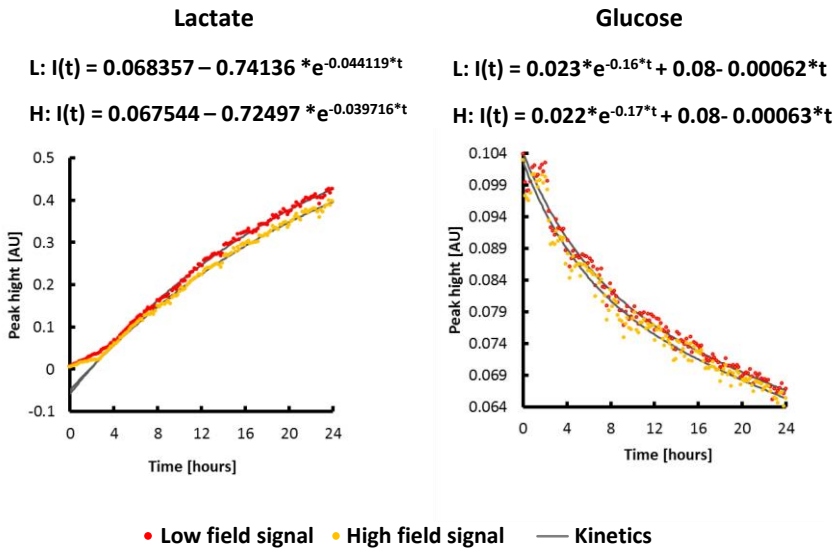

Figure 3. 13. Kinetics of different peaks corresponding to the same metabolite were similar.

Data points and fitted kinetics for two lactate and glucose signals. Kinetic parameters (L- low field signal, H- high field signal) are similar. Lactate: low field signal at 1.324 ppm and high field signal at 1.310 ppm; Glucose: low field signal at 5.226 ppm and high field signal at 5.220 ppm.

3.3 DISCUSSION

In order to measure changes in metabolism in living cells by NMR spectroscopy required to overcome two challenges. First, the NMR experiment needed to be designed in a way that does not affect the metabolism of cells. This is challenging for an experimental procedure, which is carried out away from the standard, sterile tissue culture conditions. Presented data confirm that CLL cells remained viable throughout a 24 h time course, and showed comparable viability to control cells incubated in the tissue culture incubator. Maintenance of cell viability allows to use cells for further analyses (here they were used for gene and protein expression assays). Secondly, to obtain good quality and informative NMR spectra two key requirements had to be fulfilled: a sufficiently high concentration of metabolites and good sample homogeneity. A lack of homogeneity causes broad lines in NMR spectra and therefore low spectral resolution. Broad lines would also be expected if the mobility was significantly reduced by embedding the sample in a gel matrix that significantly affects rotational diffusion of small molecules. Optimal spectra were obtained for 1-5x10^7 CLL cells/ml. While the concentration of cells does not directly affect metabolite concentrations, it does affect the rate of changes. Moreover, using the 0.1% low melting agarose matrix, with carefully suspended CLL cells yields good sample homogeneity over 24 h without causing any significant line

broadening. The low concentration of agarose gel does not disturb the free movements of metabolites in the suspension.

Comparison of spectra obtained from samples containing cells and medium without cells indicated that the observed metabolic changes were solely caused by the metabolic activity of CLL cells. A high similarity between the last spectrum of a time course and the spectrum of medium after removing cells indicates that the observed signals represent metabolites present in the medium and not inside cells. This may be a consequence of the small proportion of cell biomass in comparison to the total sample volume. It is also possible that metabolite signals inside cells are too broad to be observed. The sensitivity obtained from this method was sufficient to investigate metabolic kinetics of 30 of the most abundant metabolites.

The assignment of 30 metabolites was confirmed using 2D ^{1}H-^{1}H J-resolved (Ludwig and Viant 2010) and ^{13}C-^{1}H HSQC spectra. These spectra were recorded on medium obtained from the sample with CLL cells after the time course experiment. Because both J-res and HSQC libraries were acquired at 25°C and at pH=7.0, it is difficult to assign the spectra recorded with living cells as the pH changes during the experiment causing significant chemical shift changes.

The observed metabolic changes indicate that CLL cells consume both glucose and glutamine and produce large amounts of lactate as well as alanine and

glutamate. The metabolism of these compounds will be investigated and discussed in the next chapters.

Another metabolite secreted by CLL cells, 3-hydroxybutyrate represents a ketone body (together with acetone and aceto-acetate), an end product of fatty acid beta-oxidation. It allows the production of acetyl-CoA and provides a route whereby fatty acids can be utilised to provide energy via the TCA cycle. Ketone bodies can also be produced from excess acetyl-CoA which cannot be used by the citric acid cycle. This state is referred to as the fasted state in humans. Ketone bodies can also be produced from certain amino acids (leucine, isoleucine, lysine, phenylalanine, tyrosine and tryptophan). Ketone bodies have previously been reported to be implicated in carcinogenesis and can be seen as indicators of mitochondrial dysfunction (Kennaway, Buist et al. 1984; Robinson, McKay et al. 1985). Increased levels of 3-HB have been detected in the serum of patients with colorectal malignancy (Ludwig, Ward et al. 2009; Ma, Liu et al. 2009) as well as in patients with late stage head and neck cancer compared to early stage diseases (Tiziani, Lopes et al. 2009). On the other hand, lower levels of 3-hydroxybutyrate have been found in the serum of patients with pancreatic cancer compared to healthy controls (OuYang, Xu et al. 2011). It has recently been shown that administration of 3-HB in a xenograft model of breast cancer increased tumour growth 2.5-fold, and has been suggested that this finding may explain the increased incidence of cancer in diabetic patients,

due to increased ketone production (Bonuccelli, Tsirigos et al. 2010). Moreover 3-HB has been shown to act as a chemo-attractant, stimulating the migration of epithelial cancer cells (Bonuccelli, Tsirigos et al. 2010). It has been suggested that 3-HB detected in patient serum/plasma, or homogenates of fresh tumour tissue, might be useful as a marker to identify high-risk cancer patients at diagnosis, for treatment stratification and/or for evaluating therapeutic efficacy during anticancer therapy (Pavlides, Tsirigos et al. 2010). Elevated levels of ketone bodies in plasma can also be a result of accelerated catabolism of fatty acids (Laffel 1999), therefore 3-HB may be seen in samples of CLL cells, both as a product of starvation and as a fuel for the growth of the cancer.

Another increasing metabolite detected during time course experiments was the purine derivative hypoxanthine. Purine nucleotides are essential components of any cell, not only as the raw material for the synthesis of DNA but also being vital cofactors for many enzymatic reactions responsible for cell proliferation. Purine biosynthesis proceeds along two known routes. These include de novo synthesis and recycling of endogenous or exogenous purines through a salvage pathway.

The de novo pathway for purine nucleotide synthesis leads to the formation of inosine 5'-monophosphate (IMP) in ten metabolic steps and requires hydrolysis of ATP to drive several reactions along this pathway.

The salvage pathway involves the housekeeping protein hypoxanthine-guanine phosphoribosyl transferase (Hx-PRTase) which catalyses the addition of phosphoribosyl pyrophosphate to guanine or hypoxanthine to form guanosine monophosphate and inosine monophate respectively. In the absence of this pathway, hypoxanthine would proceed to form the waste product uric acid, through the formation of xanthine (Harrison 2002).

The salvage pathways are used to recover bases and nucleosides that are formed during degradation of RNA and DNA, offsetting the potential waste into a vital resource. Purine salvage enables ingested purines or those synthesised in one tissue to be available to other tissues (Murray 1971). Given its importance, it is not surprising that the purine salvage pathway has been implicated in human cancer development (Sanfilippo, Camici et al. 1994). In order to cope with rapid cell replication, tumour cells use the more efficient purine salvage pathway for energy production and nucleic acid synthesis (Ong, Zou et al. 2010).

An increased level of hypoxanthine in plasma and a reduced level in urine has been previously demonstrated in patients with gastric and colonic carcinomas (Vannoni, Porcelli et al. 1989). In plasma from children with acute lymphoblastic leukaemia or non- Hodgkin lymphoma, hypoxanthine levels have been reported to be higher than in healthy controls and these levels decreased after methotrexate administration (Hashimoto, Kubota et al. 1992). An increased level of hypoxanthine

in the urine has been noticed in mesothelioma transplanted nude mice. Moreover, the level of this metabolite was reduced in response to chemotherapy (Buhl, Dragsholt et al. 1985). On the other hand, a reduced level of urinary hypoxanthine was reported by Yoo et al. in patients with non-Hodgkin lymphoma. They reasoned that the level of hypoxanthine might be decreased due to consumption by tumour cells (Yoo, Kong et al. 2010). To my knowledge the hypoxanthine levels have never been reported in Chronic Lymphocytic Leukaemia, however an indication of an imbalance in purine metabolism in CLL has been published (Carlucci, Rosi et al. 1997). There it was shown that enzymes of the salvage pathway, including hypoxanthine-guanine phosphoribosyltransferase-HGPRT were greatly reduced in lymphocytes from leukaemia patients.

Beside the observation that primary CLL cells used in presented study produced hypoxanthine, especially in hypoxia, this phenomenon was not further investigated. Nevertheless, as there is not a lot of recent literature about hypoxanthine in leukaemic cells, it would be interesting to further investigate this abnormality, and to compare it with hypoxanthine levels in healthy B-cells.

All of the metabolites detected in samples containing primary CLL cells are presented in Figure 3.13 in the form of a metabolic map.

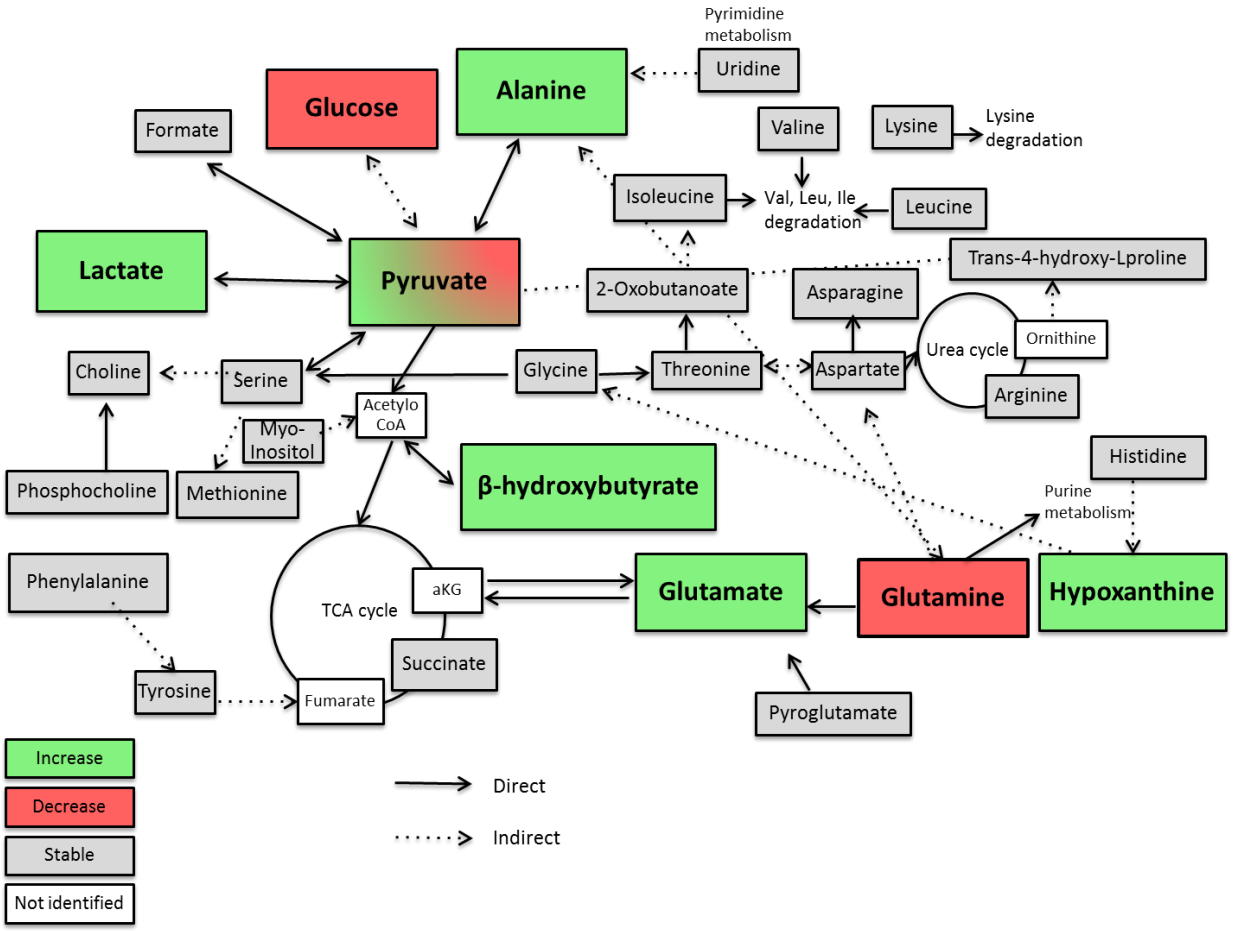

Figure 3. 14. Metabolic map presenting all of the metabolites assigned in the ^{1}H NOESY spectra recorded on samples with primary CLL cells.

Metabolites presented on this map are part of the formulation of RPMI medium except for: lactate, pyruvate, β-hydroxybutyrate, hypoxanthine, pyroglutamate, formate, succinate, uridine, 2-oxobutanoate, choline and phosphocholine.

After the time course, it was observed that the medium changed colour to yellow which indicates the acidification of pH. Histidine-based pH analysis, showed that extracellular pH changed from ~7.8 to 6.5, with slight variations between different CLL samples. As the pH changes strongly correlated with lactate production, it indicates that lactate was the main contributor to the acidification of pH. Time courses performed using RPMI with extra HEPES buffer, showed that controlling the extracellular pH did not affect the metabolic changes of glucose consumption and lactate production. It has been reported that the acidification of intracellular pH may drive the metabolic switch from aerobic glycolysis to oxidative phosphorylation, however evidence indicates that tumour cells prevent cytosolic acidification by activating a number of transporters that export excess protons produced during glycolysis (Huber, De Milito et al. 2010). This active proton transport across the cellular membrane suggests that the intracellular pH is controlled and not affected by the extracellular pH changes. It has been shown that tumour cells have alkaline intracellular pH values (7.12–7.65 compared with 6.99–7.20 in normal tissues) and acidic interstitial extracellular pH values (6.2–6.9 compared with 7.3–7.4) (Gillies, Raghunand et al. 2002; Cardone, Casavola et al. 2005). This indicates that the pH values in the NMR tube represent the natural tumour microenvironment conditions. The crucial role of intracellular pH for cancer cells is supported by the fact that the inhibition of H^+ transporters has been proposed

as an attractive anticancer strategy that could potentially be used in a wide range of cancer types (Harguindey, Arranz et al. 2009) .

Another important component of the microenvironment of cells is oxygen. Using the NMR based method for monitoring metabolism, determination of the oxygen level and regulation of its consumption rate was possible, however it was not feasible to keep the percentage stable during data acquisition. The aim of our study was to investigate metabolic changes during the transition of CLL cells from normoxic to hypoxic conditions, therefore stabilisation of the oxygen on the set level was not required. Use of the fibre optic oxygen sensor, which fitted inside the narrow NMR tube allowed us to monitor oxygen consumption very precisely. In order to slow down the rate of oxygen depletion and prolong the normoxic period, lower concentrations of CLL cells ($1x10^7$/ml) were used. This allowed very accurate identification of the time of the transition to hypoxia and to correlate it with the corresponding NMR spectra. The following chapters will present data obtained using our method together with other biochemical methods, used to better understand the adaptation of CLL cells to different oxygen environments.

Importantly, real-time NMR time-courses of glucose, lactate, alanine, glutamate and glutamine (Figure 3.11.A) revealed potential metabolic subtypes amongst the CLLs. In A0 CLL samples, the least aggressive subtype of CLL associated with lymphocytosis but no lymphadenopathy, glucose consumption was

low, glutamine consumption was equally low, and lactate/alanine as well as glutamate production showed also decreased metabolic activity. For one patient sample we observed exceedingly high glutamate production. Although not the aim of the study, these data suggest that metabolic subtypes exist which may correlate with clinical phenotype and may provide information regarding biomarkers. However patient numbers are still too small in this study to demonstrate this unequivocally.

Another metabolomics study conducted with CLL patient-derived samples was presented by MacIntyre et al. They compared metabolic profiles of serum from untreated CLL patients (Binet stage A) and healthy controls (MacIntyre, Jimenez et al. 2010). The main differences showed elevated levels of pyruvate and glutamate in the CLL samples. MacIntyre et al. did not investigate more advanced stages of CLL therefore it would be difficult to compare their results to data presented in this thesis, however the common increase of glutamate production by CLL cells can be observed for both studies. Additionally MacIntyre et al. have compared serum of patients with or without Immunoglobulin variable region heavy chain (IgVH) mutation. They observed decreased levels of cholesterol derived from VLDL, lactate, uridine as well as increased glycerol, 3-hydroxybutyrate and methionine in serum from patients with IgVH mutation, associated with poor prognosis.

In our study comparisons of the metabolic profiles of 11 primary CLL samples allowed us to distinguish two groups of cells with higher or lower metabolic activity.

Interestingly, all of the patients exhibiting the slower rates were characterised in the A0 stage of the disease (see Table 3.1). The stage A0 is often described as the "watch and wait" stage, in which patients do not receive any treatment, however remain under observation. More advanced stages, starting from A1 indicate progression of the disease. Therefore although the number of compared CLL samples was only small, the correlation between the stage of the disease and the metabolic activity was observed, suggesting the potential of this method in diagnostics or investigations of clinical and prognostic markers. A clinical test could involve short term kinetic analysis, possibly taking a series of time points for 2 metabolites in the growth medium, to characterise the 'stage' in which the cancer cells exist.

Chapter IV

Metabolic plasticity of CLL cells

4.1. INTRODUCTION

Metastatic cancer leads to the majority of cancer deaths, creates profound economic burden and remains poorly understood (Bocker 2002; Weigelt, Peterse et al. 2005; Mehlen and Puisieux 2006). It remains to be determined how metastatic cancer cells, having become adapted to the hypoxic tumour environment, survive transit in the peripheral normoxic circulation and then re-populate and survive in, *de novo* hypoxic sites. A major challenge in the study of these processes in most cancers is the rarity and transient nature of metastatic cells. In order to successfully analyse their metabolism, it would be necessary to experimentally isolate the migratory cells.

Chronic lymphocytic leukaemia (CLL) is the most common form of leukaemia in Western countries (D'Arena, Di Renzo et al. 2003; Chiorazzi, Rai et al. 2005; Parker and Strout 2011) and despite recent improvements in prolonging survival, remains incurable (Chiorazzi, Rai et al. 2005; Hayden, Pratt et al. 2012). CLL patients present elevated lymphocyte counts in the peripheral blood. In most cases these lymphocyte numbers increase progressively over months and years. However, these cancer cells are out of the cell cycle and superficially highly quiescent (Dameshek 1967). Despite this, isotopic labelling studies have determined that peripheral blood CLL cells include those that have undergone a number of divisions and also that rates of cell death within the tumour are high (Messmer, Messmer et al. 2005). The picture that emerges is that circulating CLL cells represent a large pool of non-dividing cancer

cells that are able to enter and exit tissue sites, predominantly lymph nodes, spleen and bone marrow, wherein they proliferate and drive the progressive expansion of the tumour (Messmer, Messmer et al. 2005; Calissano, Damle et al. 2011). The microenvironments of the lymph nodes, spleen and bone marrow differ from that of the blood, and entry into tissue sites provides important survival signals that protect against chemotherapeutics and thus lead to relapsed disease (Burger 2011). Moreover, tissues where CLL cells have their proliferation centres are often hypoxic (Star-Lack, Adalsteinsson et al. 2000; Sison and Brown 2011) with a pH much less controlled than in the blood. Accordingly, CLL cells must be able to quickly alter their metabolism to adapt to these different conditions. Therefore, understanding how peripheral blood CLL cells can survive transitions between normoxia and hypoxia is likely to identify novel strategies to tackle this disease.

Figure 1.4 presents a model of the lifecycle of CLL B cells including their migration between tissues and the factors regulating it. CLL is an unusual cancer where a large proportion of cells within the tumour exhibit metastatic capacity, therefore the study of its metabolic adaptations permits the potential discovery of mechanisms applicable to cancers in general. Currently however, very few studies have been conducted to investigate the potential of cell metabolism as a therapeutic target in CLL (Tura, Cavo et al. 1984; Samudio, Fiegl et al. 2008; MacIntyre, Jimenez et al. 2010). CLL cells were shown to survive considerably longer in circulation than

normal B cells (Defoiche, Debacq et al. 2008). This increases their chances of re-entry into solid tissues where they receive proliferation stimuli, enhancing their survival. Both apoptosis resistance mechanisms and metabolic adaptations that increase cell viability are likely to be responsible for the prolonged lifespan of CLL cells in the circulation.

One of the metabolic adaptations could be the increased expression of HIF-1α which may maintain CLL cells in a quiescent state through the inhibition of the mammalian target of rapamycin (mTOR) (Cam, Easton et al. 2010; Forristal, Winkler et al. 2013). HIF-1α is known as the main factor responsible for adaptation of various cells to low oxygen conditions. It was reported that CLL B cells express constitutive levels of HIF-1α under normoxia as a result of the low level of the von Hippel-Lindau gene product (pVHL) required for HIF-1α degradation (Ghosh, Shanafelt et al. 2009). Figure 1.2 shows the regulation of the HIF-1α degradation mechanism, as well as a possible effect on the quiescence of CLL cells via inhibition of the mTOR pathway. In this chapter, investigations into the role of HIF-1α in the plasticity of CLL cells and metabolic adaptation to transition between different oxygen environments are presented.

Using a novel nuclear magnetic resonance spectroscopy (NMR) based method to monitor real time metabolism in living primary CLL cells described in the previous chapter, rapid changes of metabolism over extended periods of time were

detected. Using this system, changes in CLL cell metabolism in response to oxygenation levels were studied. This chapter presents observations of a remarkable plasticity of metabolic adaptations displayed by 'quiescent' CLL cells.

4.2 RESULTS

4.2.1 Primary CLL cells adapt their metabolism to hypoxic conditions

Western blot analyses were performed in order to investigate changes in levels of key proteins during the transition from normoxia to hypoxia. Consistent with the oxygen consumption and depletion during the NMR time course experiment (described in Chapter Three), western blot analysis of CLL cells incubated in the agarose matrix in the NMR tube for different time periods, showed that levels of stabilised HIF-1α rose after one hour (Figure 4.1) and increased further over the following 4 hours. The time at which hypoxia was detected varied slightly between samples but it consistently correlated with the HIF-1α increase.

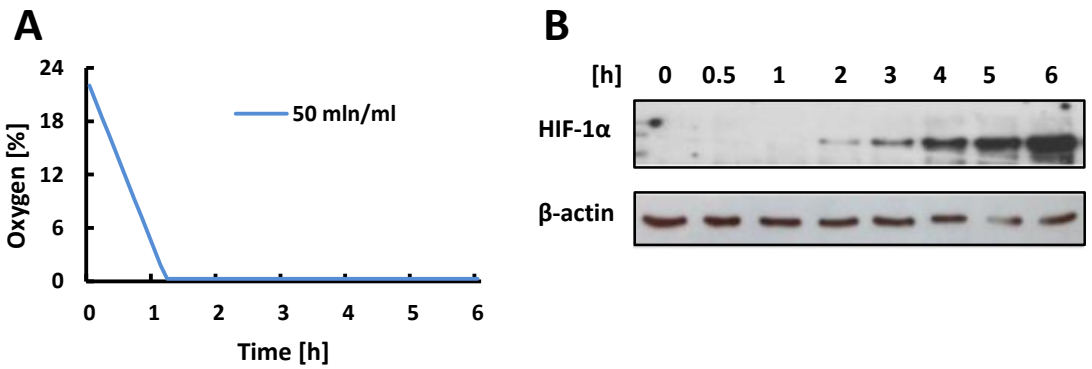

Figure 4. 1. HIF-1α level increases immediately after CLL cells reach hypoxia.

A) Oxygen measurement carried out during the NMR time course experiment, inside the NMR tube with 5x10^{7}cells/ml. Readings were taken every 10 minutes. After 70 minutes the oxygen level reached 0.2% and stabilised. B) Level of HIF-1α increase after the oxygen depletion. Cells were incubated in the agarose matrix in the NMR tube, at 36°C and the Laemmli buffer was used after different time points in order to lyse cells. Western blot was performed using the anti HIF-1α antibodies.

PCR analysis showed that selected HIF-1α target genes were expressed in CLL cells in both oxygenated and hypoxic conditions but their levels were elevated in hypoxia (Figure 4.2.A). In order to confirm that HIF-1α was responsible for the expression of the genes of interest, a commonly used inhibitor of HIF-1α transcriptional activity – chetomin (CTM) was used. CTM binds to HIF-1α transcriptional co-activator p300, disrupting its interaction with HIF-1α and attenuating hypoxia-inducible transcription (see Figure 1.2). A range of CTM concentrations were used in order to determine the dose inhibiting the expression of the chosen HIF-1α target genes. The expression of the glucose transporter GLUT1 and lactate dehydrogenase A (LDHA) in oxygenated conditions was sensitive to chetomin, whereas the expression of vascular endothelial growth factor (VEGF) was not affected (Figure 4.2.C). High levels of VEGF in CLL cells in normoxia have previously been reported (Frater, Kay et al. 2008). However, in hypoxia, the elevated expression of all three genes (including VEGF) was sensitive to inhibition by CTM (Figure 4.2.D). This was confirmed by reduced protein levels of all three HIF-1α targets after 24 hour treatment with 100 nM CTM (Figure 4.2.B). Surprisingly, levels of HIF-1α target proteins detected by western blot were similar in normoxia and hypoxia (Figure 4.2.B).

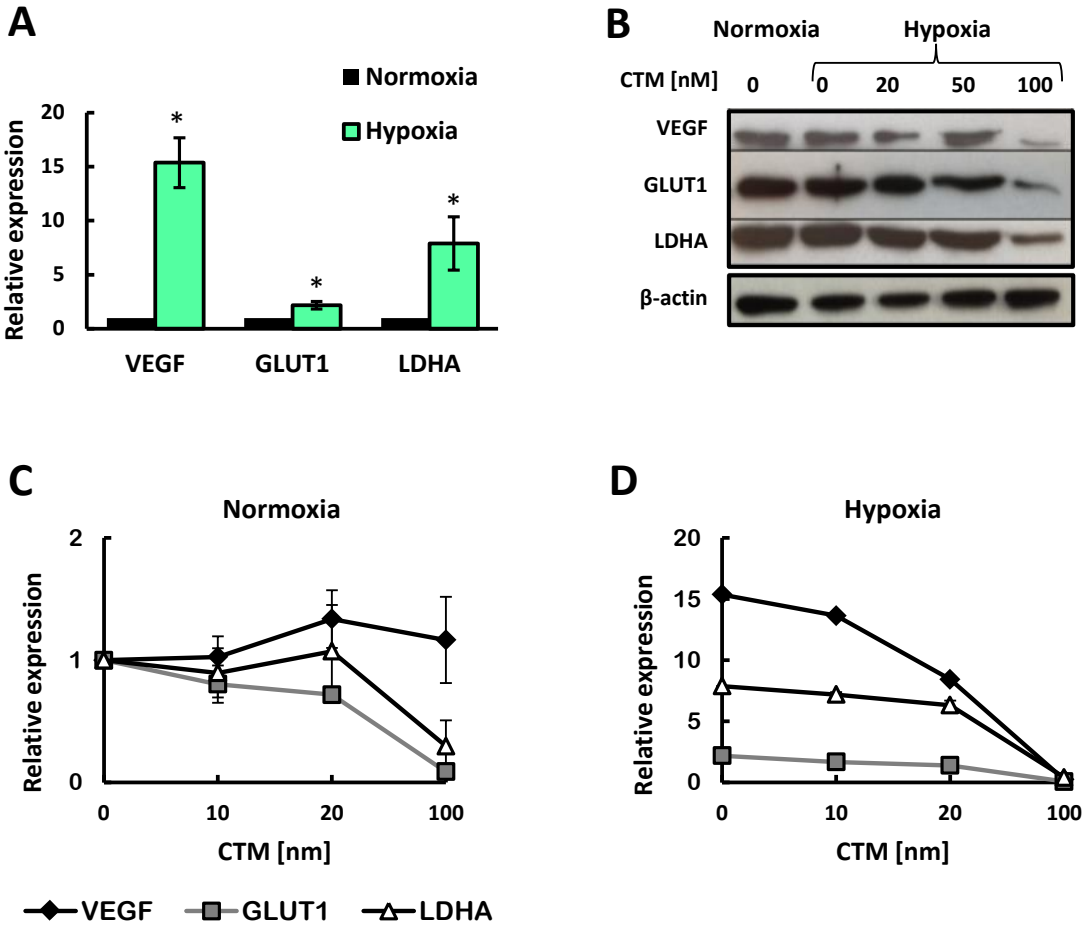

Figure 4. 2. Level of HIF-1α increases in hypoxia together with the expression of its target genes, which can be blocked by chetomin.

A) Real-time PCR analysis of VEGF, GLUT1 and LDHA expression in CLL cells incubated in normoxia or hypoxia (in the NMR tube) for 24 hours. Values are normalised to the normoxia control =1. Data are mean ± SEM n=4; *$p < 0.05$ by student's t-test for paired data. B) Western blot analysis of levels of VEGF, GLUT1 and LDHA in cells treated with CTM in normoxia or hypoxia. Cells were pre-treated with CTM 3 hours before placing in hypoxia, images are representative of 3 experiments. C&D) Real-time PCR analysis of VEGF, GLUT1 and LDHA expression in CLL cells incubated for 24 hours in normoxia (C) or hypoxia (D) with or without chetomin (CTM). Cells were pre-treated with CTM 3 hours before placing in hypoxia. Values are normalised to the normoxia control without CTM =1. Data are mean ± SEM n=3. Note that the scales of the Y axis in C&D are dissimilar reflecting the induced expression of genes in hypoxia.

4.2.2 HIF-1α shows hypoxia-inducible nuclear import

In order to verify the presence of HIF-1α in normoxic and hypoxic CLL cells, primary CLL cells were immuno-stained using HRP and fluorescent antibodies (Figures 4.3-4.5). HIF-1α was detected in both oxygenated and hypoxic CLL cells, a finding consistent with previous reports of HIF-1α activity in circulating CLL cells despite the normoxic environment of peripheral blood (Ghosh, Shanafelt et al. 2009). HRP staining demonstrated that although HIF-1α was detected in both oxygenated and hypoxic conditions, there was a difference in the localisation as well as in the strength of the HIF-1α signal (Figure 4.3). In cells incubated in normoxia, HIF-1α was detected only in the scant cytoplasm, while in cells incubated for 6 hours in 0.1% O_2, the staining signal was more intense and localised in the nucleus for the majority of cells. Confocal microscopy images (Figures 4.4 and 4.5) show the same phenomenon. It has been reported that only a small proportion of CLL cells incubated in normoxia showed detectable levels of HIF-1α localised in the cytoplasm, while hypoxic cells exhibited elevated levels of HIF-1α in the nucleus stained by DAPI and the B-cell-specific nuclear transcription factor PAX-5 (Desouki, Post et al. 2010). HIF-1α hypoxia-inducible nuclear import has previously been reported in a range of cell types, for example COS7 and Caco-2 cells but not in CLL cells (Kallio, Okamoto et al. 1998; Huang, Kuo et al. 2013).

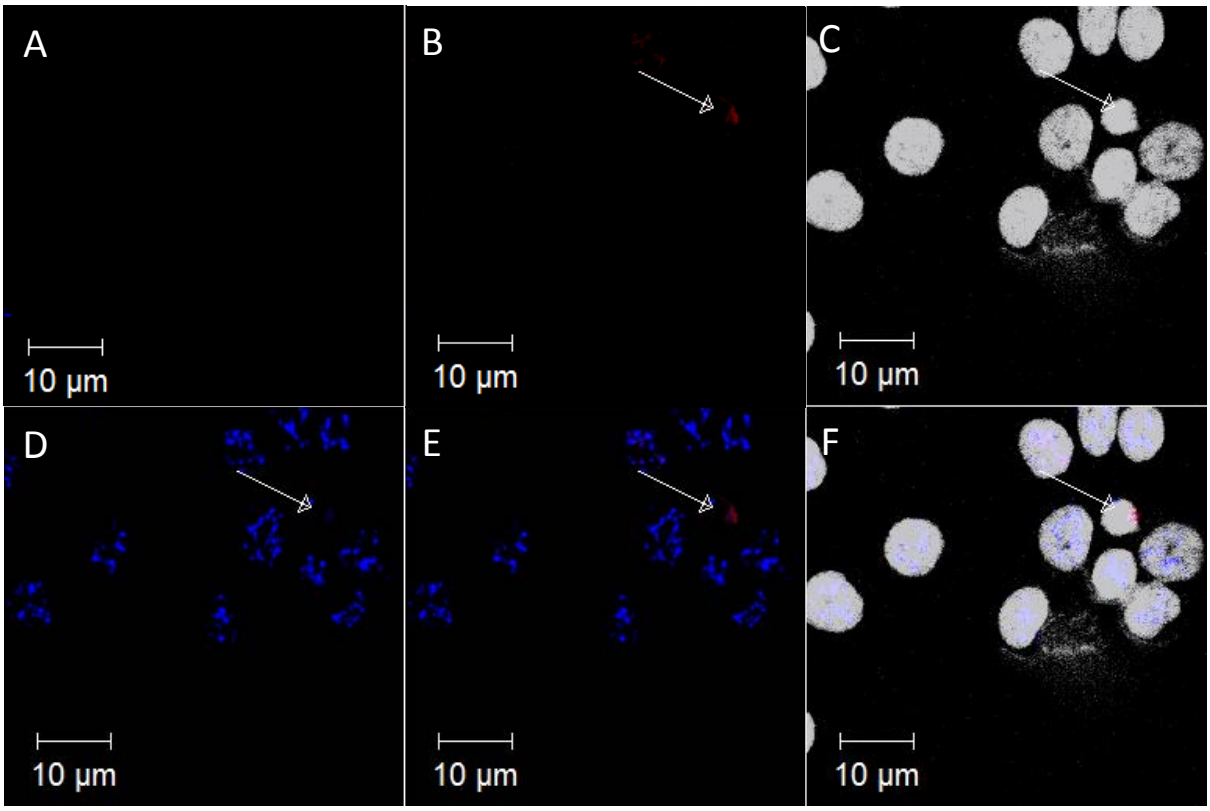

Figure 4. 4. HIF-1α is present at a low level in the cytoplasm of normoxic CLL cells.

Normoxic CLL cells cytospins stained with anti HIF-1α antibody (red), anti PAX-5 (blue) and DAPI (white). A) Isotype control for rabbit (red) and goat (blue) IgG. B) HIF-1α staining. C) DAPI staining. D) PAX-5 staining of B-cells. E) Merged HIF-1α and PAX-5. F) Merged nuclei, HIF-1α and PAX-5.

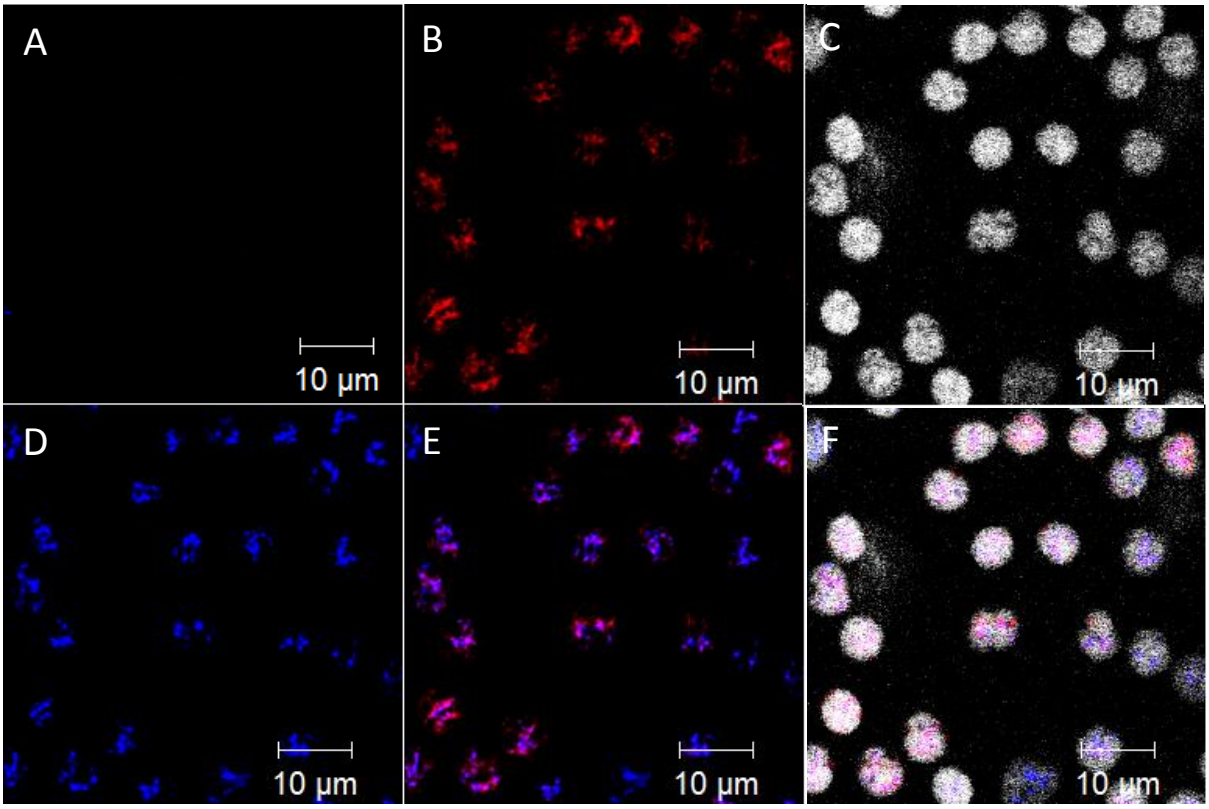

Figure 4. 5. HIF-1α is present in the nuclei of hypoxic CLL cells.

Cytospins of CLL cells incubated for 6 hours in 0.1% O_2 stained with anti HIF-1α antibody (red), anti PAX-5 (blue) and DAPI (white). A) Isotype control for rabbit (red) and goat (blue) IgG. B) HIF-1α staining. C) DAPI staining. D) PAX-5 staining of B-cells. E) Merged HIF-1α and PAX-5. F) Merged nuclei, HIF-1α and PAX-5.

4.2.3 Primary CLL cells exhibit reversible metabolic plasticity during the transition between different oxygen environments

The observations described previously (Chapter 3) identified that CLL cells can rapidly adapt to an environment of depleted oxygen by applying coordinated changes in metabolism and activation of HIF-1α. *In vivo*, CLL cells cycle from hypoxic and normoxic tissue compartments (see Figure 1.3), thus if the changes observed in our experiments are physiologically relevant it would be expected that they are plastic and reversible. To test this hypothesis CLL cells were cultured under conventional conditions containing abundant oxygen, transferred to hypoxic conditions for 24 hours (cycle 1), and retuned to high oxygen conditions for a further 24 hours before NMR analysis of a second transition to hypoxia (cycle 2) (Figure 4.6 and 4.7). The viability of cells was unaffected after the second cycle of transition from oxygenated conditions to hypoxia (Figure 4.6 B). As shown in Figure 4.7 and in Table 4.1, the kinetics of glucose and glutamine consumption, as well as lactate, glutamate and alanine production during a primary or secondary exposure to normoxia, were comparable. Moreover, oxygen was consumed at a similar rate, suggesting that mitochondrial functions were not affected by severe hypoxia or by re-oxygenation.

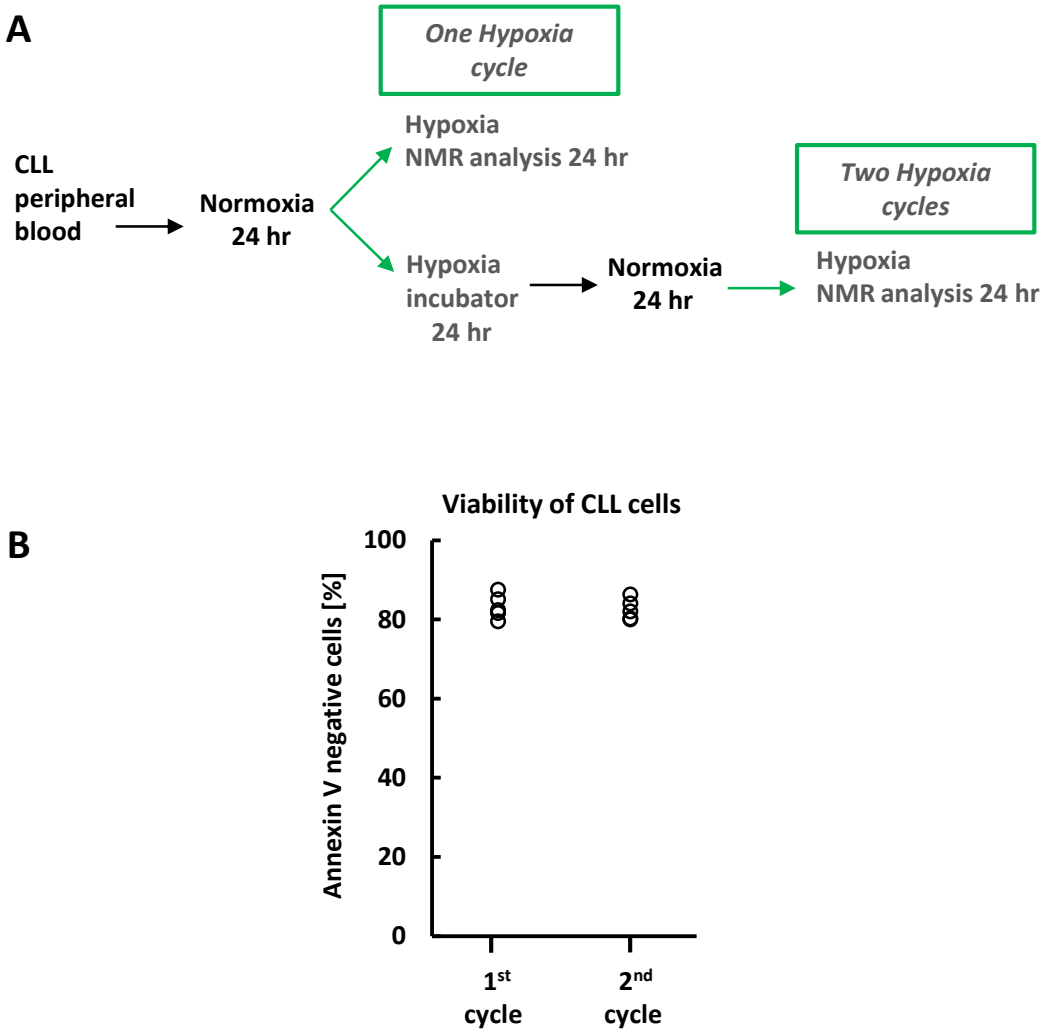

Figure 4. 6. Viability of CLL cells is not affected by extreme changes in oxygen levels.

A) Scheme of the experiment performed. Primary CLL cells were isolated from peripheral blood and incubated for 24 hours in normoxia. Then the sample was split into two parts. One was analysed by NMR for 24 hours in hypoxia, the second was incubated for 24 hours in hypoxia, then for another 24 hours in normoxia and finally analysed by NMR in hypoxia for a further 24 hours. The first sample was cycled between normoxia and hypoxia once, while the second sample was cycled twice. B) Viability data for 5 primary CLL samples. Percentage of Annexin V negative cells were compared between cells which had undergone one or two hypoxic cycles.

Table 4. 1. Kinetics of metabolic changes in CLL cells measured by the NMR during two normoxia-hypoxia cycles.

Using the time series analysis user interface (TSATool) in the MetaboLab program, the kinetic functions were applied to fit the data in order to describe the changes in metabolite concentrations. For lactate, alanine, glutamate and 3-hydroxybutyrate we assumed first order kinetics according to: $I(t)=I_0-I_1*e^{-rt}$ where I(t) is the current metabolite concentration at time point t, I_0 the theoretical metabolite concentration at infinite time, $I_0 - I_1$ the concentration at time point 0 and r the rate of change; for lactate before hypoxia $I_0*(1-\exp(-r*t))$ kinetics were applied as the concentration at time point 0 was close to 0; for glucose and glutamine the assumed kinetics was a bi-exponential decay to: $I(t)=I_0*e^{-rt}+I_1-r_1t$ where again I(t) is the metabolite concentration at the current time point t, $I_0 + I_1$ is the starting concentration and r and r_1 are the rate constants describing the glucose usage. For hypoxanthine the x=a+r*t function was used to approximate the linear part of a mono-exponential kinetics like the one assumed for lactate. r again represents the rate constant.

Metabolite	First cycle				Second cycle			
	I_0	I_1	r	r_2	I_0	I_1	r	r_2
Lactate (before hypoxia)	0.079		0.046		0.062		0.051	
Lactate (in hypoxia)	3.971	4.325	0.0451		3.072	3.42	0.065	
Glucose	0.136	0.507	0.287	0.005	0.123	0.468	0.303	0.005
Glutamine	0.071	0.092	0.517	0.0009	0.0332	0.095	0.825	0.0009
Alanine	0.0758	0.058	0.088		0.07	0.058	0.118	
Glutamate	0.058	0.043	0.209		0.038	0.019	0.2	
Pyruvate	0.069	0.052	0.37		0.056	0.037	0.437	
3-Hydroxy butyrate	0.028	0.02	0.07		0.025	0.021	0.094	
Hypoxanthine	0.0004		0.038		0.0004		0.049	

4.2.4 HIF-1α inhibition reverses changes in metabolism associated with hypoxia.

Key metabolites displayed bi-phasic kinetics as oxygen became depleted, with rate changes being tightly associated with the transition to hypoxia (Figure 4.8). These included increased accumulation of lactate and an accompanied accelerated consumption of glucose consistent with a transition to elevated anaerobic glycolysis. This indicates that CLL cells display adaptive metabolic alternations depending on oxygen availability. There was also a marked onset of alanine synthesis upon entry into hypoxia (Figure 4.8), suggesting hypoxia induced alanine aminotransferase activity. These tight associations of coordinated metabolic-rate shifts with the onset of severe hypoxia (0.8-0.1% O_2) required investigation of their dependence on HIF-1α. Two concentrations of chetomin 20 nM and 100 nM (which have been shown to decrease the expression of the chosen HIF-1α target genes in hypoxia (Figure 4.2)) were tested showing a dose dependent effect of metabolic adaptations to hypoxia in CLL cells. Enhanced glutamine consumption was detected following CTM treatment and the consumption of glucose was attenuated as a result of HIF-1α inhibition. Thus, although HIF-1α activity promoted anaerobic glycolysis in hypoxia and the consumption of glucose, it acted to suppress overall utilisation of glutamine. After CTM treatment, glutamine uptake may compensate for the blocked HIF-1α dependent glycolysis pathway.

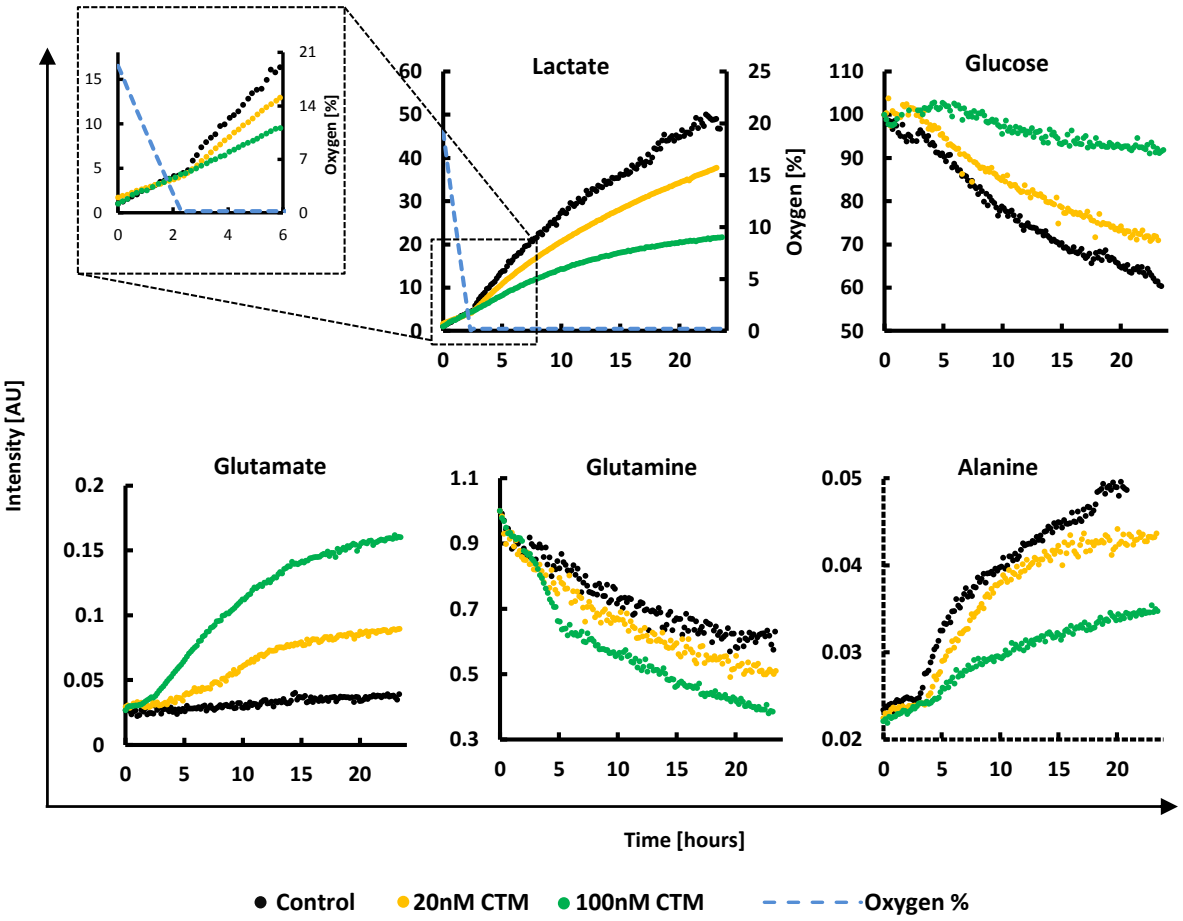

Figure 4. 8. Metabolic adaptation of CLL cells to hypoxia involves HIF-1α.

NMR time course data for the control CLL experiment and cells treated with 20 nM and 100 nM chetomin (CTM). Cells were pre-treated with CTM for 3 hours before starting the NMR experiment. Graphs present changes of chosen metabolites over time: Lactate, Glucose, Glutamate, Glutamine and Alanine. The broken blue line on the lactate graph shows the oxygen changes inside the NMR tube. The top left corner depicts an enlarged representation of the first 6 hour portion with the visible shift of lactate kinetics after oxygen depletion, which is inhibited by CTM.

4.2.5 HIF-1α inhibition by chetomin is toxic to CLL cells regardless of the oxygen level

The next goal was to determine whether CTM caused preferential killing of CLL cells in hypoxia. However, exposure of CLL cells to CTM for 48 hours induced cell death in the presence and absence of hypoxia (Figure 4.9.A). CTM inhibits the formation of functional HIF-1α/HIF-1β/p300 (CBP) transcriptional complexes by acting upon the p300 coactivator (Cook, Hilton et al. 2009). The actions of p300 as a coactivator are not restricted to HIF signalling and other targets in CLL include the NFκB pathway (Pekarsky, Palamarchuk et al. 2008). It is therefore likely that cell death induced by CTM exposure relates to this or some other non-HIF function of p300 that is constant between normoxia and hypoxia.

Nonetheless, the CTM data described, suggests that at least in the first 24 hours of exposure to hypoxia, activation of HIF signalling was not required for survival. Although the reason for this is unclear, it is notable that at a protein level, equivalent amounts of HIF-targets GLUT1, LDHA and VEGF were expressed in cells prior to and after 24 hours exposure to hypoxia; perhaps indicating that circulating CLL cells are primed to survive the immediate transition to hypoxia (Figure 4.2.B).

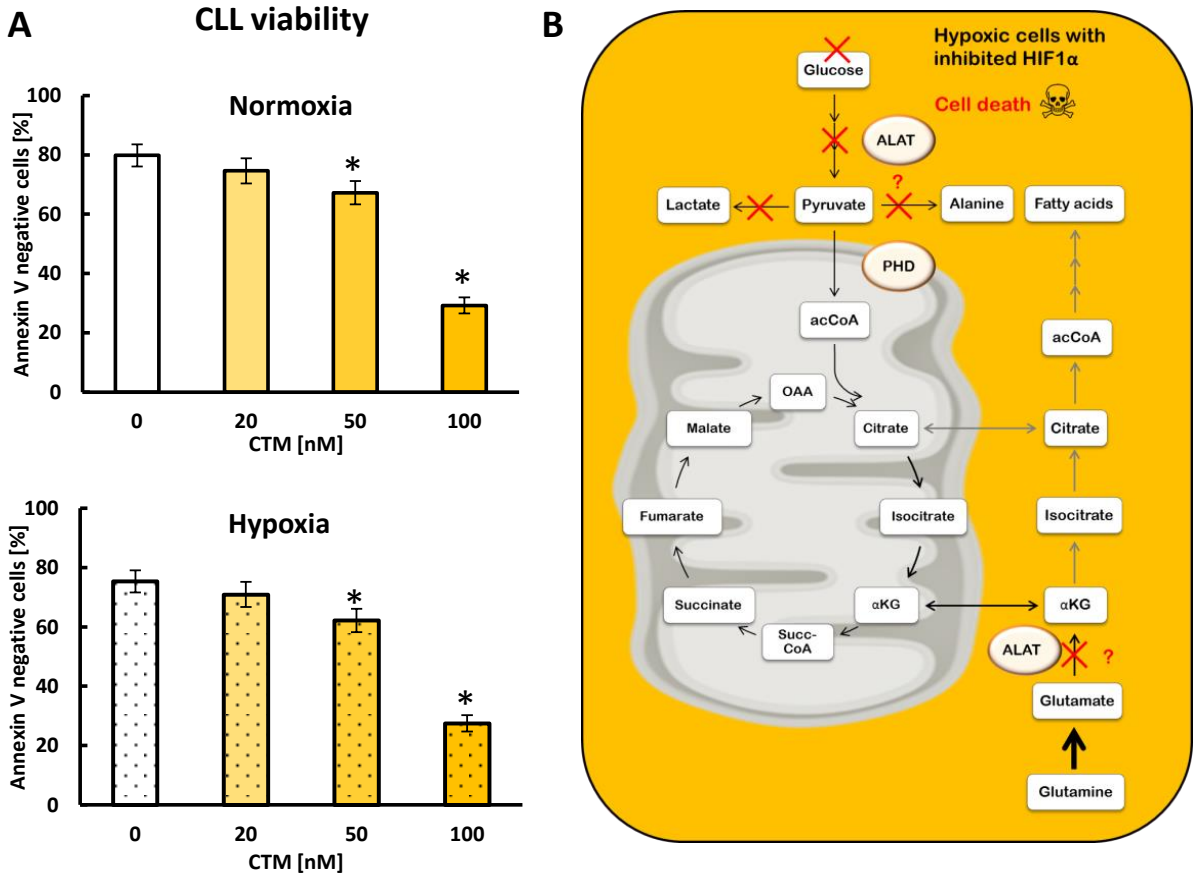

Figure 4. 9. HIF-1α inhibition by chetomin is toxic to CLL cells in both normoxia and hypoxia.

A) Viability of CLL cells after 48 hours of incubation with CTM in normoxia and hypoxia. Cells were pre-treated with CTM for 3 hours before entering hypoxia. Data are mean of n=4 ± SEM; *p < 0.05 by student's t-test for paired data. The CTM killing curves for both 24 and 48h are shown in Appendix 3. B) Effect of CTM on the metabolism of CLL cells based on the NMR time course data. Lower glucose consumption, decreased lactate and alanine secretion, increased glutamine uptake and increased glutamate secretion, which may be a result of higher intracellular glutamate accumulation was seen. Decreased alanine extraction and increased glutamate accumulation may indicate the lower activity of alanine aminotransferase (ALAT).

4.2.6 Alanine aminotransferase is not involved in the mechanism of hypoxic adaptation.

Time course NMR data, recorded on CLL cells treated with chetomin showed decreased alanine secretion correlated with higher glutamate export. The only enzyme using alanine and glutamate as its substrates is alanine aminotransferase – ALAT (a diagram of these reactions is shown in Figure 4.10.A). A possible hypothesis for the observed changes is the loss of ALAT activity. In order to test this, two ALAT inhibitors, cycloserine and β-chloro-l-alanine, were used to investigate how they affect the metabolism of CLL cells. NMR analysis of CLL cell culture media after 24 hour treatment with ALAT inhibitors showed that both compounds were able to inhibit alanine production at concentrations as low as 10 μM (Figure 4.10.B). Interestingly, the concentration of extracellular glutamate was unaffected by the blocked ALAT transformation of glutamate to α-ketoglutarate. This may be explained by the high complexity of glutamate metabolism compared to that of alanine, as the latter has only one precursor - pyruvate. An example of the complexity of glutamate metabolism is the alternative reaction that converts glutamate to α-KG, catalysed by aspartate aminotransferase (AST). One possibility is that the production of glutamate as an end product of the TCA cycle exceeds the conversion of pyruvate to alanine, with concurrent conversion of glutamate to α-KG.

Alternatively it is also feasible that the process of glutaminolysis is blocked, leaving larger amounts of glutamate unprocessed.

Beside the previously described differences in metabolite levels in CLL cell medium incubated in normoxia/hypoxia, no additional significant changes were observed after treatment with ALAT inhibitors (Figure 4.10.B). However, pyruvate showed slight (statistically insignificant) increases in hypoxia consistent across all samples, which may be a consequence of the reduced transformation of pyruvate to alanine. The reduced (statistically insignificant) accumulation of pyruvate in normoxia may be explained by the utilisation of pyruvate in the TCA cycle, a process which is blocked by HIF-1α in hypoxia. Neither cycloserine nor β-chloro-l-alanine at low and high doses affected the viability of cells either in normoxia or in hypoxia over 48 hours (Figure 4.11). In addition, supplementation with cell membrane permeable octyl-α-ketoglutaric acid did not have a significant effect on the viability of CLL cells with inhibited ALAT metabolism (Figure 4.12). These observations combined suggest that alanine aminotransferase was not the essential enzyme for CLL cell survival and/or adaptation to hypoxia. It is possible that CLL cells can retrieve required alanine from the degradation of proteins or peptides.

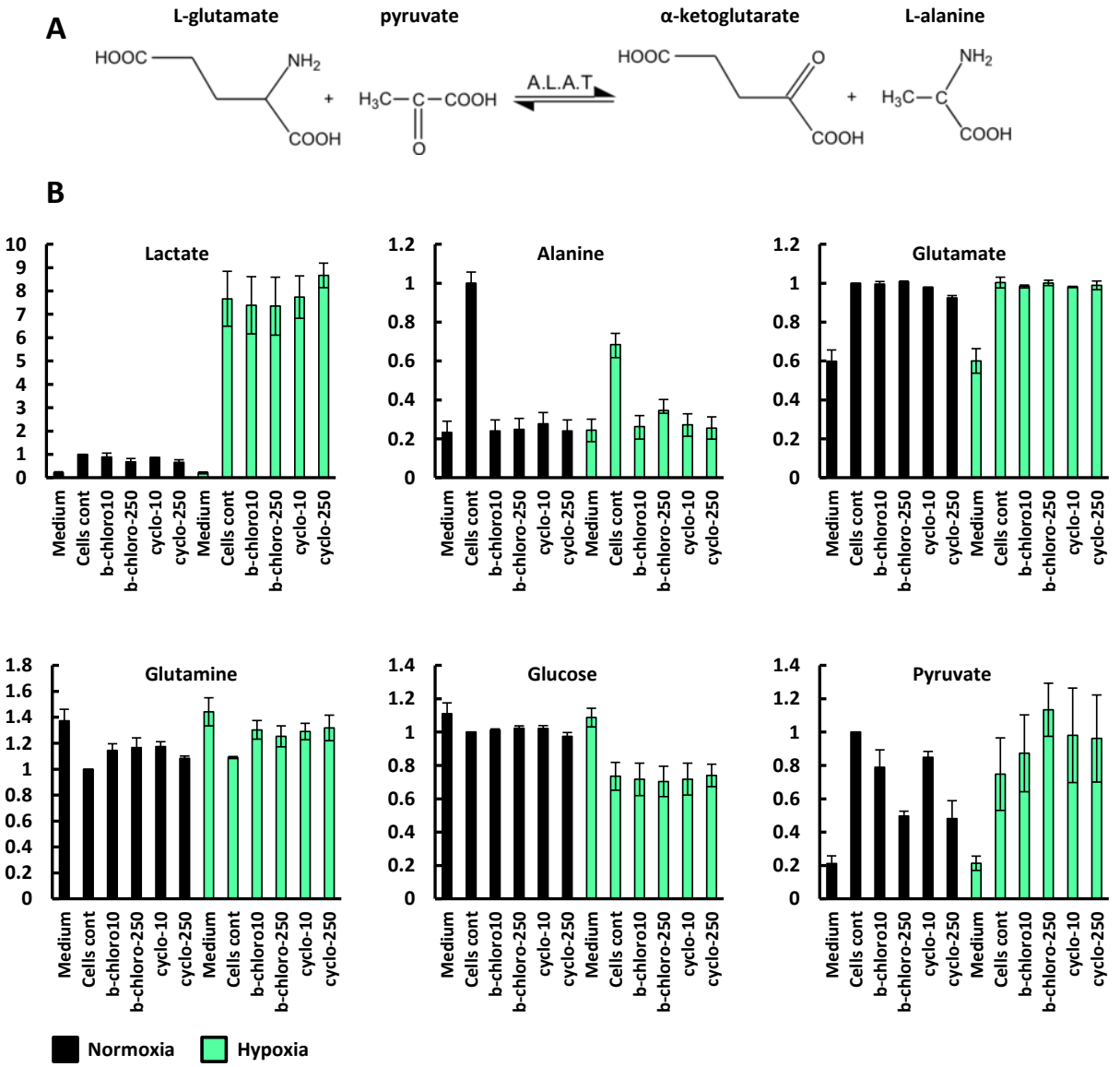

Figure 4. 10. Alanine aminotransferase (ALAT) inhibition in CLL cells.

A) ALAT catalyses the transfer of an amino group from L-alanine to α-ketoglutarate, the products of this reversible transamination reaction being pyruvate and L-glutamate. B) The ALAT inhibitors cycloserine (cyclo) and β-chloro-l-alanine (b-chloro), were used at two concentrations - 10 μM and 250 μM. Cells were incubated with inhibitors for 24 hours in normoxia and hypoxia. The concentration of metabolites in medium was subsequently measured using ^{1}H NMR. Selected metabolites are presented. Values are normalised to the normoxia control =1. Data are mean of n=3 ± SEM. Data were analysed by student's t-test for paired data and no significant difference was obtained for any metabolite for any treatment compared to control cells.

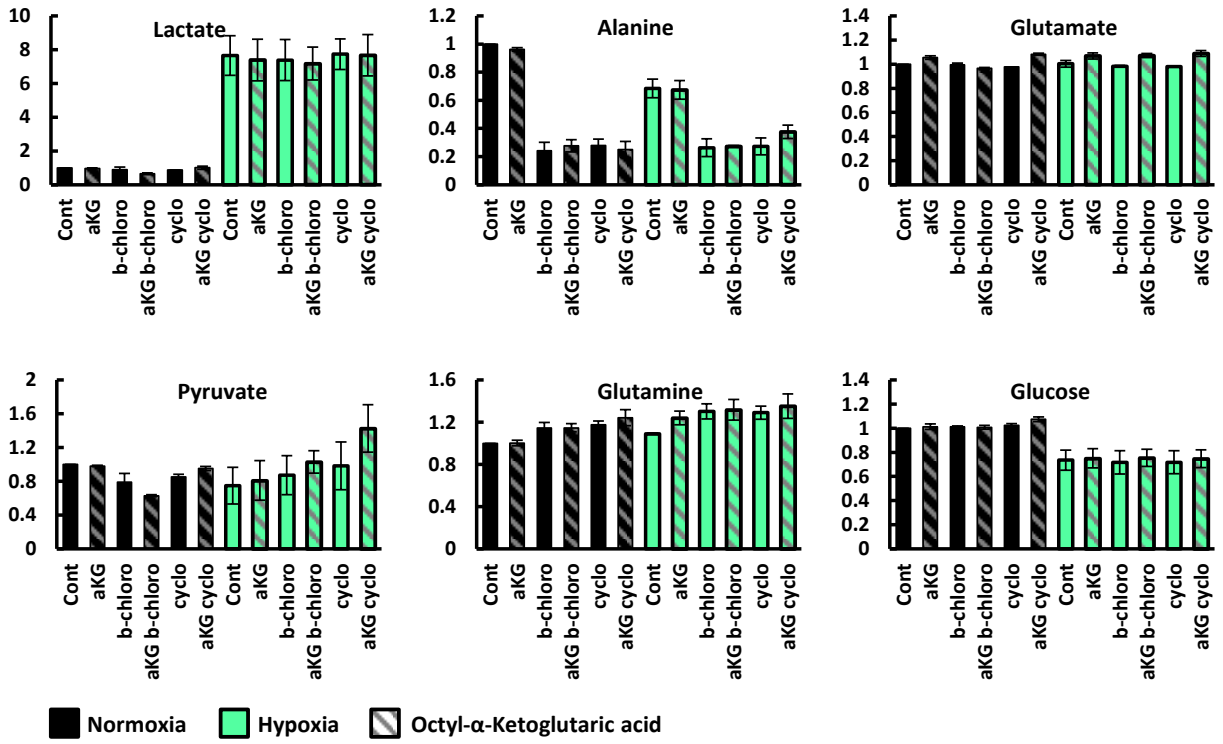

Figure 4. 12. Membrane permeable αKG did not affect ALAT inhibition.

Cells were incubated with ALAT inhibitors +/- octyl-α-ketoglutaric acid (aKG) for 24 hours in normoxia and hypoxia, then the concentration of metabolites in medium was measured using ^{1}H NMR. 10 μM ALAT inhibitors were used: cycloserine (cyclo) and β-chloro-l-alanine (b-chloro). Values are normalised to the normoxia control =1. Data are mean of n=3 ± SEM.

4.3 DISCUSSION

The influence of the microenvironment on CLL cells is important, particularly in the context of apoptotic resistance and induction of cell proliferation. Many recent studies have been focused on the interactions of CLL cells with supportive cells such as bone marrow stromal cells and endothelial cells, as well as transgenic fibroblasts expressing CD40 ligand (CD40L) which *in vivo*, is delivered by T helper cells and stimulates CLL cell proliferation. In order to replicate cytokines secreted by T cells, soluble factors such as IL-21 and IL-4 have also been added to co-culture systems to replicate the *in vivo* microenvironment of CLL cells (Ghia, Circosta et al. 2005; Ahearne, Willimott et al. 2013). This allows for the induction of cell activation, division and enhanced survival of cells. The present study on the other hand, focuses on the physical cues of the cellular microenvironment - oxygen and extracellular pH- which play roles just as important as biological factors in the regulation of cellular responses and metabolism.

The effect of hypoxia in cancer cell metabolism has been widely investigated in the last decade, however the vast majority of studies have been conducted on solid tumours. Adaptations of cancer cells to low oxygen environments have been shown to be responsible for anti-drug resistance as well as defence against ionising radiation-induced DNA damage (Wachsberger, Burd et al. 2003; Adamski, Price et al. 2013). Moreover, hypoxic tumour cells promote tumour progression and metastasis

through a variety of direct and indirect mechanisms. It has also been shown that patients with primary tumours that contain high proportions of hypoxic cells have decreased disease-free and overall survival rates after surgical resection of the primary tumour (Fyles, Milosevic et al. 2002; Vergis, Corbishley et al. 2008). Until recently there had been little interest in the investigation of the effect of hypoxia on leukaemic cells. This study postulates that CLL can potentially constitute a model for the metabolic studies of other metastatic cancers.

It has previously been reported that CLL cells express HIF-1α in normoxic conditions (Ghosh, Shanafelt et al. 2009) and the importance of its target gene VEGF has been investigated. An increase in microvessel density was observed in CLL bone marrows and lymph nodes, suggesting the increased tissue site angiogenesis in CLL (Chen, Treweeke et al. 2000; Kini, Kay et al. 2000) and VEGF has been shown to be elevated in serum and urine of some CLL patients (Menzel, Rahman et al. 1996; Molica, Vitelli et al. 1999; Aguayo, O'Brien et al. 2000). Moreover, upregulation of mRNA encoding VEGF and its receptors (Kay, Jelinek et al. 2001) suggest that angiogenic factors are important in the biology of the malignant B-cell clone. The present study showed an almost immediate increase of HIF-1α protein in hypoxia, correlated with increases of transcription of its target genes (Figures 4.1. and 4.2.A). However, only low levels (not detectable by Western blot analysis) of HIF-1α localised in the cytoplasm (Figures 4.3.-4.4.) were detected in CLL cells incubated in

normoxic conditions. Similar to previous reports, the translocation of HIF-1α to the nucleus in hypoxic cells was observed (Figure 4.5.) (Chilov, Camenisch et al. 1999). Comparable levels of LDHA and GLUT1 proteins in normoxia and hypoxia (Figure 4.2.B) may be the consequence of the longevity of these proteins or the stability of their mRNA. This data suggests that CLL cells are pre-programmed for quick oxygen depletion, which enables them to immediately adapt their metabolism to hypoxic conditions.

This pre-programming may be the key to the plasticity of CLL cells which allows them to circulate between different oxygen environments. This study has investigated how the transitions between normoxia and hypoxia influence the metabolism of CLL cells and multiple adaptations. Metabolic plasticity- which could be described as metabolic flexibility, enabling prioritisation of metabolic pathways to match anabolic and catabolic demands of evolving phenotype during cell fate determination- was widely described in stem cell research (Folmes, Dzeja et al. 2012) but has not been extensively investigated in primary CLL cells.

The NMR time course analysis proved to be a useful method to investigate the metabolism of primary cells using cycling experiments. Firstly, this proves that this NMR technique is very reproducible and experiments performed on different days can provide comparable metabolic data characterised by very similar kinetics. Secondly, the viability and the oxygen consumption rates proved not only that CLL

cells are metabolically plastic, but also that the NMR experiment does not affect their metabolism. Cells were able to re-set their metabolic pathways during the re-oxygenation without causing damage to mitochondria as observed in endothelial cells (Dhar-Mascareno, Carcamo et al. 2005).

In order to distinguish which metabolic pathways are controlled by HIF-1α, chetomin a well-known HIF-1α inhibitor was used (Kung, Zabludoff et al. 2004). Beyond the well-described toxic effect of CTM on hypoxic cells, the kinetic changes of CTM treated cells were monitored. The data presented in this chapter suggest that alongside the well understood inhibition of lactate production and glucose consumption (as a consequence of GLUT1 down regulation), HIF-1α upregulates glutaminolysis as the alternative source of carbon when glucose metabolism is blocked. Sun and Denko proposed an interesting model connecting HIF-1α with glutamine metabolism (Sun and Denko 2014). They identified the mechanism by which HIF-1 activation results in a dramatic reduction of the activity of mitochondrial enzyme complex α-ketoglutarate dehydrogenase (αKGDH). HIF-1 activation promotes SIAH2 targeted ubiquitination and proteolysis of the subunit of the αKGDH complex. Therefore inhibition of HIF-1 may reverse the hypoxic drop in αKGDH activity and stimulate glutamine oxidation, inducing its uptake as a consequence.

Another interesting consequence of HIF-1α inhibition was the decreased alanine production. The hypothesis that ALAT may have been deactivated by HIF-1α blockage did not prove to be correct in CLL cells. Alanine is often described as a by-product of the metabolism of pyruvate (DeBerardinis and Cheng 2010), which concurs with the data from the present investigation showing that ALAT inhibitors did not affect the viability of cells or have a significant effect on cell metabolism, even though alanine production was profoundly inhibited (Figure 4.10. and 4.11.). Knowing that ALAT inhibition does not increase glutamate secretion, the glutamate accumulation after CTM treatment, remains unexplained. MacIntyre *et al*. reported higher levels of glutamate and pyruvate in the serum of CLL patients compared to that of healthy donors, suggesting decreased activity of ALAT as a possible explanation (MacIntyre, Jimenez et al. 2010). The results presented in this chapter however dispute the theory that ALAT inhibition causes such an effect.

While others studies have reported that ALAT inhibition in lung carcinoma cells impaired glucose uptake (Beuster, Zarse et al. 2011), this relation in CLL cells was not observed in this investigation. Moreover it has been shown that ALAT inhibitors induced impaired growth of the cell line and reduced tumour mass in the xenograft mouse model, while no cytotoxic effect was observed in the present study. This may indicate the difference in alanine metabolism between quiescent and proliferating cells. Alternatively, CLL cells may use proteolysis in order to fulfil their

alanine demand. This is however not supported by our metabolic data showing no increase of essential amino acids.

We have demonstrated that treatment with 100mM CTM for 48h resulted in significant decrease of CLL cells viability (Figure 4.9 A) in both normoxia and hypoxia with suggests strong HIF-1α independent toxicity of high CTM dose. This suggests that the effect of 100nM CTM demonstrated on the figure 4.8 could result from cell death rather than a specific metabolic change or the combination of both. The first metabolic shift of the CLL cells treated with CTM can be observed after only 5 (when hypoxia is reached) therefore measurement of CLL cells viability after 5h of treatment with 100nM CTM should help to distinguish if those changes were triggered by cell death or only the Hif-1α inhibition.

Not only malignant B-cells, but all immune cells are exposed to low oxygen tensions as they develop and migrate between blood and different tissues, and the mechanisms by which lymphocytes adapt to hypoxia are poorly understood. A study by Kojima *et al.* showed that B-cells but not T-cells were strongly dependent on HIF-1α. The HIF-1α deficient T-cells showed unchanged phenotype (compared to the wild-type), while dramatic distortions in phenotype of HIF-1α deficient B-cells were observed (Kojima, Gu et al. 2002). Recent studies have shown that lymphocyte activation has strong links with altered metabolism. Activation of T- lymphocytes, combined with increased cell proliferation increases their bioenergetic and

biosynthetic demands, forcing cells to adapt their metabolism. Changes in the microenvironment resulting from limitations of nutrient and oxygen require further metabolic reprogramming (Pearce, Poffenberger et al. 2013). It has been shown that Naïve T cells are metabolically quiescent and use oxidative phosphorylation as the main source of ATP. As they are activated, they consume more nutrients and increase their glycolysis and gutaminolysis rates, but fully activated memory T cells are characterised by quiescent metabolism with oxidative phosphorylation mainly fuelled by fatty acid oxidation and increased mitochondrial mass which suggest they are metabolically primed to respond during the next infection (van der Windt, O'Sullivan et al. 2013).

The fact that other immune cells need to reprogram their metabolism depending on the environment suggests that CLL cells may be a good model to investigate the biology of B-cells in general. This study intended to compare observations regarding both the plasticity of CLL cells and the effect of CTM on their metabolism, with similar analysis conducted on healthy B-cells. The difficulty was that NMR spectroscopy as a relatively insensitive method requires reasonably large amounts of cells to obtain a good signal to noise ratio. Therefore primary CLL cells, although quiescent and unable to increase the biomass by division, are a very good model as CLL patient blood samples provide large amounts of B-cells which are otherwise difficult to obtain.

Chapter V

Investigating the role of pyruvate in adapting to hypoxia

5.1 INTRODUCTION

Pyruvate is known to play an important role in protecting cancer cells from hypoxic stress (Roudier and Perrin 2009; Huang, Kuo et al. 2013; Cipolleschi, Marzi et al. 2014). Some of the signals from metabolites shown in the 1D ^{1}H-NMR spectrum (Figure 3.1) are represented by distinct separated peaks, while others are more difficult to assign and analyse because of overlapping chemical shifts with neighbouring peaks. One of the more difficult metabolites to identify in spectra obtained in the previous chapter was pyruvate.

Many studies have linked pyruvate metabolism with hypoxia. The most direct link between hypoxia and pyruvate metabolism is the fact that HIF-1α directly activates the gene encoding pyruvate dehydrogenase kinase 1 (PDK1). PDK1 inactivates the TCA cycle enzyme, pyruvate dehydrogenase (PDH), which converts pyruvate to acetyl-CoA (Kim, Tchernyshyov et al. 2006) (See Figure 6.17). Active suppression of mitochondrial pyruvate catabolism resulting in decreased respiration is partially compensated by increased anaerobic glycolysis promoted by HIF-1α (Seagroves, Ryan et al. 2001). However, increased ATP production may not be sufficient for hypoxic adaptations since hypoxia causes oxidative stress from uncontrolled mitochondrial generation of reactive oxygen species (ROS), which may affect cell survival. ROS which is a by-product of mitochondrial respiration arising from electron transfer to O_2, can be efficiently neutralized by catalase,

peroxiredoxins, and superoxide dismutase. In hypoxia however, perturbation in electron transport is associated with leakage of electrons from the respiratory chain, resulting in increased ROS that could be toxic to cells if ROS levels are not attenuated (Kim, Tchernyshyov et al. 2006).

Pyruvate and its derivatives have been shown to be important endogenous scavengers of certain reactive oxygen species (ROS), especially hydrogen peroxide (H_2O_2). Pyruvate scavenges H_2O_2 by virtue of a non-enzymatic oxidative decarboxylation reaction, which was first described by Holleman in 1904 (Holleman 1904):

$$CH_3\text{-}CO\text{-}CO_2\text{-}H + HO\text{-}OH \leftrightarrow CH_3\text{-}CO\text{-}OH + CO_2H\text{-}OH \leftrightarrow CH_3\text{-}CO\text{-}OH + CO_2 + H_2O$$

Scavenging of H_2O_2 by endogenously generated pyruvate has been shown to be the key cellular defence against oxidative stress in proliferating cells (Brand and Hermfisse 1997).

In addition to H_2O_2, other important cellular reactive oxygen species include superoxide radical anion ($O_2^{\bullet -}$), hydroxyl radical ($OH^{\bullet}$), and peroxynitrite ($ONOO^-$) (Fink 2002). Although $O_2^{\bullet -}$ is only moderately reactive, it can undergo a one-electron reduction forming H_2O_2, or react with nitric oxide (NO) to form the potent oxidising and nitrosating agent, $ONOO^-$ (Pacher, Beckman et al. 2007). Evidence has been shown to support the hypothesis that pyruvate is not only capable of scavenging H_2O_2, but also $OH^{\bullet}$ (Ervens et al. 2003) and peroxynitrite (Varma and Hegde 2007).

It has been previously reported that pyruvate (together with glutamate) was increased in the serum of CLL patients compared to the serum of healthy donors (MacIntyre, Jimenez et al. 2010). Suggested causes of the elevated levels of pyruvate included deficiencies in thiamine- of which the physiologically active form (thiamine pyrophosphate) acts as a coenzyme in pyruvate decarboxylation (Seligmann, Levi et al. 2001); decreased activity of alanine aminotransferase (discussed in the previous chapter) and elevated serum levels of pyruvate kinase type M2 (Oremek, Teigelkamp et al. 1999).

The aim of this part of the study was to compare pyruvate kinetics in normoxic and hypoxic conditions in CLL cells, to investigate its importance for the metabolic adaptations and to test the hypothesis of its role in ROS protection. The analysis of pyruvate in ^{1}H-NMR spectra is challenging as there is only a singlet representing the methyl group in a crowded region of the spectrum, and its chemical shift changes with pH. Despite this challenge, this work aimed to investigate its kinetics in CLL cells.

5.2 RESULTS

5.2.1 Analysis of pyruvate changes during the NMR time course.

Figure 5.1 shows the pyruvate and glutamate resonances during the ^{1}H-NMR time course experiment with CLL cells. The glutamate multiplet H-C4 consists of 6 signals, two of which overlap with the pyruvate signal when it shifts upfield (to the lower ppm values) as a consequence of a decreasing pH. In order to assess the concentration of extracellular pyruvate in the NMR tube, Chenomx software was used. Chenomx has a build-in library of pH dependent spectra for many metabolites and can stimulate spectra of overlapping signals for deconvolution. First, glutamate resonances were assigned in Chenomx, using intensities from the non-overlapping glutamate signals to obtain correct intensities for overlapping resonances. Subsequently the pyruvate signal was assigned and its intensity was estimated by adjusting the sum of the glutamate and pyruvate signals until the overall signal was reasonably well represented. In order to obtain the pyruvate concentration, the glutamate concentration was subtracted from the sum (Figure 5.1.B). In order to confirm the assignment of pyruvate, the same sample was spiked with additional pyruvate (Figure 5.1.C,D). The pyruvate signals of the sample overlapped and spiked pyruvate exhibited the same pH dependent signal shift, moving towards the glutamate signals. Chenomx analysis showed that the additional spiked pyruvate was also taken up by CLL cells in hypoxic conditions (Figure 5.1.C,D).

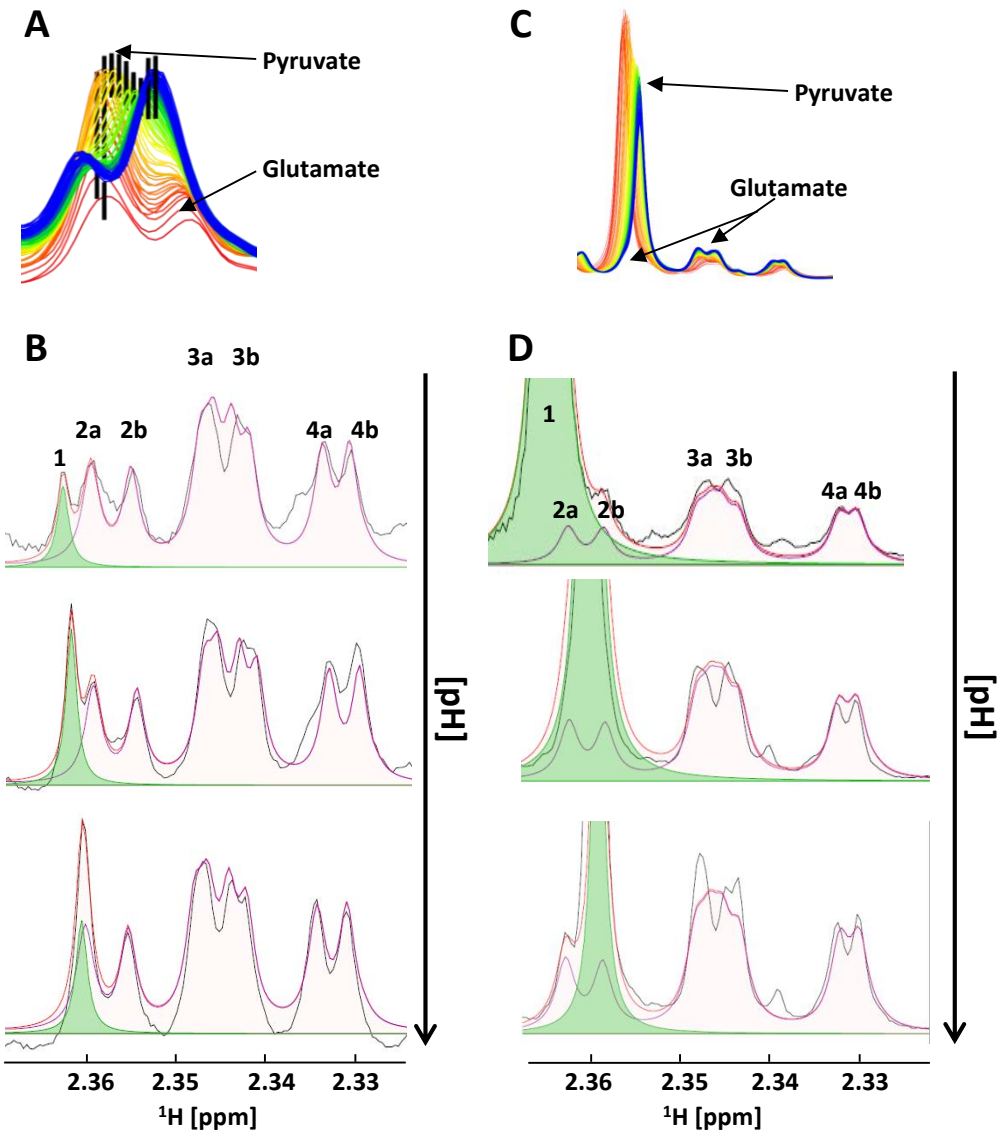

Figure 5. 1. Analysis of the pyruvate concentration during the time course with CLL cells.

A) Superimposed time course spectra with the pyruvate peak. As the pH decreased the pyruvate signal shifted upfield causing overlap with one of the glutamate resonances. B) Pyruvate intensities (green signal 1) were derived using the Chenomx and glutamate signal intensities (purple signals 2ab, 3ab, 4ab). The glutamate concentration (corresponding to area under the curve) was estimated using glutamate signals 2b, 3ab and 4ab. In order to estimate the pyruvate concentration, from the area under the overall signal arising from the overlapping pyruvate-glutamate signals, the estimated area under the signal 2b was subtracted. C) The sample with CLL cells was spiked with pyruvate, the same pH dependent shift was observed. D) The concentration of glutamate and pyruvate was estimated accordingly using Chenomx software.

5.2.2. CLL cells export pyruvate in normoxia and take it up again in hypoxia.

Across the 24 hours of recording the NMR spectra, lactate continued to accumulate and glucose was continually consumed. Similarly, once initiated in hypoxia, alanine accumulation continued throughout the experiment. In stark contrast, pyruvate kinetics were more complex. During the early stages, prior to complete oxygen depletion, pyruvate signals were seen to increase and then to fall during the period in hypoxia, suggesting a key differential functional importance of this metabolite in oxygenated and hypoxic conditions (Figure 5.2). Pyruvate uptake occurred after an average of 1.5-2 hours following oxygen consumption (Figure 5.2 B). Footprint analysis of media taken from CLL cells cultured in oxygenated conditions and hypoxia demonstrated that CLL cells release pyruvate in the presence of oxygen but not in hypoxia, suggesting that the fall in pyruvate in hypoxia relates to the re-uptake of pyruvate by CLL cells. Consistent with this, incubation of CLL cells with [2,3-^{13}C]pyruvate in hypoxia demonstrated pyruvate uptake by CLL cells with the label being detected in both lactate and alanine (Figure 5.2 C,D). ^{13}C incorporation to lactate was very quick and by the time the first spectrum was recorded, the label incorporation had reached a plateau at around 50%. This suggests that around 50% of lactate was produced from pyruvate that had been taken up by cells, while the remaining 50% was produced from the unlabelled glucose. Although

the incorporation of ^{13}C into the alanine signal was visibly increasing in the spectrum containing only signals originating from protons bound to ^{13}C compared to the spectrum containing NMR signals originating from all protons in the sample, it was not possible to calculate the ^{13}C incorporation due to the pyruvate keto tautomer signal overlapping with alanine resonance (Muller, Baumberger 1939) (See 5.2.7 for more information about the pH dependent pyruvate tautomerisation).

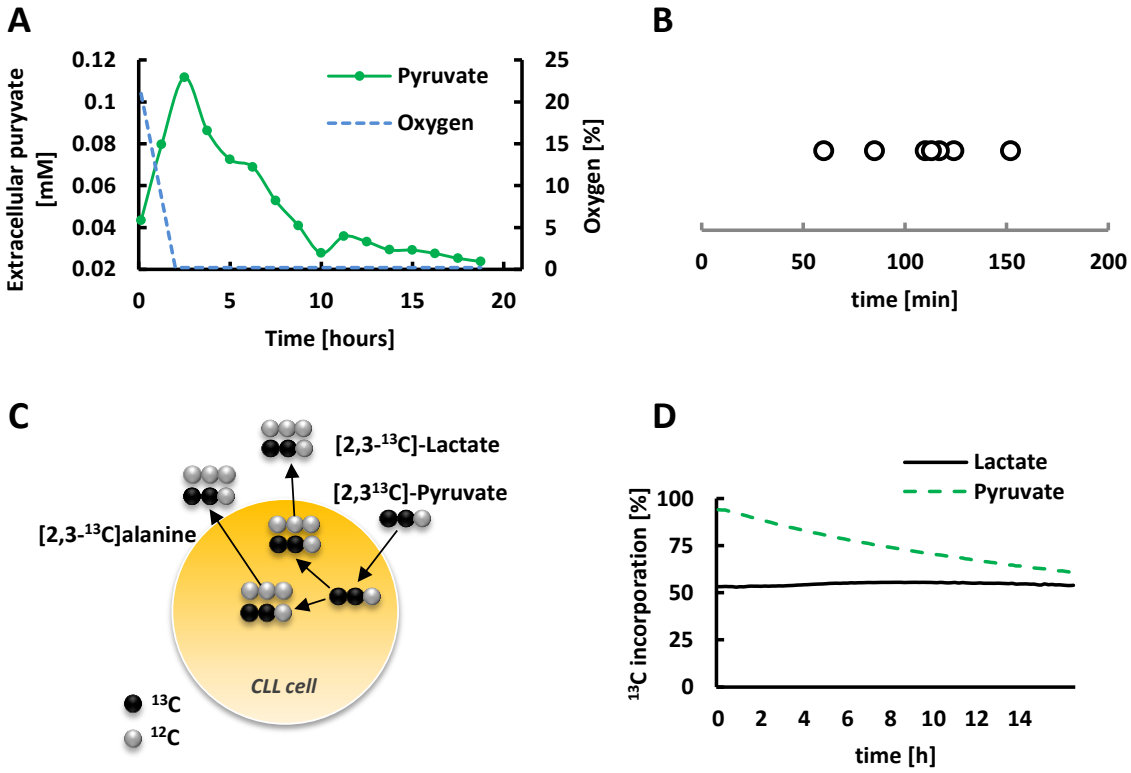

Figure 5. 2. Flux of pyruvate.

A) The extracellular pyruvate concentration together with the oxygen decrease during the NMR time course experiment derived from Chenomx analysis of ^{1}H-NMR spectra. B) The time difference between the oxygen depletion and the start of pyruvate uptake in 8 different experiments. C) The scheme of the experiment performed. 5 mM of the [2,3-^{13}C]pyruvate was added to the CLL cells and the NMR time course was performed. As a result a build-up of the label incorporation into alanine and lactate was observed. D) Graph shows the ^{13}C label incorporation to the total pool of pyruvate and lactate.

5.2.3 Pyruvate dynamics were not HIF-1α dependent.

Exposure of CLL cells to CTM indicated the transition in pyruvate dynamics was not tightly dependent on HIF-1α activation (Figure 5.3). The two chetomin concentrations investigated, 50 nM and 100 nM, did not alter the pyruvate profile in a concentration dependent manner. Secretion of pyruvate in normoxia declined slightly, following HIF-1α inhibition, which may be a consequence of the increased PDH activity, allowing pyruvate to enter the TCA cycle. However pyruvate uptake in hypoxia was not affected by chetomin, suggesting its importance in the metabolism of CLL cells independently from HIF-1α activation.

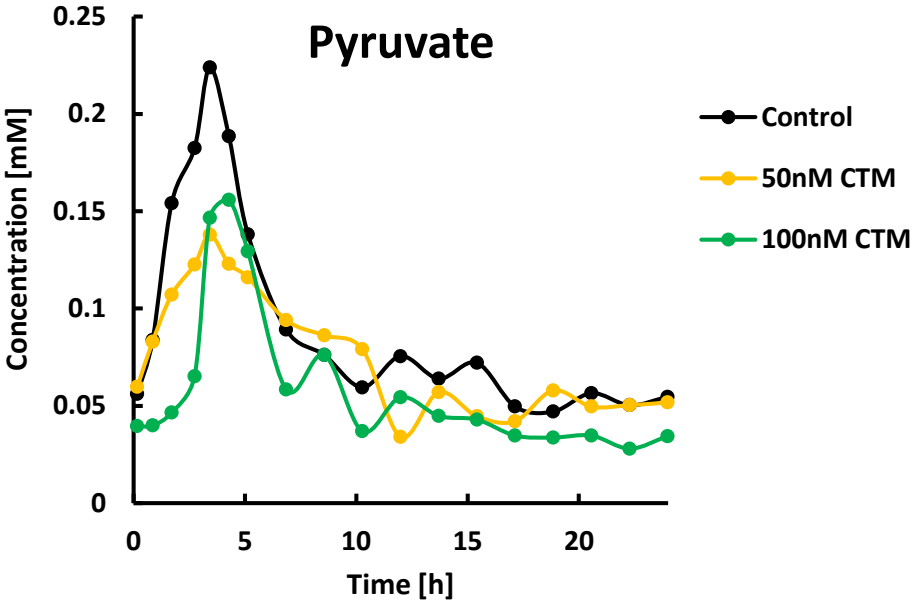

Figure 5. 3. The transition in pyruvate dynamics was independent of HIF-1α activation.

The NMR timecourse data for the control CLL experiment and cells treated with 20 mM and 100 nM CTM. Cells were pre-treated with CTM for 3 hours before starting the NMR experiment. Graph presents changes of extracellular pyruvate concentration over time. Concentration values were calculated using Chenomx software.

5.2.4 Inhibition by MCT1 prevents pyruvate re-uptake and causes apoptosis of CLL cells.

Pyruvate has recently been demonstrated to directly protect cells against hypoxic stress (Cipolleschi, Marzi et al. 2014). It was therefore hypothesised that CLL cells utilise pyruvate in hypoxia as a defence mechanism against hypoxia induced ROS. To test this hypothesis, investigations into the dependence of hypoxic CLL cells on pyruvate uptake were conducted using the inhibitor α-cyano-4-hydroxycinnamate (CHC). This inhibitor prevents the cellular uptake of pyruvate via the monocarboxylate transporter 1 (MCT1) (Figure 5.4). As shown in Figure 5.4 C, CHC concentrations of 2 mM and 5 mM only slightly diminished the rate of pyruvate accumulation whilst oxygen was available, but completely reversed its re-uptake upon entry into hypoxia. Exposure to CHC also reduced cell viability in a dose dependent fashion (Figure 5.4.B). As the role of MCT1 is to transport both lactate as well as pyruvate (through cellular and mitochondrial membranes), it was possible that lactate kinetics would also be affected by CHC. In fact, the time course data demonstrated a decrease of lactate export but not its complete blockage (Figure 5.5). Lactate and alanine secretion is decreased in hypoxia which could be linked to the lower uptake of the extracellular pyruvate. The observed lower glutamine and glucose consumption may reflect the decreased cell viability. Interestingly, glutamate production was not affected by CHC.

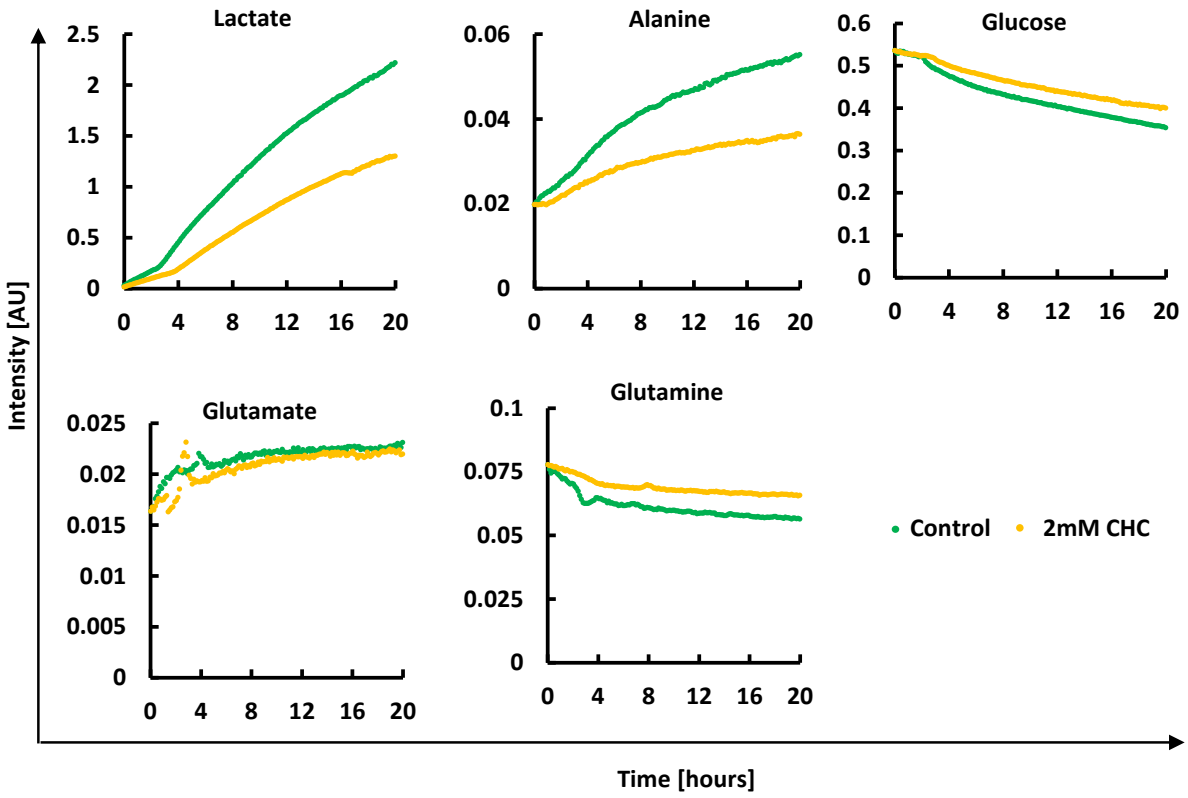

Figure 5. 5. Metabolic changes during CHC treatment.

NMR time course data for the control CLL experiment and cells treated with 2 mM CHC. Cells were pre-treated with CHC for 3 hours before starting the NMR experiment. The signal intensities of chosen metabolites (lactate, alanine, glutamate, glutamine and glucose) over time are presented in the graphs.

5.2.5 Methyl pyruvate does not rescue CLL cells from CHC.

It was observed that CHC also had an effect on the viability of CLL cells in oxygenated conditions. As MCT1 is not a pyruvate-specific transporter, an investigation was conducted to determine whether the toxicity of CHC was solely a consequence of pyruvate transport inhibition. CLL cells were supplemented with 2 mM methyl pyruvate before CHC treatment. Methyl pyruvate is a permeable derivative of pyruvate entering cells through the cell membrane without the need for a specific transporter. In this experiment, if cell viability decreased as a result of blocked extracellular pyruvate uptake through MCT1, a decrease of apoptosis after supplementing cells with methyl pyruvate would be seen. However, addition of methyl pyruvate did not rescue cells from apoptosis caused by CHC, suggesting that blocked pyruvate transport was not the sole cause of cell death (see figure 5.6). Interestingly, ROS levels were significantly decreased in cells supplemented with methyl pyruvate, supporting the hypothesis that CLL cells take up the extracellular pyruvate in order to use it as an anti-ROS defence. In contrast, levels of mitochondrial ROS – mitochondrial superoxide (mitosox) – did not decrease when membrane permeable methyl pyruvate was added. It is possible that methyl pyruvate is able to cross both cellular and mitochondrial membranes, therefore the absence of mitosox decreases suggest that methyl pyruvate must have been

demethylated or degraded in some other way, preventing its entrance into the mitochondria.

The reduced viability of CLL cells after CHC treatment may also have been a consequence of lactate build up inside cells, reducing the intracellular pH.

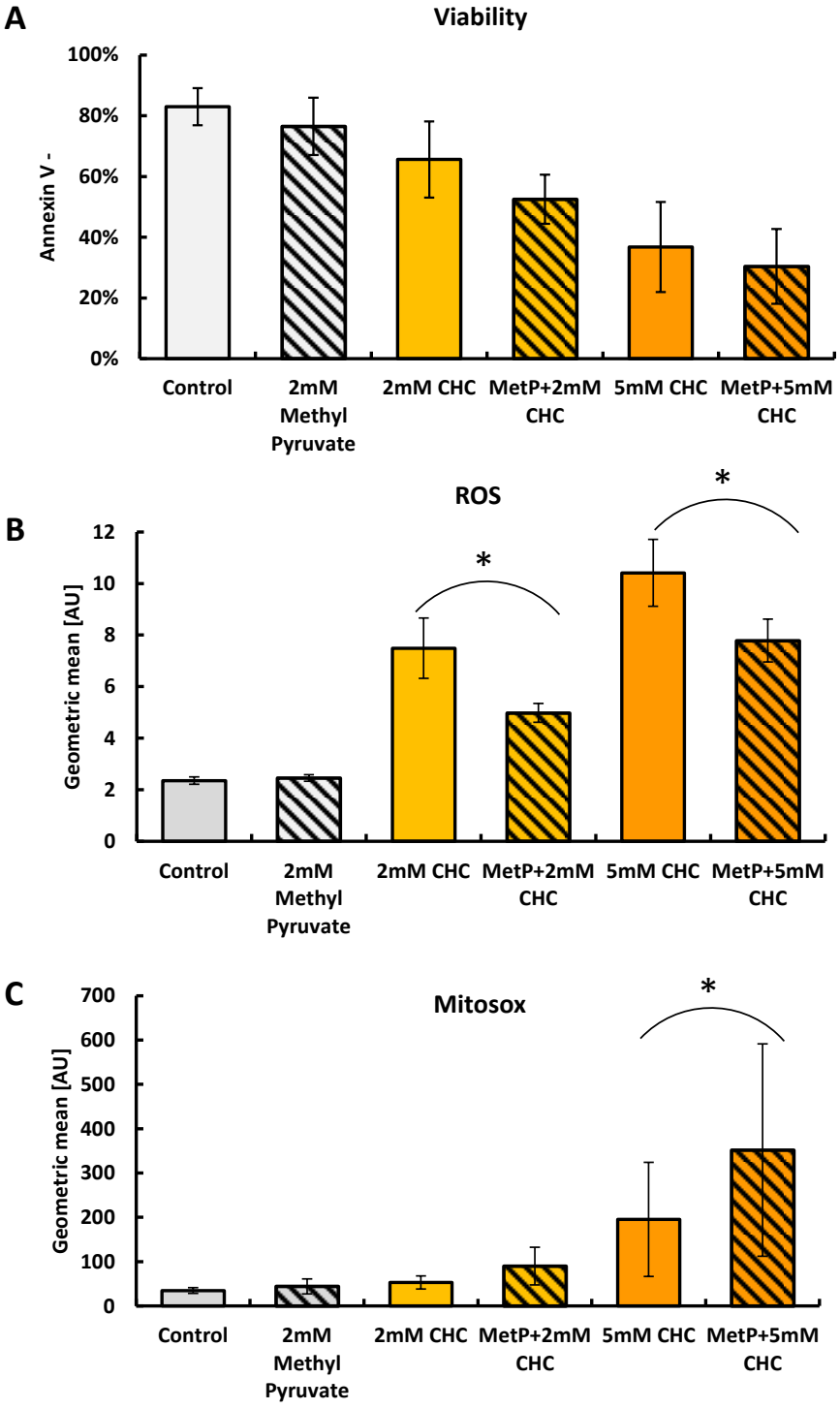

Figure 5. 6. Methyl pyruvate does not rescue cells from CHC induced apoptosis.

A) Methyl pyruvate did not rescue cells from CHC induced apoptosis. B) Methyl pyruvate decreased ROS in CLL cells treated with CHC. C) Methyl pyruvate increased mitosox in CLL cells treated with CHC. Data are mean of n=3 ± SEM, *p < 0.05 by student's t-test for paired data.

5.2.6 Exogenous pyruvate reduces mitosox and ROS levels in CLL cells.

The demonstration of the ability of CLL cells to utilise the availability of exogenous pyruvate for protection against stress, required the exacerbation of stress and supply of exogenous MCTI-transport dependent pyruvate. As shown in Figures 5.7 and 5.8, exposure of CLL cells to H_2O_2 for 24 hours resulted in elevated levels of mitosox and other ROS in both hypoxic and normoxic conditions. However, supply of exogenous sodium pyruvate significantly diminished both measures of cellular stress. Likewise, provision of exogenous pyruvate reversed H_2O_2-induced CLL cell killing. These data suggest that CLL cells do not only alter their metabolism in relation to the availability of oxygen, but that they can also modulate their utilisation of available metabolites, when experiencing ROS-induced stress. Cytospins stained with Jenner-Giemsa stain clearly presented the H_2O_2-induced apoptosis and rescue of cell phenotype when sodium pyruvate was added to the medium (Figure 5.7 D). There was no morphologically visible difference between cells treated in normoxia, from those in hypoxia (0.1% of O_2). However, histograms presented in Figure 5.8 show that levels of both mitosox and ROS were elevated in hypoxia.

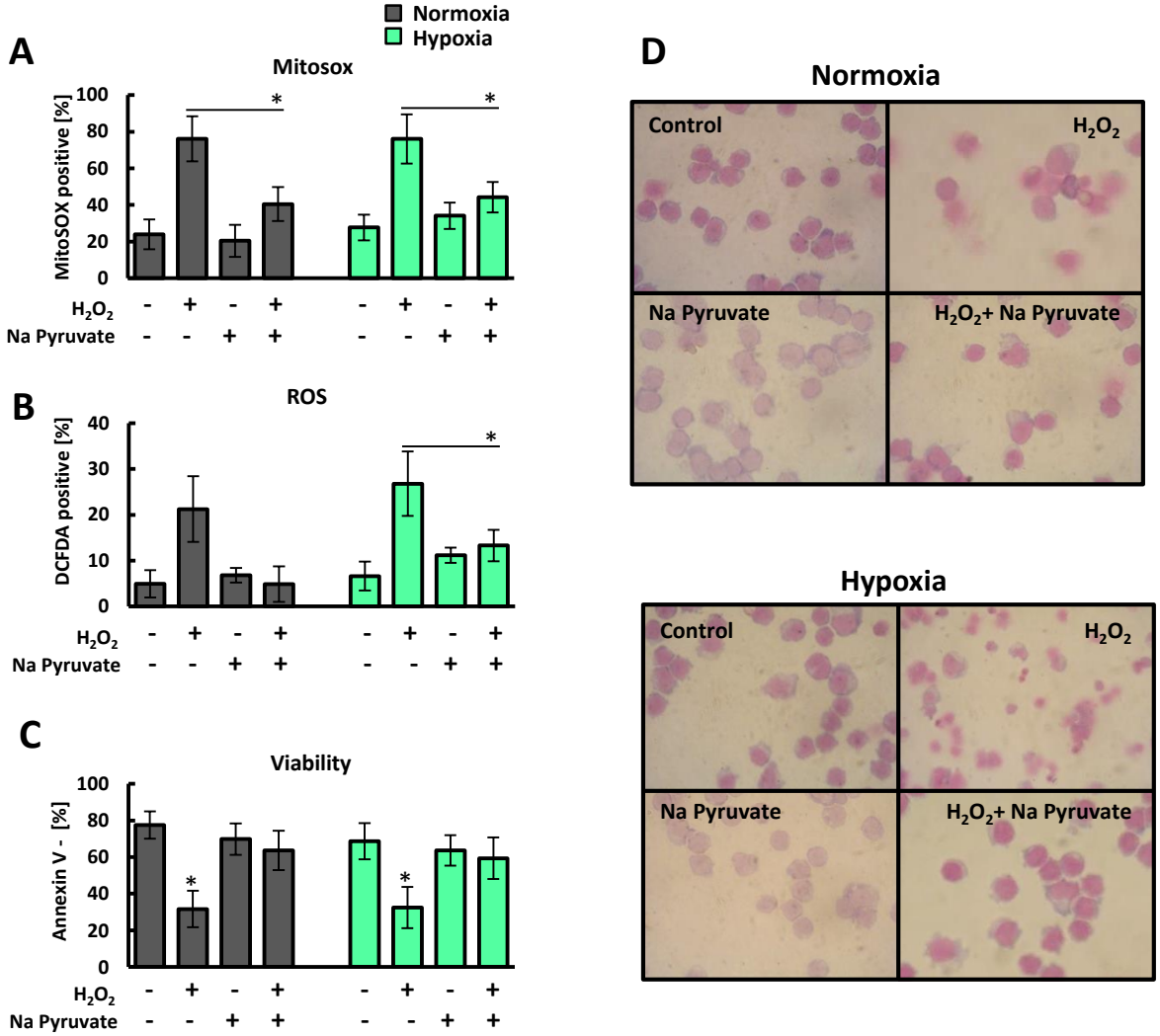

Figure 5. 7. Exogenous pyruvate reduces mitosox and ROS levels in CLL cells.

CLL cells were incubated for 24 hours with H_2O_2 and Na pyruvate in normoxia or hypoxia (0.1% O_2) prior to harvesting, transferring to the FACS tube, washing and incubating with A) MitoSOX for 10 minutes, B) H2DCFDA for 40 minutes or C) AnnexinV/PI for 15 minutes and analysed by FC. Data are the mean ± SEM from n=5 patients; *$p < 0.05$ by student's t-test for paired data. D) Cytospins of CLL cells from each treatment stained with Jenner-Giemsa.

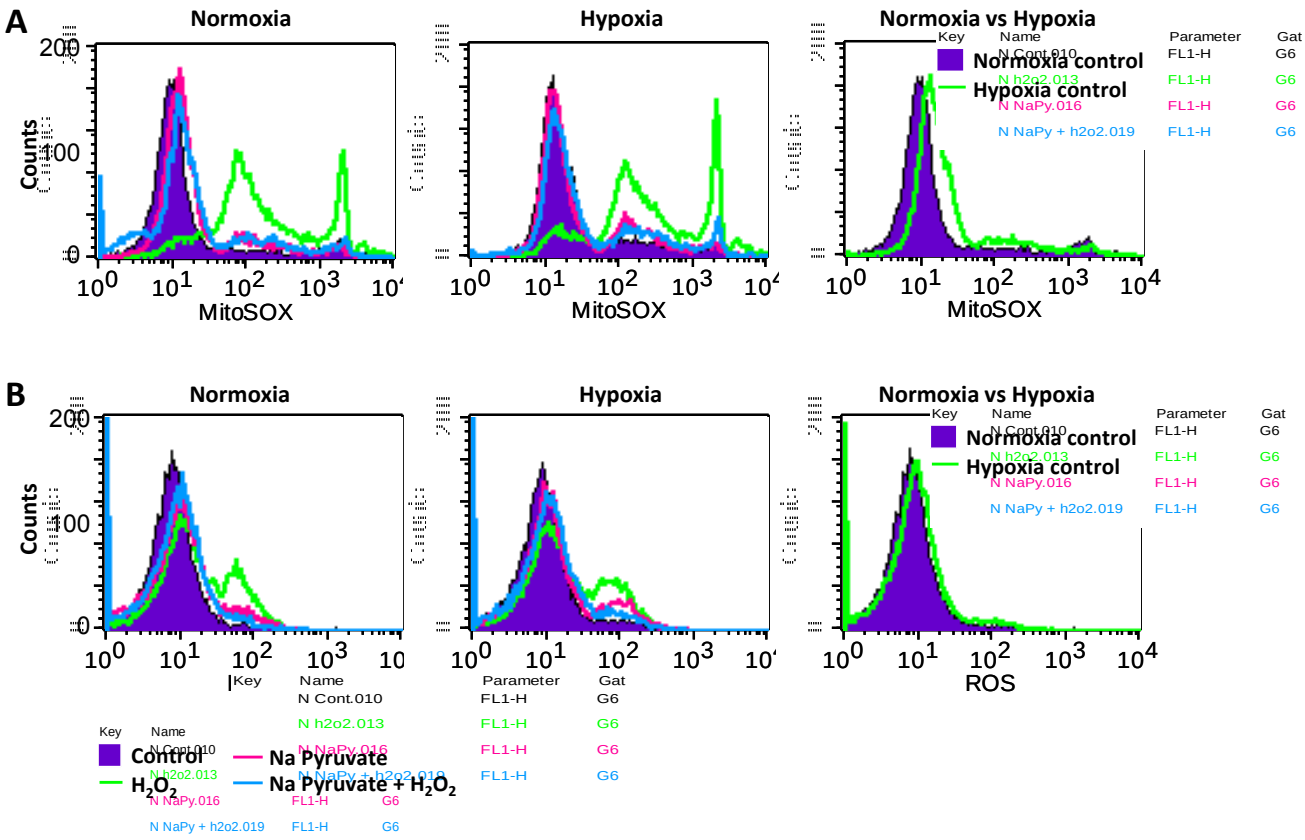

Figure 5. 8. Exogenous pyruvate reduces mitosox and ROS levels in CLL cells.

CLL cells were incubated for 24 hours with H_2O_2 and sodium pyruvate in normoxia or hypoxia (0.1% O_2) prior to harvesting, transferring to the FACS tube, washing and incubating with A) MitoSOX for 10 minutes, B) H2DCFDA for 40 minutes and analysed by FC.

5.2.7 Keto-enol tautomerism of pyruvate

Pyruvate can appear in one of two tautomer forms depending on the pH. The pyruvate keto ion has two C=O double bonds which are conjugated (see figure 5.9 A). The enol form tautomer of the pyruvate ion has one C=C double bond and a C=O group which is also conjugated. Unfortunately, metabolomics NMR databases such as HMDB do not provide the information about the keto tautomer and present only one peak in the pyruvate spectrum (at 2.46 ppm) corresponding to the enol form, described as a keto form. Using the NMR time course setup as described previously, a set of two 1D-^{1}H ^{13}C decoupled NMR spectra of CLL cells enriched with 5 mM [2,3-^{13}C]pyruvate was recorded. The acquired spectrum was edited in order to contain only signals originating from protons bound to ^{13}C, allowing for the observation of clearly identifiable peaks corresponding to keto and enol forms, without the background noise of other peaks (Figure 5.10). Using the intensities of pyruvate peaks, it was possible to calculate changes in the ratio of keto : enol forms throughout the time course. pH changes were calculated using the histidine peak (as shown in chapter 3.2.7) from spectra containing NMR signals from all protons in the sample. From these, the correlation between the tautomer changes and decreasing pH were described. During 19 hours of the time course, pH changed from 7.79 to 6.33, while the enol form of the protons decreased from 89.4% to 86.4% and the keto form increased from 10.6% to 13.6% (Figure 5.9 and 5.10). Although there was a strong

correlation between pH changes and tautomerisation and pH changed substantially for 1.46 units, the 3% change in the ratio of tautomers did not have an impact on the metabolic interpretation of the pyruvate kinetic data shown previously. Nevertheless, it is important to be aware of the possible tautomer balances while interpreting NMR spectra.

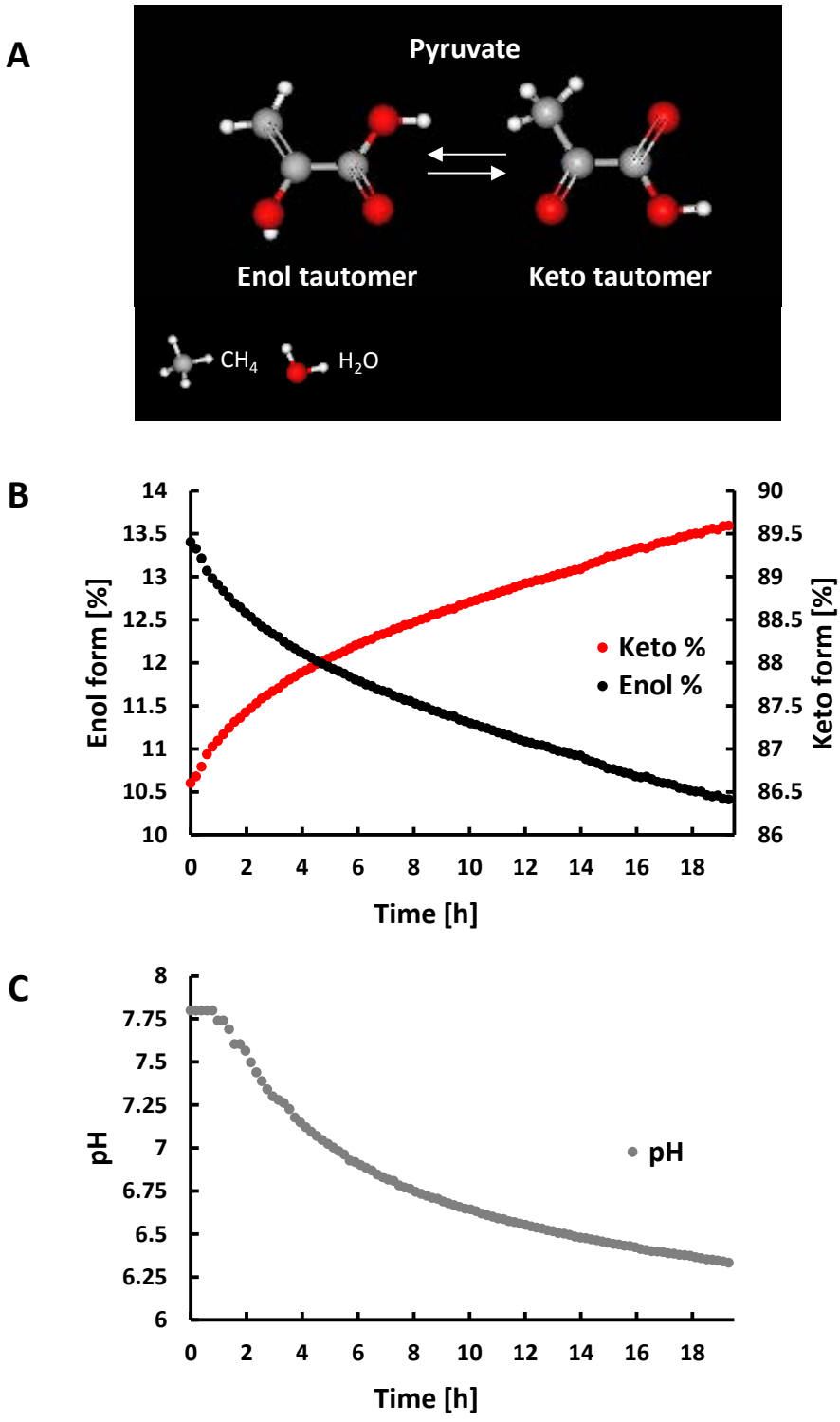

Figure 5.9. Keto-enol pyruvate tautomerism.

A) Pyruvate undergoes tautomerization depending on pH. B) 5 mM of the [2,3-^{13}C]pyruvate was added to the CLL cells and the NMR time course experiment was carried out. The percentage of enol and keto tautomers of pyruvate was calculated and the changes during the time course were plotted. C) pH Changes during the same time course experiment.

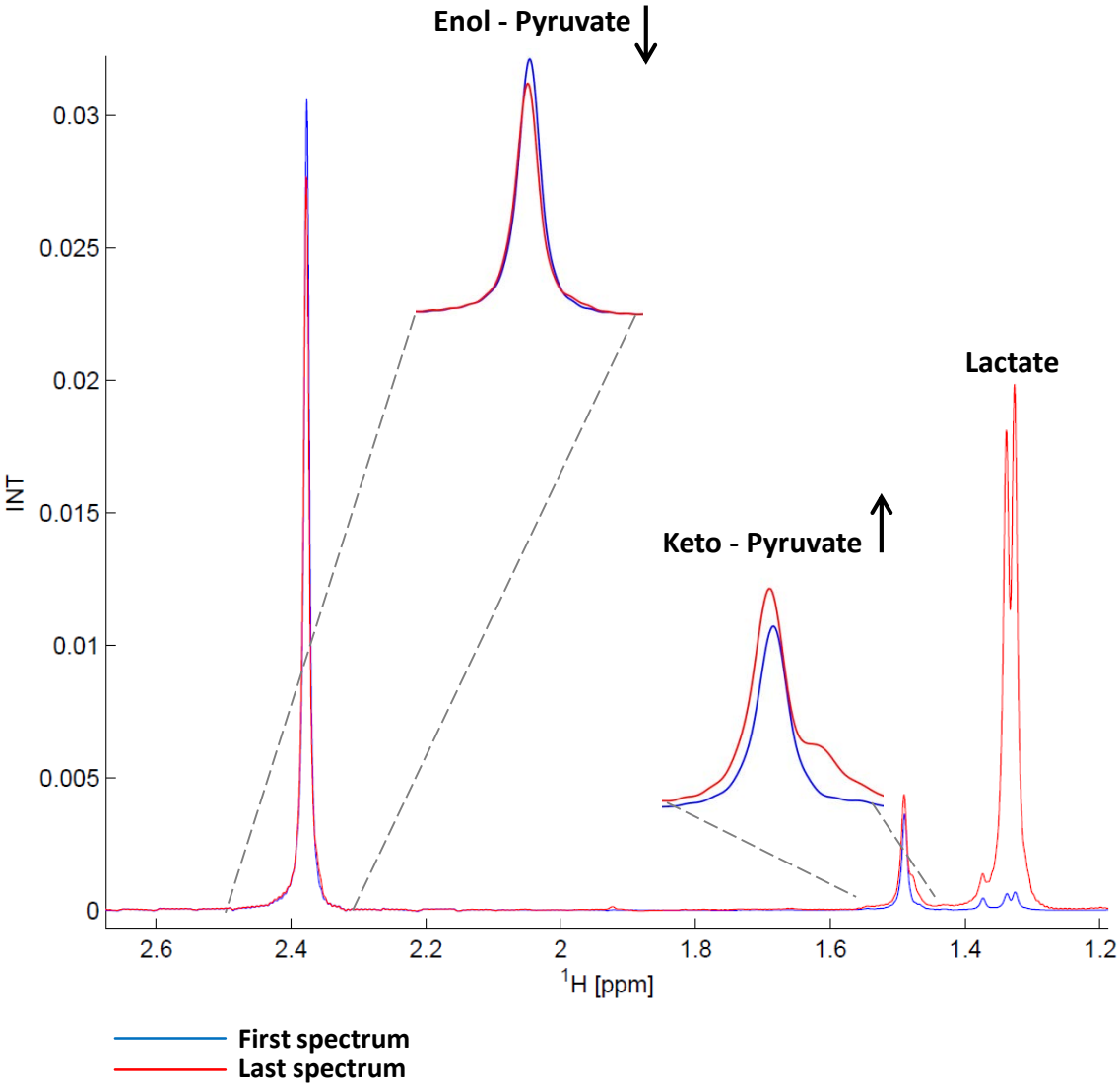

Figure 5. 10. Keto-enol pyruvate tautomerism in the NMR spectrum.

CLL cells were measured over 24 hours with ^{13}C pyruvate. As lactate was produced and pH subsequently decreased, the level of the enol tautomer of pyruvate declined due to its transformation to the keto form. 1D-^{1}H NMR spectra containing only signals originating from protons bound to ^{13}C are presented. The first specturm of the time course is shown in blue, the last spectrum in red. Spectra were scaled to the total amount of the ^{13}C pyruvate in the spectrum.

5.3 DISCUSSION

One of the difficulties of accurate assignment and quantification of metabolite NMR spectra arises from the problem of chemical shift degeneracy of individual metabolites. This chapter presents solutions to overcome this obstacle and to extract the relevant data from overlapping signals. The focus of the investigation was the methyl resonance of pyruvate at 2.46 ppm at pH 7. Keto-enol tautomerisation of pyruvate at acidic pH, with a related increase in the proportion of the enol form, at 1.47 ppm in the ^{1}H NMR spectrum, was observed. This has been taken into account for the analysis of the real-time changes in the NMR spectra with changing pH.

Using the Chenomx software, the precise quantification of pyruvate concentrations was possible from overlapping signals and signal multiplets, by stimulating spectra and subtracting glutamate resonances. The data produced showed that primary CLL cells secrete pyruvate while in normoxia and take it up after approximately 2 hours of incubation in hypoxic conditions. Export of pyruvate by CLL cells has previously been reported in studies detecting increased serum pyruvate in CLL patients when compared to healthy donors (MacIntyre, Jimenez et al. 2010). One of the proposed explanations for the elevated pyruvate level in MacIntyre's study (MacIntyre, Jimenez et al. 2010) is a deficiency in thiamine, which in its physiologically active form - thiamine pyrophosphate- acts as a coenzyme in pyruvate decarboxylation (Seligmann, Levi et al. 2001). Although thiamine deficiency

has been reported in CLL patients, it is unlikely that CLL cells used in the present *in vitro* investigation suffered from lack of thiamine, as RPMI medium contains 1 mg/l of thiamine hydrochloride and cells were suspended in fresh medium for each NMR time course experiment.

It has also been shown that human fibroblasts, as well as breast adenocarcinoma cell lines, secrete pyruvate when incubated in pyruvate-free medium (O'Donnell-Tormey, Nathan et al. 1987). This pyruvate secretion was attributed to protection from ROS. Although it is surprising that primary cancer cells divert a substantial portion of their potential energy supply by export of pyruvate, there is an obvious advantage for cells in scavenging exogenous H_2O_2 before it reaches the cell. Under the experimental conditions of the present study, the oxygen level decreased from the 0 time point, therefore the level of ROS may have been gradually rising. After about 100 minutes of hypoxia, intracellular ROS must have been substantially increased, inducing the uptake of pyruvate to scavenge ROS and mitosox inside cells.

Considering that the pyruvate NMR signal observed in this experiment reflected only the extracellular pyruvate, a subsequent investigation was conducted to determine whether the metabolite was indeed taken up and used by cells (and not degraded or used in some biochemical reaction outside cells). A ^{1}H and proton filtered ^{13}C 1D spectra approach was used to detect ^{13}C-incorporation from

extracellular pyruvate into lactate and alanine in real time. The pulse sequence was recently developed in our NMR group and real time experiments with CLL cells were the first time course spectra obtained using this method. During the optimisation of the method keto-enol tautomerism of pyruvate was observed, although it did not significantly influence the overall intensities within the pH range observed for the samples used (max 3%).

Pyruvate uptake has been reported as an important factor that correlates with cancer invasiveness. It has been shown that more invasive ovarian cancer cells exhibit higher pyruvate uptake than their less invasive counterparts (Caneba, Bellance et al. 2012). Moreover, pyruvate had an effect on the migration ability of highly invasive ovarian cancer cells. Pyruvate uptake has therefore been suggested to be potentially used in cancer diagnostics. The possible suggested explanation of this phenomenon was that pyruvate may fuel the TCA cycle and may play a role in the increased oxygen consumption rate. A possible mechanism is that pyruvate can be converted into glycerate 2-phosphate in the glycolysis pathway. Pyruvate and serine are taken up to create hydroxypyruvate (in the transamination reaction), which is then converted to glycerate via NADPH and further into glycerate 2-phosphate through conversion of ADP into ATP (Mazurek 2011). In this way, pyruvate may be another metabolite consumed during glycolysis.

Although pyruvate uptake in CLL cells in the time course experiments presented here was driven by hypoxia and considering that hypoxia induces MCT1 expression (De Saedeleer, Porporato et al. 2013), the data shown above demonstrates that pyruvate uptake is independent of HIF-1α activation and is not affected by chetomin treatment. In order to disrupt pyruvate import, the monocarboxylate transporter 1 (MCT1) inhibitor CHC was used. Blockage of this transporter resulted in the complete inhibition of pyruvate uptake and partial decrease of lactate export. As both lactate and pyruvate are transported by MCT1, it is not possible to specifically inhibit pyruvate transport. MCT1 treatment resulted in dose dependent apoptosis which was not the sole cause of the blockage of pyruvate uptake, as the addition of the membrane soluble pyruvate derivative - methyl pyruvate did not rescue cells. Although methyl pyruvate did not increase cell viability, it decreased the ROS levels significantly. Importantly, lactate export was not completely blocked by CHC, therefore the mechanism of CLL cell apoptosis resulting from MCT1 inhibition may be more complex than just the inhibition of lactate and pyruvate transport. Although the metabolic consequences of MCT1 inhibitors are not yet completely clear and little is known about its regulation by typical parameters of the tumour microenvironment (Asada, Miyamoto et al. 2003; Kennedy and Dewhirst 2010; Halestrap and Wilson 2012), the first MCT1 inhibitor is currently undergoing clinical trials for treatment of various types of cancer (Porporato, Dhup et al. 2011; Polanski, Hodgkinson et al. 2014).

Finally the current investigation revealed that the addition of extracellular sodium pyruvate to CLL cells treated with H_2O_2 resulted in decreased ROS and mitosox levels and helped to rescue cells from apoptotic death. Therefore we sustain the hypothesis that CLL cells take up extracellular pyruvate in hypoxia for ROS protection. Interestingly, it was shown that ROS is responsible for the re-oxygenation damage of endothelial cells (Dhar-Mascareno, Carcamo et al. 2005) which also suggests that CLL cells may protect themselves from apoptosis after entering the oxygenated environment, by storing the ROS scavenging pyruvate.

Recently, additional studies have emphasised the importance of the ability of Chronic Lymphocytic Leukaemia in fighting ROS. Another proposed adaptation of CLL cells to intrinsic oxidative stress is the up-regulation of the stress-responsive heme-oxygenase-1 (HO-1). New data indicates that HO-1 is also, involved in promoting mitochondrial biogenesis beyond its function as an antioxidant. Thus ROS, adaptation to ROS and mitochondrial biogenesis appear to form a self-amplifying feedback loop in CLL-cells. Taking advantage of such altered metabolism, it may be possible to selectively target CLL cells. Targeting the respiratory chain (by blocking the mitochondrial F1F0-ATPase) and promoting mitochondrial ROS, the benzodiazepine derivative PK11195 has recently been shown to induce cell death in CLL cells (Jitschin, Hofmann et al. 2014). These findings, together with the work

presented in this chapter, suggest that bioenergetics and redox characteristics could be therapeutically exploited for CLL treatment.

Chapter VI

Metabolic Flux Analysis of CLL cells in different oxygen environments

6.1. INTRODUCTION

Metabolic Flux Analysis (MFA) involving ^{13}C-labelled tracers requires a large number of cells, as the sensitivity of NMR to detect ^{12}C carbon is 4 times lower than that of protons due to the difference in the gyromagnetic ratio of ^{13}C nuclei compared to ^{1}H. The signal intensity in NMR spectra is a product of metabolite concentration, percentage of ^{13}C incorporation and several physical properties including the gyromagnetic ration and relaxation rates, and for proton observed HSQC spectra also heteronuclear scalar coupling constants between ^{1}H and ^{13}C. For this reason, an additional unlabelled cell sample is needed as a control for investigations of ^{13}C incorporation in tracer based analyses (^{13}C natural abundance is 1.07%). Therefore in standard procedures, the number of cells required is higher. Chronic lymphocytic leukaemia is clinically extremely heterogeneous and some patients are characterised by very high white blood cell counts, which indicate that their blood samples may provide a lot of biological material. One purpose of this study was to investigate if B-cells purified from 14 ml of peripheral blood from a CLL patient would provide enough biological material to perform good quality MFA. To date, this is the first such study performed on primary human CLL cells.

So far, investigation of the metabolism of CLL cells presented in this thesis has mainly been based on the examination of extracellular metabolites being taken up from or secreted into the media. This chapter describes in greater depth the analysis

of metabolic flux carried out using cell extracts using expression metabolic flux analysis (MFA). This is an approach in which the distribution of individual atoms through metabolic networks is observed, employing isotopically labelled metabolic precursors such as glucose and glutamine as tracers. Using MFA, it is possible to follow isotopic labels to investigate the pathways that are favoured in specific conditions for a particular cell type. For example, the labelled carbons of glucose would distribute differently to lactate carbons, depending on the pathway through which they are metabolised (See Figure 6.1). This chapter presents the use of an MFA approach for further investigations into the metabolic adaptations of CLL cells to different oxygen environments. The 2D ^{13}C-^{1}H HSQC analysis of CLL cells incubated in normoxia and hypoxia in medium containing [1,2-^{13}C]glucose and [3-^{13}C]glutamine will be presented.

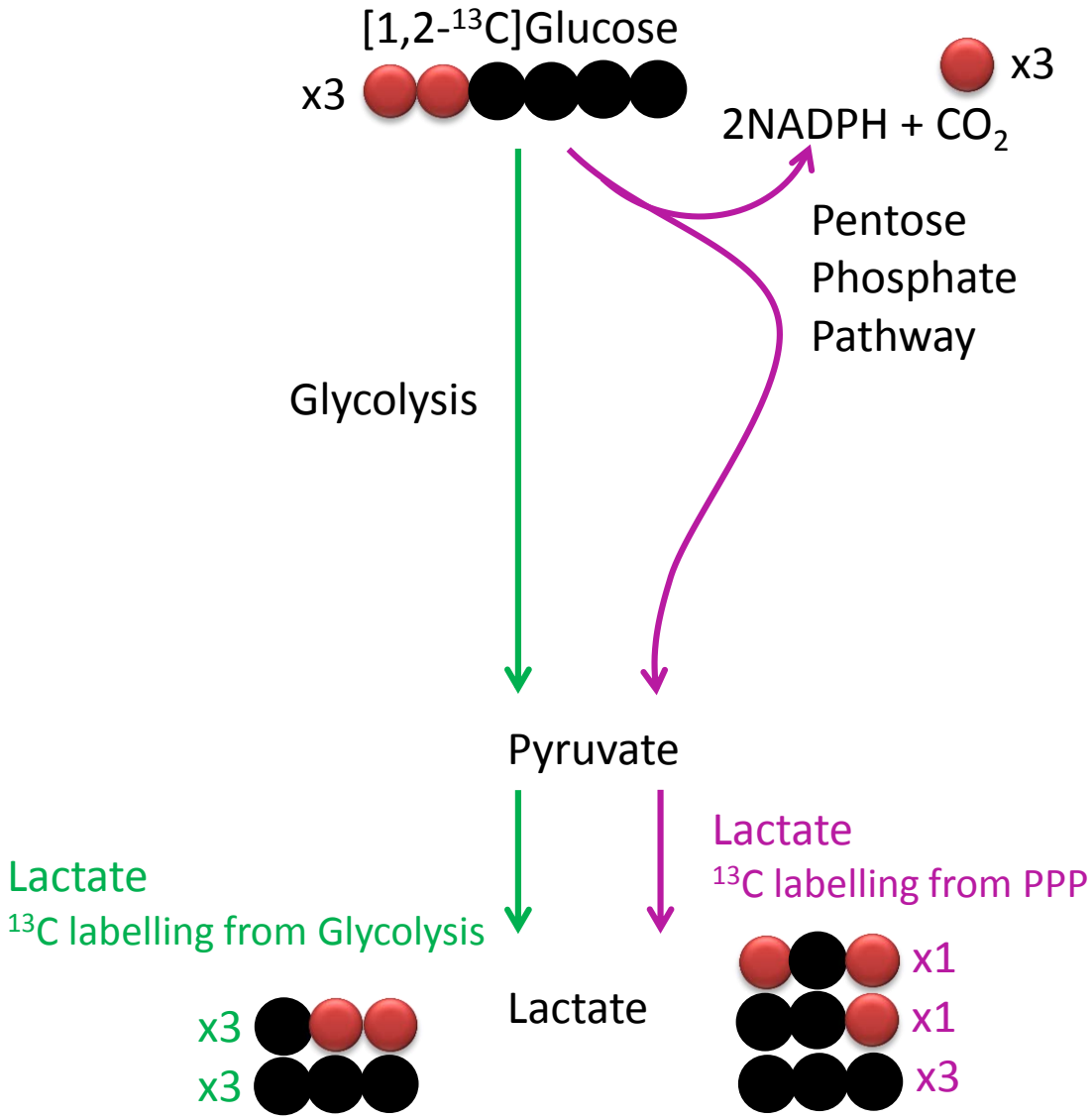

Figure 6. 1. ^{13}C labelled glucose flux to lactate through glycolysis and PPP.

The distribution of labelled carbons differs depending on whether glucose is metabolised through glycolysis or through the pentose phosphate pathway.

When multiple neighbouring carbon atoms are labelled, complex multiplet patterns of NMR signals arise (Figure 6.2), and the degree of the label incorporation into the adjacent carbons can be interpreted. In the case of one-dimensional ^{13}C-observed spectra, these multiplets are directly observed in the spectra. For this, the ^{1}H-^{13}C coupling must be removed using a decoupling sequence. The disadvantage of directly observed ^{13}C NMR spectra is lower sensitivity. Two-dimensional ^{1}H-^{13}C-HSQC spectra, offer a significantly improved sensitivity over ^{13}C-observed spectra by starting and ending on ^{1}H. The second dimension (ω1) in ^{1}H-^{13}C-HSQC spectra matches that of ^{13}C-observed spectra for ^{13}C atoms bound to protons, whereas the observed dimension (ω2) represents an ^{1}H spectrum showing only resonances of protons bound to ^{13}C. HSQC spectra require large numbers of increments (at least 4096) in order to be able to observe the ^{13}C-^{13}C scalar couplings in the incremented dimension, which prolongs the acquisition times to > 4 hours. This is however still faster than acquiring ^{13}C spectra, and provides additional spectral information through the ^{1}H resonances. ^{13}C-^{13}C scalar couplings provide valuable information about adjacent label incorporation.

6.2 RESULTS

In order to obtain good quality spectra with a good signal-to-noise ratio, ~180x10^6 CLL cells had to be extracted for each sample. Cells were obtained from a single patient (characterized by high white cell counts in blood) and individual samples were used for a single experiment which consisted of the 6 following conditions:

Cells incubated for 24h in normoxia	**Medium lacking labelled tracers**	**Medium with [1,2-^{13}C]glucose**	**Medium with [3-^{13}C]glutamine**
Cells incubated for 24h in hypoxia (1% O_2)	**Medium lacking labelled tracers**	**Medium with [1,2-^{13}C]glucose**	**Medium with [3-^{13}C]glutamine**

Labelled tracers replaced unlabelled precursors present in the control medium at the same concentrations.

6.2.1 [1,2-^{13}C]glucose flux through Glycolysis and Pentose Phosphate Pathway

Figure 6.4 presents the theoretical label distribution from glucose, when the PPP is involved and when it is not active. Depending on the pathway, distinctly labelled species of metabolites will be formed. After the multiple TCA cycle rounds, the pattern combinations became very complex, as an example the label distribution

in the glutamate molecule coming from the [1,2-^{13}C]glucose after multiple TCA rounds is shown on the Figure 6.5.

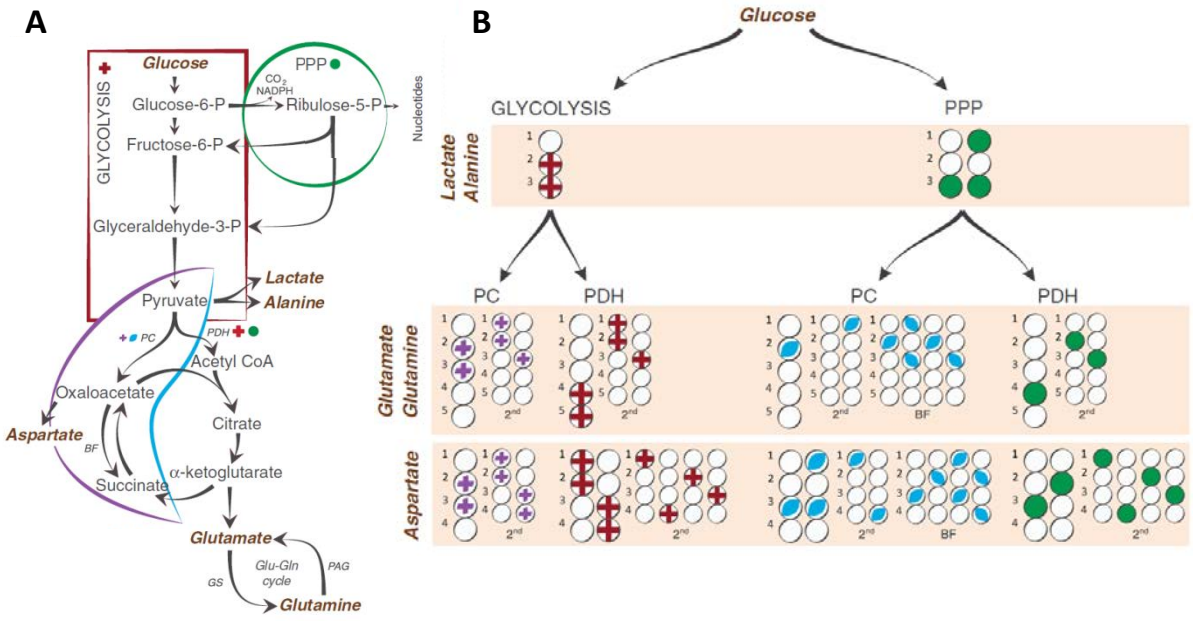

Figure 6. 4. Simplified presentation of ^{13}C labelling patterns of metabolites after incubating cells with [1,2-^{13}C]glucose.

A) Overview of the principal metabolic pathways. B) Labelling patterns in lactate, alanine, glutamate, glutamine and aspartate after metabolism of [1,2-^{13}C]glucose. Circles symbolise the carbon backbone of the molecules. Red crosses mark the position of the label resulting from glycolysis, followed by conversion to acetyl-CoA by PDH where applicable. Purple crosses indicate that the pyruvate (resulting from glycolytic metabolism) has instead undergone pyruvate carboxylation before being converted to the metabolite in question. Green circles represent labelling from the PPP, also followed by conversion to acetyl-CoA by PDH where applicable. Blue ovals indicate that the pyruvate (resulting from the metabolism in the PPP) has instead entered the TCA cycle via PC. After PC, the metabolite can undergo back-flux from oxaloacetate to succinate. BF, back-flux; GS, glutamine synthetase; P, phosphate; PAG, phosphate activated glutaminase; PC, pyruvate carboxylase; PDH, pyruvate dehydrogenase; PPP, pentose phosphate pathway. Adapted from (Brekke, Morken et al. 2014).

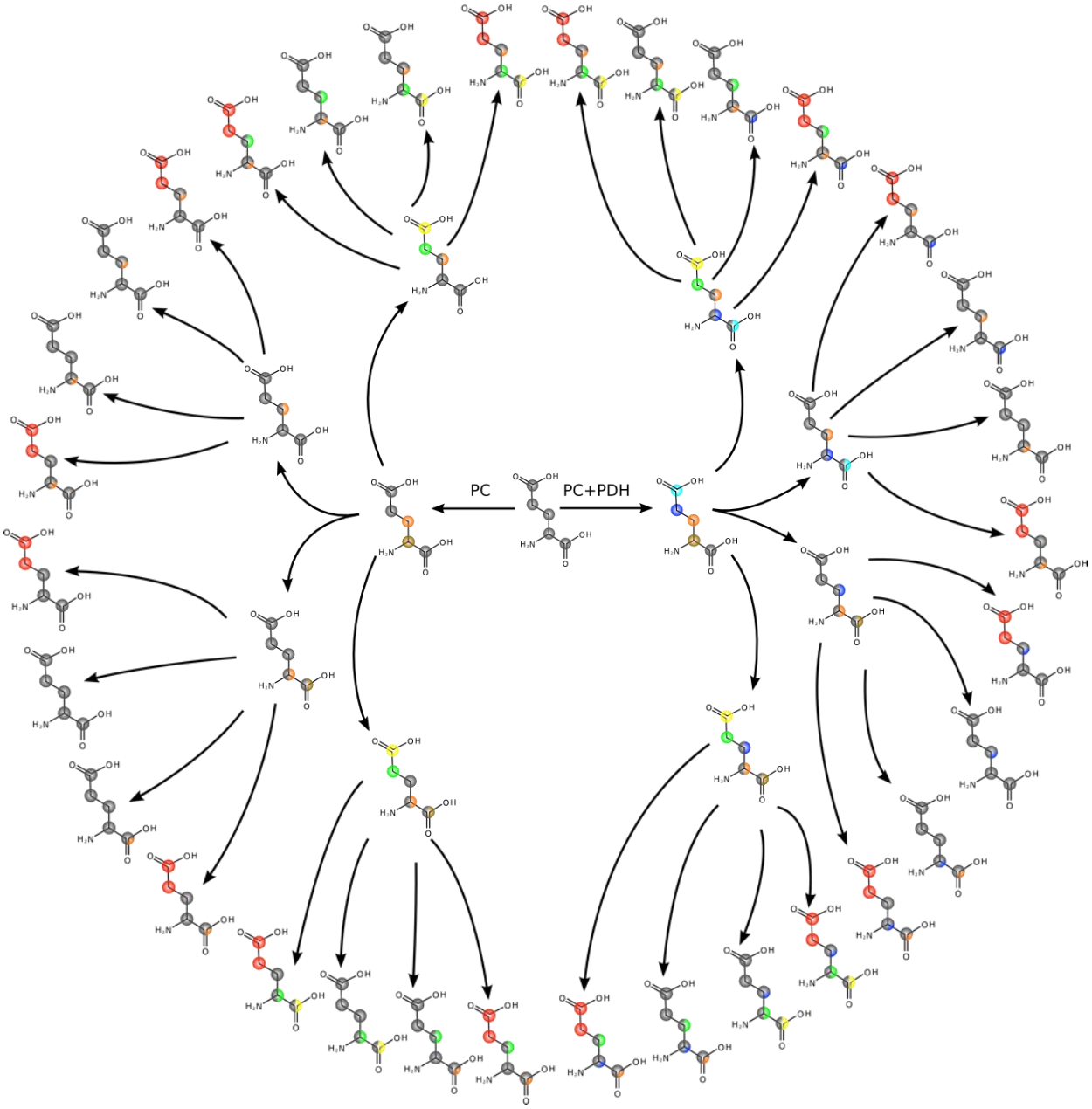

Figure 6. 5. The theoretical label distribution in the glutamate molecule derived from [1,2-^{13}C]glucose, after multiple TCA rounds.

The label distribution is different when only PC is active compared to the situation when both PC and PDH are active. Labelled distributions after 1, 2 and 3 TCA cycle rounds are presented. Adapted from a presentation made by C. Ludwig.

Figure 6.6 shows the analysis of the labelled glucose flux in normoxic conditions in CLL cells. Carbons C-1 and C-2 were transferred from the glucose molecule through the process of glycolysis, to pyruvate, then to lactate and finally to alanine, with labelled carbons in positions C-2 and C-3. Moreover, in depth analysis of the lactate and alanine line shapes revealed additional label in position C-3, derived from glucose metabolised through the pentose phosphate pathway, leading to lactate species labelled either in the C-3 position only, or simultaneously in positions C-1 and C-3 (see Figures 6.1 and 6.4). ^{13}C in position C-1 of both lactate and alanine molecules could not be seen in proton edited HSQC NMR spectra, as they are not protonated and both species (molecules with C-1 labelled and unlabelled) result in the same NMR spectrum. Therefore only the visible C-3 labelled lactate and alanine species were used as an indicator of PPP activity.

In common with the glucose flux in normoxia, in hypoxic conditions, carbon nuclei in lactate and alanine were labelled in positions C-2 and C-3 (Figure 6.7). The PPP activity, investigated by the multiplet analysis of C-3 in lactate and alanine, was shown to be less pronounced in hypoxia than in normoxia (Figure 6.8). For quantitative HSQC analysis 1D slices of HSQC spectra were evaluated using in house built software by C. Ludwig based on the MetaboLab software (Gunther, Ludwig et al. 2000; Ludwig and Gunther 2011) using a quantum mechanical spin system simulation, using the pygamma library (Smith, Levante et al. 1994).

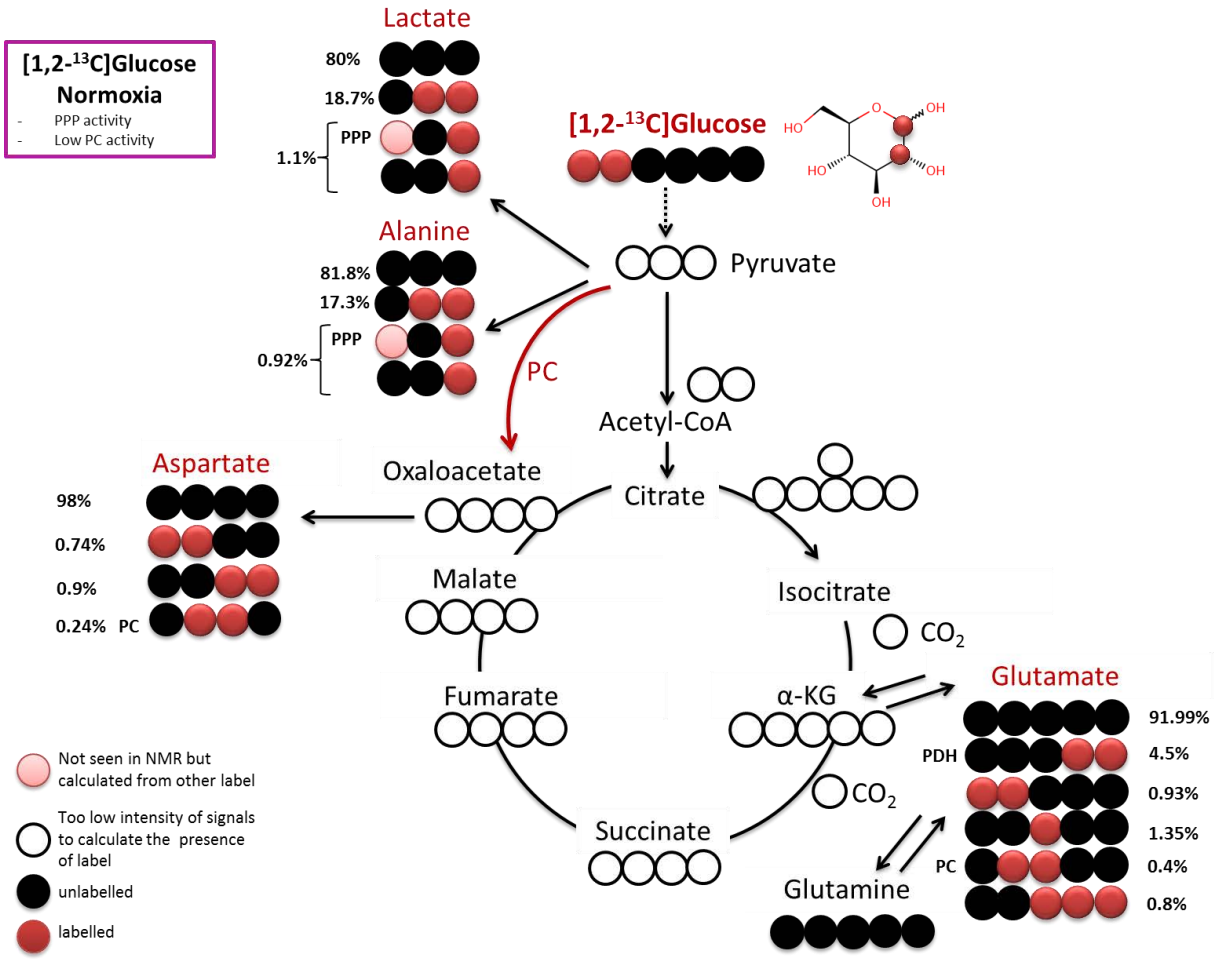

Figure 6. 6. Glucose flux in CLL cells in normoxia.

Label distribution in metabolites arising from [1,2-^{13}C]glucose under normoxic conditions. CLL cells were incubated for 24 hours in a normoxic incubator in RPMI medium with [1,2-^{13}C]glucose. Cells were extracted and the polar fraction was analysed by NMR spectroscopy. ^{1}H^{13}C – HSQC and 1D ^{1}H spectra were recorded. Data were analysed using the NMRlab software.

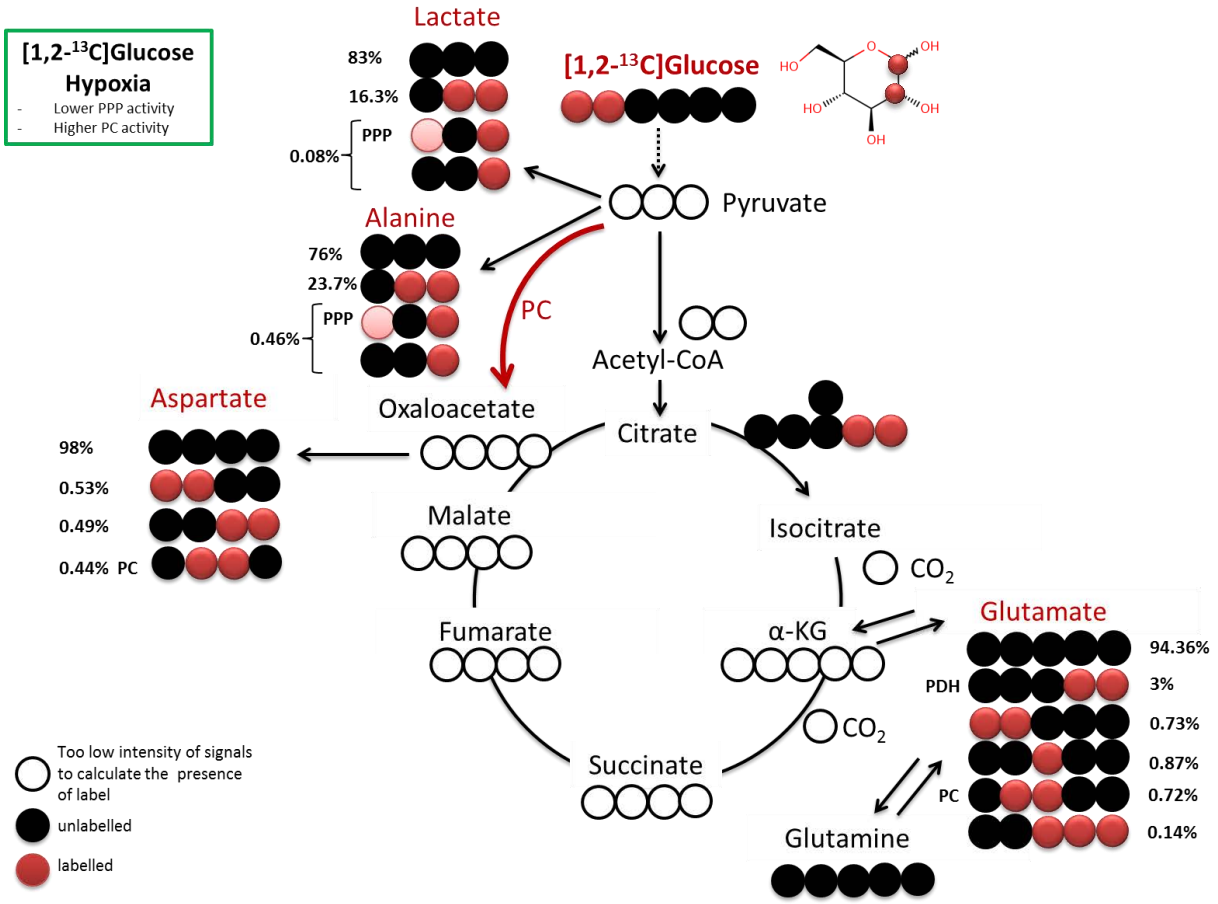

Figure 6. 7. Glucose flux in CLL cells in hypoxia.

Label distribution in metabolites arising from [1,2-^{13}C]glucose under hypoxic conditions. CLL cells were incubated for 24 hours in a hypoxic incubator (1% O_2) in RPMI medium with [1,2-^{13}C]glucose. Cells were extracted and the polar fraction was analysed by NMR spectroscopy. $^{1}H^{13}C$ – HSQC and 1D ^{1}H spectra were recorded. Data were analysed using the NMRlab software.

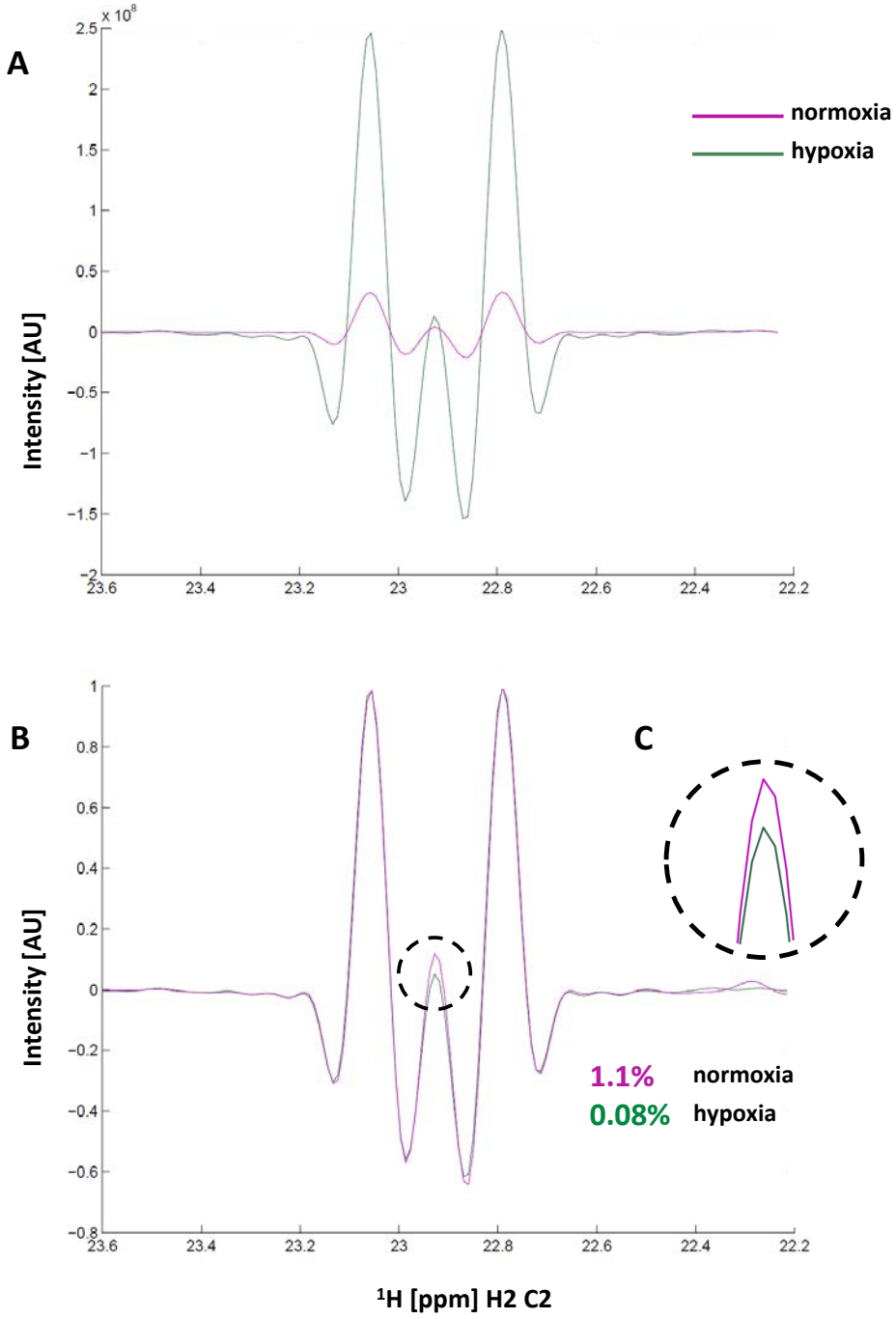

Figure 6. 8. Pentose Phosphate Pathway is more active in normoxia.

A) Comparison of the lactate peak line shape in spectra recorded from extracts of CLL cells incubated in normoxia (green) and hypoxia (purple). B) After scaling spectra intensities, the middle peak was higher in normoxia (1.1% label incorporation) than in hypoxia (0.08% label incorporation). This peak reflects the higher amount of label in position C-3 which came from the labelled glucose metabolised through the pentose phosphate pathway. C) Enlarged middle peak.

6.2.2 Pyruvate carboxylase is active only in hypoxic conditions

The labelling pattern of aspartate arising from [1,2-^{13}C]glucose informs about the entry of pyruvate into the TCA cycle. If the entry point is via pyruvate dehydrogenase (PDH) and the TCA cycle turns entirely clockwise (Figure 6.4.), the C-1,2 or C-3,4 positions should be labelled. For the anaplerotic pathway via pyruvate carboxylase (anti-clockwise entry to the TCA cycle) oxaloacetate would be labelled in position C-2,3, and consequently aspartate also in the position C-2,3 as it is directly derived from OA. It is well-known that malate can be formed from OA with the TCA cycle proceeding anti-clockwise, at least for these steps, in which case malate would show the same labelling pattern as aspartate. Labelling gets more complex if the PC product runs clockwise through the TCA cycle, but the product from PC activity and anti-clockwise operation is always unique.

Aspartate signals were sufficiently strong to distinguish the label in positions C-2 and C-3, but a lack of a $^{2}J_{CC}$ coupling in the ^{13}C-dimension suggests that neighbouring positions C-2 and C-3 were not labelled in the same molecule. Therefore two species of labelled aspartate must have been present: [1,2-^{13}C] and [3,4-^{13}C]aspartate. However, multiplet analysis of aspartate also revealed the presence of a third species, [2,3-^{13}C]aspartate (Figure 6.9). Comparison of J-coupling between C-2 aspartate peaks was used to distinguish labelling patterns. As the splitting value depends on the properties of the neighbouring atom (aliphatic-aliphatic - lower

value, aliphatic- carbonyl – higher value), the size of the coupling constant is smaller for [2,3-^{13}C]aspartate (J=36,4 Hz) than the coupling constant for 1,2-^{13}C (J=50 Hz) (see Figure 6.9 B).

In contrast to normoxic conditions, spectra from hypoxic samples showed approximately two times higher pyruvate carboxylase (PC) activity based on the percentage of [2,3-^{13}C]aspartate (Figure 6.9 C). Unfortunately it was not possible to determine label incorporation ratios by comparing signal intensities between HSQC spectra from labelled and unlabelled samples because the sensitivity in spectra of unlabelled samples was too low.

Further proof of PC activity arose from the glutamate spectrum, which suggested the presence of [2,3-^{13}C]glutamate with approximately 0.15% label incorporation in hypoxia but much lower incorporation under normoxic conditions. Because the values were so low, it was difficult to quantify the label incorporation under these circumstances. However, the line shape analysis shown in Figures 6.10 and 6.11 showed the differential line broadening due to the simultaneous presence of [1,2-^{13}C] and [2,3-^{13}C]glutamate in hypoxia but not in normoxia, further confirming higher PC activity in hypoxia. The formation of [2,3-^{13}C]glutamate isotopomer is a specific indicator for PC activity when [1,2-^{13}C]glucose is used as a tracer (Brekke, Morken et al. 2014).

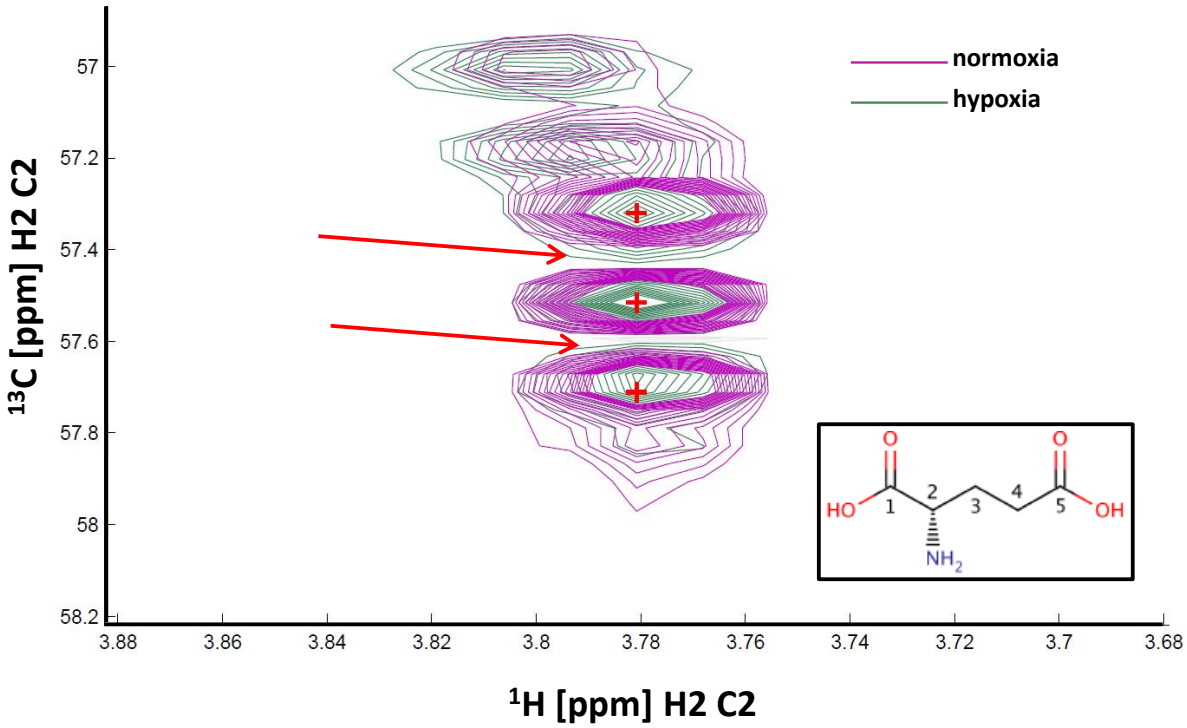

Figure 6. 10. The glutamate HSQC signal proves pyruvate carboxylase activity in CLL cells is higher in hypoxia than in normoxia.

CLL cells were incubated for 24 hours in a hypoxic incubator (1% O_2) in RPMI medium with [1,2-^{13}C]glucose. Cells were extracted and the polar fraction was analysed by NMR spectroscopy. $^{1}H^{13}C$ – HSQC and 1D ^{1}H spectra were recorded. Data were analysed using the NMRlab software. Red arrows indicate the differential line broadening due to the simultaneous presence of [1,2-^{13}C]glutamate and [2,3-^{13}C]glutamate. [2,3-^{13}C]glutamate is derived from the pyruvate carboxylase pathway.

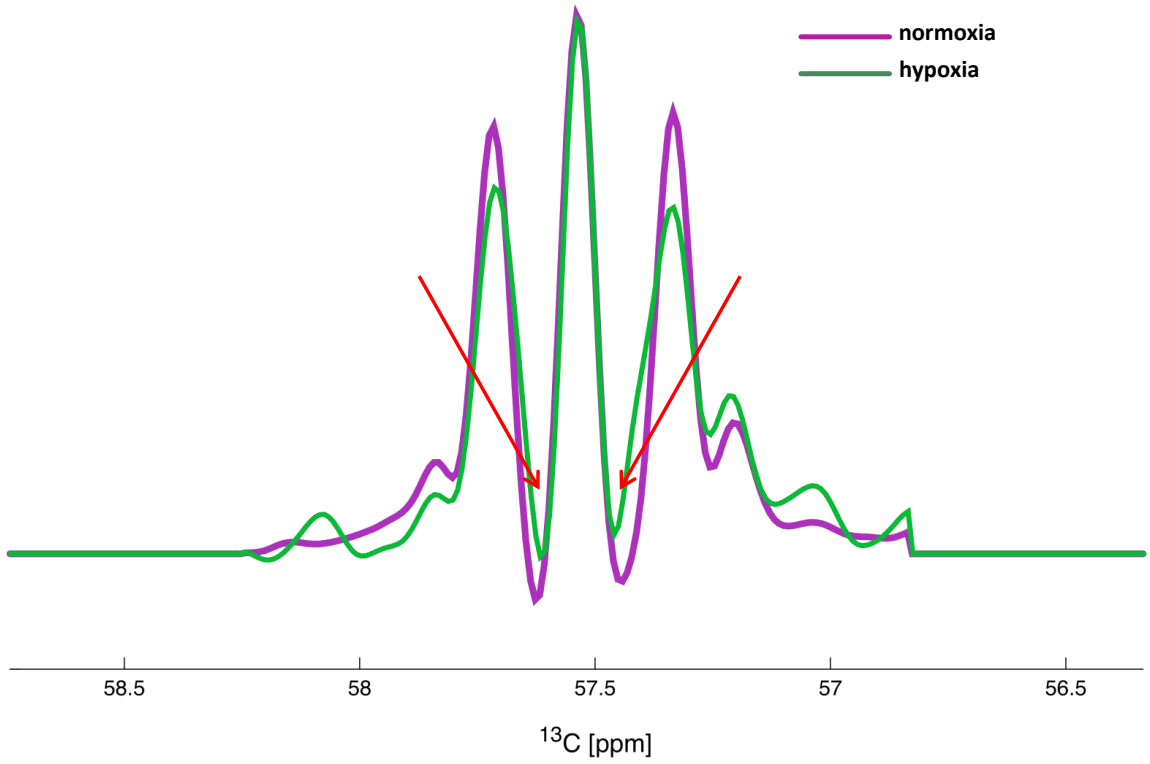

Figure 6. 11. A 1D ^{13}C column from the HSQC experimental data proves pyruvate carboxylase activity in CLL cells is higher in hypoxia than in normoxia.

CLL cells were incubated for 24 hours in a hypoxic incubator (1% O_2) in RPMI medium with [1,2-^{13}C]glucose. Cells were extracted and the polar fraction was analysed by NMR spectroscopy. $^{1}H^{13}C$ – HSQC and 1D ^{1}H spectra were recorded. Data were analysed using the NMRlab software. Red arrows indicate the differential line broadening due to simultaneous presence of [1,2-^{13}C]glutamate and [2,3-^{13}C]glutamate. [2,3-^{13}C]glutamate is derived from the pyruvate carboxylase pathway.

6.2.3 Glucose flux into the TCA cycle via PDH/PC

The majority of TCA cycle intermediates were identified with larger intensities in the HSQC spectrum obtained from cells incubated with labelled glucose, compared to those from the unlabelled sample, suggesting the incorporation of the label into TCA cycle intermediates. This was the case under both, normoxic and hypoxic conditions. However, the signal of unlabelled peaks was too low in both cases, which meant it was not possible to accurately calculate the label incorporation percentage.

Glutamate appeared highly abundant in HSQC spectra, therefore it was possible to quantify its label incorporation by comparing intensities in spectra of labelled and unlabelled cells. [4,5-^{13}C]glutamate indicates one round of the TCA cycle involving PDH, and 4.5% of this species was detected in normoxic samples, which was higher than in hypoxia (3%) (Figures 6.6 and 6.7). The presence of [1,2-^{13}C], [3-^{13}C] and the triple labelling [3,4,5-^{13}C]glutamate suggests that the label from [1,2-^{13}C]glucose went through several rounds of TCA cycles (Figure 6.5), these species were observed in both normoxic and hypoxic samples (data were analysed using the spin system simulations). The higher percentages in normoxic samples, suggest slower TCA rounds in hypoxia. On the other hand, the higher percentage of [2,3-^{13}C]glutamate indicates increased PC activity in hypoxia. Interestingly, higher percentages of [1,2-^{13}C]glutamate and [3-^{13}C]glutamate detected in normoxic

conditions compared to hypoxia indicate that more rounds of the TCA cycle were performed in normoxia

6.2.4 ^{13}C-3-Glutamine flux

Analysis of label distributions arising from [3-^{13}C]glutamine revealed glutaminolysis in both normoxic and hypoxic conditions (Figures 6.12 and 6.13). The label was detected in TCA cycle intermediates such as α-KG, succinate, fumarate, malate, oxaloacetate and citrate as well as in aspartate (positions C-2 in some compounds and C-3 in others). In the case of active reductive carboxylation of glutamine, [3-^{13}C]citrate would be labelled. However the only carbons it is possible to detect using NMR are C-2 and C-4. Therefore the only indication of labelled C-3 can be the splitting from C-3 to C-2. In the presented study, no splitting was observed which may suggest that the reductive carboxylation of glutamine did not occur in normoxia and hypoxia, or that the absolute level of label incorporation was not high enough to detect it.

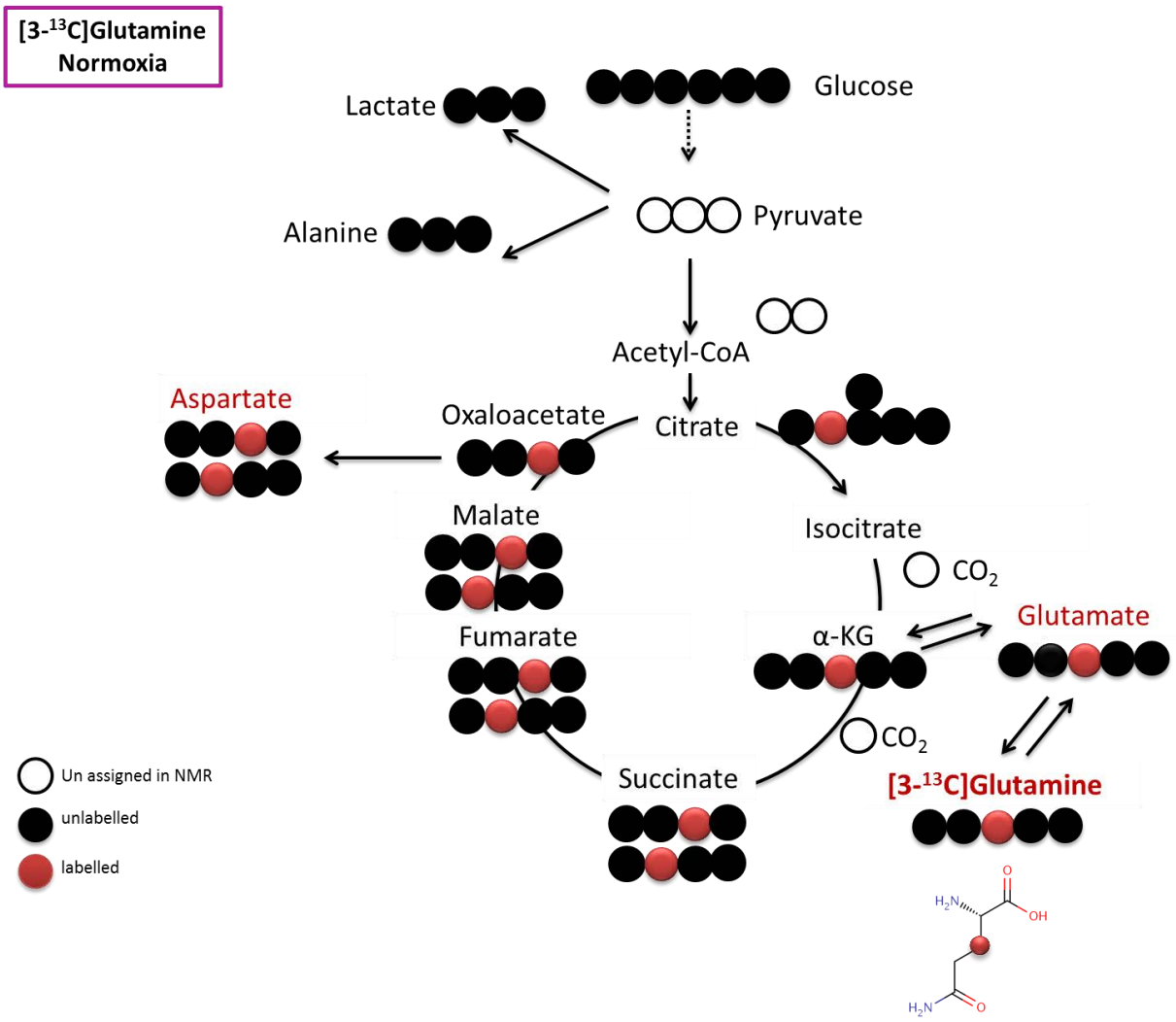

Figure 6. 12. Glutamine flux in CLL cells in normoxia.

CLL cells were incubated for 24 hours in a normoxic incubator in RPMI medium with [3-^{13}C]glutamine. Cells were extracted and the polar fraction was analysed by NMR spectroscopy. ^{1}H^{13}C – HSQC and 1D ^{1}H spectra were recorded. Data were analysed using the NMRlab software.

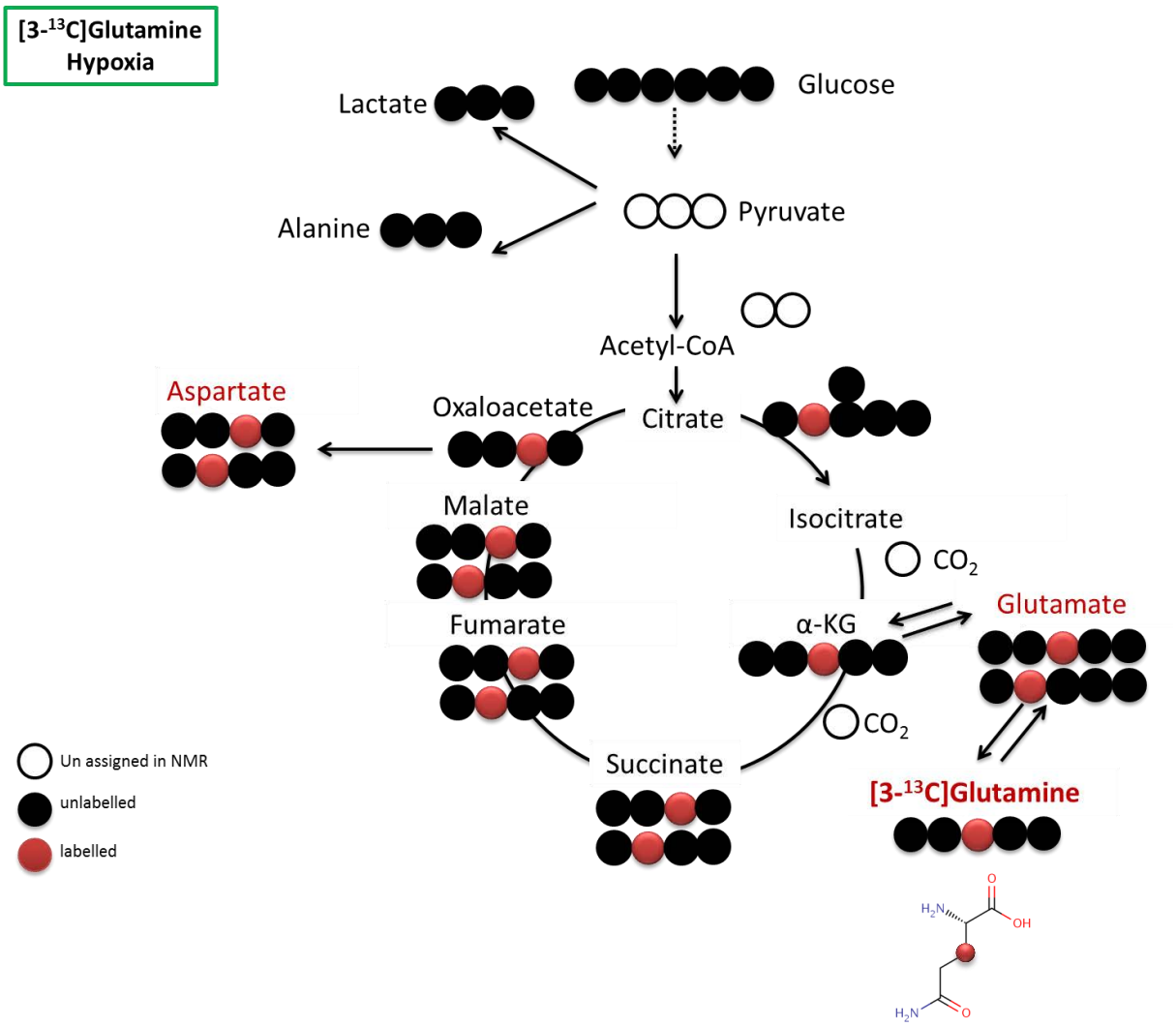

Figure 6. 13. Glutamine flux in CLL cells in hypoxia.

CLL cells were incubated for 24 hours in a hypoxic incubator (1% O_2) in RPMI medium with [3-^{13}C]glutamine. Cells were extracted and the polar fraction was analysed by NMR spectroscopy. $^{1}H^{13}C$ – HSQC and 1D ^{1}H spectra were recorded. Data were analysed using the NMRlab software.

Lack of the label in lactate and alanine identified by the absolute incorporation of label into C-3 of lactate via 1D spectra, suggests the absence of the malic enzyme activity which transforms malate into pyruvate (Figures 6.14 and 6.15). In addition lactate labelled from glucose in normoxia and hypoxia is produced in a similar percentage (Figure 6.16).

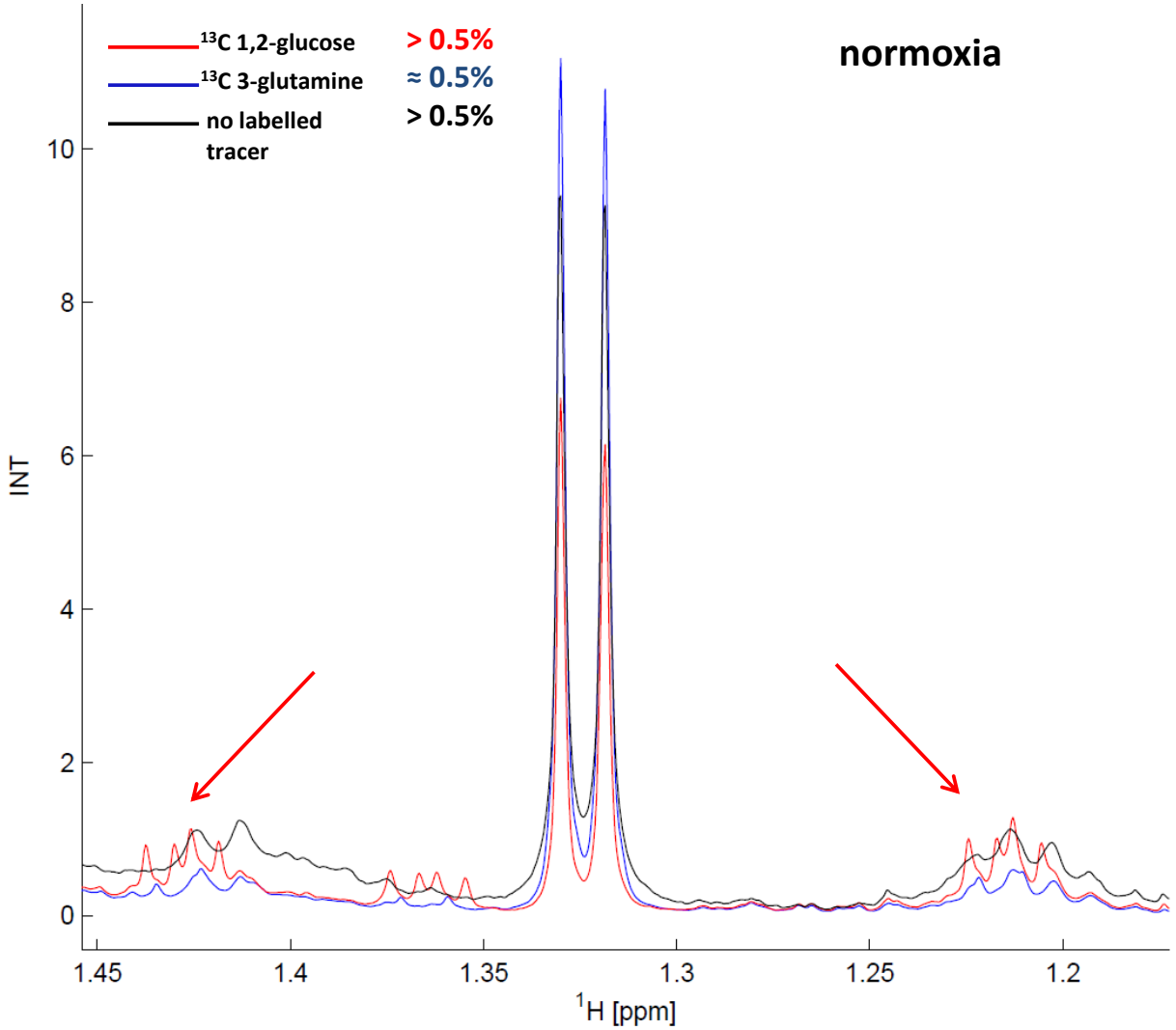

Figure 6. 14. In normoxia lactate can be labelled from glucose but not from glutamine in CLL cells.

1D ^{1}H NMR spectra were recorded on CLL cell extracts. The red line represents the spectrum of cells fed with the [2,3-^{13}C]glucose; the blue line represents the spectrum recorded on extracts of cells fed with [3-^{13}C]glutamine and the black spectrum was recorded on extracts of cells fed with standard RPMI medium, without labelled tracers. Cells were incubated for 24 hours in normoxia. The label incorporation in satellites was approximately 0.5% for the (blue line) sample labelled from glutamate (which is the natural abundance 1%: two satellites = 0.5%). In the case of sample labelled from glucose (red line), the percentage of labelling was above 0.5 indicating transfer of the label from glucose to lactate. In the case of the unlabelled spectrum (black line), the percentage was also higher than 0.5% but this was the result of other overlapping peaks.

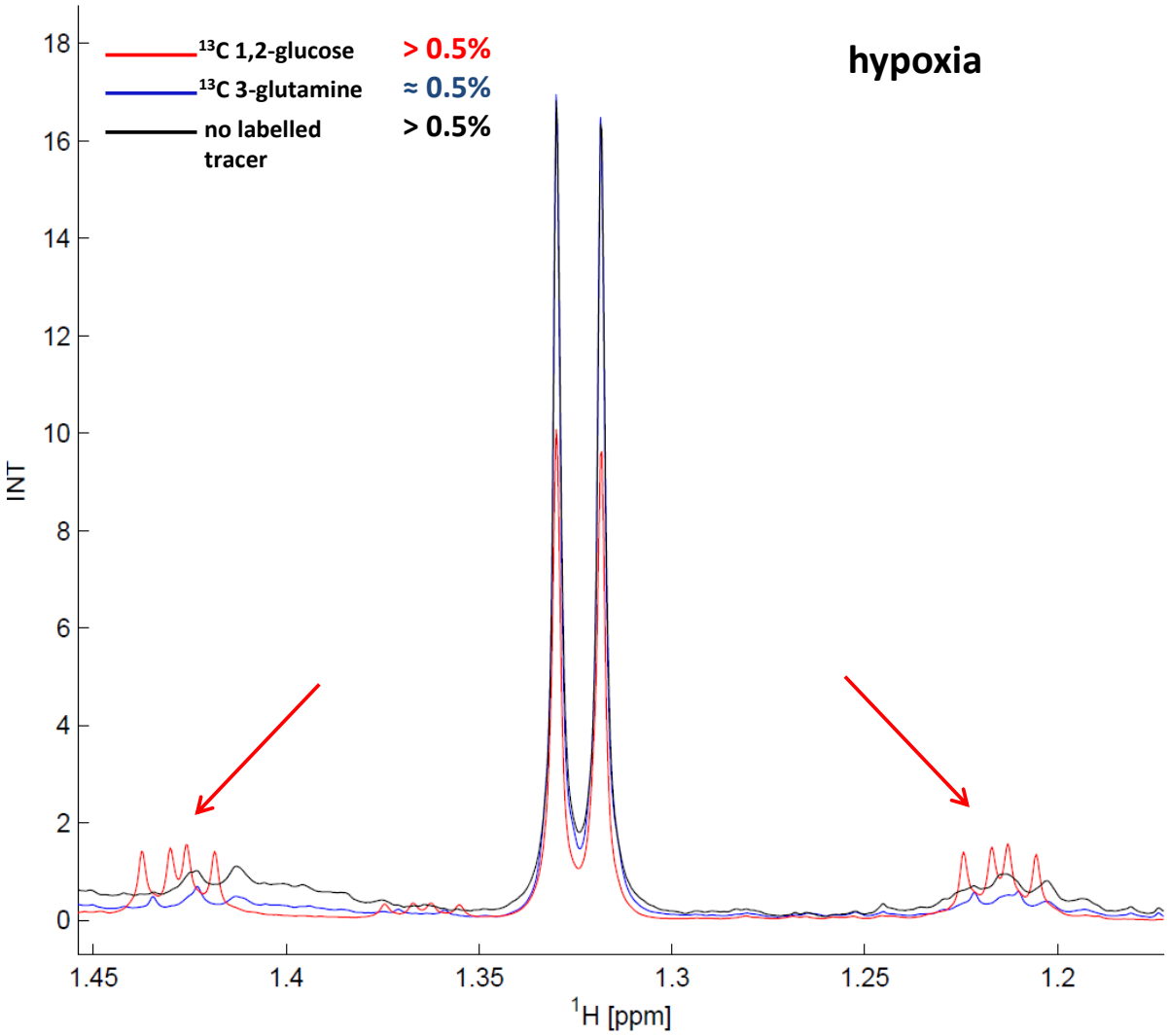

Figure 6. 15. In hypoxia lactate can be labelled from glucose but not from glutamine in CLL cells.

1D ^{1}H NMR spectra were recorded on CLL cell extracts. The red line represents the spectrum of cells fed with the [2,3-^{13}C]glucose; the blue line represents the spectrum recorded on the extract of cells fed with [3-^{13}C]glutamine and the black spectrum was recorded on extracts of cells fed with standard RPMI medium, without labelled tracers. Cells were incubated for 24 hours in 0.1% O_2. The label incorporation in satellites was approximately 0.5% for the (blue line) sample labelled from glutamate (which is the natural abundance 1%: two satellites = 0.5%). In the case of sample labelled from glucose (red line), the percentage of labelling was above 0.5 indicating transfer of the label from glucose to lactate. In the case of the unlabelled spectrum (black line) the percentage was also higher than 0.5% but this was the result of other overlapping peaks.

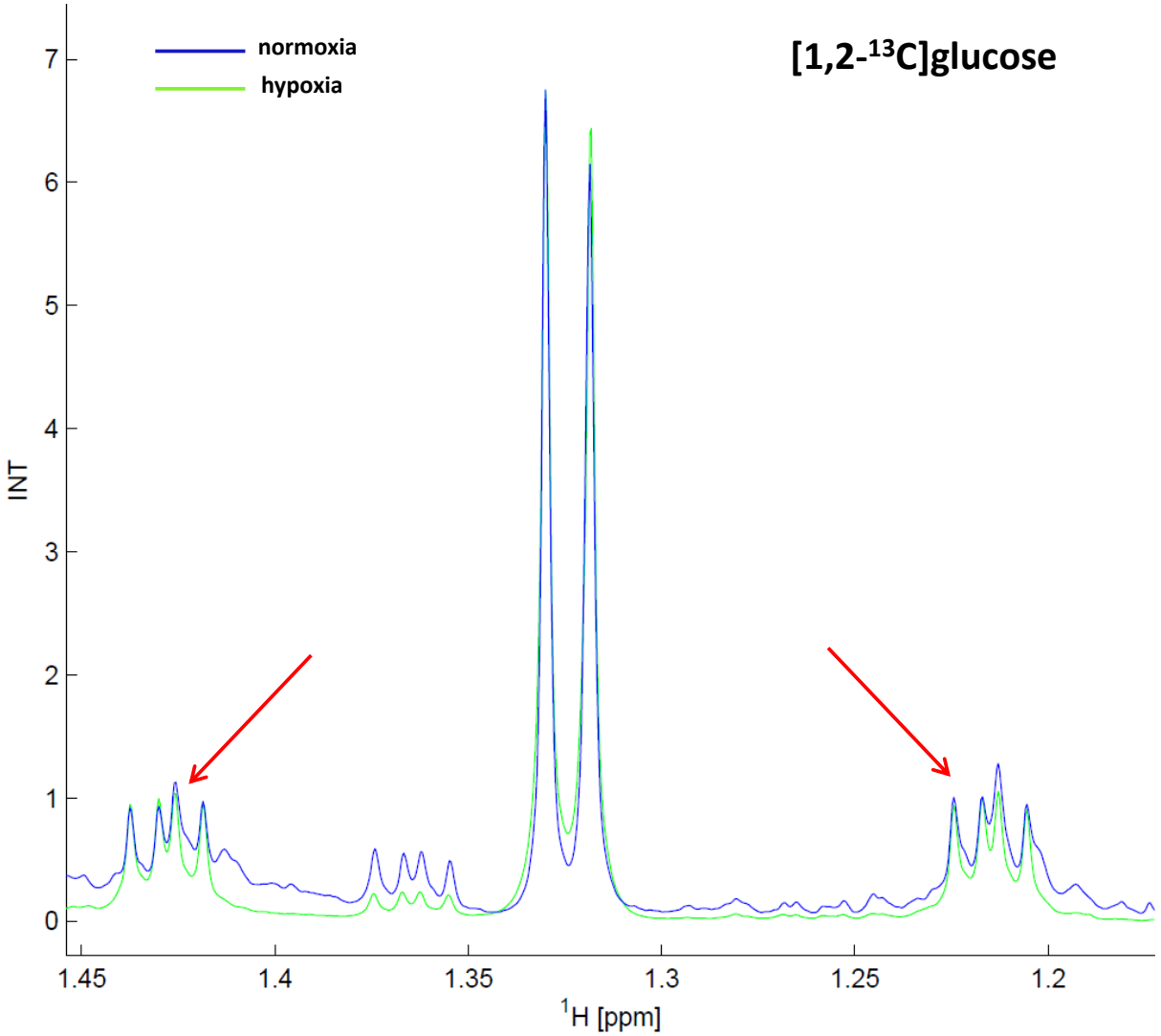

Figure 6. 16. In CLL cells, lactate can be labelled from glucose in similar percentages in both normoxia and hypoxia.

1D ^{1}H NMR spectra were recorded on the CLL cell extracts. Cells were fed with the [2,3-^{13}C]glucose and incubated for 24 hours in normoxia (blue line) or in 0.1% O_2 (green line).

6.3 DISCUSSION

Although it is difficult to obtain large amounts of primary cells, and the size of CLL cells is relatively small due to their scant cytoplasm, HSQC analysis of CLL cell extracts provided some information about their metabolic flux. Use of labelled glucose and glutamine precursors revealed differences between normoxic and hypoxic metabolism (see Figures 6.17 and 6.18).

CLL cells consumed glucose and glutamine in both normoxic and hypoxic conditions and incorporated their carbons to newly produced metabolites. Interestingly, early studies examining glucose uptake by CLL cells show that they consume less glucose than normal B lymphocytes (Brody, Oski et al. 1969). Moreover, studies using fluorodeoxyglucose positron emission tomography (FDG-PET) to visualise CLL cells *in vivo,* have yielded poor results; the sensitivity of detection was 53% and the extent of disease was often underestimated (Karam, Novak et al. 2006). This may be because CLL is composed of malignant cell fractions with different proliferative activities, whereby recently divided cells and older/quiescent cells may have different glucose requirements. This notion is supported by a report indicating that CLL patients have two populations of circulating malignant cells with different degrees of mitochondrial polarization and dependencies on glucose (Gardner, Devlin et al. 2012). FDG-PET has been used effectively in CLL management with respect to the detection of Richter's transformation (Bruzzi, Macapinlac et al. 2006). Regarding

the methods used in the present study, as yet, it has not been possible to obtain sufficient numbers of healthy B-cells after the purification of CD19 positive cells to accurately perform metabolic analysis including measurements of glucose consumption. It would be interesting to see if the kinetics of glucose and glutamine consumption by CLL cells differs from the kinetics shown by healthy B-cells.

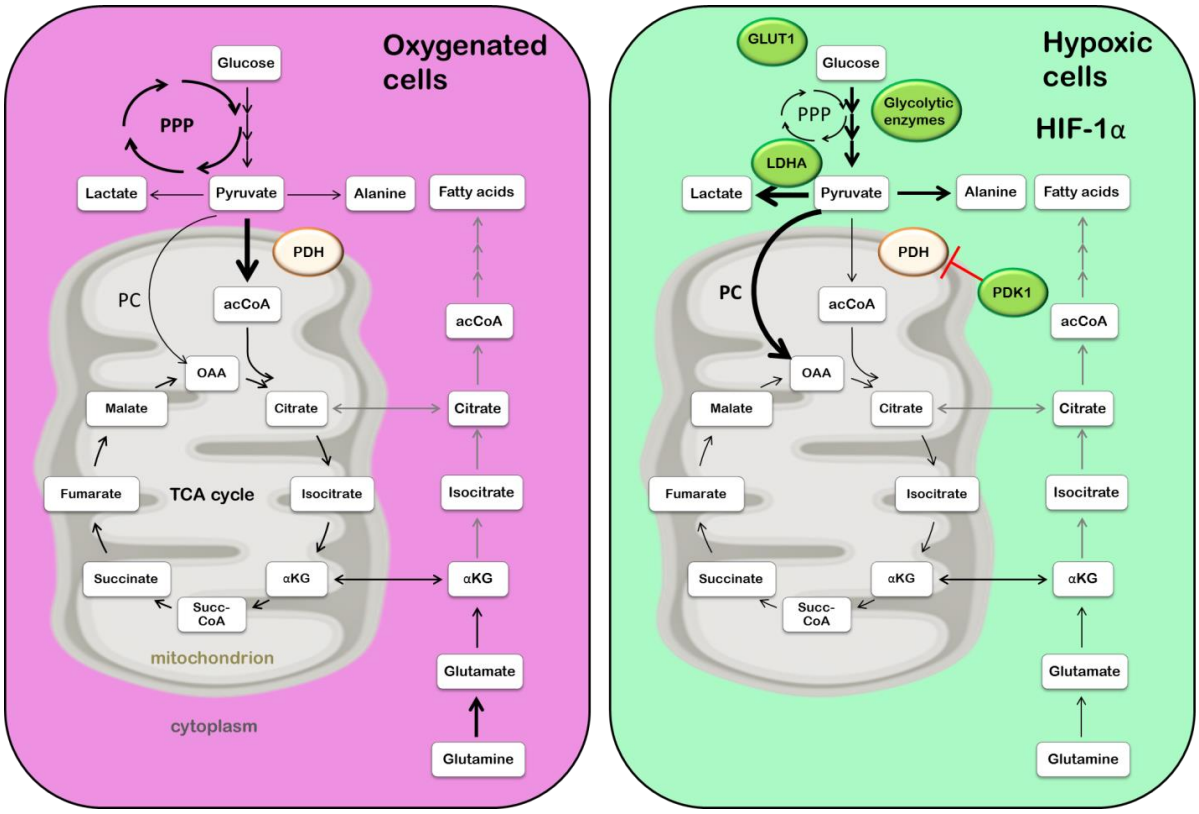

Figure 6. 17. Metabolic shift of CLL cells entering hypoxia.

A) In well oxygenated CLL cells, the pentose phosphate pathway is active, pyruvate is converted to acetyl-CoA by PDH to enter into the TCA cycle and PC activity is low. B) In hypoxia, HIF-1α is imported to the nucleus and activates the transcription of several genes: glucose transporter (GLUT1), glycolytic enzymes, lactate dehydrogenase (LDHA) or pyruvate dehydrogenase kinase (PDK1). As a result, more glucose is consumed and more lactate is produced as the pyruvate conversion to acetyl-CoA is blocked. As an alternative path of pyruvate entry to the TCA cycle, pyruvate carboxylation (PC) is more active than in normoxia. On the other hand, PPP activity is decreased compared to normoxia. Glutamine consumption is increased. Reactions marked in grey have not been investigated.

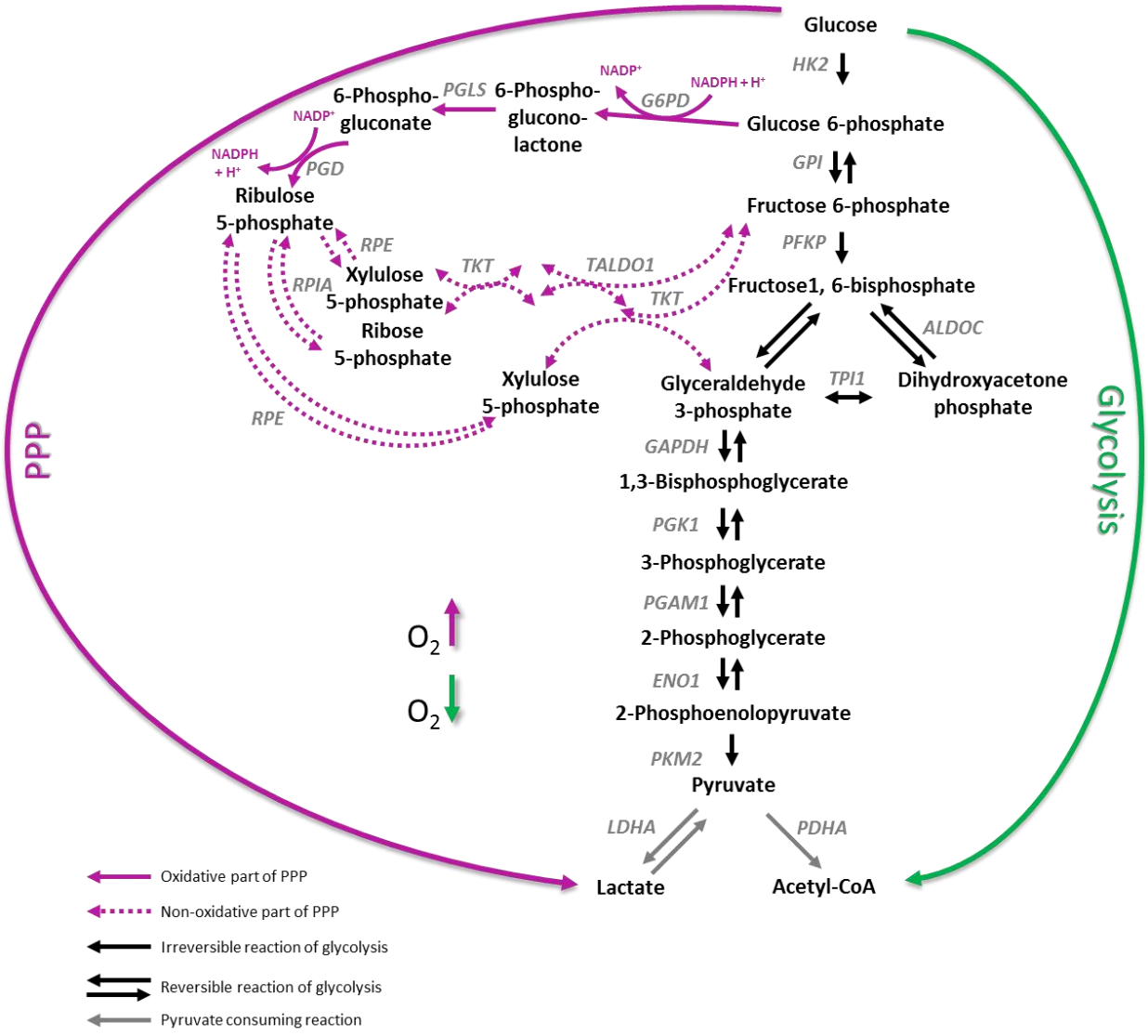

Figure 6. 18. Glycolysis is interconnected with PPP in CLL cells.

In CLL cells, PPP is more active in normoxia compared to hypoxia, while glycolysis increases in hypoxia. HK2: hexokinase 2, GPI: glucose-6-phosphate isomerase, PFKP: 6-phosphofructokinase, ALDOC: aldolase C, TPI1: triosephosphate isomerase 1, GAPDH: glyceraldehyde-3-phosphate dehydrogenase, PGK1: phosphoglycerate kinase 1, PGAM1: phosphoglycerate mutase 1, ENO1: enolase 1, PKM2: pyruvate kinase M2, LDHA: lactate dehydrogenase A, PDHA: pyruvate dehyrogenase, G6PD: glucose-6-phosphate dehydrogenase, PGLS: 6-phosphogluconolactonase, PGD: 6-phosphogluconate dehydrogenase, RPE: ribulose-5-phosphate 3-epimerase, RPIA: ribose-5-phosphate isomerase, TKT: transketolase, TALDO1: transaldolase 1, NADPH: nicotinamide adenine dinucleotide phosphate.

The observations presented in this study indicate that CLL cells use the pentose phosphate pathway (PPP) in normoxia but it appeared to be down regulated in hypoxia. A similar phenomenon has been reported in a study using glioblastoma stem-like cells, where an upregulation of genes involved in PPP in normoxia, combined with a downregulation of glycolytic enzymes and reciprocal adaptive switch between induction of glycolysis and PPP in hypoxia was shown (Kathagen, Schulte et al. 2013). Previous studies of the metabolism of CLL cells showed decreased levels of glucose consumption as well as diminished levels of [1-^{14}C]glucose-derived $^{14}CO_2$ compared with healthy cells (Brody, Oski et al. 1969). This suggests lower activity of the PPP pathway in CLL lymphocytes. This may be a consequence of the lower levels of PPP enzymes such as glucose-6-phosphate dehydrogenase and 6-phosphogluconate dehydrogenase, which were shown to be decreased in CLL (Beck 1958; Ghiotto, Perona et al. 1963; Brody, Oski et al. 1969). Moreover, it has been shown that in CLL, certain oxidative and glycolytic enzymes may not be correctly spatially oriented which would prevent substrate binding (Koshland 1963). This abnormality may be analogous to the defective mechanism responsible for the impaired assembly of new ribosomes in CLL (Rubin 1971).

The Pentose phosphate pathway synthesises precursors of nucleotides and amino acids which are required for tumour cell growth and proliferation. When cells do not require these precursors, intermediates of the pentose phosphate pathway

(fructose-6-phosphate and glyceraldehyde-3-phosphate) can be recycled back into glycolysis to produce pyruvate and lactate. Based on observations described in the previous chapter, it was hypothesised that CLL cells in hypoxia are exposed to high levels of ROS and are in high demand for ROS scavenging pyruvate. Therefore, rather than utilising the PPP, it would be more beneficial for CLL cells to use fructose-6-phosphate and glyceraldehyde-3-phosphate in the glycolytic pathway to produce more pyruvate. This is an interesting observation as other cancer cells use PPP to reduce ROS (through the generation of NADPH) (Jiang, Du et al. 2014). It seems to be a particular feature of CLL cells to reduce PPP in hypoxia.

Many of the macromolecular precursors for cell growth such as lipids, nucleotides and nonessential amino acids are generated within the TCA cycle. The TCA cycle uses pyruvate as its main fuel but can also use glutamine. The latter is often referred to as an anaplerotic pathway. Another anaplerotic reaction is the usage of pyruvate via pyruvate carboxylation (PC) providing oxaloacetate, the metabolite which forms the cycle's canonical entry point following condensation with acetyl-CoA. The HSQC analysis showed that under hypoxic conditions, pyruvate carboxylase activity increases in CLL cells. It was shown that in many tumours pyruvate carboxylase is required for glutamine- independent growth (Cheng, Sudderth et al. 2011). Glutamine is the preferred anaplerotic precursor in some transformed cell lines, contributing up to 90% of the OAA pool (Portais, Voisin et al.

1996); DeBerardinis, Mancuso et al. 2007), therefore when the contribution of glutamine is reduced, cells require an alternative source of OAA which may be pyruvate. Consequently, cancer cells exhibiting high PC activity did not require glutamine for survival and growth (Cheng, Sudderth et al. 2011). The data presented in this chapter show that PC activity was more pronounced in hypoxia and glutamine consumption was lower after oxygen depletion – supporting the previously described relation.

[1,2-^{13}C]glutamate and [3-^{13}C]glutamate derived from [1,2-^{13}C]glucose in normoxia is evidence of the TCA cycle having passed multiple rounds during 24 hours of label exposure. In contrast, spectra recorded on hypoxic cell extracts showed much lower intensions of these labelling patterns. This suggests that, compared to normoxia, in hypoxic conditions CLL cells slow down their TCA cycle metabolism. This observation is consistent with the common view that in hypoxia, cells switch their metabolism from oxidative phosphorylation to glycolytic flux, leading to the accumulation of lactate. Hypoxia promotes glycolytic flux, in part due to the activation of HIF-1α and its downstream target genes, which include many glycolytic enzymes (Tennant, Frezza et al. 2009). Both hypoxia and ROS decrease the flux of glucose through pyruvate dehydrogenase into the TCA cycle, through activation of pyruvate dehydrogenase kinase (PDK). In such cases, the TCA cycle can be fed by alternative substrates such as glutamine. It has been shown that some cancer cells use

glutamine in conjunction with a reverse TCA cycle activity for acetyl-CoA production which is the substrate for lipid synthesis (Metallo, Gameiro et al. 2012). CLL cells fed with labelled glutamine did not contain citrate labelled in the C-3 position suggesting that neither in normoxia, nor in hypoxia, the reverse TCA cycle occurs in CLL cells.

It would have been interesting to compare the metabolic characteristics of CLL cells observed in the present study, with data from healthy human B-cells, but the high number of cells required for the carbon NMR analysis proved to be an insurmountable obstacle.

Chapter VII

General Discussion

7.1 General discussion

Until relatively recently, CLL was considered the "Cinderella" of leukaemia, receiving less attention from biologists and clinicians than many other malignancies and in particular other haematological malignancies (Caligaris-Cappio 2009). However, in recent years this has changed dramatically. Studies of the genetics and physiology of CLL has uncovered novel targets for clinical exploitation using monoclonal antibodies (MoAbs), engineered T cells, or kinase inhibitors (Kharfan-Dabaja, Wierda et al. 2014). Ibrutinib, an inhibitor of Bruton's tyrosine kinase which signals downstream of the B-cell receptor (BCR) signalling pathway, is showing great promise in high-risk patients, whether alone or as an adjunctive therapy with MoAbs or chemotherapy. Similarly PI3K-δ, inhibitors are showing promise (Aalipour and Advani 2013; Danilov 2013). Despite this, for the overwhelming majority of patients the disease remains incurable. Furthermore, the hope that BTK and/or PI3K-δ inhibitors will become the 'imatinib' (blockbuster therapeutic for the treatment of CML) of CLL is perhaps as yet prematurely optimistic.

Unlike CML, which is defined by a single defining founding mutation that can be targeted by imatinib (Breccia, Efficace et al. 2011), CLL is genetically heterogeneous (Landau and Wu 2013). Previous knowledge of the successes in the development of cancer medicine indicates that combination therapies provide the most efficacious cures and remission rates and that having a pathway of treatments

available at first and subsequent relapses, prolongs both survival and with increasing commonality quality of life (Hallek 2013). It is therefore likely that new agents and new treatment strategies are still required for CLL.

From another point of view, there is a required urgency to study CLL as a generic model of human B-cell malignancies and of human cancer in general. The accessibility of CLL cells provides a unique opportunity to study primary human cancer cells that is not afforded to such studies in any other setting. However, the forecasted arrival of an arsenal of drugs and therapeutic approaches that may in the near future achieve increased survival by driving down tumour burden and halting disease progression means that this opportunity will thankfully be short lived (Hallek 2013).

Many agents that are effective in CLL are also effective in B cell lymphomas, for example the CD20 targeting antibody rituximab (Keating 2010). Therefore, studies in CLL are likely to provide additional information for the development of therapies in settings beyond this disease where outcomes remain poor. However, I believe that CLL cells provide a wider model of human cancer with particular advantages in the study and understanding of the processes of metastasis.

Although when circulating, CLL cells remain out of the cell cycle, the majority of these cells have previously undergone cell divisions within malignant lymph nodes (Chiorazzi 2007). This indicates that CLL cells can alternate between being 'in'

and 'out' of the cell cycle. Cells that are 'out' of the cell cycle are often described as 'quiescent'. However, in the age of metabolomics, the definition of quiescence is likely to change. 'Quiescence' relates to the state of being 'out' of the cell cycle, termed G_0. However not all 'out of cell cycle' cells may be metabolically quiescent. The transition to cell cycle quiescence in primary human fibroblasts has been shown to be associated with changes in gene expression, histone modification and the extension of chromatin compaction, although there is no evidence that these events regulate the cell cycle in cells (Everts, Manning et al. 2013). However, entry to the quiescent state is almost certainly associated with dramatic changes in metabolism as the requirements of proliferating and quiescent cells are vastly different. Evidence that cell cycle quiescence may not be associated with metabolic quiescence has again been shown in 'out of cycle' fibroblasts that maintain comparable metabolic rates to proliferating cells (Lemons, Feng et al. 2010)

To date, little is known about quiescent haematological cancer cells. Experiments presented here demonstrate that 'out of cell cycle' primary CLL cells also maintain a high level of metabolic activity. Data presented here describe a reversibly adaptive Warburg effect in these cancer cells where glucose consumption and lactate production were present in oxygenated conditions but became elevated upon transition to hypoxia as shown by increased lactate production. At the same time, TCA cycle activity appeared to be supported by a shift towards glutaminolysis

in hypoxia as evidenced by consumption of glutamine associated with production of glutamate, pyruvate, lactate and alanine. However, it is interesting to note that the HIF-1α inhibitor CTM had an effect on hypoxia induced CLL cell glutaminolysis by accelerating glutamine consumption and glutamate production in hypoxia. In contrast, CTM diminished glucose consumption and lactate production. These findings suggest that hypoxia induced HIF-1α activity acts to sustain glycolysis and 'spare' glutaminolysis, as CLL cells transit from oxygenated to hypoxic environments and that lactate production is largely mediated by the consumption of glucose.

A key observation was the discontinuous kinetics of pyruvate; being externalised early in the experiments and then reabsorbed in hypoxia. Pyruvate reabsorbtion was halted by CHC, implicating the MCT1-transporter in this process. Importantly, provision of exogenous pyruvate diminished the production of ROS and mitosox in response to stress induced by reactive oxygen species (H_2O_2) and reversed CLL cell killing by H_2O_2. These data are the first to demonstrate that CLL cells not only display metabolic plasticity in response to environmental change but also change their utilisation of metabolites under different conditions and can do so to enhance their survival.

The study presented here is one of a growing number of studies that have analysed metabolism in living cells. A recent study used ^{13}C-pyruvate formulations in a comparative flux study of pyruvate metabolism between a glioblastoma and a

hepatocarcinoma cell line (Yang, Harrison et al. 2014). Similarly, hyperpolarised ^{13}C NMR studies of glucose metabolism in living T47D breast cancer cell cultures have also been recently described (Harris, Degani et al. 2013). However, the work presented here provides a significant progression of this type of study.

To the author's knowledge this is the first report of real-time NMR measurements using primary patient cancer cells purified from the blood of patients but not otherwise modified nor cultured. Using these cells, fast metabolic adaptations to niche conditions using a simple model of oxygen depletion were observed. By embedding cells in a dilute agarose matrix in an NMR tube, oxygen access was restricted, while cells were preserved in a stable 'out of cell cycle' state. The agarose matrix prevented the cells from sinking to the bottom of the NMR tube, thus preserving the homogeneity of the NMR sample (in which the CLL cells account for less than 10% of the overall volume), which is important to obtain high resolution NMR spectra. Line widths of 1-1.5 Hz in 0.1% agarose were obtained, suggesting that the matrix preserves the mobility of small molecules, probably arising from large cavities in the polymer. Using ^{1}H-NMR spectra, sufficient sensitivity to obtain one-dimensional spectra in 7-10 minutes in a standard 5 mm NMR tube with a volume of just 550 μl was achieved.

However, the integration in this study of advanced NMR technologies with both cancer and cell biological expertise has been of equal importance. This

multidisciplinary approach allowed for the interrogation of previously unknown aspects of the physiology of CLL cells that underpin this complex disease. Moreover, it has provided insight to new therapeutic avenues in combating not only CLL but more generally all metastatic cancers. Beyond this, potential evidence that the basal metbolism of CLL cells displays heterogeneity from patient to patient has been identified; an observation that would not be possible using established cell lines. A future, larger scale study would permit correlation of kinetic metabolic activity with disease parameters such as prior or ongoing treatment, as well as correlative studies with disease progression and association with prognostic markers.

Finally, the methodology presented here has considerable potential for applications in personalised medicine. Unlike most other analytical technologies, NMR is completely non-invasive and preserves cells. This opens new avenues to test the effect of treatment options 'ex vivo', using primary cells from patients which can be further characterised afterwards.

7.2 Future work

1. Knowing that the presented real time metabolic analysis method can detect differences in the metabolic profiles of CLL cells treated under a range of specific conditions reproducibly, it would be interesting to select different "types" of CLL patients. For example, stage A indolent vs relapsed refractory CLL patients, to

distinguish possible differences between the cells isolated from the groups. Larger numbers of samples would be required to perform statistical analysis.

2. This study compared the metabolism of CLL cells in oxygenated and in hypoxic conditions. Lymph nodes, (where CLL cells proliferate (Herishanu, Perez-Galan et al. 2011)) are likely to be hypoxic, however, to fully prove that the metabolism of CLL cells in lymph nodes corresponds to the metabolism of CLL cells in hypoxia described in the present study, measurements of CLL cells derived directly from the lymph nodes would be required. Such analyses are feasible and should be performed after obtaining biopsy samples under appropriate ethical approval.

3. Assessment of the metabolism of heathy B-cells is also required to identify the differences and commonalities with CLL cells. Crucially, the comparisons of the metabolic plasticity and the adaptation to hypoxic environments must be made to elucidate the specificity of the alternations presented here and whether they are solely recorded in malignant B-cells.

4. It would be interesting to investigate whether the system of real time NMR analysis can be applied to other cell types. Preliminary studies using the proliferating KG1a cell line have been carried out and results suggest that these

cells are tolerant of NMR real time measurements and changes in metabolism upon transition to hypoxia can be observed.

5. A considerable experimental improvement of the NMR probe could be the addition of a flow cell, where cells can be kept temperature controlled, with a defined oxygen status and would allow for the possibility of drug supplementation in real time. This would remove the necessity of using agarose as cells could be kept in suspension by carefully adjusting the flow of medium in the NMR cell.

7.3 The future of NMR Metabolomics for beating cancer

Recently, there has been a shift in the way that cancers are being described and treated. Currently, tumours are defined not only by where they exist (e.g. lung, blood or breast), but also by their molecular characteristics. Mutations in oncogenes or those coding for receptors such as K-RAS in colorectal tumours or HER-2 in breast cancer, are an important factor to consider when choosing the treatment plan (Aiello, Vella et al. 2011; Orphanos and Kountourakis 2012). However, for the majority of tumour types, no markers have been identified so far. Patients who receive the same diagnosis react very differently to the same treatment and as a consequence, have

different outcomes. Therefore, there is a need for targeted therapeutics, characterised by higher specificity and efficiency, combined with fewer side effects.

In recent years, NMR spectroscopy has been successfully used to evaluate existing and potential therapies, as well as to analyse toxicology, sensitivity, optimal doses and biological mechanisms of therapeutic compounds (Coen, Holmes et al. 2008; Bayet-Robert, Morvan et al. 2010; Dewar, Keshari et al. 2010). NMR metabolomics has also been used to assess the efficiency of both radiation and chemotherapy treatments (Blankenberg, Katsikis et al. 1997; Lyng, Sitter et al. 2007). Moreover, it can provide a metabolic insight into different tumour subtypes as well as their responses to drugs, indicating for which groups of patients therapies are likely to be the most effective, or in which groups substantial side-effects will manifest. Identification of pre-treatment metabolic profiles correlating with the aforementioned data can be very useful for tumour treatment, leading effectively to more tailored medicine and giving rise to personalised treatments in the future.

One of the fields in which NMR metabolomics is rapidly expanding is the identification of specific cancer biomarkers in blood. Simple blood testing providing metabolic biomarker information, is considerably cheaper than genome sequencing or complete proteome analysis, and is equally informative, providing indications for early cancer detection and the information needed for selecting optimal treatments. Moreover, because of its high sensitivity and quick response to environmental

changes, the metabolome often reflects the phenotype more accurately than information derived from other –omics techniques such as genomics and proteomics (Putri, Nakayama et al. 2013). At present there is still no FDA approved metabolomics tests for cancer, however metabolomics is used by the FDA in biomarker discovery (FDA, 2006).

The identification of cancer specific metabolic patterns or alterations can accelerate the process by which new molecular targets are defined. Metabolomics approaches can also be used to evaluate drugs that are already in use. Obtaining a deeper understanding of the mechanism of action of drugs, will enhance the identification of new combinations of drugs with higher potency and/or lower toxicity, as well as identifying diseases that may respond to unconventional drug. Such a strategy will lead to novel and better use of exisiting therapeutics.

To date, a limited number of approved anticancer drugs have been investigated using metabolomics methods. However, recent improvements have opened new avenues for NMR metabolomics approaches in the context of drug discovery and patient stratification. Investigating unique molecular characteristics, will provide sensitive indicators of how drugs are tolerated and how this in turn influences the outcome of the patient. By using more specific molecular targeted drugs and suitable stratification of patients, cancer treatments can become better tailored towards the individuality of the tumor and patient. The ability to quickly

identify the best drug for a particular patient will lead to more efficient treatment, reduced patient suffering and enhanced health-economical benefits. The complete mechanisms of action of many drugs is still poorly understood, which leads to less than optimal usage, but NMR (as well as MS) metabolomics can provide much better insight. Moreover, metabolomics studies are constantly improving our understanding of tumor biology, as shown by the recent identification of new potential biomarkers. Ultimately, recognition of the specific drug targets will lead to a new generation of rationally-designed drugs.

7.4 Concluding remarks

The metabolomics era has garnered a return of interest in cancer cell metabolism. At the same time, the cancer field has become increasingly interested in the tumour cell niche. It is believed that these areas will yield the next step change in therapeutic benefits for cancer patients. The study presented here is among the first, to address the interplay between the micro-environment and cancer cell metabolism in living primary cancer cells.

Understanding the complexity of the cancer cell niche is challenging. However, reductionist approaches can provide invaluable insights. The present study addressed the important issue of oxygen supply as part of the cancer cell niche. The unusual, perhaps unique, availability of CLL cells to work as a primary cancer cell model has been exploited. However, whilst an important cancer in its own right,

CLL cells also provide the opportunity to study the more general cancer characteristic of metastasis. This is because CLL cells continually recirculate between the oxygenated blood stream and hypoxic tissues, a process that metastatic cells have to recapitulate to populate new tumour sites. The demonstration of metabolic plasticity and the differential utilisation of pyruvate presented in this study has a potential to foster new research which may lead to new therapeutic approaches. The observation that CLL cells appear to have heterogeneous basal metabolism that may relate to disease state, may be further developed in the area of biomarker discovery, prognostication and treatment stratification.

References

(1989). "Chronic lymphocytic leukemia: recommendations for diagnosis, staging, and response criteria. International Workshop on Chronic Lymphocytic Leukemia." Ann Intern Med **110**(3): 236-238.

Aalipour, A. and R. H. Advani (2013). "Bruton tyrosine kinase inhibitors: a promising novel targeted treatment for B cell lymphomas." Br J Haematol **163**(4): 436-443.

Ackerman, D. and M. C. Simon (2014). "Hypoxia, lipids, and cancer: surviving the harsh tumor microenvironment." Trends Cell Biol **24**(8): 472-478.

Adamski, J., A. Price, et al. (2013). "Hypoxia-induced cytotoxic drug resistance in osteosarcoma is independent of HIF-1Alpha." PLoS One **8**(6): e65304.

Advani, S. H. (2010). "Targeting mTOR pathway: A new concept in cancer therapy." Indian J Med Paediatr Oncol **31**(4): 132-136.

Aguayo, A., S. O'Brien, et al. (2000). "Clinical relevance of intracellular vascular endothelial growth factor levels in B-cell chronic lymphocytic leukemia." Blood **96**(2): 768-770.

Ahearne, M. J., S. Willimott, et al. (2013). "Enhancement of CD154/IL4 proliferation by the T follicular helper (Tfh) cytokine, IL21 and increased numbers of circulating cells resembling Tfh cells in chronic lymphocytic leukaemia." Br J Haematol **162**(3): 360-370.

Ahluwalia, G. S., J. L. Grem, et al. (1990). "Metabolism and action of amino acid analog anti-cancer agents." Pharmacol Ther **46**(2): 243-271.

Aiello, M., N. Vella, et al. (2011). "Role of genetic polymorphisms and mutations in colorectal cancer therapy (Review)." Mol Med Rep **4**(2): 203-208.

Alduaij, W., A. Ivanov, et al. (2011). "Novel type II anti-CD20 monoclonal antibody (GA101) evokes homotypic adhesion and actin-dependent, lysosome-mediated cell death in B-cell malignancies." Blood **117**(17): 4519-4529.

Anastasiou, D. and L. Cantley (2012). "Breathless cancer cells get fat on glutamine." Cell Res **22**(3): 443-446.

Asada, K., K. Miyamoto, et al. (2003). "Reduced expression of GNA11 and silencing of MCT1 in human breast cancers." Oncology **64**(4): 380-388.

Bagnara, D., M. S. Kaufman, et al. (2011). "A novel adoptive transfer model of chronic lymphocytic leukemia suggests a key role for T lymphocytes in the disease." Blood **117**(20): 5463-5472.

Bailey, K. M., J. W. Wojtkowiak, et al. (2012). "Targeting the metabolic microenvironment of tumors." Adv Pharmacol **65**: 63-107.

Bayet-Robert, M., D. Morvan, et al. (2010). "Pharmacometabolomics of docetaxel-treated human MCF7 breast cancer cells provides evidence of varying cellular responses at high and low doses." Breast Cancer Res Treat **120**(3): 613-626.

Beck, W. S. (1958). "Occurrence and control of the phosphogluconate oxidation pathway in normal and leukemic leukocytes." J Biol Chem **232**(1): 271-283.

Beckonert, O., H. C. Keun, et al. (2007). "Metabolic profiling, metabolomic and metabonomic procedures for NMR spectroscopy of urine, plasma, serum and tissue extracts." Nat Protoc **2**(11): 2692-2703.

Ben-Tchavtchavadze, M., J. Chen, et al. (2010). "A noninvasive technique for the measurement of the energetic state of free-suspension mammalian cells." Biotechnol Prog **26**(2): 532-541.

Benjamin, D. I., B. F. Cravatt, et al. (2012). "Global profiling strategies for mapping dysregulated metabolic pathways in cancer." Cell Metab **16**(5): 565-577.

Beuster, G., K. Zarse, et al. (2011). "Inhibition of alanine aminotransferase in silico and in vivo promotes mitochondrial metabolism to impair malignant growth." J Biol Chem **286**(25): 22323-22330.

Blankenberg, F. G., P. D. Katsikis, et al. (1997). "Quantitative analysis of apoptotic cell death using proton nuclear magnetic resonance spectroscopy." Blood **89**(10): 3778-3786.

Boag, J. M., A. H. Beesley, et al. (2006). "Altered glucose metabolism in childhood pre-B acute lymphoblastic leukaemia." Leukemia **20**(10): 1731-1737.

Bochner, B. R., P. Gadzinski, et al. (2001). "Phenotype microarrays for high-throughput phenotypic testing and assay of gene function." Genome Res **11**(7): 1246-1255.

Bocker, W. (2002). "The WHO classification of breast tumours and tumours of the female genital organs: Pathology and genetics." Pathology of the Kidneys and Urinary Passages - Molecular Vascular Pathology and Angiogenesis **86**: 116-119.

Bonnet, S., S. L. Archer, et al. (2007). "A mitochondria-K+ channel axis is suppressed in cancer and its normalization promotes apoptosis and inhibits cancer growth." Cancer cell **11**(1): 37-51.

Bonuccelli, G., A. Tsirigos, et al. (2010). "Ketones and lactate "fuel" tumor growth and metastasis: Evidence that epithelial cancer cells use oxidative mitochondrial metabolism." Cell Cycle **9**(17): 3506-3514.

Borcherds, W., F. X. Theillet, et al. (2014). "Disorder and residual helicity alter p53-Mdm2 binding affinity and signaling in cells." Nat Chem Biol **10**(12): 1000-1002.

Borge, M., P. R. Nannini, et al. (2013). "CXCL12 is a costimulator for CD4+ T cell activation and proliferation in chronic lymphocytic leukemia patients." Cancer Immunol Immunother **62**(1): 113-124.

Bottcher, S., M. Ritgen, et al. (2012). "Minimal residual disease quantification is an independent predictor of progression-free and overall survival in chronic lymphocytic leukemia: a multivariate analysis from the randomized GCLLSG CLL8 trial." J Clin Oncol **30**(9): 980-988.

Brand, K. A. and U. Hermfisse (1997). "Aerobic glycolysis by proliferating cells: a protective strategy against reactive oxygen species." FASEB J **11**(5): 388-395.

Breccia, M., F. Efficace, et al. (2011). "Imatinib treatment in chronic myelogenous leukemia: What have we learned so far?" Cancer Lett **300**(2): 115-121.

Brekke, E. M., T. S. Morken, et al. (2014). "The pentose phosphate pathway and pyruvate carboxylation after neonatal hypoxic-ischemic brain injury." J Cereb Blood Flow Metab **34**(4): 724-734.

Brody, J. I., F. A. Oski, et al. (1969). "Impaired pentose phosphate shunt and decreased glycolytic activity in lymphocytes of chronic lymphocytic leukemia. Metabolic pathway." Blood **34**(4): 421-429.

Bruzzi, J. F., H. Macapinlac, et al. (2006). "Detection of Richter's transformation of chronic lymphocytic leukemia by PET/CT." J Nucl Med **47**(8): 1267-1273.

Buhl, L., C. Dragsholt, et al. (1985). "Urinary hypoxanthine and pseudouridine as indicators of tumor development in mesothelioma-transplanted nude mice." Cancer Res **45**(3): 1159-1162.

Burger, J. A. (2011). "Nurture versus nature: the microenvironment in chronic lymphocytic leukemia." Hematology Am Soc Hematol Educ Program **2011**: 96-103.

Burger, J. A., M. Burger, et al. (1999). "Chronic lymphocytic leukemia B cells express functional CXCR4 chemokine receptors that mediate spontaneous migration beneath bone marrow stromal cells." Blood **94**(11): 3658-3667.

Burger, J. A., P. Ghia, et al. (2009). "The microenvironment in mature B-cell malignancies: a target for new treatment strategies." Blood **114**(16): 3367-3375.

Burger, J. A., M. P. Quiroga, et al. (2009). "High-level expression of the T-cell chemokines CCL3 and CCL4 by chronic lymphocytic leukemia B cells in nurselike cell cocultures and after BCR stimulation." Blood **113**(13): 3050-3058.

Burger, J. A., N. Tsukada, et al. (2000). "Blood-derived nurse-like cells protect chronic lymphocytic leukemia B cells from spontaneous apoptosis through stromal cell-derived factor-1." Blood **96**(8): 2655-2663.

Byrd, J. C., R. R. Furman, et al. (2013). "Targeting BTK with ibrutinib in relapsed chronic lymphocytic leukemia." N Engl J Med **369**(1): 32-42.

Caligaris-Cappio, F. (2000). "Biology of chronic lymphocytic leukemia." Rev Clin Exp Hematol **4**(1): 5-21.

Caligaris-Cappio, F. (2009). "Chronic lymphocytic leukemia: "Cinderella" is becoming a star." Mol Med **15**(3-4): 67-69.

Calissano, C., R. N. Damle, et al. (2011). "Intraclonal complexity in chronic lymphocytic leukemia: fractions enriched in recently born/divided and older/quiescent cells." Mol Med **17**(11-12): 1374-1382.

Cam, H., J. B. Easton, et al. (2010). "mTORC1 signaling under hypoxic conditions is controlled by ATM-dependent phosphorylation of HIF-1alpha." Mol Cell **40**(4): 509-520.

Caneba, C. A., N. Bellance, et al. (2012). "Pyruvate uptake is increased in highly invasive ovarian cancer cells under anoikis conditions for anaplerosis, mitochondrial function, and migration." Am J Physiol Endocrinol Metab **303**(8): E1036-1052.

Cantor, J. R. and D. M. Sabatini (2012). "Cancer cell metabolism: one hallmark, many faces." Cancer Discov **2**(10): 881-898.

Cardone, R. A., V. Casavola, et al. (2005). "The role of disturbed pH dynamics and the Na+/H+ exchanger in metastasis." Nat Rev Cancer **5**(10): 786-795.

Carlucci, F., F. Rosi, et al. (1997). "Purine nucleotide metabolism: specific aspects in chronic lymphocytic leukemia lymphocytes." Biochim Biophys Acta **1360**(3): 203-210.

Chen, A. P., M. J. Albers, et al. (2007). "Hyperpolarized C-13 spectroscopic imaging of the TRAMP mouse at 3T-initial experience." Magn Reson Med **58**(6): 1099-1106.

Chen, E. I., J. Hewel, et al. (2007). "Adaptation of energy metabolism in breast cancer brain metastases." Cancer Res **67**(4): 1472-1486.

Chen, H., A. T. Treweeke, et al. (2000). "In vitro and in vivo production of vascular endothelial growth factor by chronic lymphocytic leukemia cells." Blood **96**(9): 3181-3187.

Chen, R., Y. Zou, et al. (2014). "The general amino acid control pathway regulates mTOR and autophagy during serum/glutamine starvation." J Cell Biol **206**(2): 173-182.

Cheng, L. L., C. L. Lean, et al. (1996). "Enhanced resolution of proton NMR spectra of malignant lymph nodes using magic-angle spinning." Magn Reson Med **36**(5): 653-658.

Cheng, T., J. Sudderth, et al. (2011). "Pyruvate carboxylase is required for glutamine-independent growth of tumor cells." Proc Natl Acad Sci U S A **108**(21): 8674-8679.

Chilov, D., G. Camenisch, et al. (1999). "Induction and nuclear translocation of hypoxia-inducible factor-1 (HIF-1): heterodimerization with ARNT is not necessary for nuclear accumulation of HIF-1alpha." J Cell Sci **112 (Pt 8)**: 1203-1212.

Chiorazzi, N. (2007). "Cell proliferation and death: forgotten features of chronic lymphocytic leukemia B cells." Best Pract Res Clin Haematol **20**(3): 399-413.

Chiorazzi, N., K. R. Rai, et al. (2005). "Chronic lymphocytic leukemia." N Engl J Med **352**(8): 804-815.

Cipolleschi, M. G., I. Marzi, et al. (2014). "Hypoxia-resistant profile implies vulnerability of cancer stem cells to physiological agents, which suggests new therapeutic targets." Cell Cycle **13**(2): 268-278.

Coen, M., E. Holmes, et al. (2008). "NMR-based metabolic profiling and metabonomic approaches to problems in molecular toxicology." Chem Res Toxicol **21**(1): 9-27.

Cohen, J. S., M. Motiei, et al. (2004). "Determination of intracellular pH and compartmentation using diffusion-weighted NMR spectroscopy with pH-sensitive indicators." Magn Reson Med **51**(5): 900-903.

Collins, R. J., L. A. Verschuer, et al. (1989). "Spontaneous programmed death (apoptosis) of B-chronic lymphocytic leukaemia cells following their culture in vitro." Br J Haematol **71**(3): 343-350.

Cook, K. M., S. T. Hilton, et al. (2009). "Epidithiodiketopiperazines block the interaction between hypoxia-inducible factor-1alpha (HIF-1alpha) and p300 by a zinc ejection mechanism." J Biol Chem **284**(39): 26831-26838.

D'Arena, G., N. Di Renzo, et al. (2003). "Biological and clinical heterogeneity of B-cell chronic lymphocytic leukemia." Leuk Lymphoma **44**(2): 223-228.

Dalvit, C. and A. Vulpetti (2011). "Fluorine–Protein Interactions and 19F NMR Isotropic Chemical Shifts: An Empirical Correlation with Implications for Drug Design." ChemMedChem **6**(1): 104-114.

Dameshek, W. (1967). "Chronic lymphocytic leukemia--an accumulative disease of immunolgically incompetent lymphocytes." Blood **29**(4): Suppl:566-584.

Dang, L., D. W. White, et al. (2009). "Cancer-associated IDH1 mutations produce 2-hydroxyglutarate." Nature **462**(7274): 739-744.

Danilov, A. V. (2013). "Targeted therapy in chronic lymphocytic leukemia: past, present, and future." Clin Ther **35**(9): 1258-1270.

Davids, M. S. and J. A. Burger (2012). "Cell Trafficking in Chronic Lymphocytic Leukemia." Open J Hematol **3**(S1).

Day, S. E., M. I. Kettunen, et al. (2007). "Detecting tumor response to treatment using hyperpolarized 13C magnetic resonance imaging and spectroscopy." Nat Med **13**(11): 1382-1387.

De Saedeleer, C. J., P. E. Porporato, et al. (2013). "Glucose deprivation increases monocarboxylate transporter 1 (MCT1) expression and MCT1-dependent tumor cell migration." Oncogene.

DeBerardinis, R. J. and T. Cheng (2010). "Q's next: the diverse functions of glutamine in metabolism, cell biology and cancer." Oncogene **29**(3): 313-324.

DeBerardinis, R. J., A. Mancuso, et al. (2007). "Beyond aerobic glycolysis: transformed cells can engage in glutamine metabolism that exceeds the requirement for protein and nucleotide synthesis." Proc Natl Acad Sci U S A **104**(49): 19345-19350.

DeBerardinis, R. J. and C. B. Thompson (2012). "Cellular metabolism and disease: what do metabolic outliers teach us?" Cell **148**(6): 1132-1144.

Defoiche, J., C. Debacq, et al. (2008). "Reduction of B cell turnover in chronic lymphocytic leukaemia." Br J Haematol **143**(2): 240-247.

Denkert, C., E. Bucher, et al. (2012). "Metabolomics of human breast cancer: new approaches for tumor typing and biomarker discovery." Genome Med **4**(4): 37.

Desouki, M. M., G. R. Post, et al. (2010). "PAX-5: a valuable immunohistochemical marker in the differential diagnosis of lymphoid neoplasms." Clin Med Res **8**(2): 84-88.

Dewar, B. J., K. Keshari, et al. (2010). "Metabolic assessment of a novel chronic myelogenous leukemic cell line and an imatinib resistant subline by H NMR spectroscopy." Metabolomics **6**(3): 439-450.

Dhar-Mascareno, M., J. M. Carcamo, et al. (2005). "Hypoxia-reoxygenation-induced mitochondrial damage and apoptosis in human endothelial cells are inhibited by vitamin C." Free Radic Biol Med **38**(10): 1311-1322.

Dona, A. C., B. Jimenez, et al. (2014). "Precision high-throughput proton NMR spectroscopy of human urine, serum, and plasma for large-scale metabolic phenotyping." Anal Chem **86**(19): 9887-9894.

Eagle, H. (1955). "Nutrition needs of mammalian cells in tissue culture." Science **122**(3168): 501-514.

Eichhorst, B. F., R. Busch, et al. (2006). "Fludarabine plus cyclophosphamide versus fludarabine alone in first-line therapy of younger patients with chronic lymphocytic leukemia." Blood **107**(3): 885-891.

Evans, S. M., S. M. Hahn, et al. (2001). "Hypoxic heterogeneity in human tumors: EF5 binding, vasculature, necrosis, and proliferation." Am J Clin Oncol **24**(5): 467-472.

Evertts, A. G., A. L. Manning, et al. (2013). "H4k20 Methylation Regulates Quiescence and Chromatin Compaction." Mol Biol Cell.

Faderl, S., D. A. Thomas, et al. (2003). "Experience with alemtuzumab plus rituximab in patients with relapsed and refractory lymphoid malignancies." Blood **101**(9): 3413-3415.

Favaro, E., S. Lord, et al. (2011). "Gene expression and hypoxia in breast cancer." Genome Med **3**(8): 55.

Fernando, H., K. K. Bhopale, et al. (2011). "Lipidomic changes in rat liver after long-term exposure to ethanol." Toxicol Appl Pharmacol **255**(2): 127-137.

Fiegl, M., I. Samudio, et al. (2010). "Physiological hypoxia promotes lipid raft and PI3K-dependent activation of MAPK 42/44 in leukemia cells." Leukemia **24**(7): 1364-1367.

Filipp, F. V., D. A. Scott, et al. (2012). "Reverse TCA cycle flux through isocitrate dehydrogenases 1 and 2 is required for lipogenesis in hypoxic melanoma cells." Pigment Cell Melanoma Res **25**(3): 375-383.

Fink, M. P. (2002). "Role of reactive oxygen and nitrogen species in acute respiratory distress syndrome." Curr Opin Crit Care **8**(1): 6-11.

Florian, C. L., N. E. Preece, et al. (1995). "Characteristic metabolic profiles revealed by 1H NMR spectroscopy for three types of human brain and nervous system tumours." NMR Biomed **8**(6): 253-264.

Florian, C. L., N. E. Preece, et al. (1995). "Cell type-specific fingerprinting of meningioma and meningeal cells by proton nuclear magnetic resonance spectroscopy." Cancer Res **55**(2): 420-427.

Folmes, C. D., P. P. Dzeja, et al. (2012). "Metabolic plasticity in stem cell homeostasis and differentiation." Cell Stem Cell **11**(5): 596-606.

Forristal, C. E., I. G. Winkler, et al. (2013). "Pharmacologic stabilization of HIF-1alpha increases hematopoietic stem cell quiescence in vivo and accelerates blood recovery after severe irradiation." Blood **121**(5): 759-769.

Frater, J. L., N. E. Kay, et al. (2008). "Dysregulated angiogenesis in B-chronic lymphocytic leukemia: morphologic, immunohistochemical, and flow cytometric evidence." Diagn Pathol **3**: 16.

Fujiwara, S., Y. Kawano, et al. (2013). "PDK1 inhibition is a novel therapeutic target in multiple myeloma." Br J Cancer **108**(1): 170-178.

Fyles, A., M. Milosevic, et al. (2002). "Tumor hypoxia has independent predictor impact only in patients with node-negative cervix cancer." J Clin Oncol **20**(3): 680-687.

Gambhir, S. (2002). "Molecular imaging of cancer with positron emission tomography." Nat Rev Cancer **2**(9): 683-693.

Gao, P., H. Zhang, et al. (2007). "HIF-dependent antitumorigenic effect of antioxidants in vivo." Cancer cell **12**(3): 230-238.

Garcia-Segura, J. M., M. Sanchez-Chapado, et al. (1999). "In vivo proton magnetic resonance spectroscopy of diseased prostate: spectroscopic features of malignant versus benign pathology." Magn Reson Imaging **17**(5): 755-765.

Garrido, C., L. Galluzzi, et al. (2006). "Mechanisms of cytochrome c release from mitochondria." Cell Death Differ **13**(9): 1423-1433.

Gates, S. C. and C. C. Sweeley (1978). "Quantitative metabolic profiling based on gas chromatography." Clin Chem **24**(10): 1663-1673.

Gebregiworgis, T. and R. Powers (2012). "Application of NMR metabolomics to search for human disease biomarkers." Comb Chem High Throughput Screen **15**(8): 595-610.

Ghia, P., P. Circosta, et al. (2005). "Differential effects on CLL cell survival exerted by different microenvironmental elements." Curr Top Microbiol Immunol **294**: 135-145.

Ghiotto, G., G. Perona, et al. (1963). "Hexokinase and TPN-dependent dehydrogenases of leucocytes in leukaemia and other haematological disorders." Br J Haematol **9**: 345-350.

Ghosh, A. K., T. D. Shanafelt, et al. (2009). "Aberrant regulation of pVHL levels by microRNA promotes the HIF/VEGF axis in CLL B cells." Blood **113**(22): 5568-5574.

Giannoni, E., F. Buricchi, et al. (2005). "Intracellular reactive oxygen species activate Src tyrosine kinase during cell adhesion and anchorage-dependent cell growth." Mol Cell Biol **25**(15): 6391-6403.

Gillies, R. J., N. Raghunand, et al. (2002). "MRI of the tumor microenvironment." J Magn Reson Imaging **16**(4): 430-450.

Golman, K., R. in 't Zandt, et al. (2006). "Real-time metabolic imaging." Proc Natl Acad Sci U S A **103**(30): 11270-11275.

Gorrini, C., I. S. Harris, et al. (2013). "Modulation of oxidative stress as an anticancer strategy." Nat Rev Drug Discov **12**(12): 931-947.

Gottlieb, E. and I. P. Tomlinson (2005). "Mitochondrial tumour suppressors: a genetic and biochemical update." Nat Rev Cancer **5**(11): 857-866.

Graeber, T. G., C. Osmanian, et al. (1996). "Hypoxia-mediated selection of cells with diminished apoptotic potential in solid tumours." Nature **379**(6560): 88-91.

Griffin, J. L. and O. Corcoran (2005). "High-resolution magic-angle spinning 13C NMR spectroscopy of cerebral tissue." MAGMA **18**(1): 51-56.

Griffin, J. L., E. Sang, et al. (2002). "Metabolic profiles of dystrophin and utrophin expression in mouse models of Duchenne muscular dystrophy." FEBS Lett **530**(1-3): 109-116.

Griffin, J. L. and J. P. Shockcor (2004). "Metabolic profiles of cancer cells." Nat Rev Cancer **4**(7): 551-561.

Griffiths, M., D. Keast, et al. (1993). "The role of glutamine and glucose analogues in metabolic inhibition of human myeloid leukaemia in vitro." Int J Biochem **25**(12): 1749-1755.

Gromova, M. and C. Roby (2010). "Toward Arabidopsis thaliana hydrophilic metabolome: assessment of extraction methods and quantitative 1H NMR." Physiol Plant **140**(2): 111-127.

Gross, S., R. A. Cairns, et al. (2010). "Cancer-associated metabolite 2-hydroxyglutarate accumulates in acute myelogenous leukemia with isocitrate dehydrogenase 1 and 2 mutations." J Exp Med **207**(2): 339-344.

Gunther, U. L., C. Ludwig, et al. (2000). "NMRLAB-Advanced NMR data processing in matlab." J Magn Reson **145**(2): 201-208.

Hakumaki, J. M., H. Poptani, et al. (1998). "Quantitative 1H nuclear magnetic resonance diffusion spectroscopy of BT4C rat glioma during thymidine kinase-mediated gene therapy in vivo: identification of apoptotic response." Cancer Res **58**(17): 3791-3799.

Halestrap, A. P. and M. C. Wilson (2012). "The monocarboxylate transporter family--role and regulation." IUBMB Life **64**(2): 109-119.

Hallek, M. (2013). "Signaling the end of chronic lymphocytic leukemia: new frontline treatment strategies." Blood **122**(23): 3723-3734.

Hallek, M., B. D. Cheson, et al. (2008). "Guidelines for the diagnosis and treatment of chronic lymphocytic leukemia: a report from the International Workshop on Chronic Lymphocytic Leukemia updating the National Cancer Institute-Working Group 1996 guidelines." Blood **111**(12): 5446-5456.

Hamanaka, R. and N. Chandel (2012). "Targeting glucose metabolism for cancer therapy." J Exp Med **209**(2): 211-215.

Hanahan, D. and R. Weinberg (2011). "Hallmarks of cancer: the next generation." Cell **144**(5): 646-674.

Hanahan, D. and R. A. Weinberg (2000). "The hallmarks of cancer." Cell **100**(1): 57-70.

Hanlon, E. B., R. Manoharan, et al. (2000). "Prospects for in vivo Raman spectroscopy." Phys Med Biol **45**(2): R1-59.

Harguindey, S., J. L. Arranz, et al. (2009). "Proton transport inhibitors as potentially selective anticancer drugs." Anticancer Res **29**(6): 2127-2136.

Harris, T., H. Degani, et al. (2013). "Hyperpolarized 13C NMR studies of glucose metabolism in living breast cancer cell cultures." NMR Biomed **26**(12): 1831-1843.

Harris, T., G. Eliyahu, et al. (2009). "Kinetics of hyperpolarized 13C1-pyruvate transport and metabolism in living human breast cancer cells." Proc Natl Acad Sci U S A **106**(43): 18131-18136.

Harrison, R. (2002). "Structure and function of xanthine oxidoreductase: where are we now?" Free Radic Biol Med **33**(6): 774-797.

Hashimoto, H., M. Kubota, et al. (1992). "Effect of high-dose methotrexate on plasma hypoxanthine and uridine levels in patients with acute leukemia or non-Hodgkin lymphoma in childhood." Leukemia **6**(11): 1199-1202.

Hayden, R. E., G. Pratt, et al. (2012). "Treatment of chronic lymphocytic leukemia requires targeting of the protective lymph node environment with novel therapeutic approaches." Leuk Lymphoma **53**(4): 537-549.

Herishanu, Y., P. Perez-Galan, et al. (2011). "The lymph node microenvironment promotes B-cell receptor signaling, NF-kappaB activation, and tumor proliferation in chronic lymphocytic leukemia." Blood **117**(2): 563-574.

Hirayama, A., K. Kami, et al. (2009). "Quantitative metabolome profiling of colon and stomach cancer microenvironment by capillary electrophoresis time-of-flight mass spectrometry." Cancer Res **69**(11): 4918-4925.

Hoellenriegel, J., S. A. Meadows, et al. (2011). "The phosphoinositide 3'-kinase delta inhibitor, CAL-101, inhibits B-cell receptor signaling and chemokine networks in chronic lymphocytic leukemia." Blood **118**(13): 3603-3612.

Hoult, D. I., S. J. Busby, et al. (1974). "Observation of tissue metabolites using 31P nuclear magnetic resonance." Nature **252**(5481): 285-287.

Huang, C. Y., W. T. Kuo, et al. (2013). "Resistance to hypoxia-induced necroptosis is conferred by glycolytic pyruvate scavenging of mitochondrial superoxide in colorectal cancer cells." Cell Death Dis **4**: e622.

Huber, V., A. De Milito, et al. (2010). "Proton dynamics in cancer." J Transl Med **8**: 57.

Hulleman, E., K. M. Kazemier, et al. (2009). "Inhibition of glycolysis modulates prednisolone resistance in acute lymphoblastic leukemia cells." Blood **113**(9): 2014-2021.

Hurtaud, C., C. Gelly, et al. (2007). "Glutamine stimulates translation of uncoupling protein 2mRNA." Cell Mol Life Sci **64**(14): 1853-1860.

Jang, Y. Y. and S. J. Sharkis (2007). "A low level of reactive oxygen species selects for primitive hematopoietic stem cells that may reside in the low-oxygenic niche." Blood **110**(8): 3056-3063.

Jiang, P., W. Du, et al. (2014). "Regulation of the pentose phosphate pathway in cancer." Protein Cell **5**(8): 592-602.

Jitschin, R., A. D. Hofmann, et al. (2014). "Mitochondrial metabolism contributes to oxidative stress and reveals therapeutic targets in chronic lymphocytic leukemia." Blood **123**(17): 2663-2672.

Kaelin, W. G., Jr. and C. B. Thompson (2010). "Q&A: Cancer: clues from cell metabolism." Nature **465**(7298): 562-564.

Kallio, P. J., K. Okamoto, et al. (1998). "Signal transduction in hypoxic cells: inducible nuclear translocation and recruitment of the CBP/p300 coactivator by the hypoxia-inducible factor-1alpha." EMBO J **17**(22): 6573-6586.

Kathagen, A., A. Schulte, et al. (2013). "Hypoxia and oxygenation induce a metabolic switch between pentose phosphate pathway and glycolysis in glioma stem-like cells." Acta Neuropathol **126**(5): 763-780.

Kay, N. E., D. F. Jelinek, et al. (2001). "Angiogenesis in B-chronic lymphocytic leukemia." Leuk Res **25**(8): 709-710.

Keating, G. M. (2010). "Rituximab: a review of its use in chronic lymphocytic leukaemia, low-grade or follicular lymphoma and diffuse large B-cell lymphoma." Drugs **70**(11): 1445-1476.

Keating, M. J., S. O'Brien, et al. (2005). "Early results of a chemoimmunotherapy regimen of fludarabine, cyclophosphamide, and rituximab as initial therapy for chronic lymphocytic leukemia." J Clin Oncol **23**(18): 4079-4088.

Kennaway, N. G., N. R. Buist, et al. (1984). "Lactic acidosis and mitochondrial myopathy associated with deficiency of several components of complex III of the respiratory chain." Pediatr Res **18**(10): 991-999.

Kennedy, K. M. and M. W. Dewhirst (2010). "Tumor metabolism of lactate: the influence and therapeutic potential for MCT and CD147 regulation." Future Oncol **6**(1): 127-148.

Keshari, K. R., J. Kurhanewicz, et al. (2010). "Hyperpolarized (13)C spectroscopy and an NMR-compatible bioreactor system for the investigation of real-time cellular metabolism." Magn Reson Med **63**(2): 322-329.

Khajeh, M., M. A. Bernstein, et al. (2010). "A simple flowcell for reaction monitoring by NMR." Magn Reson Chem **48**(7): 516-522.

Kharfan-Dabaja, M. A., W. G. Wierda, et al. (2014). "Immunotherapy for chronic lymphocytic leukemia in the era of BTK inhibitors." Leukemia **28**(3): 507-517.

Kim, J. W., I. Tchernyshyov, et al. (2006). "HIF-1-mediated expression of pyruvate dehydrogenase kinase: a metabolic switch required for cellular adaptation to hypoxia." Cell Metab **3**(3): 177-185.

Kim, Y., Q. Lin, et al. (2009). "Hypoxic tumor microenvironment and cancer cell differentiation." Curr Mol Med **9**(4): 425-434.

Kini, A. R., N. E. Kay, et al. (2000). "Increased bone marrow angiogenesis in B cell chronic lymphocytic leukemia." Leukemia **14**(8): 1414-1418.

Kintner, D. B., M. K. Anderson, et al. (2000). "31P-MRS-based determination of brain intracellular and interstitial pH: its application to in vivo H+ compartmentation and cellular regulation during hypoxic/ischemic conditions." Neurochem Res **25**(9-10): 1385-1396.

Ko, Y. H., B. L. Smith, et al. (2004). "Advanced cancers: eradication in all cases using 3-bromopyruvate therapy to deplete ATP." Biochem Biophys Res Commun **324**(1): 269-275.

Kojima, H., H. Gu, et al. (2002). "Abnormal B lymphocyte development and autoimmunity in hypoxia-inducible factor 1alpha -deficient chimeric mice." Proc Natl Acad Sci U S A **99**(4): 2170-2174.

Koppenol, W. H., P. L. Bounds, et al. (2011). "Otto Warburg's contributions to current concepts of cancer metabolism." Nat Rev Cancer **11**(5): 325-337.

Koshland, D. E., Jr. (1963). "Correlation of Structure and Function in Enzyme Action." Science **142**(3599): 1533-1541.

Kovacevic, Z. (1971). "The pathway of glutamine and glutamate oxidation in isolated mitochondria from mammalian cells." Biochem J **125**(3): 757-763.

Kung, A. L., S. D. Zabludoff, et al. (2004). "Small molecule blockade of transcriptional coactivation of the hypoxia-inducible factor pathway." Cancer cell **6**(1): 33-43.

Kurtoglu, M., J. C. Maher, et al. (2007). "Differential toxic mechanisms of 2-deoxy-D-glucose versus 2-fluorodeoxy-D-glucose in hypoxic and normoxic tumor cells." Antioxid Redox Signal **9**(9): 1383-1390.

Laffel, L. (1999). "Ketone bodies: a review of physiology, pathophysiology and application of monitoring to diabetes." Diabetes Metab Res Rev **15**(6): 412-426.

Landau, D. A. and C. J. Wu (2013). "Chronic lymphocytic leukemia: molecular heterogeneity revealed by high-throughput genomics." Genome Med **5**(5): 47.

Lee, S. R., K. S. Yang, et al. (2002). "Reversible inactivation of the tumor suppressor PTEN by H2O2." J Biol Chem **277**(23): 20336-20342.

Lemons, J. M., X. J. Feng, et al. (2010). "Quiescent fibroblasts exhibit high metabolic activity." PLoS Biol **8**(10): e1000514.

Leni, Z., G. Parakkal, et al. (2013). "Emerging metabolic targets in the therapy of hematological malignancies." Biomed Res Int **2013**: 946206.

Leslie, N. R., D. Bennett, et al. (2003). "Redox regulation of PI 3-kinase signalling via inactivation of PTEN." EMBO J **22**(20): 5501-5510.

Lindon, J. C., E. Holmes, et al. (2006). "Metabonomics techniques and applications to pharmaceutical research & development." Pharm Res **23**(6): 1075-1088.

Lindon, J. C., J. K. Nicholson, et al. (2003). "Contemporary issues in toxicology the role of metabonomics in toxicology and its evaluation by the COMET project." Toxicol Appl Pharmacol **187**(3): 137-146.

Lodi, A., S. Tiziani, et al. (2013). "Proton NMR-based metabolite analyses of archived serial paired serum and urine samples from myeloma patients at different stages of disease activity identifies acetylcarnitine as a novel marker of active disease." PLoS One **8**(2): e56422.

Longo, P. G., L. Laurenti, et al. (2008). "The Akt/Mcl-1 pathway plays a prominent role in mediating antiapoptotic signals downstream of the B-cell receptor in chronic lymphocytic leukemia B cells." Blood **111**(2): 846-855.

Ludwig, C. and U. L. Gunther (2011). "MetaboLab--advanced NMR data processing and analysis for metabolomics." BMC Bioinformatics **12**: 366.

Ludwig, C. and M. R. Viant (2010). "Two-dimensional J-resolved NMR spectroscopy: review of a key methodology in the metabolomics toolbox." Phytochem Anal **21**(1): 22-32.

Ludwig, C., D. G. Ward, et al. (2009). "Fast targeted multidimensional NMR metabolomics of colorectal cancer." Magn Reson Chem **47 Suppl 1**: S68-73.

Lukey, M. J., K. F. Wilson, et al. (2013). "Therapeutic strategies impacting cancer cell glutamine metabolism." Future Med Chem **5**(14): 1685-1700.

Lyng, H., B. Sitter, et al. (2007). "Metabolic mapping by use of high-resolution magic angle spinning 1H MR spectroscopy for assessment of apoptosis in cervical carcinomas." BMC cancer **7**: 11.

Ma, Y. L., W. J. Liu, et al. (2009). "[Study on specific metabonomic profiling of serum from colorectal cancer patients by gas chromatography-mass spectrometry]." Zhonghua Wei Chang Wai Ke Za Zhi **12**(4): 386-390.

MacIntyre, D. A., B. Jimenez, et al. (2010). "Serum metabolome analysis by 1H-NMR reveals differences between chronic lymphocytic leukaemia molecular subgroups." Leukemia **24**(4): 788-797.

Maloney, D. G., B. Smith, et al. (2002). "Rituximab: mechanism of action and resistance." Semin Oncol **29**(1 Suppl 2): 2-9.

Mancuso, A., N. J. Beardsley, et al. (2004). "Real-time detection of 13C NMR labeling kinetics in perfused EMT6 mouse mammary tumor cells and betaHC9 mouse insulinomas." Biotechnol Bioeng **87**(7): 835-848.

Mancuso, A., A. Zhu, et al. (2005). "Artificial tumor model suitable for monitoring 31P and 13C NMR spectroscopic changes during chemotherapy-induced apoptosis in human glioma cells." Magn Reson Med **54**(1): 67-78.

Mardis, E. R., L. Ding, et al. (2009). "Recurring mutations found by sequencing an acute myeloid leukemia genome." N Engl J Med **361**(11): 1058-1066.

Mardor, Y., O. Kaplan, et al. (2000). "Noninvasive real-time monitoring of intracellular cancer cell metabolism and response to lonidamine treatment using diffusion weighted proton magnetic resonance spectroscopy." Cancer Res **60**(18): 5179-5186.

Martindale, J. L. and N. J. Holbrook (2002). "Cellular response to oxidative stress: signaling for suicide and survival." J Cell Physiol **192**(1): 1-15.

Mazurek, S. (2011). "Pyruvate kinase type M2: a key regulator of the metabolic budget system in tumor cells." Int J Biochem Cell Biol **43**(7): 969-980.

Mazurek, S., C. B. Boschek, et al. (2005). "Pyruvate kinase type M2 and its role in tumor growth and spreading." Semin Cancer Biol **15**(4): 300-308.

McKnight, S. L. (2010). "On getting there from here." Science **330**(6009): 1338-1339.

Meehan, A. J., C. J. Eskey, et al. (1992). "Cultivator for NMR studies of suspended cell cultures." Biotechnol Bioeng **40**(11): 1359-1366.

Mehlen, P. and A. Puisieux (2006). "Metastasis: a question of life or death." Nature Reviews Cancer **6**(6): 449-458.

Menzel, T., Z. Rahman, et al. (1996). "Elevated intracellular level of basic fibroblast growth factor correlates with stage of chronic lymphocytic leukemia and is associated with resistance to fludarabine." Blood **87**(3): 1056-1063.

Messmer, B. T., D. Messmer, et al. (2005). "In vivo measurements document the dynamic cellular kinetics of chronic lymphocytic leukemia B cells." J Clin Invest **115**(3): 755-764.

Metallo, C. M., P. A. Gameiro, et al. (2012). "Reductive glutamine metabolism by IDH1 mediates lipogenesis under hypoxia." Nature **481**(7381): 380-384.

Molica, S., G. Vitelli, et al. (1999). "Increased serum levels of vascular endothelial growth factor predict risk of progression in early B-cell chronic lymphocytic leukaemia." Br J Haematol **107**(3): 605-610.

Mullen, A. R., W. W. Wheaton, et al. (2012). "Reductive carboxylation supports growth in tumour cells with defective mitochondria." Nature **481**(7381): 385-388.

Murray, A. W. (1971). "The biological significance of purine salvage." Annu Rev Biochem **40**: 811-826.

Murray, J. A., F. L. Khanim, et al. (2010). "Combined bezafibrate and medroxyprogesterone acetate have efficacy without haematological toxicity in elderly and relapsed acute myeloid leukaemia (AML)." Br J Haematol **149**(1): 65-69.

Nathan, C. and A. Ding (2010). "SnapShot: Reactive Oxygen Intermediates (ROI)." Cell **140**(6): 951-951 e952.

Newsholme, P., J. Procopio, et al. (2003). "Glutamine and glutamate--their central role in cell metabolism and function." Cell Biochem Funct **21**(1): 1-9.

Nishio, M., T. Endo, et al. (2005). "Nurselike cells express BAFF and APRIL, which can promote survival of chronic lymphocytic leukemia cells via a paracrine pathway distinct from that of SDF-1alpha." Blood **106**(3): 1012-1020.

O'Donnell-Tormey, J., C. F. Nathan, et al. (1987). "Secretion of pyruvate. An antioxidant defense of mammalian cells." J Exp Med **165**(2): 500-514.

Oberley, L. W. (1988). "Free radicals and diabetes." Free Radic Biol Med **5**(2): 113-124.

Ong, E. S., L. Zou, et al. (2010). "Metabolic profiling in colorectal cancer reveals signature metabolic shifts during tumorigenesis." Mol Cell Proteomics.

Oremek, G. M., S. Teigelkamp, et al. (1999). "The pyruvate kinase isoenzyme tumor M2 (Tu M2-PK) as a tumor marker for renal carcinoma." Anticancer Res **19**(4A): 2599-2601.

Orphanos, G. and P. Kountourakis (2012). "Targeting the HER2 receptor in metastatic breast cancer." Hematol Oncol Stem Cell Ther **5**(3): 127-137.

Oscier, D., C. Dearden, et al. (2012). "Guidelines on the diagnosis, investigation and management of chronic lymphocytic leukaemia." Br J Haematol **159**(5): 541-564.

OuYang, D., J. Xu, et al. (2011). "Metabolomic profiling of serum from human pancreatic cancer patients using 1H NMR spectroscopy and principal component analysis." Appl Biochem Biotechnol **165**(1): 148-154.

Pacher, P., J. S. Beckman, et al. (2007). "Nitric oxide and peroxynitrite in health and disease." Physiol Rev **87**(1): 315-424.

Palomino-Schatzlein, M., P. V. Escrig, et al. (2011). "Evaluation of nonpolar metabolites in plant extracts by 13C NMR spectroscopy." J Agric Food Chem **59**(21): 11407-11416.

Panayiotidis, P., D. Jones, et al. (1996). "Human bone marrow stromal cells prevent apoptosis and support the survival of chronic lymphocytic leukaemia cells in vitro." Br J Haematol **92**(1): 97-103.

Parker, T. L. and M. P. Strout (2011). "Chronic lymphocytic leukemia: prognostic factors and impact on treatment." Discov Med **11**(57): 115-123.

Pavlides, S., A. Tsirigos, et al. (2010). "The autophagic tumor stroma model of cancer: Role of oxidative stress and ketone production in fueling tumor cell metabolism." Cell Cycle **9**(17): 3485-3505.

Pearce, E. L., M. C. Poffenberger, et al. (2013). "Fueling immunity: insights into metabolism and lymphocyte function." Science **342**(6155): 1242454.

Pekarsky, Y., A. Palamarchuk, et al. (2008). "Tcl1 functions as a transcriptional regulator and is directly involved in the pathogenesis of CLL." Proc Natl Acad Sci U S A **105**(50): 19643-19648.

Pfeuffer, J., I. Tkac, et al. (1999). "Toward an in vivo neurochemical profile: quantification of 18 metabolites in short-echo-time (1)H NMR spectra of the rat brain." J Magn Reson **141**(1): 104-120.

Pianet, I., P. Canioni, et al. (1992). "Beta-adrenergic stimulation of C6 glioma cells: effects of cAMP overproduction on cellular metabolites. A multinuclear NMR study." Eur J Biochem **209**(2): 707-715.

Polanski, R., C. L. Hodgkinson, et al. (2014). "Activity of the monocarboxylate transporter 1 inhibitor AZD3965 in small cell lung cancer." Clin Cancer Res **20**(4): 926-937.

Popovici-Muller, J., J. O. Saunders, et al. (2012). "Discovery of the First Potent Inhibitors of Mutant IDH1 That Lower Tumor 2-HG in Vivo." ACS Med Chem Lett **3**(10): 850-855.

Porporato, P. E., S. Dhup, et al. (2011). "Anticancer targets in the glycolytic metabolism of tumors: a comprehensive review." Front Pharmacol **2**: 49.

Portais, J. C., P. Voisin, et al. (1996). "Glucose and glutamine metabolism in C6 glioma cells studied by carbon 13 NMR." Biochimie **78**(3): 155-164.

Putri, S. P., Y. Nakayama, et al. (2013). "Current metabolomics: practical applications." J Biosci Bioeng **115**(6): 579-589.

Ramsay, A. D. and M. Rodriguez-Justo (2013). "Chronic lymphocytic leukaemia--the role of the microenvironment pathogenesis and therapy." Br J Haematol **162**(1): 15-24.

Ranjan, P., V. Anathy, et al. (2006). "Redox-dependent expression of cyclin D1 and cell proliferation by Nox1 in mouse lung epithelial cells." Antioxid Redox Signal **8**(9-10): 1447-1459.

Renault, M., L. Shintu, et al. (2013). "Slow-spinning low-sideband HR-MAS NMR spectroscopy: delicate analysis of biological samples." Sci Rep **3**: 3349.

Robinson, B. H., N. McKay, et al. (1985). "Defective intramitochondrial NADH oxidation in skin fibroblasts from an infant with fatal neonatal lacticacidemia." Am J Hum Genet **37**(5): 938-946.

Robinson, M. M., S. J. McBryant, et al. (2007). "Novel mechanism of inhibition of rat kidney-type glutaminase by bis-2-(5-phenylacetamido-1,2,4-thiadiazol-2-yl)ethyl sulfide (BPTES)." Biochem J **406**(3): 407-414.

Rohle, D., J. Popovici-Muller, et al. (2013). "An inhibitor of mutant IDH1 delays growth and promotes differentiation of glioma cells." Science **340**(6132): 626-630.

Roudier, E. and A. Perrin (2009). "Considering the role of pyruvate in tumor cells during hypoxia." Biochim Biophys Acta **1796**(2): 55-62.

Rubin, A. D. (1971). "Defective control of ribosomal RNA processing in stimulated leukemic lymphocytes." J Clin Invest **50**(12): 2485-2497.

Sakiyama, T., M. W. Musch, et al. (2009). "Glutamine increases autophagy under Basal and stressed conditions in intestinal epithelial cells." Gastroenterology **136**(3): 924-932.

Samudio, I., M. Fiegl, et al. (2009). "Mitochondrial uncoupling and the Warburg effect: molecular basis for the reprogramming of cancer cell metabolism." Cancer Res **69**(6): 2163-2166.

Samudio, I., M. Fiegl, et al. (2008). "The warburg effect in leukemia-stroma cocultures is mediated by mitochondrial uncoupling associated with uncoupling protein 2 activation." Cancer Res **68**(13): 5198-5205.

Samudio, I., R. Harmancey, et al. (2010). "Pharmacologic inhibition of fatty acid oxidation sensitizes human leukemia cells to apoptosis induction." J Clin Invest **120**(1): 142-156.

Sanfilippo, O., M. Camici, et al. (1994). "Relationship between the levels of purine salvage pathway enzymes and clinical/biological aggressiveness of human colon carcinoma." Cancer Biochem Biophys **14**(1): 57-66.

Schafer, Z. T., A. R. Grassian, et al. (2009). "Antioxidant and oncogene rescue of metabolic defects caused by loss of matrix attachment." Nature **461**(7260): 109-113.

Schechter, A. N., D. H. Sachs, et al. (1972). "Nuclear magnetic resonance titration curves of histidine ring protons. 3. Ribonuclease." J Mol Biol **71**(1): 39-48.

Schroeder, M. A., H. J. Atherton, et al. (2009). "Real-time assessment of Krebs cycle metabolism using hyperpolarized 13C magnetic resonance spectroscopy." FASEB J **23**(8): 2529-2538.

Seagroves, T. N., H. E. Ryan, et al. (2001). "Transcription factor HIF-1 is a necessary mediator of the pasteur effect in mammalian cells." Mol Cell Biol **21**(10): 3436-3444.

Selenko, P. and G. Wagner (2007). "Looking into live cells with in-cell NMR spectroscopy." J Struct Biol **158**(2): 244-253.

Seligmann, H., R. Levi, et al. (2001). "Thiamine deficiency in patients with B-chronic lymphocytic leukaemia: a pilot study." Postgrad Med J **77**(911): 582-585.

Sharma, R. A., W. P. Steward, et al. (2006). "Toxicity profile of the immunomodulatory thalidomide analogue, lenalidomide: phase I clinical trial of three dosing schedules in patients with solid malignancies." Eur J Cancer **42**(14): 2318-2325.

Shyh-Chang, N., G. Q. Daley, et al. (2013). "Stem cell metabolism in tissue development and aging." Development **140**(12): 2535-2547.

Silber, R., C. M. Farber, et al. (1992). "Glutathione depletion in chronic lymphocytic leukemia B lymphocytes." Blood **80**(8): 2038-2043.

Sison, E. A. and P. Brown (2011). "The bone marrow microenvironment and leukemia: biology and therapeutic targeting." Expert Rev Hematol **4**(3): 271-283.

Soto, G. E., Z. Zhu, et al. (1996). "Tumor 31P NMR pH measurements in vivo: a comparison of inorganic phosphate and intracellular 2-deoxyglucose-6-phosphate as pHnmr indicators in murine radiation-induced fibrosarcoma-1." Magn Reson Med **36**(5): 698-704.

Souers, A. J., J. D. Leverson, et al. (2013). "ABT-199, a potent and selective BCL-2 inhibitor, achieves antitumor activity while sparing platelets." Nat Med **19**(2): 202-208.

Star-Lack, J. M., E. Adalsteinsson, et al. (2000). "In vivo 1H MR spectroscopy of human head and neck lymph node metastasis and comparison with oxygen tension measurements." AJNR Am J Neuroradiol **21**(1): 183-193.

Subarsky, P. and R. P. Hill (2003). "The hypoxic tumour microenvironment and metastatic progression." Clin Exp Metastasis **20**(3): 237-250.

Sun, R. C. and N. C. Denko (2014). "Hypoxic regulation of glutamine metabolism through HIF1 and SIAH2 supports lipid synthesis that is necessary for tumor growth." Cell Metab **19**(2): 285-292.

Szyperski, T. (1995). "Biosynthetically directed fractional 13C-labeling of proteinogenic amino acids. An efficient analytical tool to investigate intermediary metabolism." Eur J Biochem **232**(2): 433-448.

Takahashi, A., N. Ohtani, et al. (2006). "Mitogenic signalling and the p16INK4a-Rb pathway cooperate to enforce irreversible cellular senescence." Nat Cell Biol **8**(11): 1291-1297.

Takubo, K., N. Goda, et al. (2010). "Regulation of the HIF-1alpha level is essential for hematopoietic stem cells." Cell Stem Cell **7**(3): 391-402.

Tate, A. R., S. Crabb, et al. (1996). "Lipid metabolite peaks in pattern recognition analysis of tumour in vivo MR spectra." Anticancer Res **16**(3B): 1575-1579.

Tate, A. R., J. R. Griffiths, et al. (1998). "Towards a method for automated classification of 1H MRS spectra from brain tumours." NMR Biomed **11**(4-5): 177-191.

Tausch, E., D. Mertens, et al. (2014). "Advances in treating chronic lymphocytic leukemia." F1000Prime Rep **6**: 65.

Tennant, D. A., C. Frezza, et al. (2009). "Reactivating HIF prolyl hydroxylases under hypoxia results in metabolic catastrophe and cell death." Oncogene **28**(45): 4009-4021.

Tiziani, S., V. Lopes, et al. (2009). "Early stage diagnosis of oral cancer using 1H NMR-based metabolomics." Neoplasia **11**(3): 269-276, 264p following 269.

Trachootham, D., J. Alexandre, et al. (2009). "Targeting cancer cells by ROS-mediated mechanisms: a radical therapeutic approach?" Nat Rev Drug Discov **8**(7): 579-591.

Tura, S., M. Cavo, et al. (1984). "Lonidamine in the treatment of chronic lymphoid leukemia." Oncology **41 Suppl 1**: 90-93.

Tweeddale, H., L. Notley-McRobb, et al. (1998). "Effect of slow growth on metabolism of Escherichia coli, as revealed by global metabolite pool ("metabolome") analysis." J Bacteriol **180**(19): 5109-5116.

Valcourt, J. R., J. M. Lemons, et al. (2012). "Staying alive: metabolic adaptations to quiescence." Cell Cycle **11**(9): 1680-1696.

van der Windt, G. J., D. O'Sullivan, et al. (2013). "CD8 memory T cells have a bioenergetic advantage that underlies their rapid recall ability." Proc Natl Acad Sci U S A **110**(35): 14336-14341.

Vander Heiden, M. G., L. C. Cantley, et al. (2009). "Understanding the Warburg effect: the metabolic requirements of cell proliferation." Science **324**(5930): 1029-1033.

Vannoni, D., B. Porcelli, et al. (1989). "[Purine metabolism in human tumors]." Medicina (Firenze) **9**(1): 51-54.

Varma, S. D. and K. R. Hegde (2007). "Lens thiol depletion by peroxynitrite. Protective effect of pyruvate." Mol Cell Biochem **298**(1-2): 199-204.

Velez, J., N. Hail, Jr., et al. (2013). "Mitochondrial uncoupling and the reprograming of intermediary metabolism in leukemia cells." Front Oncol **3**: 67.

Vergis, R., C. M. Corbishley, et al. (2008). "Intrinsic markers of tumour hypoxia and angiogenesis in localised prostate cancer and outcome of radical treatment: a retrospective analysis of two randomised radiotherapy trials and one surgical cohort study." Lancet Oncol **9**(4): 342-351.

Vernocchi, P., L. Vannini, et al. (2012). "Integration of datasets from different analytical techniques to assess the impact of nutrition on human metabolome." Front Cell Infect Microbiol **2**: 156.

Wachsberger, P., R. Burd, et al. (2003). "Tumor response to ionizing radiation combined with antiangiogenesis or vascular targeting agents: exploring mechanisms of interaction." Clin Cancer Res **9**(6): 1957-1971.

Wallace, D. C. (2012). "Mitochondria and cancer." Nat Rev Cancer **12**(10): 685-698.

Wang, F., J. Travins, et al. (2013). "Targeted inhibition of mutant IDH2 in leukemia cells induces cellular differentiation." Science **340**(6132): 622-626.

Wang, J. B., J. W. Erickson, et al. (2010). "Targeting mitochondrial glutaminase activity inhibits oncogenic transformation." Cancer cell **18**(3): 207-219.

Wang, Y. H., W. J. Israelsen, et al. (2014). "Cell-state-specific metabolic dependency in hematopoiesis and leukemogenesis." Cell **158**(6): 1309-1323.

Warburg, O. (1956). "On the origin of cancer cells." Science **123**(3191): 309-314.

Warburg, O., F. Wind, et al. (1927). "THE METABOLISM OF TUMORS IN THE BODY." The Journal of general physiology **8**(6): 519-530.

Ward, P. S. and C. B. Thompson (2012). "Metabolic reprogramming: a cancer hallmark even warburg did not anticipate." Cancer cell **21**(3): 297-308.

Wartenberg, M., F. C. Ling, et al. (2003). "Regulation of the multidrug resistance transporter P-glycoprotein in multicellular tumor spheroids by hypoxia-inducible factor (HIF-1) and reactive oxygen species." FASEB J **17**(3): 503-505.

Weigelt, B., J. L. Peterse, et al. (2005). "Breast cancer metastasis: markers and models." Nat Rev Cancer **5**(8): 591-602.

Weinhouse, S. (1976). "The Warburg hypothesis fifty years later." Z Krebsforsch Klin Onkol Cancer Res Clin Oncol **87**(2): 115-126.

Wellen, K. E. and C. B. Thompson (2010). "Cellular metabolic stress: considering how cells respond to nutrient excess." Mol Cell **40**(2): 323-332.

Wiechert, W. (2001). "13C metabolic flux analysis." Metab Eng **3**(3): 195-206.

Wierda, W. G., T. J. Kipps, et al. (2010). "Ofatumumab as single-agent CD20 immunotherapy in fludarabine-refractory chronic lymphocytic leukemia." J Clin Oncol **28**(10): 1749-1755.

Wiestner, A. (2013). "Targeting B-Cell receptor signaling for anticancer therapy: the Bruton's tyrosine kinase inhibitor ibrutinib induces impressive responses in B-cell malignancies." J Clin Oncol **31**(1): 128-130.

Williams, S. N., M. L. Anthony, et al. (1998). "Induction of apoptosis in two mammalian cell lines results in increased levels of fructose-1,6-bisphosphate and CDP-choline as determined by 31P MRS." Magn Reson Med **40**(3): 411-420.

Wise, D. R., R. J. DeBerardinis, et al. (2008). "Myc regulates a transcriptional program that stimulates mitochondrial glutaminolysis and leads to glutamine addiction." Proc Natl Acad Sci U S A **105**(48): 18782-18787.

Wise, D. R. and C. B. Thompson (2010). "Glutamine addiction: a new therapeutic target in cancer." Trends Biochem Sci **35**(8): 427-433.

Wu, P. S. and G. Otting (2005). "Rapid pulse length determination in high-resolution NMR." J Magn Reson **176**(1): 115-119.

Wullschleger, S., R. Loewith, et al. (2006). "TOR signaling in growth and metabolism." Cell **124**(3): 471-484.

Xu, R. H., H. Pelicano, et al. (2005). "Synergistic effect of targeting mTOR by rapamycin and depleting ATP by inhibition of glycolysis in lymphoma and leukemia cells." Leukemia **19**(12): 2153-2158.

Xu, W., H. Yang, et al. (2011). "Oncometabolite 2-hydroxyglutarate is a competitive inhibitor of alpha-ketoglutarate-dependent dioxygenases." Cancer cell **19**(1): 17-30.

Yang, C., C. Harrison, et al. (2014). "Simultaneous steady-state and dynamic 13C NMR can differentiate alternative routes of pyruvate metabolism in living cancer cells." J Biol Chem **289**(9): 6212-6224.

Yoo, B. C., S. Y. Kong, et al. (2010). "Identification of hypoxanthine as a urine marker for non-Hodgkin lymphoma by low-mass-ion profiling." BMC cancer **10**: 55.

Yuneva, M., N. Zamboni, et al. (2007). "Deficiency in glutamine but not glucose induces MYC-dependent apoptosis in human cells." J Cell Biol **178**(1): 93-105.

Zhang, W., D. Trachootham, et al. (2012). "Stromal control of cystine metabolism promotes cancer cell survival in chronic lymphocytic leukaemia." Nat Cell Biol **14**(3): 276-286.

Zhao, S., Y. Lin, et al. (2009). "Glioma-derived mutations in IDH1 dominantly inhibit IDH1 catalytic activity and induce HIF-1alpha." Science **324**(5924): 261-265.

Zhao, Y., E. Butler, et al. (2013). "Targeting cellular metabolism to improve cancer therapeutics." Cell death & disease **4**.

Zhao, Y., H. Liu, et al. (2011). "Overcoming trastuzumab resistance in breast cancer by targeting dysregulated glucose metabolism." Cancer Res **71**(13): 4585-4597.

Zhou, M., Y. Zhao, et al. (2010). "Warburg effect in chemosensitivity: targeting lactate dehydrogenase-A re-sensitizes taxol-resistant cancer cells to taxol." Mol Cancer **9**: 33.

Appendices

Appendix A1: Buffers and Recipes

2.3.2 Cell Cycle Buffer

30µg PI, 0.1mM $NaCl_2$, 1% (w/v) sodium citrate, 0.1% Triton X100 in ddH_2O

2.8.4 10x TBE Buffer

108g Tris base, 55g Boric acid, 9.3g EDTA made up to 1L in ddH_2O. Diluted to 1 x before use.

2.9.1 RIPA buffer

1% (v/v) NP40, 0.5% (w/v) sodium deoxycholate, 0.1% (w/v) SDS in distilled water. Kept at 4ºC. Protease inhibitor added prior to use.

2.9.2 Buffers and gels used for SDS PAGE and Western Blot

4x SDS gel loading buffer

62.5mM Tris HCl pH6.8, 25% (v/v) glycerol, 2% (v/v) SDS, 5% (v/v) 2-β-ME, Bromophenol Blue, in distilled water. Stored at RT.

10% Resolving gel

30% Bis/Acrylamide (Geneflow) 3.3ml

1.5M Tris HCl pH8.8 2.5ml

10% (v/v) SDS 0.1ml

Distilled water 4.1ml

10% Ammonium persulphate ((w/v)APS; Sigma) 60µl

TEMED (VWR international) 4.5µl

Stacking gel

30 % Bis/Acrylamide 440µl

0.5M Tris HCl pH6.8 830µl

10% (w/v)SDS 33µl

distilled water 2.03ml

10% (w/v)APS 16.7µl

TEMED 1.7µl

1x SDS gel running buffer

25mM Tris, 192mM glycine, 3.5mM SDS in distilled water

2.9.3 Solutions used for the Protein Transfer

Transfer buffer

25mM Tris, 192mM glycine, 20% (v/v) methanol in distilled water

TBS-T

137mM NaCl, 20mM Tris HCl pH 7.6, 0.2% (v/v) Tween20 in distilled water

5% blocking solution

5% (w/v) milk powder (Marvel) in TBS-T